

## Letter from the Editors

**D**ear readers of *Acta Naturae*!  
We are delighted to bring you the 25<sup>th</sup> issue of our journal, with new and, we hope, interesting articles.

This issue begins with reviews that can to some extent be associated with oncology (O.V. Matveeva *et al.*, N.V. Krakhmal' and to another to the problems of oncology (O.V. Matveeva *et al.*, N.V. Krakhmal' *et al.*). One of the reviews is devoted to the new targets of antibacterial therapy (A.V. Grishin *et al.*), while the two others focus on cellular biology (V.V. Gusel'nikova *et al.*, M.A. Filatov *et al.*).

The nine research articles cover a broad range of topics, with cellular biology as the predominant theme. This is no surprise: cell

cultures and cell models are widely used today in modern biological research and we wanted to register our endorsement for such a state of affairs. Yet, we strive to cover in our journal as many topics as possible: this issue contains articles that look into the approaches used today in bioinformatics, as well as those that are devoted to the interaction between certain ligands and cellular components, not to mention biomedical reports. Our journal is gradually broadening the topics it covers, and we want to urge authors to collaborate.

Until the 26<sup>th</sup> issue of *Acta Naturae*! ●

*Editorial Board*

# INNOVATION RUSSIA

Discussion club

We create a dialogue between all socially active groups of people: students, scientists, lecturers, businessmen, managers, innovators, investors, designers, art critics, architects, photographers.

Learn more  
at [WWW.STRF.RU](http://WWW.STRF.RU)

Everyone with something to say and  
ideas to share is welcome to visit  
our events



Tel.: +7 (495) 930-87-07, 930-88-50  
E-mail: seminar@strf.ru

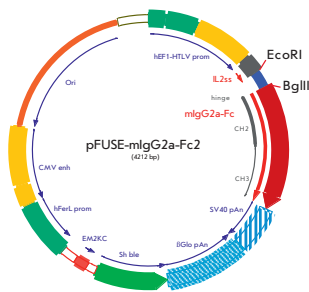
## Search for Inhibitors of Human Lactate Dehydrogenase A Using Computer Simulation

D.K. Nilov, E.A. Prokhorova, V.K. Švedas

The human lactate dehydrogenase isoform A (LDH-A) plays an important role in the survival of tumor cells with anaerobic metabolism. Therefore, the search for effective inhibitors of the enzyme is a promising direction in the development of new drugs. In order to establish new inhibitors, full atomic models of LDH-A have been generated, the structural criteria for selecting potential inhibitors have been developed, and computer screening of small molecules libraries have been performed. All these efforts have enabled us to establish a potential inhibitor: STK381370.



The open conformation of human LDH-A based on the X-ray data



A map of the pFUSE plasmid vector containing the gene of the mouse immunoglobulin constant fragment.

## Specific Depletion of Myelin-Reactive B Cells via BCR-Targeting

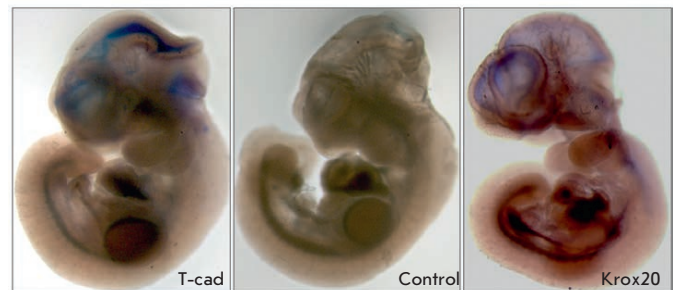
A.V. Stepanov, A.A. Belogurov, P. Kothapalli, O.G. Shamborant, V.D. Knorre, G.B. Telegin, A.A. Ovsepyan, N.A. Ponomarenko, S.M. Deyev, S. Kaveri, A.G. Gabibov

Experiments in an animal model of multiple sclerosis – SJL/J strain mice with induced experimental autoimmune encephalomyelitis (EAE) – demonstrated that a generated recombinant immunotoxin is capable of targeted elimination of an abnormal lymphocyte population *in vivo*. The suggested concept may underlie the further development of drugs for specific therapy of multiple sclerosis and other autoimmune diseases.

## Detection of T-Cadherin Expression in Mouse Embryos

K.A. Rubina, V.A. Smutova, M.L. Semenova, A.A. Poliakov, S. Gerety, D. Wilkinson, E.I. Surkova, E.V. Semina, V.Yu. Sysoeva, V.A. Tkachuk

In the present study, expression of T-cadherin at the early stages of mouse embryonic development was investigated. Using *in situ* hybridization and immunofluorescent staining of whole embryos in combination with confocal microscopy, we found that T-cadherin expression is detected in the developing brain, starting with the E8.75 stage, and in the heart, starting with the E11.5 stage. This indicates a possible role of T-cadherin in the formation of blood vessels during embryogenesis.



*In situ* hybridization of mouse embryos at the E10.5 stage

## Founders

Ministry of Education and  
Science of the Russian Federation,  
Lomonosov Moscow State University,  
Park Media Ltd

## Editorial Council

*Chairman:* A.I. Grigoriev  
*Editors-in-Chief:* A.G. Gabibov, S.N. Kochetkov

V.V. Vlassov, P.G. Georgiev, M.P. Kirpichnikov,  
A.A. Makarov, A.I. Miroshnikov, V.A. Tkachuk,  
M.V. Ugryumov

## Editorial Board

*Managing Editor:* V.D. Knorre  
*Publisher:* K.V. Kiselev

K.V. Anokhin (Moscow, Russia)  
I. Bezprozvanny (Dallas, Texas, USA)  
I.P. Bilenkina (Moscow, Russia)  
M. Blackburn (Sheffield, England)  
S.M. Deyev (Moscow, Russia)  
V.M. Govorun (Moscow, Russia)  
O.A. Dontsova (Moscow, Russia)  
K. Drauz (Hanau-Wolfgang, Germany)  
A. Friboulet (Paris, France)  
M. Issagouliants (Stockholm, Sweden)  
A.L. Konov (Moscow, Russia)  
M. Lukic (Abu Dhabi, United Arab Emirates)  
P. Masson (La Tronche, France)  
K. Nierhaus (Berlin, Germany)  
V.O. Popov (Moscow, Russia)  
I.A. Tikhonovich (Moscow, Russia)  
A. Tramontano (Davis, California, USA)  
V.K. Švedas (Moscow, Russia)  
J.-R. Wu (Shanghai, China)  
N.K. Yankovsky (Moscow, Russia)  
M. Zouali (Paris, France)

*Project Head:* S.B. Nevskaya

*Editor:* N.Yu. Deeva

*Designer:* K.K. Oparin

*Art and Layout:* K. Shnaider

*Copy Chief:* Daniel M. Medjo

Address: 119234 Moscow, Russia, Leninskiye Gory, Nauchny  
Park MGU, vlad.1, stroeniye 75G.  
Phone/Fax: +7 (495) 727 38 60  
E-mail: vera.knorre@gmail.com, mmorozova@strf.ru,  
actanaturae@gmail.com

Reprinting is by permission only.

© ACTA NATURAE, 2015

Номер подписан в печать 13 мая 2015 г.

Тираж 200 экз. Цена свободная.

Отпечатано в типографии «МЕДИА-ГРАНД»

# CONTENTS

Letter from the Editors.....1

## FORUM

O. V. Matveeva, G. V. Kochneva,  
S. V. Netesov, S. B. Onikienko, P. M. Chumakov

**Mechanisms of Oncolysis by Paramyxovirus  
Sendai.....6**

N. V. Krakhmal, M. V. Zavyalova,  
E. V. Denisov, S. V. Vtorushin,  
V. M. Perelmuter

**Cancer Invasion: Patterns and Mechanisms...17**

A. V. Grishin, M. S. Krivozubov,  
A. S. Karyagina, A. L. Gintsburg

***Pseudomonas Aeruginosa* Lectins As Targets  
for Novel Antibacterials.....29**

V. V. Gusel'nikova, D. E. Korzhevskiy

**NeuN As a Neuronal Nuclear Antigen and  
Neuron Differentiation Marker.....42**

M. A. Filatov, Y. V. Khramova, M. L. Semenova

***In Vitro* Mouse Ovarian Follicle Growth  
and Maturation in Alginate Hydrogel:  
Current State of the Art.....48**

## RESEARCH ARTICLES

D. K. Nilov, E. A. Prokhorova, V. K. Švedas

**Search for Human Lactate  
Dehydrogenase A Inhibitors  
Using Structure-Based Modeling.....57**

J. A. Filippova, G. A. Stepanov,  
D. V. Semenov, O. A. Koval, E. V. Kuligina,  
I. V. Rabinov, V. A. Richter  
**Modified Method of rRNA Structure  
Analysis Reveals Novel Characteristics  
of Box C/D RNA Analogues .....64**

A. V. Stepanov, A. A. Belogurov Jr.,  
P. Kothapalli, O. G. Shamborant, V. D. Knorre,  
G. B. Telegin, A. A. Ovsepyan,  
N. A. Ponomarenko, S. M. Deyev, S. V. Kaveri,  
A. G. Gabibov  
**Specific Depletion of Myelin-Reactive  
B Cells via BCR-Targeting .....74**

I. E. Deyev, N. V. Popova, A. G. Petrenko  
**Determination of Alkali-Sensing Parts  
of the Insulin Receptor-Related Receptor  
Using the Bioinformatic Approach .....80**

K. A. Rubina, V. A. Smutova, M. L. Semenova,  
A. A. Poliakov, S. Gerety, D. Wilkinson,  
E. I. Surkova, E. V. Semina, V. Yu. Sysoeva,  
V. A. Tkachuk  
**Detection of T-Cadherin Expression  
in Mouse Embryos .....87**

E. I. Nagaeva, N. N. Potapieva, D. B. Tikhonov  
**The Effect of Hydrophobic Monoamines on  
Acid-Sensing Ion Channels ASIC1B .....95**

E. Yu. Trizna, E. N. Khakimullina,  
L. Z. Latypova, A. R. Kurbangaliev,  
I. S. Sharafutdinov, V. G. Evtyugin,  
E. V. Babynin, M. I. Bogachev, A. R. Kayumov  
**Thio Derivatives of 2(5H)-Furanone  
as Inhibitors against *Bacillus subtilis*  
Biofilms .....102**

E. V. Dubrovin, G. V. Presnova,  
M. Yu. Rubtsova, A. M. Egorov,  
V. G. Grigorenko, I. V. Yaminsky  
**The Use of Atomic Force Microscopy  
for 3D Analysis of Nucleic Acid  
Hybridization on Microarrays .....108**

O. E. Bryzgunova, S. N. Tamkovich,  
A. V. Cherepanova, S. V. Yarmoshchuk,  
V. I. Permyakova, O. Y. Anykeeva,  
P. P. Laktionov  
**Redistribution of Free- and Cell-Surface-Bound  
DNA in Blood of Benign and Malignant  
Prostate Tumor Patients ..... 115**

**Guidelines for Authors .....119**

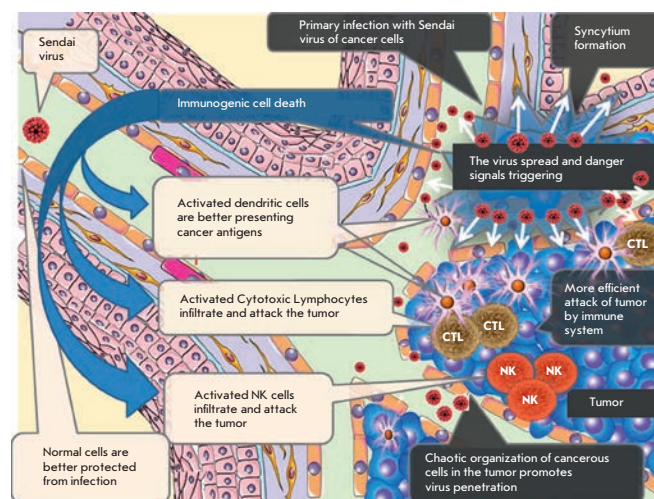


**IMAGE ON THE COVER PAGE**  
See the article by Matveeva *et al.*

# Mechanisms of Oncolysis by Paramyxovirus Sendai

O. V. Matveeva<sup>1\*</sup>, G. V. Kochneva<sup>2</sup>, S. V. Netesov<sup>3</sup>, S. B. Onikienko<sup>4</sup>, P. M. Chumakov<sup>5</sup>

<sup>1</sup>Biopolymer Design, 23 Nylander Way, Acton, Massachusetts, United States

<sup>2</sup>Center of Virology and Biotechnology "Vector", Koltsovo, Novosibirsk Region, Russia

<sup>3</sup>Novosibirsk State University, Novosibirsk, Russia

<sup>4</sup>Department of Military Field Therapy, Kirov Military Medical Academy, St. Petersburg, Russia

<sup>5</sup>Engelhardt Institute of Molecular Biology, Moscow, Russia

\*E-mail: olga.matveeva@gmail.com

Received 22.10.2014

Revised manuscript received 09.02.2015

Copyright © 2015 Park-media, Ltd. This is an open access article distributed under the Creative Commons Attribution License, which permits unrestricted use, distribution, and reproduction in any medium, provided the original work is properly cited.

**ABSTRACT** Some viral strains of the Paramyxoviridae family may be used as anti-tumor agents. Oncolytic paramyxoviruses include attenuated strains of the measles virus, Newcastle disease virus, and Sendai virus. These viral strains, and the Sendai virus in particular, can preferentially induce the death of malignant, rather than normal, cells. The death of cancer cells results from both direct killing by the virus and through virus-induced activation of anticancer immunity. Sialic-acid-containing glycoproteins that are overexpressed in cancer cells serve as receptors for some oncolytic paramyxoviruses and ensure preferential interaction of paramyxoviruses with malignant cells. Frequent genetic defects in interferon and apoptotic response systems that are common to cancer cells ensure better susceptibility of malignant cells to viruses. The Sendai virus as a Paramyxovirus is capable of inducing the formation of syncytia, multinuclear cell structures which promote viral infection spread within a tumor without virus exposure to host neutralizing antibodies. As a result, the Sendai virus can cause mass killing of malignant cells and tumor destruction. Oncolytic paramyxoviruses can also promote the immune-mediated elimination of malignant cells. In particular, they are powerful inducers of interferon and other cytokines promoting antitumor activity of various cell components of the immune response, such as dendritic and natural killer cells, as well as cytotoxic T lymphocytes. Taken together these mechanisms explain the impressive oncolytic activity of paramyxoviruses that hold promise as future, efficient anticancer therapeutics.

**KEYWORDS** attenuated measles virus strains, Newcastle disease virus, Sendai virus, oncolytic paramyxoviruses, viral anti-tumor mechanism, viral anticancer immune stimulation, cancer therapy.

**ABBREVIATIONS** NDV – Newcastle Disease Virus, MHC – Major Histocompatibility Complex, HN – Hemagglutinin Neuraminidase, DC – Dendritic Cells, IFN – Interferon, HPBL – Human Peripheral Blood Leucocytes, NA – Neuraminidase (sialidase), NK – Natural Killer, CTL – Cytotoxic T-Cells, UV – Ultraviolet light.

## INTRODUCTION

The existing approaches to the treatment of metastatic cancer are often ineffective. Therefore, new antitumor agents and new methods for the destruction of tumor cells are required. The idea of using viruses to treat malignant diseases is not a novel one. It dates back to the beginning of the XX century, when spontaneous regression of tumors was first reported in some patients after viral infection or vaccination with a live virus. The first reviews discussing this issue were published in the 1950s [1–3]. Viruses capable of specific destruction of malignant cells without affecting normal cells were later referred to as oncolytic. Specific destruction of cancer cells is caused by selective replication of

a virus in these cells and virus-induced activation of anticancer immunity.

Various viruses with both DNA and RNA genomes possess oncolytic activity. The genomic DNA of such viruses may be single-stranded, e.g. in parvoviruses [4], or double stranded, e.g. in oncolytic adenoviruses [5] and poxviruses [6]. The genomic RNA of oncolytic viruses can also have different forms: positive sense single-stranded RNA (enteroviruses [7]), double stranded RNA (reoviruses [8]), or negative sense single-stranded RNA (paramyxoviruses and rhabdoviruses in [9]).

Some members of the Paramyxoviridae family, including a number of attenuated vaccine strains of the measles virus [10], various animal viruses that are

non-pathogenic for humans, such as Newcastle disease virus [11–13] and Sendai virus (to which this review is dedicated), have been studied as potential anticancer agents.

## ANTITUMOR ACTIVITY OF THE SENDAI VIRUS

### Studies of the Sendai virus and its oncolytic properties

The oncolytic properties of the Sendai virus, which is also known as a murine parainfluenza virus type 1 or the hemagglutinating virus of Japan, have been studied particularly within the last 10 years. This paramyxovirus belongs to genus *Respirovirus* of the Paramyxoviridae family. *Figure 1* shows a phylogenetic tree of the family Paramyxoviridae (A), the structure of the Sendai virus virion (B), and the structure of its genome (C). The Sendai virus genome is a negative sense single-stranded RNA, which is 15.3 kb long and contains six protein-encoding genes. Two of these genes encode the surface glycoproteins HN and F; three encode the nucleocapsid proteins NP, P, and L; and the last one encodes the non-glycosylated internal matrix protein M. A distinctive feature of paramyxoviruses is the presence of an F protein, which promotes membrane fusion at neutral pH. The F protein is synthesized as an inactive precursor protein, the F0 protein, which is subsequently cleaved by cellular proteases into two subunits, F1 and F2, which remain linked to each other via disulfide bridges [14].

In nature, the arginine-specific serine protease “Clara” is most likely responsible for the maturation of the virus [15–17]. The ability to process the F0 protein defines the tissue tropism of paramyxoviruses [18]. Only inactive precursor virus particles can form in the absence of proteolytic activation of F0 [19]. When the Sendai virus is grown for research purposes in cells which do not produce the protease required for the activation, this enzyme (e.g., trypsin) must be added to the extracellular environment.

The Sendai virus causes easily transmitted respiratory tract infections in mice, hamsters, guinea pigs, rats, and sometimes in pigs [20]. The Sendai virus can spread both through the air and through direct contact. It can be found in mice colonies around the world but is believed to be completely safe for humans [20]. In the USA, the Sendai virus is approved for clinical trials aimed at immunization against diseases caused by the parainfluenza type 1 virus in children. This research is based on the assumption that the Sendai virus and parainfluenza virus 1 induce production of cross-reactive antibodies. It was found that intranasal administration of the Sendai virus is well tolerated and it induces the production of antibodies that can neutralize

parainfluenza virus 1 [21]. This study is important as proof of the Sendai virus’ safety for humans.

A number of studies conducted in Japan demonstrated that the attenuated virus, genetically modified to be non-pathogenic for rodents, can spread rapidly in tumor cells and destroy them without affecting the surrounding normal cells. This property often leads to tumor growth suppression in mice. The list of tested xenotransplanted human tumor models includes fibrosarcoma cells, pancreas epithelioid carcinoma, and colon cancer [22]. The use of a recombinant Sendai virus has resulted in significant suppression of tumor growth in mouse models and even in complete eradication of mature brain tumors [23]. Similar results were obtained for xenotransplantation of human sarcoma and prostate cancer cells into mice [24, 25]. The recombinant Sendai virus has been shown to be highly efficient in destroying melanoma, hepatocellular carcinoma, neuroblastoma, squamous cell carcinoma, and human prostate cancer in rat xenograft models [26]. It has been demonstrated that even after inactivation by ultraviolet light (UV), Sendai virus preparations are effective against colon [27, 28], bladder [29], and kidney [30] cancer in syngeneic mice. The efficiency of UV-inactivated Sendai virus has also been demonstrated for murine xenografts of human prostate cancer [31]. In all these studies, Sendai virus therapy led to complete tumor regression or major suppression of its growth.

In 1964, a short-term remission following intravenous administration of live Sendai virus was reported in the United States in a patient with acute leukemia [32].

### Studies of the oncolytic properties of the Sendai virus in Russia

In the mid-1950s, Academician of the Academy of Medical Sciences V.M. Zhdanov obtained a Sendai virus strain from Japan; the strain was later used for research purposes as a model pathogen at the D.I. Ivanovskii Institute of Virology. At the end of the 1960s, the strain was transferred from the lab of V.M. Zhdanov to V.M. Senin (RCRC RAMS) and underwent about 30 passages in chicken embryos. The fact that the Sendai virus is non-pathogenic for humans makes it a promising therapeutic agent against malignant diseases. In the early and mid-1990s, V.M. Senin and his colleagues tested the strain of Sendai virus on volunteers, patients in Moscow and St. Petersburg hospitals, with various malignant grade III and IV diseases. Although in some patients improvement was transient or not observed at all, other patients achieved long-term remissions, even in the cases where tumors had been previously considered inoperable and the virus was used as a monotherapy. In these cases, resorption of primary tumors

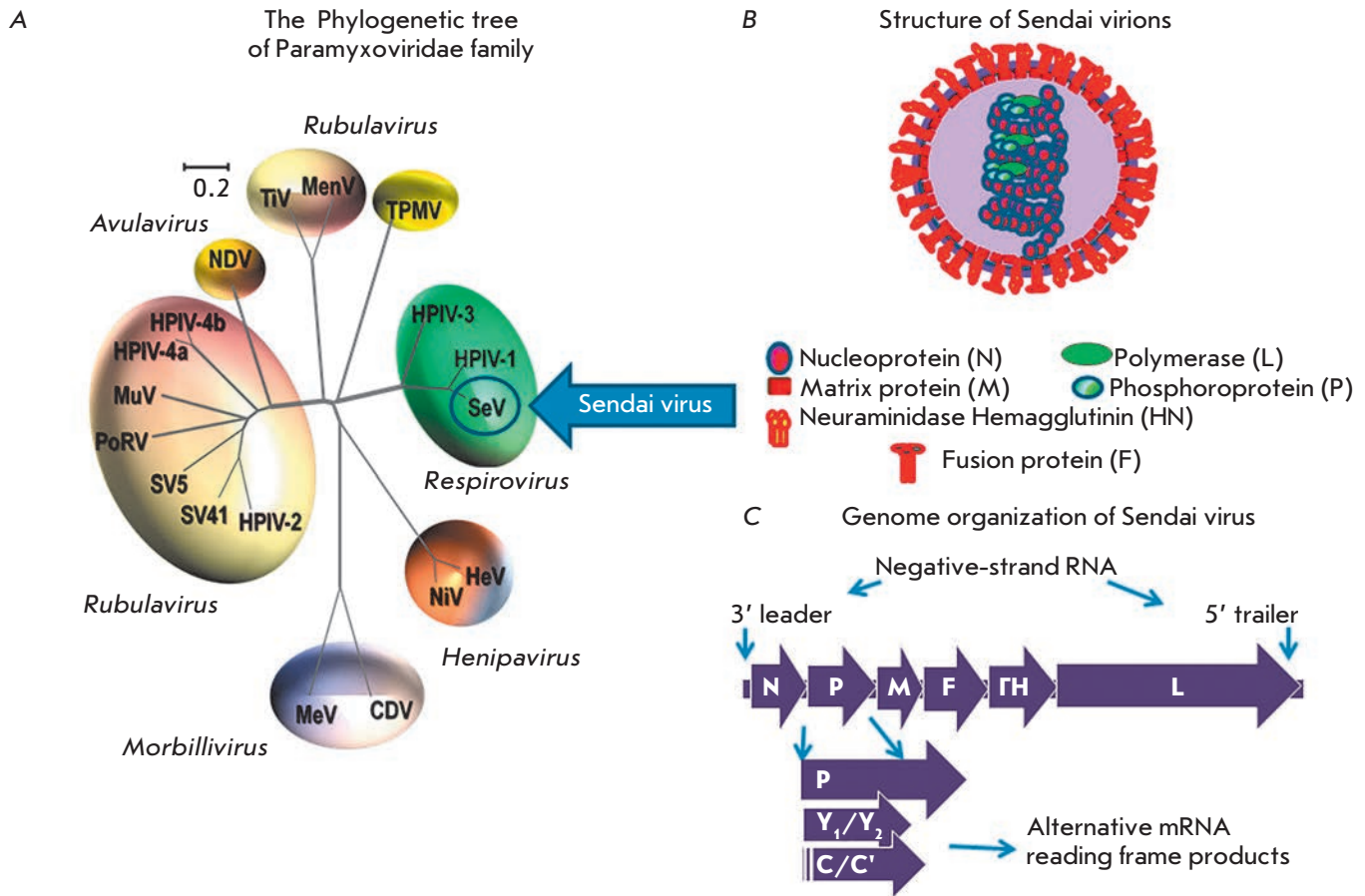


**Fig. 1.** Paramyxoviridae phylogenetic tree along with a virion composition and genomic organization scheme of the Sendai virus. A) The phylogenetic tree based on the alignment of the amino-acid sequences of the HN genes of selected *Paramyxoviridae* subfamily members. The family members with proven oncolytic properties are circled. The tree was generated by Clustal W multiple alignments using the Neighbor-Joining method. Viruses are grouped according to genus and abbreviated as follows. *Morbillivirus* genus: MV (measles virus), CDV (canine distemper virus); *Henipavirus* genus: HeV (Hendra virus), NiV (Nipah virus); *Respirovirus* genus: SeV (Sendai virus), hPIV3 (human parainfluenza virus 3); *Avulavirus* genus: NDV (Newcastle Disease Virus); *Rubulavirus* genus: hPIV2 (human parainfluenza virus 2), hPIV-4a (human parainfluenza virus 4a), hPIV-4b (human parainfluenza virus 4b), MuV (mumps virus), PoRV (porcine rubulavirus), SV5 (simian parainfluenza virus 5), SV41 (simian parainfluenza virus 41); TiV (tioman virus); MenV (menangle virus); Unclassified: TPMV (Tupaia paramyxovirus), B) Structure and composition of virion, C) Genomic organization of the Sendai virus

and metastases was observed and all objective and subjective signs of cancer disappeared. In some cases, after one or two courses of Sendai virus therapy no signs of the disease were discovered even within 5–10 years or more. Brief histories of these patients are presented in the text of the patent [33, 34]. The only reported side effect was short-term fever within 24 hours of virus administration.

The Sendai virus strain used in these tests was deposited in the American Type Culture Collection (ATCC) as PTA-13024 and PTA-121432. PTA-13024 contains the virus in frozen allantoic fluid, and PTA-121432 contains the virus in lyophilized form. The pri-

mary nucleotide sequence of the virus strain has been deposited in the database GenBank as KP717417.1.

### MECHANISMS OF ONCOLYSIS BY PARAMYXOVIRUSES

#### Direct killing of malignant cells

*Higher affinity of paramyxoviruses for malignant rather than normal cells.* Sialic acid polymers are cellular receptors for some paramyxoviruses [35, 36]. Since a virus binds to its receptor with high affinity, a large number of sialic acid residues on the surface of tumor cells contribute to preferential binding of a virus to malignant,



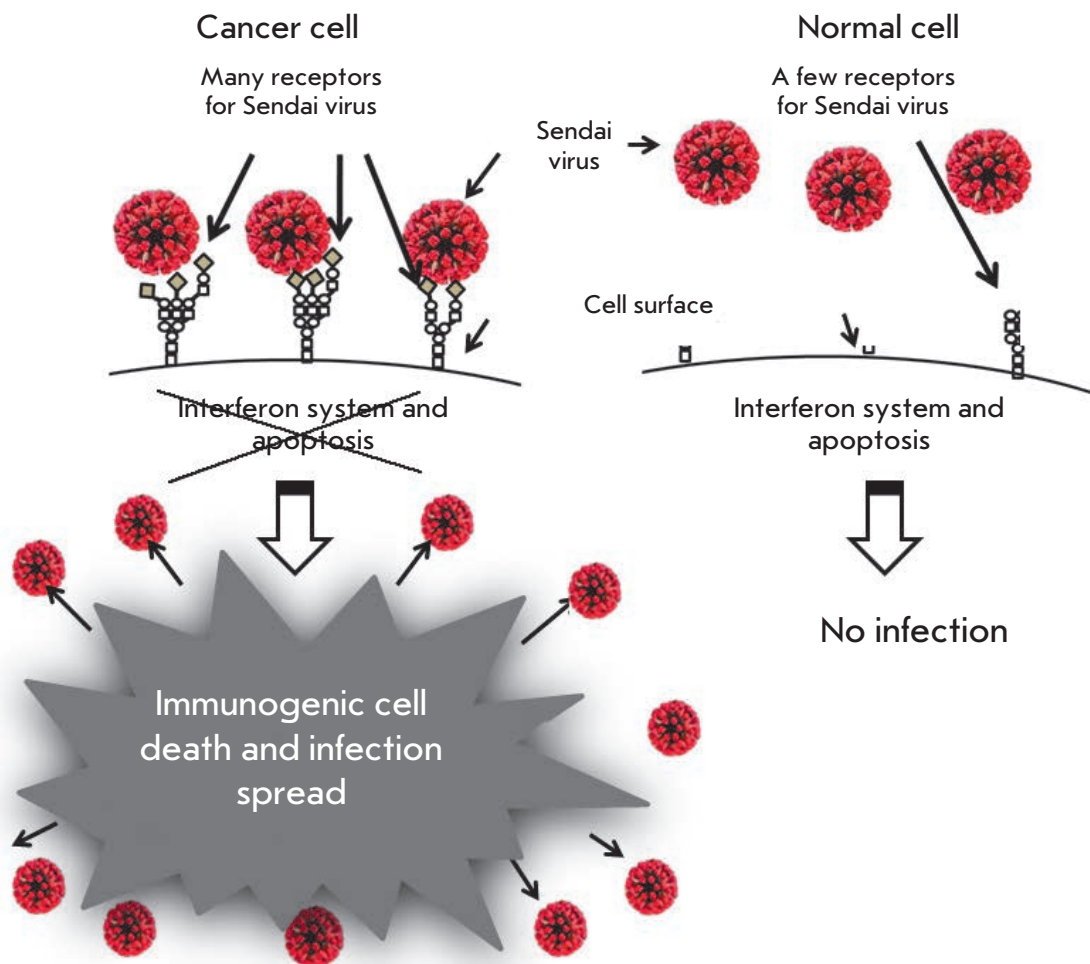


**Fig. 2.** Sendai virus infection and spread in malignant but not in normal cells. First level of virus specificity for cancer cells is related to overexpression of specific receptors for paramyxoviruses. Sialic acids residues in the form of sialoglycoproteins serve as receptors for the Sendai virus. These sialoglycoproteins are frequently overexpressed in malignant cells. Another level of oncoselectivity is related to frequent genetic defects of cancer cells that help viral replication. During the malignant progression cancer cells accumulate many genetic changes. Along with mutations that promote accelerated proliferation and invasion, many cancerous cells lose the abilities to produce interferon and to respond to interferon by induction of the antiviral state. Such abnormalities make these cells highly susceptible to viral infection. Therefore, because cancer cells are overexpressing surface receptors and are commonly defective in antiviral immunity the Sendai virus could easily replicate in malignant cells, but not in normal cells

rather than normal cells, which, in turn, leads to a higher concentration of the virus in tumors and metastases compared to normal tissues. *Figure 2* shows such preferential binding of the Sendai virus to cancer cells.

It has been shown that the viability of human prostate cancer cells, PC3 and DU145, is significantly reduced by a UV-inactivated Sendai virus. Apoptosis has been observed in PC3 cells within 24 hours of treatment with the Sendai virus, with no inhibition of normal prostate epithelium growth [31]. According to the authors, the results of this research confirm that the susceptibility of prostate cancer cells to the Sendai virus can be attributed mostly to a large number of

sialylated viral receptors on the surface of the cells and, therefore, to their greater affinity for the virus.

There is also an alternate route for Sendai virus infection of cells which does not involve sialic acid [37]. In this case, the F protein binds to the hepatocyte-specific asialoglycoprotein receptor, ASGR. However, the exact mechanism of this route, as well as its possible role in the oncolytic potential of the virus, requires further investigation.

*Disruption of interferon and apoptosis cell systems.* It is well known that mutations and other genetic alterations accumulate in tumor cells during the progression of the

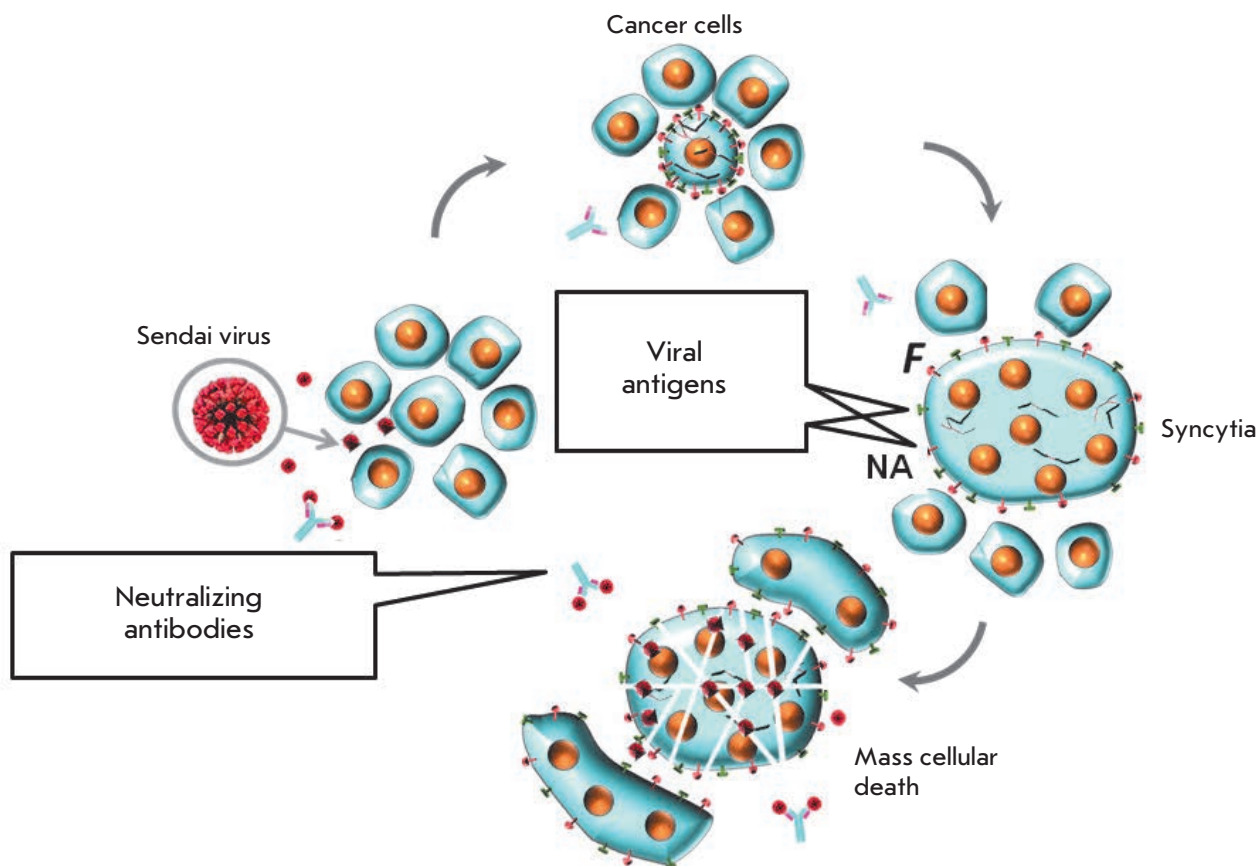


**Fig. 3.** Sendai virus infection may spread through syncytium formation to achieve an accelerated elimination of cancer cells. In natural hosts virus infected cells start expressing the viral fusion protein (F) on the cell surface that forces fusion of infected and surrounding non-infected cells into large polykaryonic structures known as syncytia. The syncytia support viral replication through continuous fusion with neighboring cells, even in the presence of high titers of neutralizing antibodies. Eventually, the syncytia die, which assists in viral oncolysis. The fusion protein of the Sendai virus is synthesized as an inactive precursor ( $F_0$ ), and proteolytic cleavage is needed to convert it to active  $F_1$  that can promote syncytia formation. A tumor-resident host protease is needed for the efficient formation of syncytia

disease, contributing to the disruption in the interferon response system [38, 39]. Moreover, the progression of malignancy unbalances the system responsible for apoptosis [39, 40]. As a result, tumor cells lose their ability to induce the synthesis of interferon, to acquire resistance to viral infections, and to respond to the interferon antiproliferative action. They also lose their ability to progress to apoptosis, despite the signal received. These changes result in tumor progression and growth.

Viruses can replicate by exploiting the same disruptions that promote tumor growth, leading to a larger scale of death among malignant cells compared to normal ones. *Figure 2* illustrates the differences between malignant and normal cells, which make the infection of cancer cells more likely, more efficient, and results in immunogenic death of malignant cells and further spread of the virus within the tumor.

**Formation of malignant cells syncytium.** Some members of paramyxoviruses have developed a mechanism for spreading the infection which involves the fusion of infected and uninfected cells. Such fusion leads to the formation of a syncytium, a large multinucleus structure. Infected cells can fuse with 50–100 neighboring cells to form a syncytium [41]. Infection of new host cells via fusion makes possible the spread of a viral infection without the release of virus particles from the cells. Therefore, the ability to form syncytium represents one of the strategies used by the virus to avoid host-neutralizing antibodies, which otherwise would inactivate it. *Figure 3* illustrates Sendai-virus-induced syncytium formation. Syncytium typically survives *in vivo* for 4–5 days only and dies afterwards.

It has been suggested that the ability of certain viruses to induce syncytium formation is related to their

oncolytic potential. This hypothesis is supported by the fact that it is possible to transfer genes that encode the fusion proteins required for syncytium formation from one type of virus to another. It has been shown that such transfer imparts oncolytic potential to viruses that had not possessed it previously [42, 43]. This potential can be further enhanced by amino acid substitutions, resulting in increased production of proteins capable of cell fusion induction [44, 45]. Even plasmids that encode membrane glycoproteins with a similar function can cause significant tumor regression [46–48].

### **Destruction of malignant cells mediated by specific anti-tumor immunity**

*Paramyxoviruses neuraminidase (NA) removes sialic acid from the surface of malignant cells.* It is known that an increased level of sialylation of cell membranes is associated with progression of the malignancy and invasive and metastatic potential of cells [49–54]. It has been demonstrated that certain sialylation inhibitors can reduce the malignancy of cancer cells [55–57].

One of the possible mechanisms linking the increased sialylation with a malignant phenotype is the creation of a thick “coat” on the cell surface that may mask cancer antigens and protect malignant cells from immunosurveillance. Desialylation of tumor cells reduces their growth potential, making them available to natural killer cells (NK). Moreover, sialidase-treated tumor cells better activated NK cells for IFN- $\gamma$  secretion. It has been shown that the activity and cytotoxicity of NK cells depend on the expression of tumor cell surface-specific sialic acids [58].

Hemagglutinin-neuraminidase (HN) is a protein that can induce hemagglutination and possesses enzymatic activity. Neuraminidase (NA), a subunit of the HN molecule, is an enzyme (sialidase) which cleaves sialic acid from the surface of a cell [35, 36]. NA is encoded and synthesized by certain members of oncolytic paramyxoviruses, including the Newcastle disease virus, Sendai virus, and mumps virus. NA recognizes sialic acid polymers as cell surface receptors [36]. NA also promotes cell fusion, which helps the forming virions to spread within the tissue, avoiding interaction with host antibodies.

Removal of sialic acid residues can lead to a significant change in the ability of B lymphoma cells to stimulate cytolytic T lymphocytes. In an experiment with three different types of sialidases, one of which was Newcastle disease virus NA [59], it was found that this enzyme can cleave 2,3-, 2,6- [60], and 2,8-linkages between sialic acid residues [61]. It has also been shown that there are no significant differences in *in vitro* specificity for the cleaved substrate between the New-

castle disease virus, Sendai virus, and the mumps virus [62]. These observations suggest that once a tumor is treated with the virus, malignant cells become desialylated and this fact contributes to enhanced anti-tumor immunosurveillance. *Figure 4* illustrates a hypothetical process of sialic acid removal from the surface of malignant cells by Sendai virus sialidase, revealing tumor antigens, which subsequently become available for recognition by cytotoxic lymphocytes.

*Stimulation of interferons (IFN) type I and II production.* The Sendai virus acts as a powerful stimulant of interferon  $\alpha$  (IFN- $\alpha$ ) production in human peripheral blood leukocytes (HPBL) [63]. The virus induces secretion of at least nine different types of IFN- $\alpha$ : 1a, 2b, 4b, 7a, 8b, 10a, 14c, 17b, and 21b. The main one among them is IFN- $\alpha$ 1a, which accounts for approximately 30% of the total leukocyte IFN- $\alpha$  [64]. The Sendai virus can also stimulate IFN- $\gamma$  production in HPBL [65]; therefore, it has been chosen for human leukocyte interferon production on an industrial scale [66].

A UV-inactivated Sendai virus can induce the secretion of IFN- $\alpha$  and IFN- $\beta$  in certain tumor cell lines [31]. The inactivated virus induces type I IFN secretion by murine dendritic cells. This induction does not depend on cell fusion; however, the F protein is apparently responsible for the effect [67].

It has been shown that stimulation of interferon synthesis promotes oncolytic immune surveillance in several ways. Type I interferons and IFN- $\gamma$  significantly improve the presentation of the antigens that are dependent on major histocompatibility complex type I (MHC I). IFN- $\gamma$  also substantially promotes MHC II-dependent antigen presentation. Both of these processes increase the presentation of tumor-specific antigens by malignant- and specific antigen-presenting cells, which promotes the proliferation and activity of anti-tumor cytotoxic T-cells. The interferons can also inhibit angiogenesis by neutralizing angiogenic stimuli coming from the tumor cells and inhibiting the proliferation of endothelial cells. This inhibition is correlated with the lower vascularity of the tumor and subsequent slowing of its growth (see Reviews [68–70]).

*Paramyxovirus stimulates the production of other cytokines.* It has been shown that the Sendai virus can stimulate production of IL-2 [65], macrophage inflammatory protein-1 $\alpha$  and - $\beta$ , and many other cytokines in HPBL [63]. Administration of the Sendai virus to animals demonstrated that both live and UV-inactivated viruses stimulate the secretion of interleukin-6 [27]. It has been determined that the fusion protein (F) of the Sendai virus is responsible for the stimulation of interleukin-6 secretion in dendritic cells [67]. Admin-

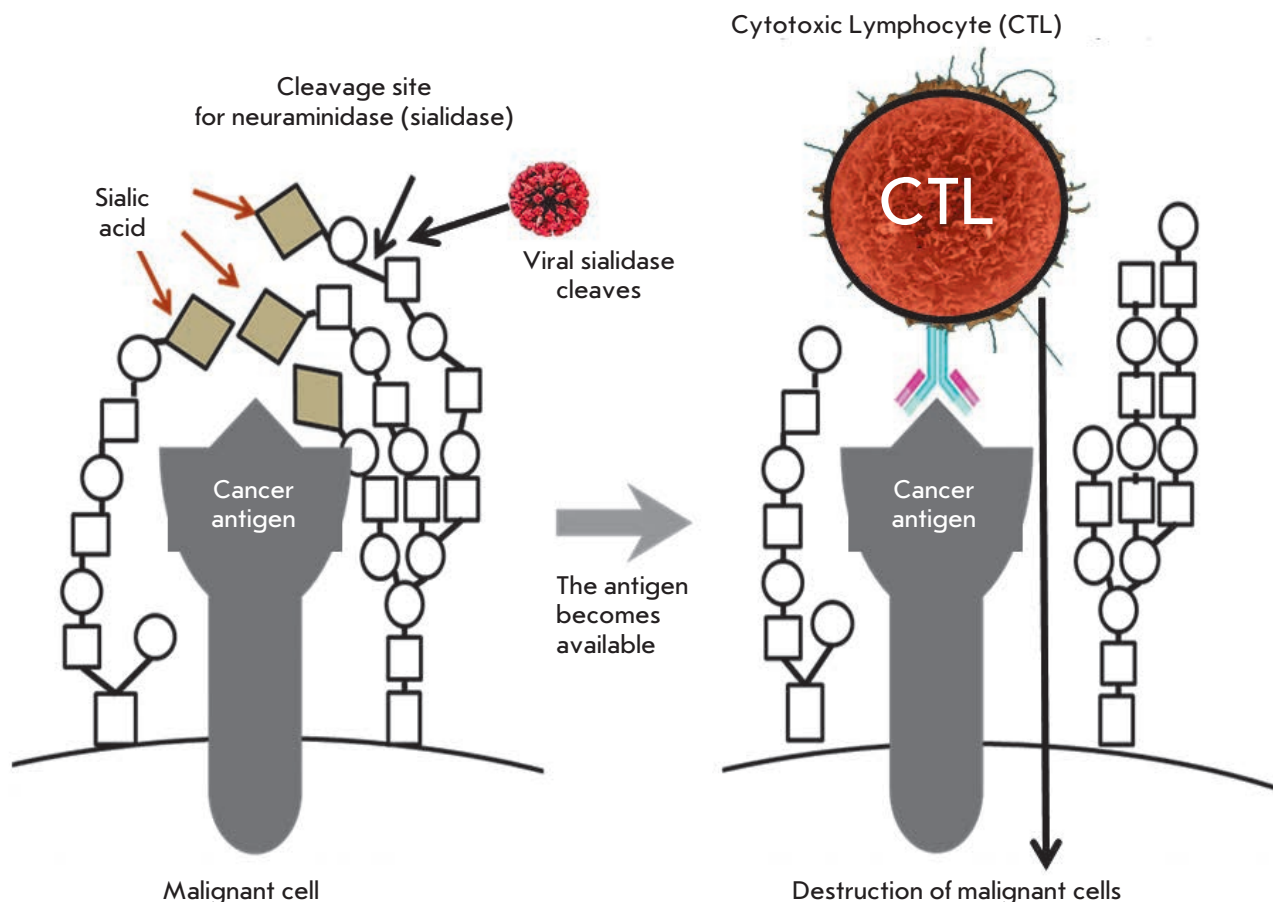


**Fig. 4.** Death of cancer cells through activation of the immune response against cancer cells triggered by the removal of sialic acid residues from the cancer cell's surface by viral sialidase. Metastatic cancer cells often overexpress sialic acid-rich cell-surface glycoproteins that render a negative charge and electrostatic repulsion between cells that facilitates cancer cells entry into the blood stream, thereby promoting metastasis. One of the possible mechanisms linking increased sialylation with a malignant phenotype is the creation of a thick "coat" on the cell surface that may mask cancer-antigens-protect malignant cells from immunosurveillance. Removing some sialic acid residues by sialidase can unmask cancer-specific antigens and make cells visible to the immune system. The removal of sialic acids from tumor cells is associated with a reduced growth potential, activation of NK cells, and secretion of IFN-gamma. The hemagglutinin-neuraminidase proteins present in the Sendai virus and some other paramyxoviruses possess neuraminidase (sialidase) activity, and, therefore, its action on the surface of cancer cells may dramatically increase the induction of the cytotoxic T-cell response

istration of a UV-inactivated Sendai virus to a patient with a kidney cancer tumor caused the expression of chemokine CXCL10 (also known as protein 10, which can induce interferon- $\gamma$ ) [30].

*Paramyxoviruses can stimulate natural killer (NK) cells.* Activated NK cells can destroy tumor cells without prior antigen stimulation. These cells are part of the important branch of the innate immune system which is activated immediately upon pathogen detection and does not involve the development of antigenic immunological memory. Several receptors, including two

proteins called natural killer proteins 46 (NKp46) and 44 (NKp44), are responsible for the activation of NK. It has been proven experimentally that only one protein of paramyxoviruses, namely HN, activates NK [71]. It is assumed that NK activation by a UV-inactivated Sendai virus [30] is caused by interaction between the HN protein and NKp46 and/or NKp44 receptors. Efficient binding of the HN protein to NKp46 and/or 44 NKp receptors results in the lysis of cells which have the HN protein or its fragments on their surface [72–74].

A study of a UV-inactivated Sendai virus showed that NK cells play an important role in the virus-me-

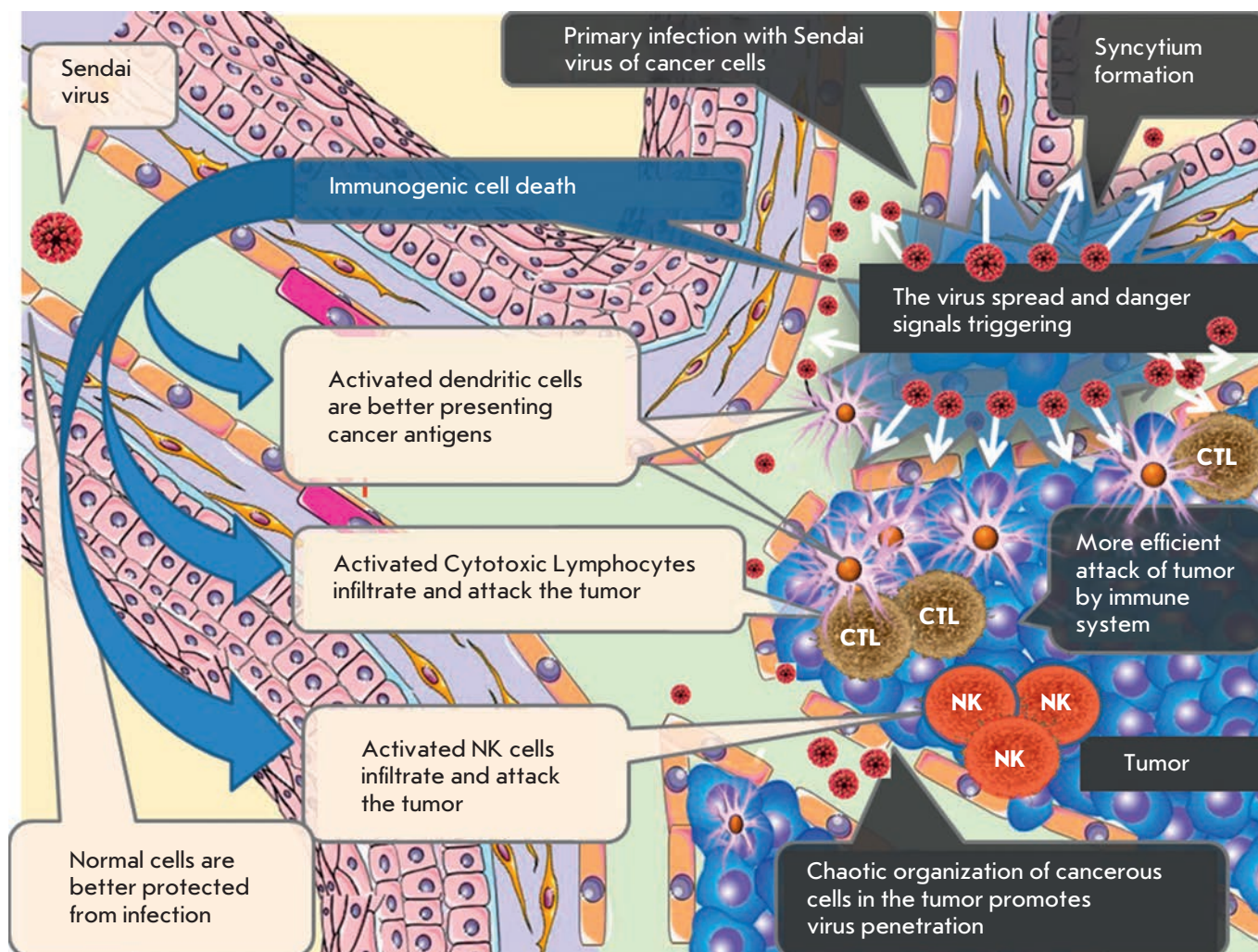


**Fig. 5.** Sendai virus induces both direct and immune-mediated death of cancer cells. Cancer cells are more accessible to viruses and susceptible to viral replication. Ordered architecture of normal tissues (blood vessels, basal membranes, tight cell-to-cell contacts etc.) protects against viral invasion from the bloodstream. Chaotic organization of a tumor, loose cell-to-cell contacts, and leakiness of immature tumor vasculature provide better access to viruses. Normal cells exposed to viruses provide antiviral protection to surrounding normal cells by secreting IFNs. Tumor cells are generally defective for IFNs induction and, therefore, support viral replication even in the presence of IFNs produced by the surrounding normal cells. The Sendai virus is capable of accelerated spread inside a tumor through the formation of syncytia. Exposure of viral antigens on the surface of infected cells induces massive immunogenic death of tumor cells. Virus-specific proteins represent danger signals triggering activation of innate and adaptive anticancer immune responses. Activated cytotoxic T lymphocytes (CTLs), natural killer (NKs), and antigen-presenting dendritic cells (DCs) migrate into the tumor and provide accelerated immune-mediated destruction of malignant cells

mediated regression of tumor growth. In a mouse model of renal cancer, the anti-tumor effect of the virus was reduced when it was co-injected with an antibody against GM1 ganglioside, which reduced the number of NK cells [30].

*Induction of anti-tumor cytotoxic activity of T lymphocytes.* It has been shown that the Newcastle disease virus (NDV) enhances tumor-specific cytotoxic

response of CD8 T-cells (CTLs) and increases the activity of T-helper CD4 cells in the absence of an antiviral T-cell response [73]. The UV-inactivated virus, which is unable to replicate, promotes the anti-tumor CTL-response as actively as intact NDV, which is capable of replication. Apparently, the effect of NDV on the CTL response is caused by the introduction of functional viral HN protein molecules into the membranes of tumor cells and stimulation of neuraminidase activity

[73] (*Fig. 4*). Since Sendai virus HN proteins are highly homologous to NDV ones, the data suggest that a HN protein, regardless of its origin (Sendai virus, NDV or other related paramyxoviruses), activates both the responses associated with cytotoxic lymphocytes and the NK cells.

**Stimulation of dendritic cells.** Dendritic cells (DCs) are specialized antigen-presenting cells that can efficiently amplify both innate and acquired immune responses against various pathogens and tumors. Detection of a virus or other pathogens initiates a specific differentiation program in DCs, which makes them capable of activating naive T-cells.

Even a UV-inactivated Sendai virus can cause intense infiltration of a tumor by dendritic cells [27], whereas *ex vivo* infection of DCs with a recombinant Sendai virus induces maturation and activation of DCs within an hour [74]. Administration of activated DCs carrying different variants of a recombinant Sendai virus significantly improves the survival of animals injected with malignant melanoma cells [75, 76], colorectal cancer [77], squamous cell carcinoma [78], hepatic cancer, neuroblastoma, and prostate cancer [26]. The use of such DCs prior to tumor cells administration has shown that DCs can prevent neuroblastoma and prostate adenocarcinoma metastasis into the lungs [79, 80]. The process of anti-tumor immunity activation by the Sendai virus is shown in *Figure 5*.

**Suppression of regulatory cells.** Animal model experiments have shown that the Sendai virus is able to suppress T-cell-mediated regulatory immunosuppression by secretion of interleukin-6 by mature DCs even after UV inactivation [27].

#### PROSPECTS FOR FURTHER RESEARCH

Clinical trials of the Sendai virus are undoubtedly of interest. Currently, Japan is conducting phase I trials on the efficiency of a UV-irradiated virus in melanoma patients [81]. Its goal is to improve the systemic delivery of the inactivated virus to the tumor and metastases by pre-binding it to blood platelets. This approach has been tested on animals. It was found that binding to platelets significantly improves delivery of the virus and causes tumor growth suppression in murine melanoma models [82].

A study of a gene-engineered Sendai virus which can be activated by an altered spectrum of proteases is being conducted in Germany [83]. Animal experiments have shown that this virus can be easier to activate in malignant cells.

Another promising approach is the study of other oncolytic viruses whose co-administration with the Sendai virus could have a positive synergistic therapeutic effect.

#### CONCLUSION

Several mechanisms explaining the oncolytic action of paramyxoviruses and, in particular, the Sendai virus have been established so far. The extent of the oncolysis and the specific mechanism of action may depend on several factors. Paramyxoviruses can directly kill cancer cells by multiplying within them and causing syncytium formation. The cells, which are fused into a syncytium, can no longer divide and are doomed to collective, synchronous death. Furthermore, paramyxoviruses induce immune-mediated killing of malignant cells via strong activation of anti-tumor NK cells, as well as via enhanced anti-tumor activity of cytotoxic T-cells, stimulation of antigen presenting dendritic cells, and immunosuppressive activity of suppressing T-cells. The neuraminidases of paramyxoviruses capsids can cleave sialic acids from the surface of malignant cells, unmasking tumor antigens present on the cell membrane. This renders cancer cells more visible to the immune system. Furthermore, viral neuraminidases can ensure strong specific affinity of the virus for sialic acid polymers, which are over-represented on cancerous cells' membranes. This increases the specificity of the virus in respect to primary tumor cells and metastases, but not normal cells. These mechanisms may substantiate antitumor activity of the Sendai virus detected in animals and humans. Therefore, there an objective rationale for further development of anticancer drugs based on paramyxoviruses and, in particular, on the Sendai virus. ●

*This work was supported by a grant from the Ministry of Education and Science (RFMEFI60714X0014) and RNF (grant № 14-15-01073). The authors are grateful to S.A. Shabalina (National Institutes of Health, USA) for the construction of the phylogenetic tree of paramyxoviruses shown in Figure 1*

#### REFERENCES

1. Svejda J. // *Lek. List.* 1950. V. 5. P. 688–689.
2. Arnesen K. // *Tidsskr Nor Laegeforen.* 1951. V. 71. P. 232–235.
3. Higgins G.K., Pack G.T. // *Bull. Hosp. Joint Dis.* 1951. V. 12. P. 379–382.
4. Loktev V.B., Ivan'kina T., Netesov S.V., Chumakov P.M. // *Vestn Ross Akad Med Nauk.* 2012. P. 42–47.
5. Sviatchenko V.A., Tarasova M.V., Netesov S.V., Chumakov P.M. // *Mol Biol (Mosk).* 2012. V. 46. P. 556–569.
6. Kochneva G.V., Sivolobova G.F., Yudina K.V., Babkin I.V., Chumakov P.M., Netesov S.V. // *Molecular Genetics, Micro-*

## REVIEWS

- biology and Virology. 2012. V. 27. P. 8-15.
7. Chumakov P.M., Morozova V.V., Babkin I.V., Baykov I.K., Netesov S.V., Tikunova N.V. // *Molecular Biology*. 2012. V. 46. P. 712-725.
  8. Kim M., Chung Y.H., Johnston R.N. // *J. Microbiol. (Seoul, Korea)*. 2007. V. 45. P. 187-192.
  9. Lech P.J., Russell S.J. // *Expert Rev. Vaccines*. 2010. V. 9. P. 1275-1302.
  10. Russell S.J., Peng K.W. // *Curr. Top. Microbiol. Immunol.* 2009. V. 330. P. 213-241.
  11. Schirmmacher V., Fournier P. // *Methods Mol. Biol.* 2009. V. 542. P. 565-605.
  12. Keshelava V.V. et al. // *Vopr Onkol*. 2009. V. 55. P. 433-435.
  13. Fournier P., Schirmmacher V. // *Biology*. 2013. V. 2. P. 936-975.
  14. Iwata S., Schmidt A.C., Titani K., Suzuki M., Kido H., Gotoh B., Hamaguchi M., Nagai Y. // *J. Virol.* 1994. V. 68. P. 3200-3206.
  15. Tashiro M., Yokogoshi Y., Tobita K., Seto J.T., Rott R., Kido H. // *J. Virol.* 1992. V. 66. P. 7211-7216.
  16. Sakai K., Kohri T., Tashiro M., Kishino Y., Kido H. // *Europ. Resp. J.* 1994. V. 7. P. 686-692.
  17. Sakai K., Kawaguchi Y., Kishino Y., Kido H. // *J. Histochem. Cytochem. Official J. Histochem. Soc.* 1993. V. 41. P. 89-93.
  18. Nagai Y. // *Microbiol. Immunol.* 1995. V. 39. P. 1-9.
  19. Scheid A., Choppin P.W. // *Virology*. 1974. V. 57. P. 475-490.
  20. Infectious diseases of mice and rats. Washington, DC: Nat. Acad. Press, 1991.
  21. Slobod K.S., Shenep J.L., Lujan-Zilbermann J., Allison K., Brown B., Scroggs R.A., Portner A., Coleclough C., Hurwitz J.L. // *Vaccine*. 2004. V. 22. P. 3182-3186.
  22. Kinoh H., Inoue M., Washizawa K., Yamamoto T., Fujikawa S., Tokusumi Y., Iida A., Nagai Y., Hasegawa M. // *Gene Ther.* 2004. V. 11. P. 1137-1145.
  23. Iwadata Y., Inoue M., Saegusa T., Tokusumi Y., Kinoh H., Hasegawa M., Tagawa M., Yamaura A., Shimada H. // *Clin. Cancer Res.* 2005. V. 11. P. 3821-3827.
  24. Kinoh H., Inoue M. // *Front. Biosci.* 2008. V. 13. P. 2327-2334.
  25. Tatsuta K., Tanaka S., Tajiri T., Shibata S., Komaru A., Ueda Y., Inoue M., Hasegawa M., Suita S., Sueishi K., Taguchi T., Yonemitsu Y. // *Gene Ther.* 2009. V. 16. P. 240-251.
  26. Yonemitsu Y., Ueda Y., Kinoh H., Hasegawa M. // *Front. Biosci.* 2008. V. 13. P. 1892-1898.
  27. Kurooka M., Kaneda Y. // *Cancer Res.* 2007. V. 67. P. 227-236.
  28. Kawano H., Komaba S., Kanamori T., Kaneda Y. // *BMC Med.* 2007. V. 5. P. 28.
  29. Kawano H., Komaba S., Yamasaki T., Maeda M., Kimura Y., Maeda A., Kaneda Y. // *Cancer Chemother. Pharmacol.* 2008. V. 61. P. 973-978.
  30. Fujihara A., Kurooka M., Miki T., Kaneda Y. // *Cancer Immunol. Immunotherapy: CII*. 2008. V. 57. P. 73-84.
  31. Kawaguchi Y., Miyamoto Y., Inoue T., Kaneda Y. // *Int. J. Cancer*. 2009. V. 124. P. 2478-2487.
  32. Wheelock E.F., Dingle J.H. // *N. Engl. J. Med.* 1964. V. 271. P. 645-651.
  33. Senin V., Senina A., Matveeva O. // *Russian issued Patent № 2519763*. 2014.
  34. Senin V., Senina A., Matveeva O. // *Patent application PCT/RU2013/001043, WO2014081346 A3*. 2014.
  35. Lamb R.A., Parks G.D. // *Fields Virology / Eds Knipe D.M., Howley P.M. Lippincott. Philadelphia: Williams & Wilkins, 2007. P. 1449-1496.*
  36. Bossart K.N., Fusco D.L., Broder C.C. // *Adv. Exp. Med. Biol.* 2013. V. 790. P. 95-127.
  37. Bitzer M., Lauer U., Baumann C., Spiegel M., Gregor M., Neubert W.J. // *J. Virol.* 1997. V. 71. P. 5481-5486.
  38. Chawla-Sarkar M., Lindner D.J., Liu Y.F., Williams B.R., Sen G.C., Silverman R.H., Borden E.C. // *Apoptosis: Internat. J. Programmed Cell Death*. 2003. V. 8. P. 237-249.
  39. Kotredes K.P., Gamero A.M. // *J. Interferon Cytokine Res.* 2013. V. 33. P. 162-170.
  40. Igney F.H., Krammer P.H. // *Nat. Rev. Cancer*. 2002. V. 2. P. 277-288.
  41. Rawling J., Cano O., Garcin D., Kolakofsky D., Melero J.A. // *J. Virol.* 2011. V. 85. P. 2771-2780.
  42. Ebert O., Shinozaki K., Kournioti C., Park M.S., Garcia-Sastre A., Woo S.L. // *Cancer Res.* 2004. V. 64. P. 3265-3270.
  43. Nakamori M., Fu X., Meng F., Jin A., Tao L., Bast R.C., Jr., Zhang X. // *Clin. Cancer Res.* 2003. V. 9. P. 2727-2733.
  44. Gainey M.D., Manuse M.J., Parks G.D. // *J. Virol.* 2008. V. 82. P. 9369-9380.
  45. Altomonte J., Marozin S., Schmid R.M., Ebert O. // *Mol. Ther.* 2010. V. 18. P. 275-284.
  46. Bateman A., Bullough F., Murphy S., Emiliusen L., Lavillette D., Cosset F.L., Cattaneo R., Russell S.J., Vile R.G. // *Cancer Res.* 2000. V. 60. P. 1492-1497.
  47. Galanis E., Bateman A., Johnson K., Diaz R.M., James C.D., Vile R., Russell S.J. // *Hum. Gene Ther.* 2001. V. 12. P. 811-821.
  48. Lin E.H., Salon C., Brambilla E., Lavillette D., Szecsi J., Cosset F.L., Coll J.L. // *Cancer Gene Ther.* 2010. V. 17. P. 256-265.
  49. Pearlstein E., Salk P.L., Yogeewaran G., Karparkin S. // *Proc. Natl. Acad. Sci. USA*. 1980. V. 77. P. 4336-4339.
  50. Yogeewaran G., Salk P.L. // *Science*. 1981. V. 212. P. 1514-1516.
  51. Benedetto A., Elia G., Sala A., Belardelli F. // *Int. J. Cancer*. 1989. V. 43. P. 126-133.
  52. Collard J.G., Schijven J.F., Bikker A., La Riviere G., Bolscher J.G., Roos E. // *Cancer Res.* 1986. V. 46. P. 3521-3527.
  53. Passaniti A., Hart G.W. // *J. Biol. Chem.* 1988. V. 263. P. 7591-7603.
  54. Bresalier R.S., Rockwell R.W., Dahiya R., Duh Q.Y., Kim Y.S. // *Cancer Res.* 1990. V. 50. P. 1299-1307.
  55. Hsu C.C., Lin T.W., Chang W.W., Wu C.Y., Lo W.H., Wang P.H., Tsai Y.C. // *Gynecol. Oncol.* 2005. V. 96. P. 415-422.
  56. Chang W.W., Yu C.Y., Lin T.W., Wang P.H., Tsai Y.C. // *Biochem. Biophys. Res. Commun.* 2006. V. 341. P. 614-619.
  57. Chiang C.H., Wang C.H., Chang H.C., More S.V., Li W.S., Hung W.C. // *J. Cell. Physiol.* 2010. V. 223. P. 492-499.
  58. Cohen M., Elkabets M., Perlmutter M., Porgador A., Voronov E., Apte R.N., Lichtenstein R.G. // *J. Immunol.* 2010. V. 185. P. 5869-5878.
  59. Powell L.D., Whiteheart S.W., Hart G.W. // *J. Immunol.* 1987. V. 139. P. 262-270.
  60. Tyagarajan K., Forte J.G., Townsend R.R. // *Glycobiology*. 1996. V. 6. P. 83-93.
  61. Drzeniek R., Gauhe A. // *Biochem. Biophys. Res. Commun.* 1970. V. 38. P. 651-656.
  62. Brostrom M.A., Bruening G., Bankowski R.A. // *Virology*. 1971. V. 46. P. 856-865.
  63. Hua J., Liao M.J., Rashidbaigi A. // *J. Leukoc. Biol.* 1996. V. 60. P. 125-128.
  64. Nyman T.A., Tolo H., Parkkinen J., Kalkkinen N. // *Biochem. J.* 1998. V. 329. P. 295-302.

## REVIEWS

65. Costas M.A., Mella D., Criscuolo M., Diaz A., Finkielman S., Nahmod V.E., Arzt E. // *J. Interferon Res.* 1993. V. 13. P. 407–412.
66. Cantell K., Hirvonen S., Kauppinen H.L., Myllyla G. // *Methods Enzymol.* 1981. V. 78. P. 29–38.
67. Suzuki H., Kurooka M., Hiroaki Y., Fujiyoshi Y., Kaneda Y. // *FEBS Lett.* 2008. V. 582. P. 1325–1329.
68. Ikeda H., Old L.J., Schreiber R.D. // *Cytokine Growth Factor Rev.* 2002. V. 13. P. 95–109.
69. Dunn G.P., Bruce A.T., Sheehan K.C., Shankaran V., Uppaluri R., Bui J.D., Diamond M.S., Koebel C.M., Arthur C., White J.M., Schreiber R.D. // *Nat. Immunol.* 2005. V. 6. P. 722–729.
70. Borden E.C., Sen G.C., Uze G., Silverman R.H., Ransohoff R.M., Foster G.R., Stark G.R. // *Nat. Rev. Drug Discov.* 2007. V. 6. P. 975–990.
71. Jarahian M., Watzl C., Fournier P., Arnold A., Djandji D., Zahedi S., Cerwenka A., Paschen A., Schirmacher V., Momburg F. // *J. Virol.* 2009. V. 83. P. 8108–8121.
72. Arnon T.I., Lev M., Katz G., Chernobrov Y., Porgador A., Mandelboim O. // *Eur. J. Immunol.* 2001. V. 31. P. 2680–2689.
73. Schirmacher V., Haas C., Bonifer R., Ertel C. // *Clin. Cancer Res.* 1997. V. 3. P. 1135–1148.
74. Harada Y., Yonemitsu Y. // *Front. Biosci.* 2011. V. 16. P. 2233–2242.
75. Shibata S., Okano S., Yonemitsu Y., Onimaru M., Sata S., Nagata-Takeshita H., Inoue M., Zhu T., Hasegawa M., Moroi Y., Furue M., Sueishi K. // *J. Immunol.* 2006. V. 177. P. 3564–3576.
76. Okano S., Yonemitsu Y., Shirabe K., Kakeji Y., Maehara Y., Harada M., Yoshikai Y., Inoue M., Hasegawa M., Sueishi K. // *J. Immunol.* 2011. V. 186. P. 1828–1839.
77. Sugiyama M., Kakeji Y., Tsujitani S., Harada Y., Onimaru M., Yoshida K., Tanaka S., Emi Y., Morita M., Morodomi Y., et al. // *Mol. Cancer Ther.* 2011. V. 10. P. 540–549.
78. Yoneyama Y., Ueda Y., Akutsu Y., Matsunaga A., Shimada H., Kato T., Kubota-Akizawa M., Okano S., Shibata S., Sueishi K., et al. // *Biochem. Biophys. Res. Commun.* 2007. V. 355. P. 129–135.
79. Komaru A., Ueda Y., Furuya A., Tanaka S., Yoshida K., Kato T., Kinoh H., Harada Y., Suzuki H., Inoue M., et al. // *J. Immunol.* 2009. V. 183. P. 4211–4219.
80. Kato T., Ueda Y., Kinoh H., Yoneyama Y., Matsunaga A., Komaru A., Harada Y., Suzuki H., Komiya A., Shibata S., et al. // *Neoplasia.* 2010. V. 12. P. 906–914.
81. Tanemura A., Kiyohara E., Katayama I., Kaneda Y. // *Cancer Gene Ther.* 2013. V. 20. P. 599–605.
82. Nishikawa T., Tung L.Y., Kaneda Y. // *Mol. Ther.* 2014. V. 22. № 12. P. 2046–2055.
83. Zimmermann M., Armeanu-Ebinger S., Bossow S., Lampe J., Smirnow I., Schenk A., Lange S., Weiss T.S., Neubert W., Lauer U.M., Bitzer M. // *PLoS One.* 2014. V. 9. P. e90508.



# Cancer Invasion: Patterns and Mechanisms

N. V. Krakhmal<sup>1</sup>, M. V. Zavyalova<sup>1,2,3</sup>, E. V. Denisov<sup>2,3\*</sup>, S. V. Vtorushin<sup>1,2</sup>, V. M. Perelmuter<sup>1,2</sup>

<sup>1</sup>Siberian State Medical University, Moskovskiy Trakt, 2, 634050, Tomsk, Russia

<sup>2</sup>Tomsk Cancer Research Institute, Kooperativny Pereulok, 5, 634050, Tomsk, Russia

<sup>3</sup>Tomsk State University, Prosp. Lenina, 36, 634050, Tomsk, Russia

\*E-mail: d\_evgeniy@oncology.tomsk.ru

Received 20.09.2014

Revised manuscript received 27.02.2015

Copyright © 2015 Park-media, Ltd. This is an open access article distributed under the Creative Commons Attribution License, which permits unrestricted use, distribution, and reproduction in any medium, provided the original work is properly cited.

**ABSTRACT** Cancer invasion and the ability of malignant tumor cells for directed migration and metastasis have remained a focus of research for many years. Numerous studies have confirmed the existence of two main patterns of cancer cell invasion: collective cell migration and individual cell migration, by which tumor cells overcome barriers of the extracellular matrix and spread into surrounding tissues. Each pattern of cell migration displays specific morphological features and the biochemical/molecular genetic mechanisms underlying cell migration. Two types of migrating tumor cells, mesenchymal (fibroblast-like) and amoeboid, are observed in each pattern of cancer cell invasion. This review describes the key differences between the variants of cancer cell migration, the role of epithelial-mesenchymal, collective-amoeboid, mesenchymal-amoeboid, and amoeboid-mesenchymal transitions, as well as the significance of different tumor factors and stromal molecules in tumor invasion. The data and facts collected are essential to the understanding of how the patterns of cancer cell invasion are related to cancer progression and therapy efficacy. Convincing evidence is provided that morphological manifestations of the invasion patterns are characterized by a variety of tissue (tumor) structures. The results of our own studies are presented to show the association of breast cancer progression with intratumoral morphological heterogeneity, which most likely reflects the types of cancer cell migration and results from different activities of cell adhesion molecules in tumor cells of distinct morphological structures.

**KEYWORDS** cancer; invasion; cell migration; collective cell migration; individual cell migration.

**ABBREVIATIONS** EMT – epithelial-mesenchymal transition; MET – mesenchymal-epithelial transition; GTPases – guanosine triphosphatases.

## INVASIVE GROWTH AND METASTASIS AS MANIFESTATION OF CANCER MALIGNANCY

The results of numerous experimental and clinical studies of malignant neoplasms have indicated that invasive growth and metastasis are the main manifestations of tumor progression, which represent two closely related processes.

A malignant tumor is characterized by the possibility to implement such a biological phenomenon as the metastatic cascade that is a unique multi-stage “program” where cell invasion is a trigger and a key factor for further cancer progression and metastasis in distant organs and tissues. Massive metastatic lesions lead to the development of severe organ failure and, therefore, a patient’s death [1–3]. The range between “end” points of a complex invasive metastatic process – invasion of the primary tumor into surrounding tissues and the formation of metastatic foci – comprises several stages, the passage of which is strictly nec-

essary for the successful development and subsequent progression of tumor growth: intravasation, survival and presence in the systemic circulation, extravasation with subsequent colonization of organs by tumor cells, and the formation of clinically detectable metastasis [1, 4–6]. Tumor growth is accompanied by increasing pressure on extracellular matrix structures, whereas the tissue microenvironment fights to retain its functional-anatomic integrity via increasing pressure on tumor cells. The factors limiting the growth of malignant neoplasm include the basal membrane and various components of the surrounding stroma, increased interstitial pressure, limited oxygen supply to tumor cells and the formation of active oxygen forms, hypoxia conditions, and permanent exposure to immune system cells. Given the intratumoral heterogeneity, in the struggle for survival, some tumor cells may be subjected to regression and death, while other cells, which resist powerful, counteracting microen-

vironmental factors, gain an aggressive phenotype and the ability of metastatic progression [7]. Invasive tumor growth is enabled by the detachment of malignant cells from the tumor mass due to a reduction in or complete loss of intercellular adhesion molecules, and, therefore, the cells gain the ability of anomalously high motility enabling penetration through the stiff structural elements of the surrounding stroma [8]. In this case, the invasion process extensively involves various molecular and cellular mechanisms that, according to published data, depend directly on another biological phenomenon – the epithelial-mesenchymal transformation, which was first described by E.D. Hay in 1995. Later, the term “epithelial-mesenchymal transition” (EMT) was put to use to clarify the reversibility of this process [9]. Currently, EMT is known to underlie the processes of embryogenesis and inflammation and regeneration of tissues and, certainly, plays a key role in the mechanisms of carcinogenesis [10, 11].

#### PHYSIOLOGICAL PROTOTYPES OF INVASIVE GROWTH

Tumor cells spreading into the surrounding tissues and distant organs are known to reproduce the mechanisms and migration types characteristic of normal, non-tumor cells during physiological processes. Tumor cells, similar to normal cells, are capable of activating these mechanisms for changing their own shape, creating conditions for moving, as well as remodeling surrounding tissues to form migration pathways. The main problem is that tumor cells, in contrast to normal cells, do not have physiological “stop signals” to terminate these processes. Most likely, this leads to the establishment of the migration mechanisms and promotes the progression and spread of the tumor [12–14].

Malignant cells were found to use built-in genetic programs to implement the processes that determine invasive growth and the possibility of metastasis. For example, the movement of a single cell is observed during embryonic development and inflammation (e.g., leukocyte migration). A similar mechanism of dissemination is typical of cancer cells during tumor progression and metastasis [13].

Along with single cell migration, collective cell migration can occur when groups of firmly interconnected tumor cells are migrating [15, 16]. This type of migration indicates tissue rearrangement, underlies the processes of embryonic morphogenesis, and also is an essential component in the healing of wound surfaces [17, 18].

Therefore, the key is that malignant tumor cells extensively use the mechanisms of both collective and single cell migration as physiological prototypes in the process of invasive growth and metastasis.

#### PATTERNS OF INVASIVE GROWTH

At present, based on a complex of certain morphological and molecular genetic parameters, two fundamentally different patterns of invasive growth are distinguished: collective (group) cell migration and single cell migration (individual migration: *Fig. 1*) [1, 2, 15, 19, 20]. In this case, the migration type is largely determined by tissue microenvironment features and depends on molecular changes in tumor cells [21].

Determination of the invasion mechanism used by single migrating cells during migration is a complex task. Unfortunately, studies examining this issue at the molecular and morphological levels are few in numbers and mostly were carried out *in vitro* using specific cell lines [22].

However, now, there is considerable increase in the number of studies that demonstrate increasing interest in research into the molecular genetic features of tumor cells that determine the main differences between the mesenchymal and amoeboid types of cell movement during individual migration, as well as collective migration.

#### Collective migration

Collective migration is characterized by the migration of whole groups of cells interconnected by adhesion molecules and other communication junctions (*Fig. 1*). It should be noted that this is the main feature of this type of invasion, since the underlying cellular mechanisms are the same key processes that largely determine single cell migration [15, 20, 23, 24].

Collective cell migration has been observed in the development and progression of breast and endometrial cancer, prostate cancer, colorectal cancer, large-cell lung carcinoma, rhabdomyosarcoma, melanoma, as well as most squamous cell carcinomas [1, 17, 20, 25, 26].

In the case of collective migration, cancer cells, being a part of the tumor mass or detaching from it in the form of multicellular groups, penetrate into the surrounding tissues and form thin short chords, clusters, stripes and wide fields, as well as structures with lumen, that indicate a wide variety of structural elements involved in tumor invasion [1, 2, 15, 20, 27].

As already mentioned, collective migration is characterized by the migration of whole cell groups interconnected by cadherins and intercellular gap junctions. A moving cell group has a “leading edge” or “leading front” that uses integrins and proteases (*Fig. 1*). Researchers indicate clear differences in the expression of genes and the morphology between the “leader” cells forming the leading edge and the “follower” cells that are located behind them, at the “trailing edge.” The “leaders” in the cell shape often resemble mesenchymal

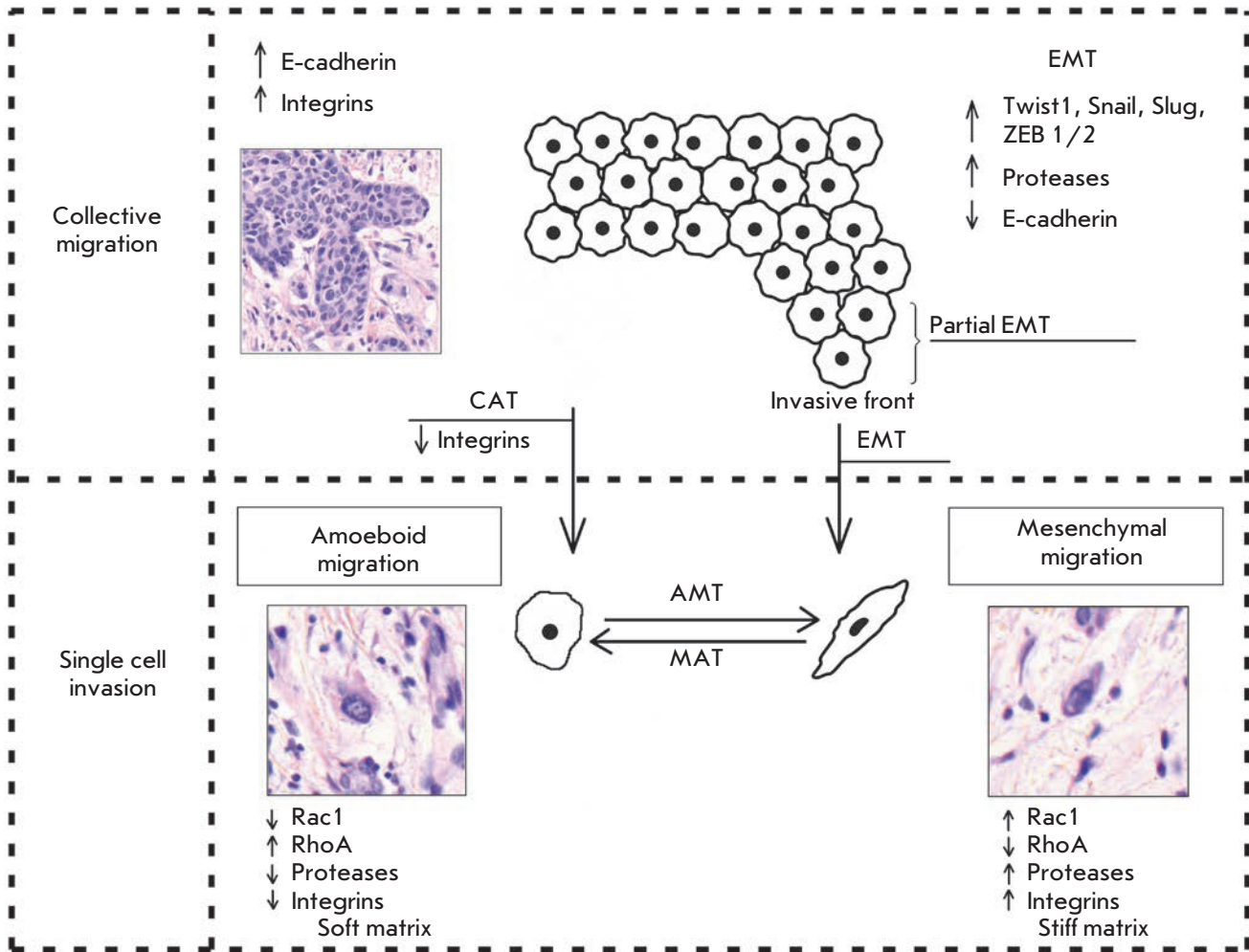


**Fig. 1.** Patterns of cancer cell invasion: collective cell and individual cell migration. In collective cell migration, tumor cells exhibit high expression of E-cadherin and integrins. Epithelial-mesenchymal (EMT) and collective-amoeboid (CAT) transitions are a trigger between collective cell invasion and individual cell migration. EMT involves activation of transcription factors, such as TWIST1, Snail, Slug, ZEB1/2, a decrease in E-cadherin expression, and an increase in protease activity. During EMT, tumor cells acquire the mesenchymal phenotype, detach from the tumor mass, and migrate by the mesenchymal mechanism. In contrast, the partial EMT that is specific to the tumor invasive front means that tumor cells retain cell-cell adhesion but already possess migratory ability. This tumor cell phenotype was named the “epithelial-mesenchymal” phenotype. In CAT, which takes place when  $\beta 1$  integrins are down-regulated, tumor cells detach from the tumor mass and move by the amoeboid mechanism. Amoeboid migration involves a decrease in protease and integrin expression and changes in the activity of GTPases – inhibition of Rac1 and activation of RhoA. This movement type occurs in the loose/soft extracellular matrix. In contrast, mesenchymal migration is associated with the opposite phenotype and predominates in the dense/stiff matrix. These two movement types are highly plastic and can convert to each other, depending on the extracellular matrix type and intracellular regulation. Thereby, the mesenchymal-amoeboid (MAT) and amoeboid-mesenchymal (AMT) transitions are suggested [1, 13, 22, 47, 68, 73, 74]

cells and are characterized by a less pronounced ordering and structural organization, while the “followers” tend to form more tightly packed, rosette-like tubular structures with tight intercellular contacts [17, 28].

In the case of collective migration, tumor cells form protrusions (pseudopodia) at the leading edge, use inte-

grins to form focal contacts with the actin cytoskeleton, and perform proteolytic degradation of the extracellular matrix, creating a space for invasion of the tumor tissue and extensively involving the actin-myosin contractile apparatus in the process to ensure successful migration [15, 20].

The differences in the polarity of collectively migrating cell groups are due to the features of expression of surface receptors, such as CXCR4 and CXCR7 chemokine receptors, in the “leader” cells [29]. The growth factors and chemokines produced by stromal cells and a diffusion gradient provide extracellular induction of cell polarization. Involvement of chemokines, such as SDF1 (CXCL12), the fibroblast growth factor (FGF), and the transforming growth factor  $\beta$  (TGF- $\beta$ ), in these processes has been under discussion [17, 30].

Much is known about the involvement of TGF- $\beta$  in carcinogenesis, with its role being twofold. Taylor *et al.* [31] have drawn attention to the fact that TGF- $\beta$ , which acts in the epithelial cells of the mammary gland as a potent tumor suppressor at the early stages of cancer, can affect tumor development via interaction with oncogenic cytokines. Increased expression of TGF- $\beta$  has been associated with the progression of tumor, which has often been observed, e.g., at the later stages of breast cancer [32, 33]. The role of TGF- $\beta$  in epithelial-stromal migration during tumor progression has not been studied sufficiently. TGF- $\beta$  is supposed to be a key regulator of the interactions between the tumor and stroma, which promotes collective cell migration in breast cancer [34].

It has been established that leader cells express podoplanin [2], a transmembrane glycoprotein that is expressed under normal conditions in kidney podocytes, type 1 lung alveolar cells, skeletal muscle cells, placenta, etc. Podoplanin expression in breast cancer cells induces cell migration and invasion with the formation of filopodia and simultaneous retention of E-cadherin expression [2, 35].

Data have been reported indicating that collectively migrating cancer cells can use the ability of adjacent mesenchymal cells to modify the structure of the matrix and rebuild it, and then follow in their “footsteps.” In *in vitro* experiments, the introduction of fibroblasts in the culture induces collective tumor cell migration to the underlying matrix in the form of chains. Therefore, fibroblasts are a “guide” for invading tumor cells, remodeling the surrounding extracellular matrix to pathways with thick collagen bundles on the sides and a lack of a matrix in the center [36, 37].

LIM-kinase, a member of one of the protein families, plays a role in the development of collective migration by tumor cells. This protein is known to be involved in the regulation of developing invadopodia, which are structures typical of malignant tumor cells and responsible for the destruction of the surrounding extracellular matrix. Excessive activation of LIM-kinase is displayed in breast cancer. Breast tumor cells with suppressed expression of the LIM-kinase gene lose their ability to invade due to the loss of their ability to disrupt the extracellular matrix [38, 39].

### Single cell invasion or individual cell migration

Such a type of invasive growth as single cell invasion is distinguished based on the detection, during morphological analysis, of individual tumor cells that invade the surrounding tissues independently of each other [2]. In this type of tumor invasion, single cell migration can occur via two different movement types: mesenchymal and amoeboid [1, 2, 15, 22]. It should be noted that a number of researchers point to the possibility of a “shift” from one type of migration to the other (from mesenchymal to amoeboid and vice versa, *Fig. 1*) in the case of single cell invasion. These transitions usually occur upon changes in the activity of certain cell molecules when tumor cells have to adapt to the peculiarities of the microenvironment [22, 40].

### Mesenchymal (fibroblast-like) cell migration

The mesenchymal mechanisms of invasive cell growth, in contrast to the amoeboid type of migration, are characterized by the occurrence of more complex processes and a need for the involvement of a larger number of cellular molecules in its implementation (*Fig. 1*).

This type of migration is typical of keratinocytes during reparative regeneration, endotheliocytes, smooth muscle cells, and fibroblasts. Since malignant cells, which use the mesenchymal type of movement, lose epithelial polarity and gain an elongated spindle shape, which resembles the fibroblast shape, invasion of this type is also called “fibroblast-like” migration [1, 2, 22, 23, 41]. Mesenchymal invasion has been detected during the development of melanoma, fibrosarcoma, glioblastoma, and other malignancies [1, 42–44].

Most of the cancer cells that detach from the tumor mass and invade the surrounding tissues are known to undergo certain changes, acquiring the morphological properties and a phenotype typical of mesenchymal cells [2, 15]. This transformation of a malignant epithelial cell, which is related to the emergence of new molecular and morphological features in the cell, was called the “epithelial-mesenchymal transition.” As already mentioned, this biological phenomenon was first described by E.D. Hay in 1995 [9]. Today, the existence of the phenomenon is supported by the results of a large number of studies that have investigated the mechanisms of invasion and metastasis of malignant tumors [1, 2, 15, 45]. The mesenchymal mechanism of invasion is believed to be the consequence of EMT, when active dedifferentiation of a malignant epithelial tumor occurs, and multicellular groups start to divide into single tumor cells, gaining a mesenchymal phenotype [13].

A number of researchers have stressed that tumor cells during the mesenchymal type of migration go through a number of specific sequential steps that constitute a five-stage model of migration. This cycle

includes the following changes: 1) formation of a protrusion on one of the cell poles – a lamellipodia or a filopodia produced by contractions of the actin cytoskeleton under the control of small GTPases Rac1 and Cdc42 with rapid involvement of integrins of the  $\beta 1$  family; 2) occurrence of focal adhesion with the involvement of integrins  $\beta 1$  and  $\beta 3$  at the contact site between the extracellular matrix and the cell; 3) assembly of focal contacts, which is based on integrin-mediated interactions, and activation of proteolytic enzymes (matrix metalloproteinases, serine and threonine proteases, cathepsins) at the “cell-matrix” interface that leads to the destruction and remodeling of the surrounding extracellular matrix; 4) a change in the actin cytoskeleton polarization under myosin II-mediated control, the occurrence of cell body contractions; and 5) “pulling” the trailing edge toward movement through the newly formed defects in the matrix structure [1, 13, 22]. Since the cells which use the fibroblast-like mechanism of invasion follow the described migration steps, their speed of movement is low: about 0.1–2  $\mu\text{m}/\text{min}$  [1, 22, 40].

The possibility of proteolysis and remodeling of tissue structures explains the fact that mesenchymal movement of a tumor cell is accompanied by minor changes, compared to amoeboid migration, in the cell's shape and by minimal deformation of the nucleus [46]. Of clear interest are the results of studies that indicate that the behavior of tumor cells during individual migration depends on the surrounding matrix' stiffness. For example, the mesenchymal or proteolytic model of migration dominates under conditions of a “stiff” (“dense”) surrounding matrix. The high migration efficiency of a single cell using the mesenchymal mechanism in dense tissues is explained by proteolysis due to the secretion of various proteases and by the ability to form focal contacts with stromal elements [47, 48].

Therefore, it is worth noting that the key points of the fibroblast-like mechanism of invasive growth are strong adhesion forces on both poles of the cell as well as between cells and extracellular matrix components, pronounced expression of integrins ( $\beta 1$  and  $\beta 3$  families), proteolysis with destruction and subsequent remodeling of tissues with the formation of defects in the matrix structure, and movement of a single cell or cell chains through the defects. The nucleus deformation is minimal, and a slow rate of cell migration is observed.

Based on the suppression of the expression of the relevant genes using small interfering RNAs, the specific activity of GTPases Rac1 and Cdc42 was demonstrated to be the characteristic feature of the mesenchymal type of invasion. Suppression of GTPase Rac1 through signaling activation of GTPase RhoA and its effector, ROCK kinase, leads to blockage of the mesenchymal migration of tumor cells [49–52].

### Amoeboid cell migration

The amoeboid mechanism of invasive growth is the most primitive and, at the same time, the most efficient mode of migration of single tumor cells. In all of its features, it is similar to the behavior and movement of a single-celled organism, such as the amoeba *Dictyostelium discoideum* [40, 53].

The use of antibodies that block integrins or protease inhibitors in clinical trials leads to the emergence of tumor cells with the amoeboid type of migration [1]. Similar results were obtained in studies of malignant tumors *in vivo*. A relationship between the application of drugs on the basis of matrix metalloproteinase inhibitors in cancer therapy and progression of the tumor process was established. The explanation of this relationship became possible only after the identification of tumor cells capable of amoeboid migration [54]. These data most likely indicate that, under conditions of a reduction in or complete loss of their ability to spread to the surrounding tissues using the main molecules that perform adhesion and destruction of the extracellular matrix, tumor cells turn to the amoeboid mechanism of invasion, which becomes the only and most effective mode of migration.

This type of migration has been described in circulating stem cells, leukocytes, and certain types of tumor cells [2, 14]. According to Zijl *et al.*, the amoeboid type of invasive growth has been observed in breast cancer, lymphoma, small cell lung cancer and prostate cancer, and melanoma [1, 42, 55].

In the case of amoeboid migration, malignant tumor cells have been demonstrated to have a round or elliptical shape (*Fig. 1*) [1, 22, 23, 40]. Amoeboid cells are characterized by fast deformability, adaption of their shapes to existing structures of the surrounding extracellular matrix, and penetration through them via narrow spaces in a compressed form. Movement and relocation are carried out through successive high-speed cycles of expansion and contraction of the cell's body with the development of “bleb-like” protrusions of the cell membrane [22, 56–58]. These blebs allow the cell to investigate the microenvironment to find the most suitable route of movement to bypass various obstacles, whereby tumor cells are capable of moving through narrow gaps in the extracellular matrix [1, 2, 15, 22]. Developing changes in the cell shape are generated by the cortical actin cytoskeleton that is, in turn, controlled by small GTPase RhoA and its effector, ROCK kinase [1, 2, 15, 59]. This GTPase belongs to the superfamily of small GTP hydrolases, whose members play key roles in the amoeboid type of invasion, since they are involved in signal transduction and, thereby, in the regulation of a wide variety of processes occurring in the cell, including reorgani-

zation of the actin cytoskeleton during migration [51, 60, 61].

It is worth noting that migration through the amoeboid mechanism of invasion is accompanied by changes not only in the cell shape, but also in the shape of the nucleus and its orientation and position relative to other internal organelles. The nucleus, which is the largest and stiffer, compared to the surrounding cytoskeleton, organelle, is mechanically firmly stabilized by an extensive network of structural proteins, and, for this reason, its shape, most likely, often does not undergo significant changes. However, the amoeboid type of migration is characterized by the most pronounced nucleus deformation, caused by the lack of proteolytic degradation of the surrounding matrix. Since tumor cells have to move through narrow spaces and pores, the nucleus in this case also occurs in a maximum compressed state [46, 62, 63]. It is assumed that, like the amoeboid movement of leukocytes, nuclei inside single migrating tumor cells move forward toward the leading edge [46].

In contrast to the mesenchymal movement, amoeboid or a non-proteolytic model of migration prevails when the surrounding matrix is characterized by relatively low stiffness (“soft” matrix). For example, amoeboid migration of tumor cells in the lymphatic and circulatory systems is considered as migration in a soft matrix [47, 48].

Condeelis and Segall [64] elucidated some features of cell migration on the example of two different tumor lines, MTC and MTLn3, under *in vitro* and *in vivo* conditions. MTLn3 cells that have a high metastatic potential and migrate probably by the amoeboid mechanism of invasive growth are characterized by a higher level of expression of epidermal growth factor receptors (EGFRs) than MTC cells with a low metastatic potential. Their migration is associated with the presence of blood vessels and collagen-containing fibers in the surrounding matrix. Tumor cell chemotaxis towards blood vessels is believed to be mediated by the signaling pathways of EGFR [64].

The amoeboid mechanism of invasion has a number of distinctive features. It is characterized by a weak interaction between cells and the surrounding matrix, as well as a lack of or weak focal contacts. The possibility to retain the rapid and non-focal assembly of receptors at the sites of cell contacts with the extracellular substrate has been noted. Integrins are not important in this type of invasive growth. Important aspects are the absence of proteolysis at the sites of cell-matrix interactions and the lack of expression of proteolytic enzymes that destroy the extracellular matrix [1, 2, 15, 62, 65]. *In vitro* studies have demonstrated that, in the case of an amoeboid type of invasive growth, it is likely

due to these properties that tumor cells are capable of moving at the highest speed in cultures (20  $\mu\text{m}/\text{min}$ ) [1, 20, 21].

### Amoeboid-mesenchymal and mesenchymal-amoeboid transitions

We have already noted the existence of a degree of plasticity and the possibility of a “shift” from one migration type to the other (from the mesenchymal type to the amoeboid one and *vice versa*) upon individual cell invasion. These events are apparently due to the appearance of changes in the activity of certain cell molecules and the need to adapt to tissue microenvironment conditions (*Fig. 1*).

These changes are described as amoeboid-mesenchymal and mesenchymal-amoeboid transitions [2, 22]. Tumor cells using the mesenchymal type of migration can be changed in a certain way and shift to the amoeboid type of movement under conditions of a weakened signal and mechanical pathways that are directly involved in the stabilization of the interactions between extracellular matrix structures and malignant cells [22, 40, 47, 66]. However, the available data were obtained primarily by means of experiments. The following mechanisms leading to the transition of cells from the mesenchymal to the amoeboid type of invasive growth (mesenchymal-amoeboid transition) have been described: 1) reduction in or complete abolition of pericellular proteolysis due to application of protease inhibitors; 2) reduction in the activity of integrin receptors and their interactions with surrounding stromal elements by their antagonists; 3) increase in and stabilization of the activity of small GTPase RhoA and its ROCK effector [16, 40]. A study by S. Berton’s group provided an interesting fact indicating that the p27 protein, despite a great variety of functions, plays an important role in the control of cell motility. In particular, a lack of this protein under *in vitro* conditions induces the mesenchymal-amoeboid transition in cells in a 3D matrix [66].

Some authors studying the mechanisms of invasive growth upon individual cell migration indicate the possibility of an amoeboid-mesenchymal transition that is the reverse process to the mesenchymal-amoeboid transition. There is a hypothesis according to which the mechanism of amoeboid-mesenchymal transition most likely relies on the same molecular basis, and that the only reliable process that determines the possibility of the described transformation is an imbalance in the activity of members of the small GTPase family and predominance of the Rac activity over the RhoA activity. It should be noted that the mechanisms that could underlie the described changes remain unclear [47].

### COLLECTIVE-INDIVIDUAL TRANSITIONS

Tumor cells within a single tumor can simultaneously move both collectively and individually. In this case, the transition from individual to collective migration is an important step towards increasing the invasive and metastatic potential of malignant neoplasms. For example, breast tumor cells detached from the solid mass gain the ability to invade lymphatic vessels [26]. Currently, two mechanisms are distinguished: epithelial-mesenchymal and collective-amoeboid transitions by which individually migrating tumor cells are produced (*Fig. 1*) [13, 67]. In turn, the latter, in particular cells that have undergone EMT, are capable under certain conditions of gaining an epithelial phenotype and forming tumor multicellular complexes. This phenotype inversion was called the “mesenchymal-epithelial transition” [15, 17].

### Epithelial-mesenchymal transition

Lately, there has been vigorous discussion of the epithelial-mesenchymal transition as a mechanism during which the tumor cell detaches from the epithelial layer and gains motility (*Fig. 1*), the so-called “locomotor phenotype,” which promotes invasive growth and metastasis [68–71]. The development of this process as a key factor of cancer progression was shown *in vitro* using specific tumor lines as well as experimental models; however, establishment of the EMT development and identification of tumor cells and their main characteristics under *in vivo* conditions is a complex task [72].

EMT is the basis of many processes of morphogenesis [71]. It is believed that under normal conditions (during embryogenesis) EMT can be induced by the HGF (hepatocyte growth factor) secreted by fibroblasts. HGF binds to specific c-Met receptors located on the membrane of epithelial cells. The binding to receptors activates a signaling pathway involving some proteins of the small GTPase system (Cdc42, Rac, RhoA, RhoC) that regulate the intensity of actin microfilament polymerization and the contractility of actin-myosin filaments, which determines the intensity of lamellipodia formation and tension of the matrix-attached cell. In this case, there is significant rearrangement of the whole actin-myosin cytoskeleton and loss of E-cadherin intercellular contacts. During carcinogenesis, epithelial cells are subjected to a morphological transformation that is phenotypically similar to EMT but develops in the absence of the relevant HGF ligand. This transformation in malignant tumors can be induced by transfection of various oncogenes. During transformation, tumor cells can leave the epithelial layer and move like fibroblasts, thereby gaining the ability of invasion and metastasis [73].

During EMT, the following major events occur: malignant epithelial cells lose their apical-basal polarity due to disruption in tight intercellular junctions and loss of cellular adhesion molecules (such as E-cadherin and integrins); the cellular actin cytoskeleton is changed and subjected to remodeling with the formation of stress fibers that are collected in certain cell parts near the cell membrane, where specific cellular protrusions begin subsequently to form; degradation of the underlying basal membrane of the epithelium occurs, which results in the fact that tumor cells lacking intercellular contacts become capable of invasive growth and penetration into the surrounding stromal matrix and begin active migration [69, 71].

EMT was found to be rarely equally pronounced in the entire tumor tissue. More likely, this process is characterized by a varying intensity of the transition of cells from the epithelial to the mesenchymal phenotype. In this regard, some researchers describe the so-called partial EMT, in which most cells in the invasive front are involved (*Fig. 1*). Partial EMT is a state when cells have already gained the properties necessary for successful migration, but continue to retain cell-cell contacts. This phenotype was called the hybrid “epithelial-mesenchymal” phenotype and was linked to the features characteristic of collectively moving tumor cells [69, 74, 75].

Taddei *et al.* have indicated that EMT develops due to the induction of programs associated with the activation of key transcription factors, such as TWIST1, Snail, Slug, and ZEB1/2 [76, 77]. This results in disruption in strong cadherin junctions and activation of polar cell migration and proteolysis of extracellular matrix components by various secreted proteases, with the functions of integrin receptors being retained [10, 17, 77, 78]. The role of the transcription factor Prrx1, which determines the ability of breast cancer cells for invasive growth, was experimentally established [79].

It was shown that ZEB1 and ZEB2 proteins with a zinc finger domain are able to directly bind to promoters, thereby inducing the expression of mesenchymal marker genes and suppressing the expression of E-cadherin and other epithelial markers [80, 81].

Similarly, Snail and Slug are able to suppress the expression of the E-cadherin gene via direct binding to its promoter, as well as production of epithelial proteins such as desmoplakin and claudin, and activate the expression of vimentin and matrix metalloproteinases, thereby increasing cell migration [82]. A team of researchers led by Sanchez-Tillo found that the transcription factor Snail does not occur in normal epithelial cells and that its detection in cells of the tumor invasive front can be considered as a predictor of poor survival

of cancer patients [83]. It is believed that ZEB1/2, Snail, and Slug are induced by TGF- $\beta$ , inflammatory cytokines, and hypoxia [84].

### Collective-amoeboid transition

Based on experimental data, a number of researchers indicate the possible existence of a so-called collective-amoeboid transition (*Fig. 1*), when tumor masses invading surrounding tissues in the form of collective multicellular groups dissociate into single migrating cells that use the amoeboid movement [40]. This event has been shown to become possible with the application of inhibitors of integrin receptors of the  $\beta 1$  family, since these molecules play a key role both in the formation of cell-cell contacts and in the interactions between tumor cells and surrounding tissue components [16, 40, 85].

### Mesenchymal-epithelial transition

There are actually no studies devoted to the investigation of the mechanisms underlying the mesenchymal-epithelial transition. However, the possibility of such a phenomenon is recognized. In this case, it is said that often, e.g. in breast and prostate cancer, the tissue structure in distant metastatic foci is similar to the primary tumor structure [15, 86]. According to Friedl and Gilmour [17], several assumptions can be made based on these data. First, invasion and metastasis can occur without EMT. Second, detection of single disseminated cells during a routine pathologic examination of tumor tissue samples seems to be a rather complex task, and identification of these cells during EMT is actually impossible. And, third, tumor cells temporarily use the EMT mechanisms for intravasation and spread to distant organs and tissues, where they return to the epithelial phenotype. This transformation is described as the mesenchymal-epithelial transition (MET) [15, 17]. MET has been induced experimentally, and individually moving cells formed multicellular complexes, but the molecular mechanisms of MET under physiological conditions remain unknown [17]. Nguyen *et al.* [5] demonstrated that the selective inhibitor PD173074 of the fibroblast growth factor receptor 1 (FGFR1) inhibits the MAPK signaling pathway regulating the activity of the AP-1 protein, which, in turn, induces the development of MET. Investigation of the possibility of using the PD173074 inhibitor as a drug, which was conducted on specific tumor cell lines, revealed a distinct suppression of tumor growth, migration ability, and invasion. In this case, a decrease in the expression of *Snail* and the matrix metalloproteinase 3, 10, 12 and 13 genes and an increase in the expression of the E-cadherin gene were observed [5].

### CLASSIFICATION OF INVASIVE GROWTH TYPES ON THE EXAMPLE OF BREAST CANCER

For many years, our research team has studied the features of breast cancer progression depending on intratumoral heterogeneity. Particular attention has been paid to the phenotypic diversity of the primary tumor in invasive carcinoma of no special type, which accounts for the bulk (80%) of all histological types of breast cancer.

Despite the considerable structural diversity of the primary breast tumor, five main types of morphological structures can be distinguished: alveolar, trabecular, tubular and solid structures, and discrete groups of tumor cells (*Fig. 2*). The alveolar structures are tumor cell clusters of round or slightly irregular shape. The morphology of the cells that form this type of structures varies from small cells with moderate cytoplasm and round nuclei to large cells with hyperchromatic nuclei of irregular shape and moderate cytoplasm. The trabecular structures are either short, linear associations formed by a single row of small, rather monomorphic cells or wide cell clusters consisting of two rows of medium-sized cells with moderate cytoplasm and round normochromic or hyperchromatic nuclei. The tubular structures are formed by a single or two rows of rather monomorphic cells with round normochromic nuclei. The solid structures are fields of various sizes and shapes, consisting of either small cells with moderate cytoplasm and monomorphic nuclei or large cells with abundant cytoplasm and polymorphic nuclei. Discrete groups of cells occur in the form of clusters of one to four cells with variable morphologies [87, 88].

According to the data accumulated to date, it may be assumed that different morphological structures of breast tumors correspond to certain types of invasion. Therefore, alveolar, trabecular, and solid structures that are characterized by the presence of cell-cell contacts may be referred to morphological manifestations of collective migration, while discrete groups of tumor cells may be referred to manifestations of individual migration. Interestingly, the first batch of data obtained in a study of the expression of cell adhesion genes fully confirms this hypothesis. For example, there was a decrease in the activity of the genes of cadherins, which are responsible for cell-cell contacts, in the order: solid – alveolar and trabecular structures – discrete groups of tumor cells. In this case, the number of expressed genes of integrins involved in the adhesion of tumor cells to the extracellular matrix was reduced in the order: solid and alveolar – trabecular structures – discrete groups of tumor cells [89].



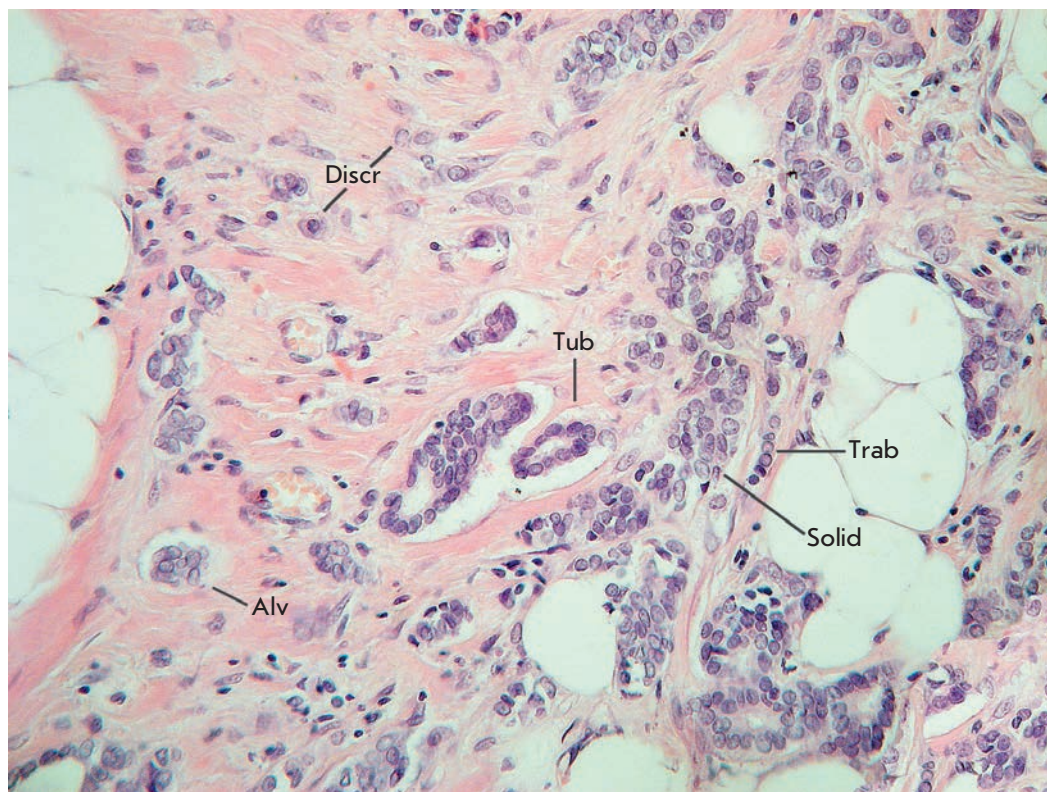


**Fig. 2.** Intratumoral morphological heterogeneity in invasive breast carcinoma. Diversity of invasive growth of breast cancer is shown, which can be classified into five main morphological structures: alveolar (Alv), trabecular (Trab), tubular (Tub), solid (Solid) structures, and discrete groups of tumor cells (Discr). Hematoxylin and eosin staining. Magnification of 200x

### TYPES OF INVASIVE GROWTH IN TUMOR PROGRESSION AND THERAPY EFFICACY

Invasive growth and the development of drug resistance are related processes that play the most important role in tumor progression: in particular in metastasis. It is very likely that the same signaling pathways are involved in cell migration and the development of tumor resistance to therapy [67, 90].

Migrating tumor cells (regardless of the movement's type) are more resistant to chemotherapy and radiotherapy than non-moving cells [90]. This is largely due to the fact that migrating cells temporarily lose their ability to divide. It is also the fact that moving tumor cells display increased activity of anti-apoptotic genes, which causes resistance to chemotherapeutic drugs aimed at induction of programmed cell death [91]. In addition, cells in the EMT state are known to also exhibit chemoresistance [92]. This drug resistance is due to induction, during EMT, of the synthesis of the ABC family proteins responsible for the efflux of chemotherapeutic drugs out of the cell. The main transcription factors that trigger EMT and, at the same time, positively regulate the activity of ABC transporters include TWIST1, Snail, etc [92–94].

Recently obtained data indicate strong association between collective migration and resistance to radio-

therapy and chemotherapy [67, 90]. According to our own research, breast tumors containing both alveolar and trabecular structures, as well as demonstrating significant morphological diversity, are characterized by increased drug resistance [95, 96]. Interestingly, the contribution of the trabecular structures to chemoresistance is probably explained by the high activity of ABC transporters in tumor cells of a given morphological variant. In contrast, resistance of breast tumors containing the alveolar structure is explained by other, yet unidentified, causes [96].

Invasive growth and its phenotypic diversity are associated, both directly and through the development of drug resistance, with metastasis. Circulating tumor cells, which are responsible for the development of future metastases, are a result of the invasion and subsequent penetration of tumor cells into lymphatic or blood vessels. Not only single migrating tumor cells, but also cell groups can have the intravasation ability. There is an assumption that collective migration much more often leads to metastasis compared to individual migration. Pioneering studies in animal models have demonstrated that metastases more often form after intravenous injection of tumor clusters rather than single tumor cells [97–99]. Furthermore, circulating tumor cell clusters have been found in the blood of pa-

tients with various cancers [100, 101]. It was assumed that collective intravasation is related to the VEGF-dependent formation of dilated vasculature and the accumulation of intravasated tumor clusters [102]. Furthermore, groups of tumor cells can enter circulation through damaged vessels [103] or by cooperation with cells in the EMT state and cancer-associated fibroblasts that disrupt the extracellular matrix by proteases [14, 104]. The dependence of metastasis on collective migration is confirmed by the results of our own research. For example, the presence of alveolar structures in tumors in postmenopausal breast cancer patients is associated with a high rate of lymphogenous metastasis, whereas the risk of this type of progression in premenopausal females increases with an increase in the number of different types of morphological structures [87, 105]. The latter dependence is also quantitative: lymphogenous metastases were detected more frequently in the case of a larger number of alveolar structures in breast tumors [87, 106]. Furthermore, patients with alveolar structures in tumors had a low metastasis-free survival rate (our own unpublished data).

The established relationship between the alveolar structures, as one of the manifestations of collective migration, and the rate of lymphogenous and hematogenous metastasis allows us to put forth the following assumptions. Apparently, the cellular elements of the alveolar structures differ from tumor cells of other structures by a set of biological properties determining the metastatic phenotype. The clearer relationship between alveolar structures and lymphogenous metastasis in the menopausal period suggests a certain role of estrogens, including also their production *in situ*, in that tumor cells of the alveolar structures gain the metastatic phenotype through the lymphogenous pathway [107].

Therefore, the data currently available on the features of invasive growth in carcinomas of different localizations and, in particular, in breast cancer present new opportunities for the investigation of tumor

progression patterns and the search for additional key parameters of prognosis and, possibly, “control” of disease progression.

## CONCLUSIONS

The significance of studies of the morphological manifestations and molecular genetic mechanisms of the invasion and metastasis of malignant tumors is not in doubt. The results of numerous studies clearly demonstrate that migration of tumor cells during invasive growth can occur both via single cells and via groups of cells. This diversity of cell migration types probably leads to the development of intratumoral heterogeneity that is represented, e.g. in breast cancer, by different morphological structures: alveolar, trabecular, and solid structures and discrete groups of tumor cells. A number of biochemical and molecular genetic mechanisms are known that enable malignant cells to invade surrounding tissues and gain the ability to spread far beyond the primary tumor site, giving rise to the development of secondary metastatic foci in distant organs and tissues. However, despite the achieved progress, there remain unexplored questions concerning a possible relationship between different types of invasive cell growth and the parameters of lymphogenous and hematogenous metastasis, the features of disease progression, as well as the efficacy of the chosen therapy. A solution to these problems could be of great help in determining the disease prognosis and, possibly, developing new approaches to the management of cancer patients. ●

*The study was supported by a grant from the Russian Science Foundation № 14-15-00318 (review of the authors' own data) and the Tomsk State University Competitiveness Improvement Program .*

*Work was partially carried out on equipment of Tomsk regional common use center, with the support of the Russian Ministry of the Agreement No.14.594.21.0001 (RFMEFI59414X0001).*

## REFERENCES

1. van Zijl F., Krupitza G., Mikulits W. // *Mutat Res.* 2011. V. 728. № 1–2. P. 23–34.
2. Spano D., Heck C., De Antonellis P., Christofori G., Zollo M. // *Semin Cancer Biol.* 2012. V. 22. № 3. P. 234–249.
3. Santibanez J.F. // *ISRN Dermatol.* 2013. V. 2013. P. 597927.
4. Mehlen P., Puisieux A. // *Nat Rev Cancer.* 2006. V. 6. № 6. P. 449–458.
5. Nguyen D.X., Bos P.D., Massague J. // *Nat Rev Cancer.* 2009. V. 9. № 4. P. 274–284.
6. Monteiro J., Fodde R. // *Eur J Cancer.* 2010. V. 46. № 7. P. 1198–1203.
7. Kovalyov A.A. // *Zdorovie Ukrainy.* 2011. V. 4. № 17. P. 26–28.
8. Kovalyov A.A., Grudinskaya T.A., Kusnezova T.P., Kovalyov K.A. // *Oncology.* 2012. V. 14. № 2. P. 126–129.
9. Hay E.D. // *Acta Anat (Basel).* 1995. V. 154. № 1. P. 8–20.
10. Kalluri R., Weinberg R.A. // *J Clin Invest.* 2009. V. 119. № 6. P. 1420–1428.
11. Tam W.L., Weinberg R.A. // *Nat Med.* 2013. V. 19. № 11. P. 1438–1449.
12. Cox E.A., Sastry S.K., Huttenlocher A. // *Mol Biol Cell.* 2001. V. 12. № 2. P. 265–277.
13. Friedl P., Hegerfeldt Y., Tusch M. // *Int J Dev Biol.* 2004.

## REVIEWS

- V. 48. № 5-6. P. 441-449.
14. Friedl P, Alexander S. // *Cell*. 2011. V. 147. № 5. P. 992-1009.
  15. Friedl P, Locker J, Sahai E, Segall J.E. // *Nat Cell Biol*. 2012. V. 14. № 8. P. 777-783.
  16. Hernandez-Caballero M.E. Molecular mechanisms of metastasis: epithelial-mesenchymal transition, anoikis and loss of adhesion. In *Carcinogenesis*, Tonissen K., ed.: Intech, 2013. 165-194.
  17. Friedl P, Gilmour D. // *Nat Rev Mol Cell Biol*. 2009. V. 10. № 7. P. 445-457.
  18. Ulrich F, Heisenberg C.P. // *Traffic*. 2009. V. 10. № 7. P. 811-818.
  19. Khalil A.A., Friedl P. // *Integr Biol (Camb)*. 2010. V. 2. № 11-12. P. 568-574.
  20. Yilmaz M., Christofori G. // *Mol Cancer Res*. 2010. V. 8. № 5. P. 629-642.
  21. Friedl P, Wolf K. // *J Cell Biol*. 2010. V. 188. № 1. P. 11-19.
  22. Pankova K., Rosel D., Novotny M., Brabek J. // *Cell Mol Life Sci*. 2010. V. 67. № 1. P. 63-71.
  23. Scott R.W., Crighton D., Olson M.F. // *J Vis Exp*. 2011. № 58.
  24. Cheung K.J., Gabrielson E., Werb Z., Ewald A.J. // *Cell*. 2013. V. 155. № 7. P. 1639-1651.
  25. Kitamura T., Kometani K., Hashida H., Matsunaga A., Miyoshi H., Hosogi H., Aoki M., Oshima M., Hattori M., Takabayashi A., et al. // *Nat Genet*. 2007. V. 39. № 4. P. 467-475.
  26. Giampieri S., Manning C., Hooper S., Jones L., Hill C.S., Sahai E. // *Nat Cell Biol*. 2009. V. 11. № 11. P. 1287-1296.
  27. Sanz-Moreno V., Marshall C.J. // *Curr Opin Cell Biol*. 2010. V. 22. № 5. P. 690-696.
  28. Lecaudey V., Cakan-Akdogan G., Norton W.H., Gilmour D. // *Development*. 2008. V. 135. № 16. P. 2695-2705.
  29. Aman A., Piotrowski T. // *Dev Cell*. 2008. V. 15. № 5. P. 749-761.
  30. Vitorino P., Meyer T. // *Genes Dev*. 2008. V. 22. № 23. P. 3268-3281.
  31. Taylor M.A., Parvani J.G., Schiemann W.P. // *J Mammary Gland Biol Neoplasia*. 2010. V. 15. № 2. P. 169-190.
  32. Barcellos-Hoff M.H., Akhurst R.J. // *Breast Cancer Res*. 2009. V. 11. № 1. P. 202.
  33. Lebrun J.J. // *ISRN Molecular Biology*. 2012. V. 2012. doi:10.5402/2012/381428
  34. Matisse L.A., Palmer T.D., Ashby W.J., Nashabi A., Chytil A., Aakre M., Pickup M.W., Gorska A.E., Zijlstra A., Moses H.L. // *Breast Cancer Res*. 2012. V. 14. № 4. P. R98.
  35. Wicki A., Christofori G. // *Br J Cancer*. 2007. V. 96. № 1. P. 1-5.
  36. Gaggioli C., Hooper S., Hidalgo-Carcedo C., Grosse R., Marshall J.F., Harrington K., Sahai E. // *Nat Cell Biol*. 2007. V. 9. № 12. P. 1392-1400.
  37. Friedl P, Wolf K. // *Cancer Res*. 2008. V. 68. № 18. P. 7247-7249.
  38. Scott R.W., Hooper S., Crighton D., Li A., Konig I., Munro J., Trivier E., Wickman G., Morin P., Croft D.R., et al. // *J Cell Biol*. 2010. V. 191. № 1. P. 169-185.
  39. Schoumacher M., Goldman R.D., Louvard D., Vignjevic D.M. // *J Cell Biol*. 2010. V. 189. № 3. P. 541-556.
  40. Friedl P. // *Curr Opin Cell Biol*. 2004. V. 16. № 1. P. 14-23.
  41. Madsen C.D., Sahai E. // *Dev Cell*. 2010. V. 19. № 1. P. 13-26.
  42. Sanz-Moreno V., Gadea G., Ahn J., Paterson H., Marra P., Pinner S., Sahai E., Marshall C.J. // *Cell*. 2008. V. 135. № 3. P. 510-523.
  43. Carragher N.O., Walker S.M., Scott Carragher L.A., Harris F., Sawyer T.K., Brunton V.G., Ozanne B.W., Frame M.C. // *Oncogene*. 2006. V. 25. № 42. P. 5726-5740.
  44. Yamazaki D., Kurisu S., Takenawa T. // *Oncogene*. 2009. V. 28. № 13. P. 1570-1583.
  45. Siletz A., Schnabel M., Kniazeva E., Schumacher A.J., Shin S., Jeruss J.S., Shea L.D. // *PLoS One*. 2013. V. 8. № 4. P. e57180.
  46. Friedl P., Wolf K., Lammerding J. // *Curr Opin Cell Biol*. 2011. V. 23. № 1. P. 55-64.
  47. Chikina A.S., Aleksandrova A.Yu. // *Molecular Biology*. 2014. V. 48. № 2. P. 165-180.
  48. Ehrbar M., Sala A., Lienemann P., Ranga A., Mosiewicz K., Bittermann A., Rizzi S.C., Weber F.E., Lutolf M.P. // *Biophys J*. 2011. V. 100. № 2. P. 284-293.
  49. Abreu-Blanco M.T., Verboon J.M., Parkhurst S.M. // *Curr Biol*. 2014. V. 24. № 2. P. 144-155.
  50. Li H., Peyrollier K., Kilic G., Brakebusch C. // *Biofactors*. 2014. V. 40. № 2. P. 226-235.
  51. Lash L.L., Wallar B.J., Turner J.D., Vroegop S.M., Kilkuskie R.E., Kitchen-Goosen S.M., Xu H.E., Alberts A.S. // *Cancer Res*. 2013. V. 73. № 22. P. 6793-6803.
  52. Militello R., Colombo M.I. // *Commun Integr Biol*. 2013. V. 6. № 5. P. e25460.
  53. Bloomfield G., Skelton J., Ivens A., Tanaka Y., Kay R.R. // *Science*. 2010. V. 330. № 6010. P. 1533-1536.
  54. Sabeih F., Shimizu-Hirota R., Weiss S.J. // *J Cell Biol*. 2009. V. 185. № 1. P. 11-19.
  55. Gadea G., Sanz-Moreno V., Self A., Godi A., Marshall C.J. // *Curr Biol*. 2008. V. 18. № 19. P. 1456-1465.
  56. Chaussepied M., Janski N., Baumgartner M., Lizundia R., Jensen K., Weir W., Shiels B.R., Weitzman J.B., Glass E.J., Werling D., et al. // *PLoS Pathog*. 2010. V. 6. № 11. P. e1001197.
  57. Tozluoglu M., Tournier A.L., Jenkins R.P., Hooper S., Bates P.A., Sahai E. // *Nat Cell Biol*. 2013. V. 15. № 7. P. 751-762.
  58. Miyazawa Y., Uekita T., Ito Y., Seiki M., Yamaguchi H., Sakai R. // *Mol Cancer Res*. 2013. V. 11. № 6. P. 628-637.
  59. Razidlo G.L., Schroeder B., Chen J., Billadeau D.D., McNiven M.A. // *Curr Biol*. 2014. V. 24. № 1. P. 86-93.
  60. Bakal C. // *J Cell Biol*. 2013. V. 203. № 3. P. 378-379.
  61. Synek L., Sekeres J., Zarsky V. // *Front Plant Sci*. 2014. V. 4. P. 543.
  62. Pinner S.E., Sahai E. // *F1000 Biol Rep*. 2009. V. 1. P. 67.
  63. Gerlitz G., Bustin M. // *Trends Cell Biol*. 2011. V. 21. № 1. P. 6-11.
  64. Condeelis J., Segall J.E. // *Nat Rev Cancer*. 2003. V. 3. № 12. P. 921-930.
  65. Ewald P.W., Swain Ewald H.A. // *Evol Appl*. 2013. V. 6. № 1. P. 70-81.
  66. Berton S., Belletti B., Wolf K., Canzonieri V., Lovat F., Vecchione A., Colombatti A., Friedl P., Baldassarre G. // *Mol Cell Biol*. 2009. V. 29. № 18. P. 5031-5045.
  67. Häger A., Alexander S., Friedl P. // *European Journal of Cancer Supplements*. 2013. V. 11. № 2. P. 291-293.
  68. Vasil'ev Yu.M., Gel'fand I.M. // *Biochemistry (Mosc)*. 2006. V. 71. № 8. P. 821-826.
  69. Micalizzi D.S., Farabaugh S.M., Ford H.L. // *J Mammary Gland Biol Neoplasia*. 2010. V. 15. № 2. P. 117-134.
  70. Said N.A., Williams E.D. // *Cells Tissues Organs*. 2011. V. 193. № 1-2. P. 85-97.
  71. Kim S., Lee J.W. // *Genomics Inform*. 2014. V. 12. № 1. P. 12-20.
  72. Tsai J.H., Yang J. // *Genes Dev*. 2013. V. 27. № 20. P. 2192-2206.

73. Gotte M., Kersting C., Radke I., Kiesel L., Wulfing P. // *Breast Cancer Res.* 2007. V. 9. № 1. P. R8.
74. Savagner P. // *Ann Oncol.* 2010. V. 21 Suppl 7. P. vii89–92.
75. Lu M., Jolly M.K., Levine H., Onuchic J.N., Ben-Jacob E. // *Proc Natl Acad Sci U S A.* 2013. V. 110. № 45. P. 18144–18149.
76. Tsai J.H., Donaher J.L., Murphy D.A., Chau S., Yang J. // *Cancer Cell.* 2012. V. 22. № 6. P. 725–736.
77. Taddei M.L., Giannoni E., Morandi A., Ippolito L., Ramazzotti M., Callari M., Gandellini P., Chiarugi P. // *Cell Commun Signal.* 2014. V. 12. P. 24.
78. Giannoni E., Parri M., Chiarugi P. // *Antioxid Redox Signal.* 2012. V. 16. № 11. P. 1248–1263.
79. Ocana O.H., Corcoles R., Fabra A., Moreno-Bueno G., Acloque H., Vega S., Barrallo-Gimeno A., Cano A., Nieto M.A. // *Cancer Cell.* 2012. V. 22. № 6. P. 709–724.
80. Bindels S., Mestdagt M., Vandewalle C., Jacobs N., Volders L., Noel A., van Roy F., Berx G., Foidart J.M., Gilles C. // *Oncogene.* 2006. V. 25. № 36. P. 4975–4985.
81. Vandewalle C., Van Roy F., Berx G. // *Cell Mol Life Sci.* 2009. V. 66. № 5. P. 773–787.
82. Samatov T.R., Tonevitsky A.G., Schumacher U. // *Mol Cancer.* 2013. V. 12. № 1. P. 107.
83. Sanchez-Tillo E., Liu Y., de Barrios O., Siles L., Fanlo L., Cuatrecasas M., Darling D.S., Dean D.C., Castells A., Postigo A. // *Cell Mol Life Sci.* 2012. V. 69. № 20. P. 3429–3456.
84. De Craene B., Berx G. // *Nat Rev Cancer.* 2013. V. 13. № 2. P. 97–110.
85. Friedl P., Wolf K. // *Nat Rev Cancer.* 2003. V. 3. № 5. P. 362–374.
86. Tsuji T., Ibaragi S., Hu G.F. // *Cancer Res.* 2009. V. 69. № 18. P. 7135–7139.
87. Zavyalova M.V., Perelmuter V.M., Vtorushin S.V., Denisov E.V., Litvyakov N.V., Slonimskaya E.M., Cherdyntseva N.V. // *Diagn Cytopathol.* 2013. V. 41. № 3. P. 279–282.
88. Gerashchenko T.S., Denisov E.V., Litviakov N.V., Zavyalova M.V., Vtorushin S.V., Tsyganov M.M., Perelmuter V.M., Cherdyntseva N.V. // *Biochemistry (Mosc).* 2013. V. 78. № 11. P. 1201–1215.
89. Denisov E.V., Geraschenko T.S., Zavyalova M.V., Litviakov N.V., Tsyganov M.M., Kaigorodova E.V., Slonimskaya E.M., Kzhyshkowska J., Cherdyntseva N.V., Perelmuter V.M. // *Neoplasma.* 2015. doi: 10.4149/neo\_2015\_041. [Epub ahead of print].
90. Alexander S., Friedl P. // *Trends Mol Med.* 2012. V. 18. № 1. P. 13–26.
91. Goswami S., Wang W., Wyckoff J.B., Condeelis J.S. // *Cancer Res.* 2004. V. 64. № 21. P. 7664–7667.
92. Mallini P., Lennard T., Kirby J., Meeson A. // *Cancer Treat Rev.* 2014. V. 40. № 3. P. 341–348.
93. Chen W.J., Wang H., Tang Y., Liu C.L., Li H.L., Li W.T. // *Chin J Cancer.* 2010. V. 29. № 2. P. 151–157.
94. Li Q.Q., Xu J.D., Wang W.J., Cao X.X., Chen Q., Tang F., Chen Z.Q., Liu X.P., Xu Z.D. // *Clin Cancer Res.* 2009. V. 15. № 8. P. 2657–2665.
95. Zavyalova M.V., Litvyakov N.V., Garbukov E.Y., Vtorushin S.V., Stakheeva M.N., Savenkova O.V., Kritskaya N.G., Perelmuter V.M., Slonimskaya E.M., Cherdyntseva N.V. // *Siberian Journal of Oncology.* 2008. V. 6. P. 30–34.
96. Denisov E.V., Litviakov N.V., Zavyalova M.V., Perelmuter V.M., Vtorushin S.V., Tsyganov M.M., Gerashchenko T.S., Garbukov E.Y., Slonimskaya E.M., Cherdyntseva N.V. // *Sci Rep.* 2014. V. 4. P. 4709.
97. Watanabe S. // *Cancer.* 1954. V. 7. № 2. P. 215–223.
98. Fidler I.J. // *Eur J Cancer.* 1973. V. 9. № 3. P. 223–227.
99. Liotta L.A., Saidel M.G., Kleinerman J. // *Cancer Res.* 1976. V. 36. № 3. P. 889–894.
100. Yu M., Stott S., Toner M., Maheswaran S., Haber D.A. // *J Cell Biol.* 2011. V. 192. № 3. P. 373–382.
101. Greene B.T., Hughes A.D., King M.R. // *Front Oncol.* 2012. V. 2. P. 69.
102. Kusters B., Kats G., Roodink I., Verrijp K., Wesseling P., Ruiter D.J., de Waal R.M., Leenders W.P. // *Oncogene.* 2007. V. 26. № 39. P. 5808–5815.
103. Hou J.M., Krebs M.G., Lancashire L., Sloane R., Backen A., Swain R.K., Priest L.J., Greystoke A., Zhou C., Morris K., et al. // *J Clin Oncol.* 2012. V. 30. № 5. P. 525–532.
104. Tsuji T., Ibaragi S., Shima K., Hu M.G., Katsurano M., Sasaki A., Hu G.F. // *Cancer Res.* 2008. V. 68. № 24. P. 10377–10386.
105. Zavyalova M.V., Perelmuter V.M., Slonimskaya E.M., Vtorushin S.V., Garbukov E.Y., Glushenko S.A. // *Siberian Journal of Oncology.* 2006. V. 1. P. 32–35.
106. Zavyalova M.V., Denisov E.V., Tashireva L.A., Gerashchenko T.S., Litviakov N.V., Skryabin N.A., Vtorushin S.V., Telegina N.S., Slonimskaya E.M., Cherdyntseva N.V., et al. // *BioResearch Open Access.* 2013. V. 2. № 2. P. 148–154.
107. Perelmuter V.M., Zavyalova M.V., Vtorushin S.V., Slonimskaya E.M., Kritskaya N.G., Garbukov E., Litviakov N.V., Stakheeva M.N., Babyshkina N.N., Malinovskaya E.A., et al. // *Adv Gerontol (Russian).* 2008. V. 21. № 4. P. 643–653.

# *Pseudomonas Aeruginosa* Lectins As Targets for Novel Antibacterials

A. V. Grishin<sup>1,2\*</sup>, M. S. Krivozubov<sup>1</sup>, A. S. Karyagina<sup>1,2,3</sup>, A. L. Gintsburg<sup>1</sup>

<sup>1</sup>Gamaleya Research Center of Epidemiology and Microbiology, Gamaleya Str., 18, Moscow, 123098, Russia

<sup>2</sup>Institute of Agricultural Biotechnology, Timiryazevskaya Str., 42, Moscow, 127550, Russia

<sup>3</sup>Belozersky Institute of Physical and Chemical Biology, Lomonosov Moscow State University, Leninskie Gory, 1, bld. 40, Moscow, 119991, Russia

\*E-mail: grishin-a1@yandex.ru

Received 29.09.2014

Revised manuscript received 27.02.2015

Copyright © 2015 Park-media, Ltd. This is an open access article distributed under the Creative Commons Attribution License, which permits unrestricted use, distribution, and reproduction in any medium, provided the original work is properly cited.

**ABSTRACT** *Pseudomonas aeruginosa* is one of the most widespread and troublesome opportunistic pathogens that is capable of colonizing various human tissues and organs and is often resistant to many currently used antibiotics. This resistance is caused by different factors, including the acquisition of specific resistance genes, intrinsic capability to diminish antibiotic penetration into the bacterial cell, and the ability to form biofilms. This situation has prompted the development of novel compounds differing in their mechanism of action from traditional antibiotics that suppress the growth of microorganisms or directly kill bacteria. Instead, these new compounds should decrease the pathogens' ability to colonize and damage human tissues by inhibiting the virulence factors and biofilm formation. The lectins LecA and LecB that bind galactose and fucose, as well as oligo- and polysaccharides containing these sugars, are among the most thoroughly-studied targets for such novel antibacterials. In this review, we summarize the results of experiments highlighting the importance of these proteins for *P. aeruginosa* pathogenicity and provide information on existing lectins inhibitors and their effectiveness in various experimental models. Particular attention is paid to the effects of lectins inhibition in animal models of infection and in clinical practice. We argue that lectins inhibition is a perspective approach to combating *P. aeruginosa*. However, despite the existence of highly effective *in vitro* inhibitors, further experiments are required in order to advance these inhibitors into pre-clinical studies.

**KEYWORDS** *Pseudomonas aeruginosa*, lectin, LecA, LecB, antibiotic resistance, biofilm, inhibitor.

**ABBREVIATIONS** IPTG – isopropyl- $\beta$ -D-thiogalactopyranoside; PQS – *Pseudomonas* quinolone signal; IFN- $\gamma$  – interferon- $\gamma$ ; Le<sup>a</sup>, Le<sup>x</sup> – Lewis oligosaccharides; TNF $\alpha$  – tumor necrosis factor  $\alpha$ ; ITC – isothermal titration calorimetry; ELLA – enzyme-linked lectin assay; SPR – surface plasmon resonance.

## INTRODUCTION

*Pseudomonas aeruginosa* is a widespread bacterium that can have both saprotrophic and parasitic lifestyles. It can colonize virtually every human tissue and cause a number of acute and chronic diseases, including acute pneumonia, bacteriemia, urinary tract infection, external otitis, dermatitis, wound and burn sepsis, keratitis, meningitis, brain abscess, endocarditis, and various bone and joint infections. *P. aeruginosa* is an opportunistic pathogen; it typically affects people with weakened immune systems, being one of the most problematic hospital-acquired pathogens. According to current data, at least 10–15% of all hospital-acquired infections are caused by *P. aeruginosa* [1, 2]. Furthermore, *P. aeruginosa* often colonizes the lungs of patients with cystic fibrosis, the hereditary disease associated with

insufficient chloride canal function and mucus accumulation in lungs, reducing the lung function and the patient's life expectancy [2].

One of the main challenges associated with the therapy of *P. aeruginosa* infections is that the pathogen shows resistance to many antibiotics. Its resistance to antibiotics consists of several aspects. First, the pathogen controls the level of porins and membrane permeability for antibacterials and expresses a large number of efflux pumps involved in the excretion of antibiotic molecules from the cell. Second, *P. aeruginosa*, similar to many other pathogens, can easily acquire specific antibiotic resistance genes (e.g., the genes coding for  $\beta$ -lactamases and aminoglycoside-inactivating enzymes) [2]. Finally, chronic infections caused by *P. aeruginosa* are accompanied by biofilm formation. Bio-

films are organized microbial communities submerged into the extracellular polymer matrix, which consists of polysaccharides, proteins, and DNA synthesized by these microorganisms [3, 4]. Inside biofilm, bacteria become significantly more resistant to unfavorable environmental conditions, as well as to antimicrobial agents and factors of the human immune system [3]. *P. aeruginosa* forms difficult-to-remove biofilms in patients' organs and tissues, as well as on implanted devices and catheters [3, 5]. One of the popular approaches to solving this problem suggests the design of new substances that would either inhibit or inactivate the virulence factors of pathogenic bacteria (toxins, adhesins, effector proteins modulating the metabolism and the immune response of the host organism, secretion systems delivering these proteins to the target site, and factors facilitating communication between the bacteria and biofilm formation) rather than kill the pathogens by inhibiting their biosynthesis [6]. In other words, the strategy consists in disarming rather than killing the pathogen. Resistance to these antiviral compounds is expected to develop in slower fashion, since they will not have a direct effect on bacterial viability but will only affect their ability to infect humans.

The *P. aeruginosa* lectins LecA and LecB are viewed as potential targets for such antiviral compounds. They are soluble proteins binding galactose (LecA) and fucose (LecB) residues both individually and within oligo- and polysaccharides. These proteins are believed to be involved in the attachment of the pathogen to human cells, to be capable of epithelial tissue damage, and to play a crucial role in the formation of *P. aerug-*

*inosa* biofilms, thus acting as key virulence factors. In this review, we have summarized the results of studies focused on the role of lectins LecA and LecB in the pathogenesis and formation of biofilms, described currently known inhibitors of these proteins, and assessed the potential for using these proteins as targets to treat infections caused by *P. aeruginosa*.

#### ***P. AERUGINOSA* LECTINS: GENERAL INFORMATION**

Lectins LecA and LecB (also commonly known as PA-IL and PA-IIL) were isolated from *P. aeruginosa* in the 1970s as proteins capable of agglutinating human and animal erythrocytes [7–9]. Both lectins are small proteins 121 (LecA) and 115 (LecB) amino acid residues in size (12.8 and 11.9 kDa, respectively) [10, 11]. LecA binds *D*-galactose and, with lower affinity, *N*-acetyl-*D*-galactosamine. *L*-fucose exhibits the highest affinity to LecB, but this lectin also binds mannose and a number of other saccharides. Although LecA and LecB have completely different amino acid sequences, their quaternary structures are similar: both lectins form homotetrameric complexes where each monomer has its own ligand-binding site. Thus, a single tetramer can bind four molecules of the corresponding carbohydrate [12, 13] (Fig. 1). In *Pseudomonas* genus, the *lecA* and *lecB* genes are unique to *P. aeruginosa*; however, homologs are found in such bacteria as *Burkholderia* and *Phototrhobdus*.

Regulation of lectins synthesis (mostly for LecA) has been studied rather thoroughly. Synthesis of both lectins is induced when the bacterial culture reaches a stationary phase and is regulated by *rhl* and the Pseu-

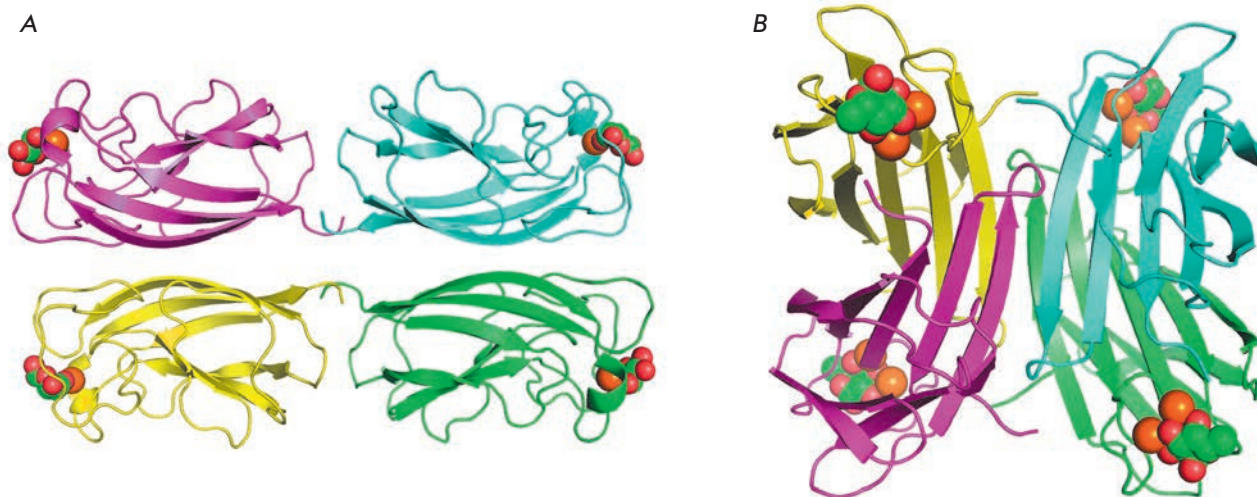


**Fig. 1.** General view of LecA (A) and LecB (B) tetramers. Individual monomers are shown as polypeptide chain trace models of different colors, where flat arrows indicate  $\beta$ -strands. Calcium ions are shown as orange spheres, and lectin-bound galactose and fucose are shown as green (carbon) and red (oxygen) spheres

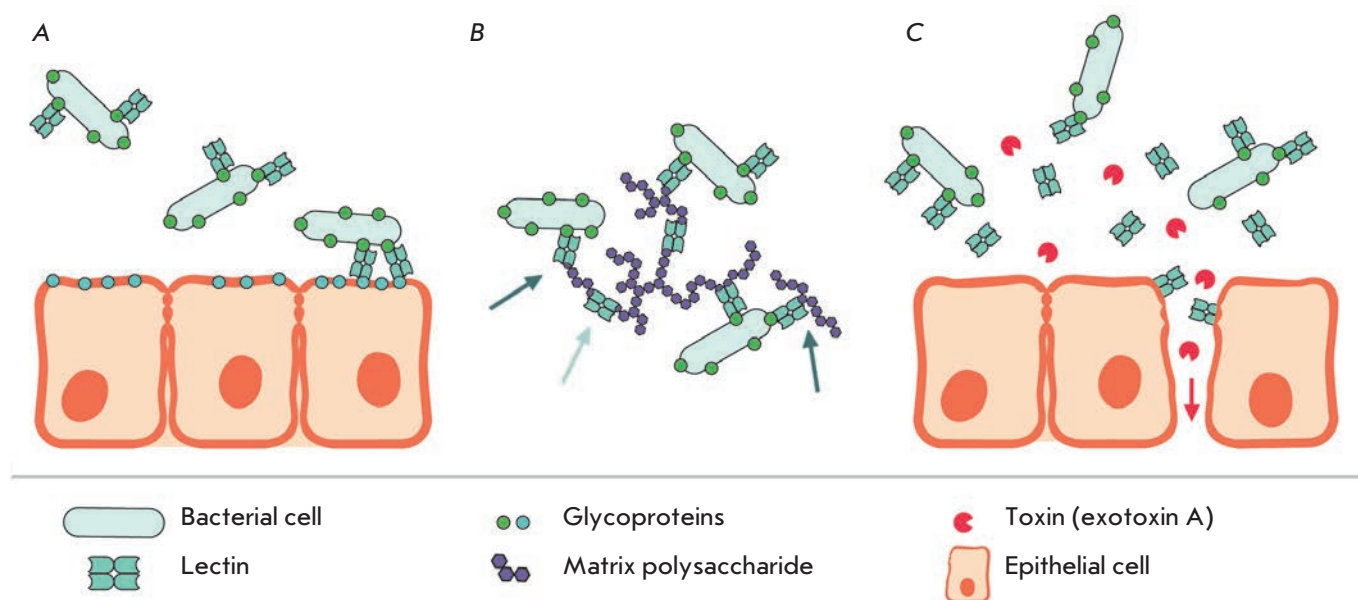


**Fig. 2.** Proposed functions of *P. aeruginosa* lectins: adhesion to host epithelial cells (A); attachment of bacterial cells to biofilm matrix polysaccharides and cross-linking of these polysaccharides (B); disruption of epithelial barrier function and increase in permeability for other virulence factors (C). Light gray arrow indicates cross-linked polysaccharides, dark gray arrows indicate polysaccharides attached to bacteria, red arrow depicts toxins permeation through the disrupted epithelium

domonas quinolone signal (PQS), components of the quorum sensing system [14, 15]. The function of this system is based on the release of low-molecular-weight substances of different natures by these bacteria (in particular, acyl homoserine lactones and quinolones), which allows them to send signals about their presence to other bacteria. That is how bacteria “feel” that a certain population density level has been reached and trigger the expression of virulence factors (such as LasA and LasB proteases, exotoxin A, alkaline protease, etc.) and biofilm formation [16]. The regulation of LecA expression is very similar to the regulation of the synthesis of pyocyanin, an important toxin inducing oxidative stress and damage to the cells of the host organism [14, 15, 17–20]. Interestingly, the level of produced LecA, as well as other virulence factors, increases when the pathogen comes into contact with certain molecules produced by the host organism under stress conditions: noradrenalin, IFN- $\gamma$ , adenosine, and  $\kappa$ -opioid peptide dynorphin [19, 21–23].

*P. aeruginosa* lectins are mostly localized in the cell cytoplasm; a certain amount of them can be found on the outer membrane surface [24, 25]. LecB on the outer membrane surface is most likely bound to fucose residues of glycolipids or glycoproteins [25, 26]. It has been demonstrated that LecB interacts with one of the main outer membrane porins of *P. aeruginosa*

OprF and is not detected on the membrane of bacteria with mutations in the *oprF* gene [26]. However, taking into account the fact that these mutations significantly change the overall properties of the *P. aeruginosa* outer membrane [27], it is not inconceivable that other proteins can also be involved in anchoring LecB to the membrane. As opposed to LecB, localization of LecA remains virtually unstudied.

### ROLE OF LECTINS IN PATHOGENESIS

The role of lectins LecA and LecB in the pathogenesis of the diseases accompanying a *P. aeruginosa* infection is not yet unambiguously determined. Some data demonstrate that these lectins enhance adhesion of the bacteria to the substrate (e.g., human cells), are involved in the aggregation of bacterial cells, biofilm formation, and interaction between a bacterium and the host organism’s tissues, resulting in tissue damage. The presumed role of lectins has been schematically summarized in Fig. 2.

#### Adhesion

LecA and LecB lectins bind the oligosaccharides of many human and mammalian glycoproteins [28–34], thus naturally suggesting that lectins are directly involved in the adhesion of *P. aeruginosa* to human tissues [35]. Adhesion is a crucial stage in pathogenesis.

Adhesion of bacterial cells to the epithelial tissue surface precedes colonization, which may subsequently lead to biofilm formation or pathogen invasion. However, the experimental data on the role of LecA and LecB lectins in *P. aeruginosa* adhesion are controversial. Wentworth *et al.* [36] studied bacterial adhesion to a rabbit corneal epithelium culture. Addition of bacterial cell lysate was shown to increase the amount of adhered intact bacteria; this effect was partially inhibited by addition of galactose, mannose, and fucose. A conclusion was drawn that stimulation of adhesion is associated with the release of lectins from the cytoplasm of the lysed bacterial cells. Binding of bacteria to fibronectin, one of the most common human glycoproteins, was also inhibited by addition of saccharides: to the greatest extent, by adding sialic acid, N-acetylglucosamine and N-acetylgalactosamine and to a lower extent, by adding galactose and fucose [37]. However, as opposed to the previous study, addition of LecA did not increase but reduced the amount of bacterial cells bound to immobilized fibronectin. *P. aeruginosa* strains with mutations in the *lecA* and *lecB* genes retain their ability to bind to mucins (glycoproteins secreted by epithelial cells) [38], while their ability to bind to A549 human lung epithelial cells significantly deteriorates [39, 40]. It was also demonstrated that binding to A549 cells is inhibited in a dose-dependent manner by lectin ligands, methyl- $\beta$ -galactoside and methyl- $\alpha$ -fucoside [40], while binding to immortalized human airway epithelial cells NuLi (derived from a healthy donor) and CuFi (derived from a cystic fibrosis patient) is inhibited by the addition of anti-LecB antibodies, but not control non-specific antibodies [41]. Contrariwise, Eierhoff *et al.* [42] demonstrated that interaction between lectin LecA and globotriaosilceramide (Gb3) is required for the invasion of *P. aeruginosa* inside H1299 human lung epithelial cells and inside artificial vesicles but plays no role in adhesion. Bacteria with mutation in the *lecA* gene bind to H1299 cells and artificial vesicles with the same efficiency as wild-type bacteria do. These contradictions probably arose from the fact that different substrates were used to study adhesion (isolated glycoproteins, epithelial cells of different origin) and on whether lectins had an effect on the binding to a certain substrate or did not depend on the range of oligosaccharides present on the substrate surface.

It should also be mentioned that in addition to lectins, *P. aeruginosa* adhesion to the cells of a host organism is also ensured by other factors, such as flagella and type IV pili [43, 44]. It is rather difficult to distinguish between the effects arising from the presence of different adhesins. Furthermore, it is known that functional LecB is required to ensure normal assembly of *P. aeruginosa* pili and secretion of certain proteins [38].

Hence, although *P. aeruginosa* lectins play a crucial role in binding the pathogen to certain types of human cells, the mechanism underlying this process has not been fully elucidated; its role in *in vivo* infection remains uncertain; and the contribution of lectins in it can be either direct (interaction with glycan structures on the cell surface) or indirect (involvement in assembly, secretion, and functioning of other adhesins, such as type IV pili).

### Biofilms

Both lectins are involved not only in adhesion, but also in the formation of *P. aeruginosa* biofilms. Independent research groups have used different experimental models to demonstrate that *P. aeruginosa* strains with mutations in the *lecA* and *lecB* genes form poorly developed biofilms without the well-defined architecture that is typical of the biofilms of wild-type strains [25, 38, 45, 46]. Furthermore, addition of isopropyl- $\beta$ -D-thiogalactopyranoside (IPTG) or nitrophenylgalactoside (galactose derivatives capable of binding to LecA with a higher affinity than galactose) when *P. aeruginosa* biofilms were grown on steel coupons inhibited biofilm formation to the level of the *lecA* mutant (the surface area of the biofilm was twice as low compared to that of wild-type biofilms grown without IPTG), while addition of galactosides to the already formed biofilms resulted in their dispersal. It is noteworthy that galactosides affected neither formation nor dispersal of the biofilm formed by the strain with a mutation in the *lecA* gene [45]. Identically, biofilms formed by *P. aeruginosa* with mutations in the *lecB* gene on cover slips were much thinner and had a smaller surface area than the wild-type biofilms [25, 46]. Similar to galactosides, LecB ligand nitrophenylfucoside prevented biofilm formation and partially dispersed wild-type biofilms but not those of *lecB* mutant. It is an interesting fact that nitrophenylfucoside inhibited biofilm formation not only by the laboratory strain PAO1, but also by three clinical isolates [46].

Unfortunately, although these studies demonstrate that functional lectins genes are needed for the formation of full-fledged biofilms, the direct function of lectins in this process remains unclear. The role of lectins may possibly be associated with the aggregation of bacterial cells and microcolony formation. At least Diggle *et al.* detected no microcolony formation by the *lecA* mutant [45]. LecB lectin is needed for proper assembly of type IV pili, which, in turn, are required for biofilm formation [38]. Lectins may potentially facilitate binding of polysaccharides of the biofilm extracellular matrix to bacterial cells or are required to cross-link individual chains of these polysaccharides. Cross-linking polysaccharide chains by multivalent lectins can po-



tentially facilitate the formation of denser biofilms that would be more resistant to physical impact. Interestingly, the extracellular polysaccharide Psl that is absolutely required for the formation of *P. aeruginosa* biofilms contains mannose and, according to some sources, galactose, which are ligands of lectins LecB and LecA, respectively [47, 48]. Binding of this polysaccharide to bacterial cells is required to initiate the biofilm formation process [49].

### Effect on epithelial cells

The direct effect of lectins on human airway and intestinal epithelial cells was investigated in several studies. It has been demonstrated that addition of LecA significantly slows the growth of nasal polyp epithelial cells and reduces the number of ciliated cells. Furthermore, LecA causes formation of large vacuoles in the cells and, when added at large concentrations, even cell detachment [50]. Incubation with LecA also significantly reduces the ciliary beat frequency [51, 52]. The effect of LecA on the ciliary beat frequency was attenuated by adding *D*-galactose. Ciliary beat was inhibited by LecB, and this effect was attenuated by adding fucose [51–54]. In the norm, movements of airway epithelium ciliated cells facilitate the removal of mucus and foreign particles trapped by it (including bacterial cells) from the lungs. Inhibition of the ciliary function is most likely to be caused by binding of lectins to glycoproteins on the surface of epithelial cells and the response of epithelial cells to this event or directly by cilia cross-linking to one another [51]. However, these effects have been demonstrated only in *in vitro* models and it remains unclear how important they are in an airway infection *in vivo*.

LecA lectin has a negative effect on intestinal epithelium. In particular, addition of LecA to Caco-2 and T-84 cell cultures significantly reduces the transepithelial electrical resistance of the cellular monolayer and increases monolayer permeability for mannite; this effect is attenuated by *N*-acetylgalactosamine [21, 55, 56]. The most likely reason is that lectin disrupts tight intercellular contacts [55]. Increased permeability of intestinal epithelium was observed *in vivo* using a mouse model of intestinal infection [21, 55, 56]. The fatality rate 48 h after LecA, in combination with exotoxin A or elastase, was injected into the cecum of mice previously subjected to 30% partial hepatectomy was 100%. This effect was not observed when LecA, exotoxin A, or elastase was injected as an individual substance. Injection of the clinical isolate of *P. aeruginosa* (but not the mutant incapable of LecA expression) caused a 100% mortality rate. Taking into account that intravenous injection of endotoxin A is fatal to mice, it is most likely that injection of LecA into the cecum renders epithe-

lium permeable to endotoxin A, which enters the blood flow.

### LECTIN LIGANDS AND INHIBITORS

Lectins perform their functions by binding oligo- and polysaccharides, whether they are human or bacterial glycoprotein oligosaccharides or matrix polysaccharides of *P. aeruginosa* biofilms. Specificity of lectins with respect to the saccharides being bound plays the key role in this process.

Lectin LecA preferentially binds to  $\alpha$ -*D*-galactose and oligo- and polysaccharides containing terminal non-reducing residues of  $\alpha$ -*D*-galactose, such as the B, P<sup>k</sup> and P<sub>1</sub> blood group antigens, melibiose and galactobiose, plant-derived galactomannans, etc. [28–30, 57]. Similar to many other lectins, the galactose-binding site of LecA contains a calcium ion bound to protein carboxyl groups via coordination bonds. The galactose molecule is present in the binding site in its most stable <sup>4</sup>C<sub>1</sub> conformation; the O3 and O4 atoms are involved in coordination bonds with an immobilized calcium ion; the O2, O3, and O4 atoms form additional hydrogen bonds with the amino acid residues of the protein; and the O6 atom forms hydrogen bonds with a water molecule that is firmly fixed by two hydrogen bonds in the binding site [12, 58] (*Fig. 3A*). The dissociation constant of the LecA–galactose complex is 88  $\mu$ M [59]. The terminal residue of  $\alpha$ -*D*-galactose plays the key role in binding of oligosaccharides by lectin LecA, while other oligosaccharide residues form few contacts with the protein [31, 58]. In this connection, the oligosaccharide affinity to LecA may vary within a rather narrow range depending on the composition of the oligosaccharide and the details of the glycoside bond connecting the terminal galactose residue to the next residue in the oligosaccharide: the dissociation constants typically vary from 30 to 130  $\mu$ M [31, 58]. In addition to  $\alpha$ -*D*-galactose, LecA can also bind *N*-acetyl-*D*-galactosamine (although with lower affinity) [7, 60], as well as adenine and acyl-homoserine lactones; however, an independent binding site is involved in the latter interaction [61, 62].

LecB has a broader specificity and higher affinity to its ligands. It can bind *L*-fucose and *L*-fucosylamine, *L*-galactose, *D*-arabinose, *D*-mannose, and *D*-fructose [63–65]. The dissociation constant of the LecB–*L*-fucose complex is 2.9  $\mu$ M; its interaction with other saccharides is weaker [65]. The reason for such high affinity for lectin is that there are two immobilized calcium ions in the LecB ligand-binding site; coordination interactions with these ions determine binding between saccharides and LecB (*Fig. 3B*). The optimal arrangement of the saccharide hydroxyl groups for coordinating two calcium ions by LecB corresponds to two hydrox-

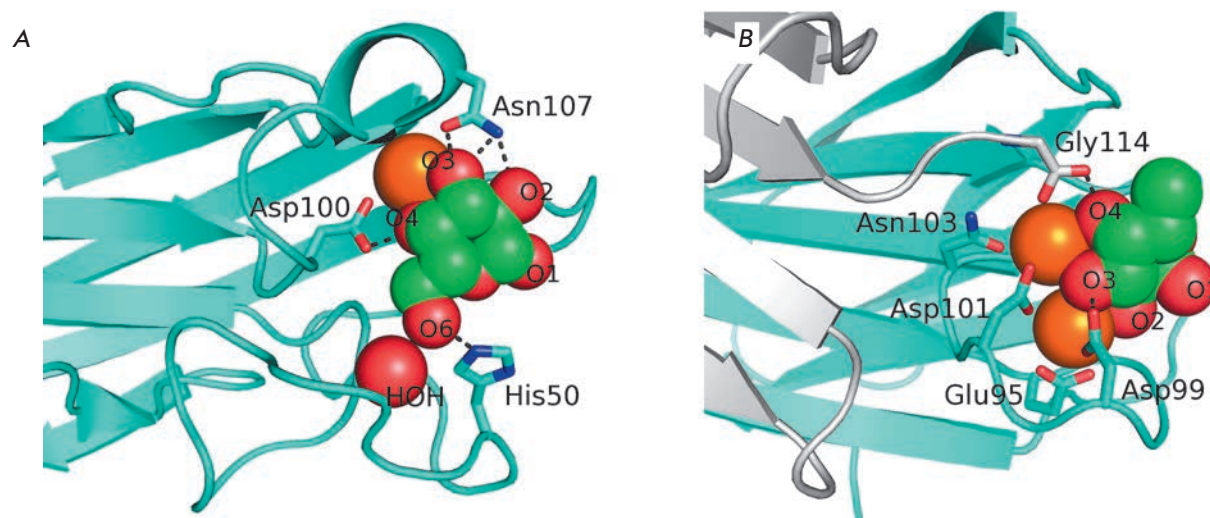


**Fig. 3.** Detailed view of LecA (A) and LecB (B) sugar-binding sites. Lectins are shown as polypeptide chain trace models, where flat arrows indicate  $\beta$ -strands. Calcium ions are shown as orange spheres, and lectin-bound galactose and fucose are shown as green (carbon) and red (oxygen) spheres. The water molecule involved in galactose binding by LecA is shown as a red sphere, and the side chains of certain amino acid residues involved in sugar binding or calcium coordination are shown as sticks. Black dotted lines depict hydrogen bonds between the sugars and side chains of amino acid residues. The additional monomer of LecB is shown in gray (B); C-terminal glycine of this monomer is involved in the formation of the sugar-binding site of the neighboring monomer

yl groups in the equatorial position and one hydroxyl group in the axial position. This fact makes a landmark contribution to LecB specificity: all the saccharides bound by LecB have this arrangement of hydroxyl groups in their most energetically favorable conformations [63, 65]. Like LecA, LecB interacts with oligosaccharides having terminal non-reducing residues of the corresponding monosaccharides, in particular *L*-fucose. It has been demonstrated that LecB can bind oligosaccharides of the A, B, H, Le<sup>a</sup> and Le<sup>x</sup> blood groups [28, 32, 66, 67]. The terminal fucose residue makes the main contribution to the energy of interaction between the oligosaccharides and LecB, although the oligosaccharide affinities can be increased 14-fold compared to that of fucose due to the composition and positions of other monosaccharide residues, which has been demonstrated for Le<sup>a</sup> [32].

A large number of various LecA and LecB inhibitors have been proposed over the past decade. Except for glycomimetic peptides [52], all of them contain residues of the corresponding saccharides as affine groups. These inhibitors include monosaccharide derivatives, multivalent glycoclusters and dendrimers of different chemical nature, and natural glycoproteins and polysaccharides.

#### Monovalent monosaccharide derivatives

Many monosaccharide derivatives bind to *P. aeruginosa* lectins with a higher affinity than the original

saccharides do. For example, even small hydrophobic substituents at the first oxygen atom increase the affinity of the corresponding saccharides both to LecA and LecB. The dissociation constant of the LecA–IPTG complex is almost threefold lower than that of the LecA–*D*-galactose complex [59, 60], while the dissociation constant of the LecB–methyl- $\alpha$ -*L*-fucoside complex is sevenfold lower than that of the LecB complex with unmodified *L*-fucose [65].

The affinity of galactosides to LecA can be further increased by inserting simple aromatic substituents.  $K_d$  of the complex between LecA and such compounds as phenylgalactopyranoside, *p*-nitrophenylgalactopyranoside (Table, compound 1), *p*-aminophenylgalactopyranoside, *p*-tolylgalactopyranoside, naphthylgalactopyranoside, etc. is 4–15  $\mu$ M (let us remember that the  $K_d$  of unsubstituted *D*-galactose is almost 90  $\mu$ M) [68]. This is associated with the formation of a contact between the hydrogen atom and the  $\epsilon$ -carbon atom of LecA His50 and the aromatic ring  $\pi$ -system (Fig. 4). This interaction is known as the CH- $\pi$  interaction, and its energy is  $\sim$  1 kcal/mol. For the sake of comparison, the energy of interaction between LecA and *D*-galactose is 6.0 kcal/mol. The mechanism of this interaction is similar to that of the hydrogen bond; however, it is not an electronegative atom with an unshared electron pair that acts as a hydrogen acceptor but the aromatic  $\pi$ -electron system [68]. Insertion of aliphatic substituents or aromatic ones separated from galactose by an

aliphatic linker preventing the formation of an CH- $\pi$  interaction provides for a much lower increase in affinity [68–71].

Lectin LecB does not exhibit such a simple dependence. Among monovalent ligands, oligosaccharide Le<sup>a</sup> (Table, compound 2) has the greatest affinity to LecB [32]. The  $K_d$  of the LecB–Le<sup>a</sup> complex is 210 nM, while that of the LecB–fucose complex is 2.9  $\mu$ M. Although several attempts have been made to design ligands that would exhibit higher affinity than Le<sup>a</sup>, this objective has not been achieved. Various derivatives of disaccharide  $\alpha$ -L-Fuc-(1 $\rightarrow$ 4)- $\beta$ -D-GlcNAc – the component of Le<sup>a</sup> – have been characterized by an affinity to LecB identical to that of Le<sup>a</sup>. An analysis of the crystalline structure of the complex has demonstrated that the inserted substituents are not involved in the formation of contacts with the protein [72]. A series of fucosylamides have been designed where the first oxygen atom of fucose is replaced with a nitrogen atom of the amide group carrying different appreciably bulky substituents of non-saccharide nature [73]. All the compounds were bound to LecB with dissociation constants of 0.68–2.1  $\mu$ M, which shows no improvement compared to Le<sup>a</sup> and even methylfucoside. The reason is that the amide group cannot interact with the conservative water molecule that participates in the ligand binding to lectin LecB. Finally, Hauck *et al.* [74] have designed several classes of derivatives of methyl-*D*-mannoside, another saccharide that binds to LecB with an affinity lower than that of LecB binding to fucose ( $K_d = 71 \mu$ M). Some amide and sulfonamide derivatives at the 6<sup>th</sup> position of mannose show a significant increase in affinity. For example,  $K_d$  for one of sulfonamides is 3.3  $\mu$ M. Although this value is 20-fold higher compared to the initial methylmannoside, no improvement compared to fucose and Le<sup>a</sup> was achieved.

Thus, there are no monovalent ligands with an affinity to lectins higher than that of unmodified monosaccharides by more than an order of magnitude. This is one of the reasons why researchers have focused on designing multivalent inhibitors.

### Multivalent compounds

Lectins, irrespective of their origin (plant, animal, or bacterial), typically bind saccharides with an appreciably low affinity [75]. This limitation can be overcome through the multivalence of both lectins and their ligands. Multivalence implies that a single molecule or the molecular complex contains several identical binding sites. For example, lectins can be organized into homomultimeric protein complexes, while glycoproteins (lectin receptors) can carry several identical glycan chains bound by lectins. This multivalence allows one to significantly increase the affinity and specificity of

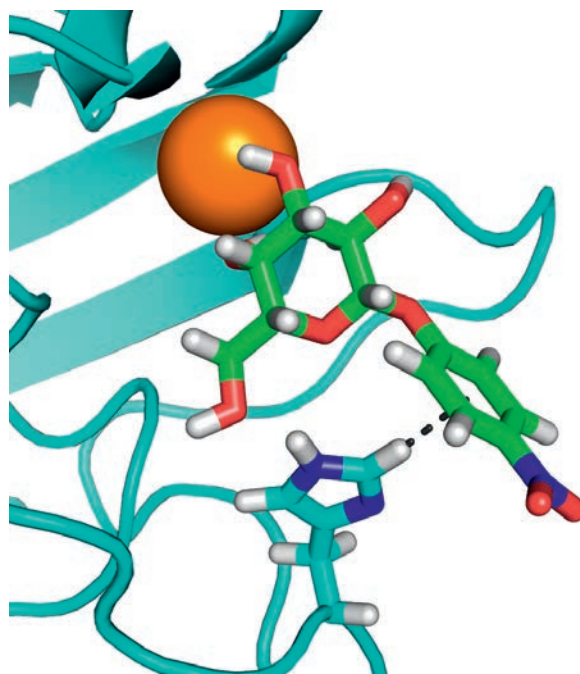


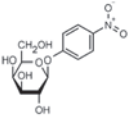
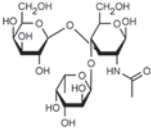
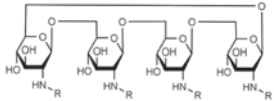
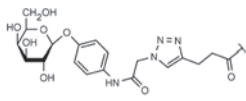
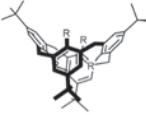
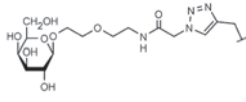
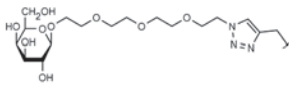
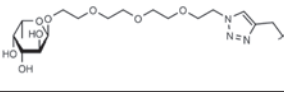
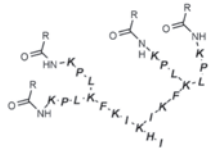
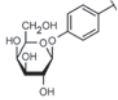
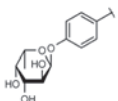
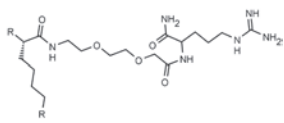
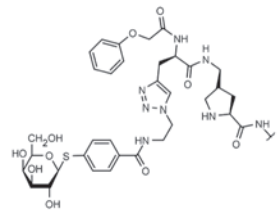
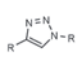
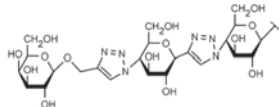
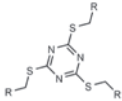
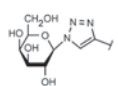
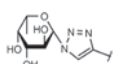
**Fig. 4.** LecA – nitrophenylgalactoside complex. Nitrophenyl-galactoside and side chain of LecA His50 are shown as sticks, and the black dotted line depicts CH- $\pi$  interaction

the interaction between lectins and glycans via several mechanisms. First, in some cases several sites of multivalent lectin can simultaneously bind several epitopes of a multivalent ligand. Such interaction is known as a chelate or bridging interaction. Second, even if simultaneous binding is impossible, the presence of several epitopes that can interact with lectin on a single ligand molecule increases the local concentration of these epitopes. During dissociation of the lectin complex with a single epitope, lectin has a high probability of binding to another identical epitope that is located nearby. This mechanism of ligand entrapment is known as statistical rebinding [76, 77]. These effects have recently been used increasingly often to design multivalent compounds inhibiting the effect of lectins: glycoclusters, glycodendrimers, and glycopolymers [76, 78].

*P. aeruginosa* lectins were no exception. A large number of compounds belonging to different chemical classes, with different valences and different linkers between the saccharide and the core of the multivalent compound, have been designed for both lectins of this pathogen (in particular, for LecA). Glycoclusters based on trithiocyanuric acid [79], calixarenes, and resorcinarenes [40, 70, 80–82]; linear and cyclic  $\beta$ -peptoids, porphyrin [81], fullerenes [83], and cyclooligosaccharides [71]; polyphenylacetylene polymers functional-

REVIEWS

Some of the most effective inhibitors of *P. aeruginosa* lectins

No.	Chemical formula of the matrix (for multivalent compounds)	Chemical formula of the functional group	Lectin target, reference	Valence	Affinity (ITC: $K_d$ ; ELLA: $IC_{50}$ )	Improvement of affinity as compared to monosaccharide (calculated per monosaccharide – shown in parentheses)
1			LecA, [59]	1	ITC: 14.1 $\mu$ M	ITC: 6 (6)
2			LecB, [32]	1	ELLA: 0.51 $\mu$ M; ITC: 0.2 $\mu$ M	ELLA: 12 (12) ITC: 14 (14)
3			LecA, [71]	4	ELLA: 57 nM; ITC: 79 nM	ELLA: 1210 (300) ITC: 1114 (278)
4			LecA, [70]	4	ELLA: 7 $\mu$ M; SPR: 1.0 $\mu$ M; ITC: 90 nM	ELLA: 50 (12) SPR: 58 (14) ITC: 978 (244)
5			LecA, [40,80]	4	SPR: 500 nM ITC: 176 nM	SPR: 143 (35) ITC: 500 (125)
6			LecB, [40]	4	ITC: 48 nM	ITC: 60 (15)
7			LecA, [59]	4	ITC: 0.1 $\mu$ M	ITC: 880 (220)
8			LecB, [46]	4	ELLA: 0.14 $\mu$ M	ELLA: 79 (20)
9			LecA, [91]	2	ITC: 82 nM	ITC: 1073 (537)
10			LecA, [89]	2	Inhibition of FITC-LecA binding, IC50: 2.7 nM; ITC: 28 nM	Inhibition of FITC-LecA binding: 7407 (3703) ITC: 3143 (1572)
11			LecA, [79]	3	ITC: 1.1 $\mu$ M	ITC: 80 (27)
12			LecB, [79]	3	ITC: 50 $\mu$ M	ITC: 0.6 (0.2)

ized with galactose residues and gold nanoparticles [85]; dendrimers of peptide [59, 86] and non-peptide nature [87, 88]; and bivalent compounds [89–91] were proposed for use as multivalent inhibitors of LecA. The LecB inhibitors included synthetic oligomers based on pentaerythrityl phosphodiester [92], dendrimers based on lysins and cyclopeptides [93], those based on *D*- and *L*-oligopeptides [46, 94, 95], glycoclusters based on tri-thiocyanuric acid [79] and calixarenes [40], as well as bi- and trivalent compounds functionalized by disaccharide  $\alpha$ -*L*-Fuc-(1→4)- $\beta$ -*D*-GlcNAc instead of fucose [96].

Many of these compounds are characterized by a significantly increased affinity to the corresponding lectin in isothermal titration calorimetry (ITC) experiments and efficiency in inhibition of lectin binding to immobilized saccharides in enzyme-linked lectin assay (ELLA). For example, the  $K_d$  values of the complexes of LecA with galactosylated glycoclusters based on cyclic oligosaccharides (*table*, compound 3) [71] and calixarenes (*table*, compound 4) [70], oligopeptide dendrimer (*table*, compound 7) [59], and the bivalent ligand selected during screening of a library consisting of 625 compounds (*table*, compound 9) [91] were  $\sim 80$ – $100$  nM, which is almost 1,000-fold lower than the  $K_d$  of galactose. The bivalent ligand where two galactose residues are connected by a rigid linker  $\sim 24$  Å long is characterized by the highest affinity to LecA; its  $K_d$  is 28 nM (*table*, compound 10) [90]. According to the molecular modeling data, all these ligands can bind two monomers of a LecA tetramer, thus providing a chelate effect, which is probably responsible for such a significant increase in affinity. In the LecB tetramer, the distance between the fucose-binding sites in the adjacent monomers is much greater ( $\sim 26$ – $28$  Å in LecA and at least  $35$ – $37$  Å in LecB), and the increase in affinity due to the multivalence in LecB inhibitors is significantly lower.

Despite the great variety of synthesized multivalent compounds, only relatively few studies have focused on their effect on bacterial cells, adhesion, or biofilm formation. Oligopeptide dendrimers are capable of inhibiting biofilm formation. One of these dendrimers, GalAG2 (*table*, compound 7) with four galactose residues, virtually completely inhibits the formation of *P. aeruginosa* biofilms on steel coupons and facilitates the dispersion of already formed biofilms. Unfortunately, attempts to optimize the amino acid sequence of the oligopeptide only slightly improved its ability to disperse the biofilms rather than to inhibit their growth [59, 86]. Similar fucosylated peptide dendrimers were synthesized as LecB inhibitors (*Table*, compound 8) [46, 94]. The tetravalent dendrimer FD2 effectively inhibited biofilm formation by the standard PAO1 strain and by three clinical isolates but not by the strain with a mutation in the *lecB* gene. Similar to GalAG2, it facilitated

the dispersion of already formed biofilms. Tetravalent glycoclusters based on calixarenes functionalized with galactose and fucose (*table*, compounds 5 and 6) proved also capable of inhibiting the formation of *P. aeruginosa* biofilms by PAO1 [40]. Interestingly, these glycoclusters inhibited the biofilm growth not only of the PAO1 strain, but also of the *lecA* and *lecB* gene mutants, thus demonstrating that these compounds can potentially affect other targets as well. These glycoclusters inhibited bacterial adhesion to A549 cells by 70 and 90% (glycosylated and fucosylated glycoclusters, respectively). The inhibition was more significant compared to that observed when the *lecA* or *lecB* genes were inactivated, which also suggests that these compounds may affect other targets. Trivalent glycoclusters based on tri-thiocyanuric acid functionalized either by galactose or by fucose (*table*, compounds 11 and 12) are also capable of inhibiting biofilm formation. Although the affinity of these glycoclusters to the corresponding lectins is significantly lower, their effective concentrations suppressing biofilm formation are the same as those for calixarenes (5 mM). Novoa *et al.* [91] demonstrated that the bivalent LecA ligand (*table*, compound 9) at a concentration of  $0.05$ – $5$   $\mu$ M can prevent the penetration of *P. aeruginosa* inside H1299 cells by 50–80%, although no dose dependence was revealed.

### Natural compounds

The ability to bind *P. aeruginosa* lectins has been revealed not only in chemically synthesized but also in many natural compounds. Unfortunately, most of these compounds have not been isolated into components and only a certain degree of assumption can be made regarding the nature of their active components. Furthermore, their ability to interact with lectins has been typically demonstrated only using hemagglutination assay and western blot hybridization, without the use of more reliable quantitative procedures.

Hemagglutination assay and western blot demonstrated that the proteins of pigeon and quail egg whites [97, 98], components of honey and royal jelly [99], human breast milk and milk from some other mammals [66, 100], and extracts from the seeds of some edible plants [101] can interact with *P. aeruginosa* lectins.

Two independent research groups have demonstrated that hemagglutination induced by lectin LecA is inhibited by galactomannans, plant-derived polysaccharides consisting of linear chains of poly-(1→4)-mannose with galactose residues bound to some mannose residues via the 1→6 glycoside bond [57, 102]. Furthermore, galactomannan from guar, rather than oat glucan and some other plant-derived polysaccharides, has inhibited biofilm formation by the clinical isolate of *P. aeru-*

*ginosa* [102]. The action of galactomannan, like that of peptide dendrimers, is probably based on the multivalence effect.

### IN VIVO LECTIN INHIBITION

The positive effect of inhibition of lectins LecA and LecB has been demonstrated both in *in vitro* and *in vivo* experiments: the use of lectin-specific monosaccharides and synthetic inhibitors was studied using animal models of the infection. Furthermore, single cases of using monosaccharides in clinical practice have been reported.

In the aforescribed experiments on a model of intestinal infection in mice subjected to 30% partial hepatectomy,  $10^7$  CFU *P. aeruginosa* injected into the cecum caused 100% fatality, and so did a combination of lectin LecA and exotoxin A. However, 13% N-acetylgalactosamine added to the injection mixture reduced the fatality rate almost to zero in both cases [55]. The effect of the addition of simple saccharides (lectin ligands) was also observed in a mouse model of lung infection [39]. Intratracheal injection of *P. aeruginosa* PAO1 increased the permeability of lung epithelium and resulted in fluid accumulation in the lungs and bacterial dissemination in the organism. Infection with strains with mutations in the *lecA* or *lecB* genes had a much smaller effect on lung permeability and caused lower bacterial dissemination both in the lungs and blood of the infected mice, although their survival rates remained the same compared to mice infected with the wild-type strain. The addition of saccharides binding to LecA (N-acetylgalactosamine and methyl- $\alpha$ -galactoside) or LecB (methyl- $\alpha$ -fucoside) at concentrations of 15–50 mM, but not glucose, reduced the negative effects caused by the injection of bacteria and bacterial dissemination in the lungs and blood. Furthermore, methyl- $\alpha$ -galactose and N-acetylgalactosamine led to a better survival rate among the infected mice. The effectiveness of synthetic lectins inhibitors, tetravalent galactosylated, and fucosylated calixarene-based glycoclusters (table, compounds 5 and 6) was studied in the same model of acute lung infection in mice [40]. As might have been expected, glycoclusters showed much higher effectiveness both in retaining the lung barrier function and in reducing the bacterial dissemination in the lungs and spleen compared to monosaccharides at same concentrations (1–5 mM). Lung permeability for labeled albumin after glycoclusters had been added was the same as after the injection of strains with mutations in the lectin genes [39]; the bacterial dissemination in lungs and spleen decreased by 1–3 orders of magnitude. The fucosylated glycocluster was more effective. Unfortunately, no data on the survival rate were available.

Several cases in which saccharide solutions were used to treat a *P. aeruginosa* infection in humans have also been reported. Steuer *et al.* [103] demonstrated the effectiveness of using D-galactose, D-mannose, and sialic acid solutions to treat external otitis caused by infection with *P. aeruginosa*, although in this case the effect could have been due to inhibition of some other adhesins besides lectins. A case of successful treatment of the upper airway infection in a child subjected to chemotherapy has also been reported [104]. The infection was resistant to antibiotics, while inhalation of galactose and fucose solutions resulted in the complete elimination of the pathogen. Finally, Hauber *et al.* studied inhalation of solutions of these saccharides to treat cystic fibrosis patients whose lungs were chronically colonized by *P. aeruginosa* [105]. A twice-daily inhalation of the saccharide solution for 21 days significantly reduced bacterial counts in the patients' sputum and inhibited TNF $\alpha$  expression. Unfortunately, no statistically significant improvement in lung function was observed, which was related to the insufficient sample size.

Although the effect of using monosaccharides in the aforementioned studies was often rather small, recent data have demonstrated that these limitations can be potentially overcome by using multivalent compounds. The results of these studies have convincingly confirmed that positive results can be achieved *in vivo* by inhibition of *P. aeruginosa* lectins.

### CONCLUSIONS

Lectins LecA and LecB seem to be among the virulence factors of *P. aeruginosa*: they contribute to the ability of this organism to colonize human tissues and organs and persist in them as biofilms, thus causing hard-to-treat chronic diseases. Both lectins affect bacteria's ability to attach to epithelial human cells, are the key components of bacterial biofilms, and can inhibit the ciliary movement and disturb the barrier function of epithelial tissue. Unfortunately, it remains unclear how important each of these lectin functions in *in vivo* infection is. Taking into account the fact that lectin specificity differs, it cannot be ruled out that *P. aeruginosa* LecA and LecB play different roles in the infection of a human organism. However, regardless of the nature of lectins function, the use of corresponding monosaccharides and multivalent glycoclusters in animal models of a *P. aeruginosa* infection has reliably demonstrated the positive effect of the inhibition of both lectins, which has also been confirmed by clinical data.

Among the variety of lectin inhibitors, the most promising ones are those where the multivalence effect is used to achieve a higher affinity to their targets. This is partially related to the multivalence of lectins: com-

pounds bearing several affine groups can simultaneously bind two monomers from a single tetramer. The molecular modeling method has demonstrated that some compounds potentially possess this ability. It was found that some classes of multivalent compounds can inhibit the development of *P. aeruginosa* biofilms and/or impede bacterial adhesion to epithelial cells. The positive effect of tetravalent calixarene-based glyco-clusters in an *in vivo* acute model of lung infection was also demonstrated.

Most multivalent lectin inhibitors are synthetic glycodendrimers and glycoclusters. The cost intensity and complexity of synthesizing many of them can be a significant obstacle in further advancement towards pre-clinical and especially clinical trials. Furthermore, there is a high risk of adverse toxic effects and non-optimal pharmacokinetic properties. In this regard, natural neutral polysaccharides, such as the galactomannan or oligosaccharides produced by their hydrolysis, seem to

have a higher potential. Plant-derived galactomannans are widely used in the food industry, are safe, and exceptionally inexpensive. However, the effectiveness of natural polysaccharides, as well as most synthetic glyco-clusters and glycodendrimers, is yet to be confirmed using animal models of infection. We believe that, taking into account the encouraging results achieved in experiments with calixarenes, the highest priority objective is to further verify the effectiveness of natural and synthetic multivalent compounds (and probably their combinations with conventional antibiotics) *in vivo* in various models of infection. ●

*The authors are grateful to Vera Gusakova for her assistance in preparing illustrations for the manuscript and Anna Ershova for meticulous proofreading and valuable comments.*

*This work was supported in part by the RF President's grant "Leading Scientific Schools" (NSh-2038.2014.7).*

#### REFERENCES

- Blanc D.S., Petignat C., Janin B., Bille J., Francioli P. // Clin. Microbiol. Infect. 1998. V. 4. № 5. P. 242–247.
- Mesaros N., Nordmann P., Plésiat P., Roussel-Delvallez M., van Eldere J., Glupczynski Y., van Laethem Y., Jacobs F., Lebecque P., Malroot A., et al. // Clin. Microbiol. Infect. 2007. V. 13. № 6. P. 560–578.
- Donlan R.M., Costerton J.W. // Clin. Microbiol. Rev. 2002. V. 15. № 2. P. 167–193.
- Hall-Stoodley L., Costerton J.W., Stoodley P. // Nat. Rev. Microbiol. 2004. V. 2. № 2. P. 95–108.
- Costerton J.W. // Science. 1999. V. 284. № 5418. P. 1318–1322.
- Clatworthy A.E., Pierson E., Hung D.T. // Nat. Chem. Biol. 2007. V. 3. № 9. P. 541–548.
- Gilboa-Garber N. // FEBS Lett. 1972. V. 20. № 2. P. 242–244.
- Gilboa-Garber N., Mizrahi L., Garber N. // Can. J. Biochem. 1977. V. 55. № 9. P. 975–981.
- Gilboa-Garber N. // Methods Enzymol. 1982. V. 83. № 1980. P. 378–385.
- Avichezer D., Katcoff D.J., Garber N.C., Gilboa-Garber N. // J. Biol. Chem. 1992. V. 267. № 32. P. 23023–23027.
- Gilboa-Garber N., Katcoff D.J., Garber N.C. // FEMS Immunol. Med. Microbiol. 2000. V. 29. P. 53–57.
- Cioci G., Mitchell E.P., Gautier C., Wimmerová M., Sudakevitz D., Pérez S., Gilboa-Garber N., Imberty A. // FEBS Lett. 2003. V. 555. № 2. P. 297–301.
- Mitchell E., Houles C., Sudakevitz D., Wimmerova M., Gautier C., Pérez S., Wu A.M., Gilboa-Garber N., Imberty A. // Nat. Struct. Biol. 2002. V. 9. № 12. P. 918–921.
- Winzer K., Falconer C., Garber N.C., Diggle S.P., Camara M., Williams P. // J. Bacteriol. 2000. V. 182. № 22. P. 6401–6411.
- Diggle S.P., Winzer K., Chhabra S.R., Worrall K.E., Cámara M., Williams P. // Mol. Microbiol. 2003. V. 50. № 1. P. 29–43.
- Bjarnsholt T., Tolker-Nielsen T., Høiby N., Givskov M. // Expert Rev. Mol. Med. 2010. V. 12. e11.
- Pessi G., Williams F., Hindle Z., Heurlier K., Holden M.T., Cámara M., Haas D., Williams P. // J. Bacteriol. 2001. V. 183. № 22. P. 6676–6683.
- Diggle S.P., Winzer K., Lazdunski A., Williams P., Camara M. // J. Bacteriol. 2002. V. 184. № 10. P. 2576–2586.
- Wu L., Estrada O., Zaborina O., Bains M., Shen L., Kohler J.E., Patel N., Musch M.W., Chang E.B., Fu Y.-X., et al. // Science. 2005. V. 309. № 5735. P. 774–777.
- Kipnis E., Sawa T., Wiener-Kronish J. // Médecine Mal. Infect. 2006. V. 36. № 2. P. 78–91.
- Alverdy J., Holbrook C., Rocha F., Seiden L., Wu R.L., Musch M., Chang E., Ohman D., Suh S. // Ann. Surg. 2000. V. 232. № 4. P. 480–489.
- Kohler J.E., Zaborina O., Wu L., Wang Y., Bethel C., Chen Y., Shapiro J., Turner J.R., Alverdy J.C. // Am. J. Physiol. Gastrointest. Liver Physiol. 2005. V. 288. № 5. P. G1048–1054.
- Zaborina O., Lepine F., Xiao G., Valuckaite V., Chen Y., Li T., Ciancio M., Zaborin A., Petroff E.O., Petroff E., et al. // PLoS Pathog. 2007. V. 3. № 3. e35.
- Glick J., Garber N. // J. Gen. Microbiol. 1983. V. 129. № 10. P. 3085–3090.
- Tielker D., Hacker S., Loris R., Strathmann M., Wingen-der J., Wilhelm S., Rosenau F., Jaeger K.-E. // Microbiology. 2005. V. 151. Pt 5. P. 1313–1323.
- Funken H., Bartels K.-M., Wilhelm S., Brocker M., Bott M., Bains M., Hancock R.E.W., Rosenau F., Jaeger K.-E. // PLoS One. 2012. V. 7. № 10. e46857.
- Fito-Boncompte L., Chapalain A., Bouffartigues E., Chaker H., Lesouhaitier O., Gicquel G., Bazire A., Madi A., Conil N., Véron W., et al. // Infect. Immun. 2011. V. 79. № 3. P. 1176–1186.
- Gilboa-Garber N., Sudakevitz D., Sheffi M., Sela R., Lev-ene C. // Glycoconj. J. 1994. V. 11. № 5. P. 414–417.
- Lanne B., Čiopruga J., Bergström J., Motas C., Karlsson K.A. // Glycoconj. J. 1994. V. 11. № 4. P. 292–298.

30. Chen C.P., Song S.C., Gilboa-Garber N., Chang K.S., Wu A.M. // *Glycobiology*. 1998. V. 8. № 1. P. 7–16.
31. Blanchard B., Nurisso A., Hollville E., Tétaud C., Wiels J., Pokorná M., Wimmerová M., Varrot A., Imberty A. // *J. Mol. Biol.* 2008. V. 383. № 4. P. 837–853.
32. Perret S., Sabin C., Dumon C., Pokorná M., Gautier C., Galanina O., Ilia S., Bovin N., Nicaise M., Desmadril M., et al. // *Biochem. J.* 2005. V. 389. Pt 2. P. 325–332.
33. Kirkeby S., Hansen A.K., d'Apice A., Moe D. // *Microb. Pathog.* 2006. V. 40. № 5. P. 191–197.
34. Kirkeby S., Wimmerová M., Moe D., Hansen A.K. // *Microbes Infect.* 2007. V. 9. № 5. P. 566–573.
35. Imberty A., Wimmerová M., Mitchell E.P., Gilboa-Garber N. // *Microbes Infect.* 2004. V. 6. № 2. P. 221–228.
36. Wentworth J.S., Austin F.E., Garber N., Gilboa-Garber N., Paterson C.A., Doyle R.J. // *Biofouling*. 1991. V. 4. № 1–3. P. 99–104.
37. Rebiere-Huët J., Di Martino P., Hulen C. // *Can. J. Microbiol.* 2004. V. 50. № 5. P. 303–312.
38. Sonawane A., Jyot J., Ramphal R. // *Infect. Immun.* 2006. V. 74. № 12. P. 7035–7039.
39. Chemani C., Imberty A., de Bentzmann S., Pierre M., Wimmerová M., Guery B.P., Faure K. // *Infect. Immun.* 2009. V. 77. № 5. P. 2065–2075.
40. Boukerb A.M., Rousset A., Galanos N., Méar J.-B., Thépaut M., Grandjean T., Gillon E., Cecioni S., Abderrahmen C., Faure K., et al. // *J. Med. Chem.* 2014. V. 57. № 24. P. 10275–10289.
41. Nosková L., Kubíčková B., Vašková L., Bláhová B., Wimmerová M., Stiborová M., Hodek P. // *Sensors*. 2015. V. 15. № 1. P. 1945–1953.
42. Eierhoff T., Bastian B., Thuenauer R., Madl J., Audfray A., Aigal S., Juillot S., Rydell G.E., Müller S., de Bentzmann S., et al. // *Proc. Natl. Acad. Sci. USA*. 2014. V. 111. № 35. P. 12895–12900.
43. Scharfman A., Arora S.K., Delmotte P., van Brussel E., Mazurier J., Ramphal R., Roussel P. // *Infect. Immun.* 2001. V. 69. № 9. P. 5243–5248.
44. Hahn H.P. // *Gene*. 1997. V. 192. № 1. P. 99–108.
45. Diggle S.P., Stacey R.E., Dodd C., Cámara M., Williams P., Winzer K. // *Environ. Microbiol.* 2006. V. 8. № 6. P. 1095–1104.
46. Johansson E.M.V., Cruz S.A., Kolomiets E., Buts L., Kadam R.U., Cacciarini M., Bartels K.-M., Diggle S.P., Cámara M., Williams P., et al. // *Chem. Biol.* 2008. V. 15. № 12. P. 1249–1257.
47. Ma L., Lu H., Sprinkle A., Parsek M.R., Wozniak D.J. // *J. Bacteriol.* 2007. V. 189. № 22. P. 8353–8356.
48. Byrd M.S., Sadovskaya I., Vinogradov E., Lu H., Sprinkle A.B., Richardson S.H., Ma L., Ralston B., Parsek M.R., Anderson E.M., et al. // *Mol. Microbiol.* 2009. V. 73. № 4. P. 622–638.
49. Ma L., Conover M., Lu H., Parsek M.R., Bayles K., Wozniak D.J. // *PLoS Pathog.* 2009. V. 5. № 3. e1000354.
50. Bajolet-Laudinat O., Girod-De Bentzmann S.G., Tournier J.M., Madoulet C., Plotkowski M.C., Chippaux C., Puchelle E. // *Infect. Immun.* 1994. V. 62. № 10. P. 4481–4487.
51. Mewe M., Tielker D., Schönberg R., Schachner M., Jaeger K.-E., Schumacher U. // *J. Laryngol. Otol.* 2005. V. 119. № 8. P. 595–599.
52. Gustke H., Kleene R., Loers G., Nehmann N., Jaehne M., Bartels K.-M., Jaeger K.-E., Schachner M., Schumacher U. // *Eur. J. Clin. Microbiol. Infect. Dis.* 2012. V. 31. № 2. P. 207–215.
53. Adam E.C., Mitchell B.S., Schumacher D.U., Grant G., Schumacher U. // *Am. J. Respir. Crit. Care Med.* 1997. V. 155. № 6. P. 2102–2104.
54. Adam E.C., Schumacher D.U., Schumacher U. // *J. Laryngol. Otol.* 1997. V. 111. № 8. P. 760–762.
55. Laughlin R.S., Musch M.W., Hollbrook C.J., Rocha F.M., Chang E.B., Alverdy J.C. // *Ann. Surg.* 2000. V. 232. № 1. P. 133–142.
56. Wu L., Holbrook C., Zaborina O., Ploplys E., Rocha F., Pelham D., Chang E., Musch M., Alverdy J. // *Ann. Surg.* 2003. V. 238. № 5. P. 754–764.
57. Zinger-Yosovich K.D., Gilboa-Garber N. // *J. Agric. Food Chem.* 2009. V. 57. № 15. P. 6908–6913.
58. Nurisso A., Blanchard B., Audfray A., Rydner L., Oscarson S., Varrot A., Imberty A. // *J. Biol. Chem.* 2010. V. 285. № 26. P. 20316–20327.
59. Kadam R.U., Bergmann M., Hurley M., Garg D., Cacciarini M., Swiderska M.A., Nativi C., Sattler M., Smyth A.R., Williams P., et al. // *Angew. Chem. Int. Ed. Engl.* 2011. V. 50. № 45. P. 10631–10635.
60. Garber N., Guempel U., Belz A., Gilboa-Garber N., Doyle R.J. // *Biochim. Biophys. Acta.* 1992. V. 1116. № 3. P. 331–333.
61. Stoitsova S.R., Boteva R.N., Doyle R. // *Biochim. Biophys. Acta – Gen. Subj.* 2003. V. 1619. № 2. P. 213–219.
62. Boteva R.N., Bogoeva V.P., Stoitsova S.R. // *Biochim. Biophys. Acta.* 2005. V. 1747. № 2. P. 143–149.
63. Loris R., Tielker D., Jaeger K.-E., Wyns L. // *J. Mol. Biol.* 2003. V. 331. № 4. P. 861–870.
64. Garber N., Guempel U., Gilboa-Garber N., Doyle R. // *FEMS Microbiol. Lett.* 1987. V. 48. № 3. P. 331–334.
65. Sabin C., Mitchell E.P., Pokorná M., Gautier C., Utille J.-P., Wimmerová M., Imberty A. // *FEBS Lett.* 2006. V. 580. № 3. P. 982–987.
66. Lesman-Movshovich E., Lerrer B., Gilboa-Garber N. // *Can. J. Microbiol.* 2003. V. 49. № 3. P. 230–235.
67. Wu A.M., Wu J.H., Singh T., Liu J.-H., Tsai M.-S., Gilboa-Garber N. // *Biochimie.* 2006. V. 88. № 10. P. 1479–1492.
68. Kadam R.U., Garg D., Schwartz J., Visini R., Sattler M., Stocker A., Darbre T., Raymond J.-L. // *ACS Chem. Biol.* 2013. V. 8. № 9. P. 1925–1930.
69. Rodrigue J., Ganne G., Blanchard B., Saucier C., Giguère D., Shiao T.C., Varrot A., Imberty A., Roy R. // *Org. Biomol. Chem.* 2013. V. 11. № 40. P. 6906–6918.
70. Cecioni S., Praly J.-P., Matthews S.E., Wimmerová M., Imberty A., Vidal S. // *Chemistry*. 2012. V. 18. № 20. P. 6250–6263.
71. Gening M.L., Titov D.V., Cecioni S., Audfray A., Gerbst A.G., Tsvetkov Y.E., Krylov V.B., Imberty A., Nifantiev N.E., Vidal S. // *Chemistry*. 2013. V. 19. № 28. P. 9272–9285.
72. Marotte K., Sabin C., Prévile C., Moumé-Pymbock M., Wimmerová M., Mitchell E.P., Imberty A., Roy R. // *ChemMedChem.* 2007. V. 2. № 9. P. 1328–1338.
73. Andreini M., Anderlüh M., Audfray A., Bernardi A., Imberty A. // *Carbohydr. Res.* 2010. V. 345. № 10. P. 1400–1407.
74. Hauck D., Joachim I., Frommeyer B., Varrot A., Philipp B., Möller H.M., Imberty A., Exner T.E., Titz A. // *ACS Chem. Biol.* 2013. V. 8. № 8. P. 1775–1784.
75. Dam T.K., Brewer C.F. // *Chem. Rev.* 2002. V. 102. № 2. P. 387–429.
76. Wittmann V., Pieters R.J. // *Chem. Soc. Rev.* 2013. V. 42. № 10. P. 4492–4503.
77. Dam T.K., Brewer C.F. // *Adv. Carbohydr. Chem. Biochem.* 2010. V. 63. № 10. P. 139–164.
78. Imberty A., Chabre Y.M., Roy R. // *Chemistry*. 2008. V. 14. № 25. P. 7490–7499.



## REVIEWS

79. Smadhi M., de Bentzmann S., Imberty A., Gingras M., Abderrahim R., Goekjian P.G. // *Beilstein J. Org. Chem.* 2014. V. 10. P. 1981–1990.
80. Cecioni S., Lalor R., Blanchard B., Praly J.-P., Imberty A., Matthews S.E., Vidal S. // *Chemistry*. 2009. V. 15. № 47. P. 13232–13240.
81. Cecioni S., Faure S., Darbost U., Bonnamour I., Parrot-Lopez H., Roy O., Taillefumier C., Wimmerová M., Praly J.-P., Imberty A., et al. // *Chemistry*. 2011. V. 17. № 7. P. 2146–2159.
82. Soomro Z.H., Cecioni S., Blanchard H., Praly J.-P., Imberty A., Vidal S., Matthews S.E. // *Org. Biomol. Chem.* 2011. V. 9. № 19. P. 6587–6597.
83. Cecioni S., Oerthel V., Iehl J., Holler M., Goyard D., Praly J.-P., Imberty A., Nierengarten J.-F., Vidal S. // *Chemistry*. 2011. V. 17. № 11. P. 3252–3261.
84. Otsuka I., Blanchard B., Borsali R., Imberty A., Kakuchi T. // *ChemBioChem*. 2010. V. 11. № 17. P. 2399–2408.
85. Reynolds M., Marradi M., Imberty A., Penadés S., Pérez S. // *Chemistry*. 2012. V. 18. № 14. P. 4264–4273.
86. Kadam R.U., Bergmann M., Garg D., Gabrieli G., Stocker A., Darbre T., Reymond J.-L. // *Chemistry*. 2013. V. 19. № 50. P. 17054–17063.
87. Chabre Y.M., Giguère D., Blanchard B., Rodrigue J., Rocheleau S., Neault M., Rauthu S., Papadopoulos A., Arnold A.A., Imberty A., et al. // *Chemistry*. 2011. V. 17. № 23. P. 6545–6562.
88. Gerland B., Goudot A., Ligeour C., Pourceau G., Meyer A., Vidal S., Gehin T., Vidal O., Souteyrand E., Vasseur J.J., et al. // *Bioconjug. Chem.* 2014. V. 25. P. 379–392.
89. Pertici F., Pieters R.J. // *Chem. Commun. (Camb.)*. 2012. V. 48. № 33. P. 4008–4010.
90. Pertici F., de Mol N.J., Kemmink J., Pieters R.J. // *Chemistry*. 2013. V. 19. № 50. P. 16923–16927.
91. Novoa A., Eierhoff T., Topin J., Varrot A., Barluenga S., Imberty A., Römer W., Winssinger N. // *Angew. Chem. Int. Ed. Engl.* 2014. V. 53. № 34. P. 8885–8889.
92. Morvan F., Meyer A., Jochum A., Sabin C., Chevolut Y., Imberty A., Praly J.-P., Vasseur J.-J., Souteyrand E., Vidal S. // *Bioconjug. Chem.* 2007. V. 18. № 5. P. 1637–1643.
93. Berthet N., Thomas B., Bossu I., Dufour E., Gillon E., Garcia J., Spinelli N., Imberty A., Dumy P., Renaudet O. // *Bioconjug. Chem.* 2013. V. 24. № 9. P. 1598–1611.
94. Kolomiets E., Swiderska M.A., Kadam R.U., Johansson E.M.V., Jaeger K.-E., Darbre T., Reymond J.-L. // *ChemMedChem*. 2009. V. 4. № 4. P. 562–569.
95. Johansson E.M.V., Kadam R.U., Rispoli G., Crusz S. A., Bartels K.-M., Diggle S.P., Cámara M., Williams P., Jaeger K.-E., Darbre T., et al. // *Med. Chem. Commun.* 2011. V. 2. № 5. P. 418–420.
96. Marotte K., Préville C., Sabin C., Moumé-Pymbock M., Imberty A., Roy R. // *Org. Biomol. Chem.* 2007. V. 5. № 18. P. 2953–2961.
97. Lerrer B., Gilboa-Garber N. // *FEMS Immunol. Med. Microbiol.* 2001. V. 32. № 1. P. 33–36.
98. Lerrer B., Gilboa-Garber N. // *Electrophoresis*. 2002. V. 23. № 1. P. 8–14.
99. Gilboa-Garber N., Zinger-Yosovich K., Lerrer B. // *J. ApiProduct ApiMedical Sci.* 2009. V. 1. № 3. P. 82–89.
100. Zinger-Yosovich K.D., Iluz D., Sudakevitz D., Gilboa-Garber N. // *J. Dairy Sci.* 2010. V. 93. № 2. P. 473–482.
101. Rachmaninov O., Zinger-Yosovich K.D., Gilboa-Garber N. // *Nutr. J.* 2012. V. 11. № 1. P. 10.
102. Grishin A., Karyagina A.S., Tiganova I.G., Dobrynina O.Y., Bolshakova T.N., Boksha I.S., Alexeyeva N.V., Stepanova T.V., Lunin V.G., Chuchalin A.G., et al. // *Int. J. Antimicrob. Agents*. 2013. V. 42. № 5. P. 471–472.
103. Steuer M.K., Herbst H., Beuth J., Steuer M., Pulverer G., Matthias R. // *Oto-Rhino-Laryngologia Nov.* 1993. V. 3. № 1. P. 19–25.
104. von Bismarck P., Schneppenheim R., Schumacher U. // *Klin. Pädiatrie*. 2001. V. 213. № 5. P. 285–287.
105. Hauber H.-P., Schulz M., Pforte A., Mack D., Zabel P., Schumacher U. // *Int. J. Med. Sci.* 2008. V. 5. № 6. P. 371–376.

# NeuN As a Neuronal Nuclear Antigen and Neuron Differentiation Marker

V. V. Gusel'nikova\*, D. E. Korzhevskiy

Federal State Budgetary Scientific Institution "Institute of Experimental Medicine", akad. Pavlov str., 12, St. Petersburg, 197376, Russia

\*E-mail: Guselnicova.Valeriia@yandex.ru

Received 19.01.2015

Copyright © 2015 Park-media, Ltd. This is an open access article distributed under the Creative Commons Attribution License, which permits unrestricted use, distribution, and reproduction in any medium, provided the original work is properly cited.

**ABSTRACT** The NeuN protein is localized in nuclei and perinuclear cytoplasm of most of the neurons in the central nervous system of mammals. Monoclonal antibodies to the NeuN protein have been actively used in the immunohistochemical research of neuronal differentiation to assess the functional state of neurons in norm and pathology for more than 20 years. Recently, NeuN antibodies have begun to be applied in the differential morphological diagnosis of cancer. However, the structure of the protein, which can be revealed by antibodies to NeuN, remained unknown until recently, and the functions of the protein are still not fully clear. In the present mini-review, data on NeuN accumulated so far are summarized and analyzed. Data on the structure and properties of the protein, its isoforms, intracellular localization, and hypothesized functions are reported. The application field of immunocytochemical detection of NeuN in scientific and clinical studies, as well as the difficulties in the interpretation of the obtained experimental data and their possible causes, is described in details.

**KEYWORDS** NeuN nuclear protein, neuron specific marker, neurons.

**ABBREVIATIONS** IHC – immunohistochemical analysis; NeuN – neuronal nuclear protein; shRNA – small hairpin RNA; MAP-2 – microtubule-associated protein 2; GFAP – Glial Fibrillary Acidic Protein; TUNEL – Terminal Deoxynucleotidyl Transferase-Mediated dUTP (2'-Deoxyuridine 5'-Triphosphate) Nick-End Labeling; BrdU – 5-bromo-2'-deoxyuridine.

## INTRODUCTION

Studies of the neural tissue proteome and immunocytochemical studies of nervous system organs have established that neurons contain a number of specific proteins, whose appearance in postmitotic cells is indicative of their neuronal differentiation. Some of these proteins are characteristic of only a number of specific neuronal types. Thus, tyrosine hydroxylase, an enzyme involved in the synthesis of catecholamines, can be detected in the population of catecholaminergic neurons and monoenzyme neurons involved in the synthesis of catecholamines [1, 2], while choline acetyltransferase allows one to label cholinergic neurons [3]. Other specific proteins are present in the vast majority of neurons. One of them is the neuronal nuclear protein NeuN, which is often used as a marker of postmitotic neurons due to some of its properties (primarily nuclear localization) [4–7]. Monoclonal antibodies to the NeuN protein have been actively used in immunohistochemical studies of neuronal differentiation to assess the functional state of neurons in norm and pathology for more than 20 years. Currently, they are also used in the differential morphological diagnosis of cancer [8–10]. However, the structure of the protein, which can be revealed by antibodies to NeuN, remained unknown

until recently, and the functions of this protein remain not entirely clear.

The purpose of our study was to summarize and analyze data on the NeuN protein accumulated to date. Data on the structure and properties of the protein, its isoforms, intracellular localization, and hypothesized functions are reported. The application field of immunocytochemical detection of NeuN in scientific and clinical studies, as well as the difficulties in the interpretation of the obtained experimental data and their possible causes, is described in details.

## NeuN protein expression in nervous system cells

The neuronal nuclear protein (NeuN) was discovered in 1992, when a research team managed to obtain monoclonal antibodies (A60 clone) to this hitherto unknown nuclear protein [11]. Comprehensive immunohistochemical (IHC) analyses have shown that the expression of the NeuN protein throughout the whole ontogeny is exclusively associated with the nervous tissue. This marker has not been detected in tissues other than nervous ones. Moreover, the protein has never been detected in glial cells, which suggests it is a specific neuronal marker. Subsequent studies have shown that anti-NeuN antibodies can identify most types of

neurons in the whole nervous system with rare exceptions. Thus, Cajal-Retzius cells in the neocortex, some cerebellar cells (including Purkinje cells), inferior olive neurons, cells of the inner nuclear layer of the retina,  $\gamma$ -motor neurons in the spinal cord, and ganglion cells of the sympathetic chain are not immunohistochemically stained with antibodies to NeuN. There also exist conflicting reports on the expression of NeuN cells in the substantia nigra cells of the brain [12–14]. The causes behind the lack of NeuN immunoreactivity in certain types of neurons have not been established. For example, inferior olive neurons are believed to share a common origin with neurons in the base of the pons, but the latter demonstrate high NeuN immunoreactivity for almost the entire ontogeny, whereas the inferior olive neurons are NeuN-immunonegative in both the fetal and postnatal life periods [15]. Thus, NeuN immunoreactivity apparently reflects some other side of cell biology, rather than a close relationship in embryonic neurohistogenesis.

It is believed that NeuN emerges during early embryogenesis in postmitotic neuroblasts and remains in differentiating and terminally differentiated neurons throughout the whole subsequent ontogeny. Antibody binding to the NeuN protein is predominantly associated with cell nuclei and, to a lesser extent, with the perinuclear cytoplasm [11]. It was shown that two hypothesized isoforms of the NeuN protein (46 and 48 kDa) are present in both locations, but differ in their relative concentration in the nucleus and cytoplasm. Thus, both isoforms of the protein are approximately equally represented in the nucleus, and isoform with a molecular mass of 46 kDa only occasionally predominates, while the isoform with a molecular mass of 48 kDa always predominates in the cytoplasm. It is believed that NeuN isoforms differ in a short amino acid sequence, which is responsible for the localization of the different variants of this protein in the cell [16].

In the nucleus, NeuN is primarily located in the areas with low chromatin density, and it is absent in areas with dense packing of DNA [16]. Most of the intranuclear NeuN is bound to the nuclear matrix [17]. The results of chromatographic analysis of cerebral nuclear proteins demonstrate the ability of the NeuN protein to bind to DNA [11]. It remains not fully clear how specific this binding is and whether NeuN binds to DNA *in vivo*. The nuclear localization of the NeuN protein, its DNA binding properties that were demonstrated *in vitro*, as well as its solubility suggest that NeuN is a neurospecific regulatory molecule functioning at the level of the cell nucleus [11]. More recent studies [17] have confirmed the validity of this assumption. However, the capability of binding to RNA rather than DNA is currently considered to be a more important property

of NeuN [18]. Nevertheless, the fact that the expression of NeuN is associated with neuronal differentiation and persists throughout the whole cell life can be an indication that NeuN is a permanent regulator of the general presentation of the neuronal phenotype. In this case, the lack of NeuN expression in certain neuronal populations implies the presence of alternative, but functionally similar to NeuN regulatory molecules in these cells. This assumption is consistent with the general idea that a variety of alternative regulatory mechanisms, providing comprehensive control of the differentiation processes of nerve elements and formation of nervous system organs, should be present in such a complex system as the nervous system of vertebrates.

The accumulated so far experimental data provide evidence that the intensity of the immunocytochemical reactions for NeuN in the nucleus and cytoplasm may vary both within the same type of neurons and between different types of neurons. Thus, an investigation in NeuN distribution in the substantia nigra cells of the rat brain revealed that it is poorly expressed in some neurons, while in other neurons it is completely absent [12]. In humans, the population of neurons of the substantia nigra is also heterogeneous in terms of NeuN distribution. Both weakly immunopositive and immunonegative cells have been detected [13]. The neurons of the substantia nigra differ both in their ability to be stained in an immunohistochemical reaction for NeuN and neuromelanin content in their cytoplasm. Neurons that contain neuromelanin and the NeuN protein; neurons that contain neuromelanin, but give a negative reaction for the NeuN protein; and neurons that do not contain neuromelanin, but contain NeuN were detected. Interestingly, the concentration of the NeuN protein in substantia nigra neurons is significantly lower than that in the neurons of the red nucleus located anatomically close to the substantia nigra and other areas of the human brain [13].

Although NeuN expression in substantia nigra neurons has been convincingly determined in laboratory animals and humans, we can state that, in general, no clear correlation between the intensity of NeuN immunoreactivity and a certain type of neurons has been established. Obviously, the differences in the intensity of the reaction for NeuN reflect the differences in the expression of this protein in a cell, which are associated with both the constitutive characteristics of the neuron and its functional state. Thus, the intensity of the immunocytochemical reaction for NeuN consistently varies during the stimulation of primary neuronal culture cells [19]. Injuries to the nervous system can affect the expression of the NeuN protein in the cell in various ways. For example, axonal injury leads to an almost complete loss of NeuN immunoreactivity in motoneu-

rons of the facial nerve nucleus, while a transection of the rubrospinal tract only leads to a minor reduction in NeuN immunoreactivity in red nucleus neurons [20]. In the latter case, the less pronounced changes may be due to a more distal transection of axons having a sufficient amount of collaterals.

The complexity associated with interpreting the results of immunohistochemical staining for the NeuN protein is associated with the fact that a negative result of the reaction may be due to several reasons. On the one hand, this may be due to the absence of NeuN protein expression in a cell or protein synthesis in such a small amount that it cannot be detected by immunohistochemistry. On the other hand, there is experimental evidence of the influence of NeuN protein phosphorylation on its ability to bind known antibodies to NeuN [16]. It has been shown that there are seven post-translational modifications (forms) of the NeuN protein characterized by varying degrees of phosphorylation. Enzymatic dephosphorylation experiments demonstrated that antibodies to the NeuN protein (clone A60) recognize only phosphorylated forms of the protein, and that at least one phosphate group in the NeuN molecule is required for proper formation of the antigenic determinant recognized by these antibodies [16]. Later on, it was suggested that the epitope for antibody binding to a non-phosphorylated NeuN protein is involved in protein-protein interactions, and, therefore, it is masked and incapable of binding to antibodies [21]. This hypothesis is indirectly confirmed by the fact that the aforementioned epitope has proline-rich amino acid sequences that are considered to be the main actors in protein-protein interactions in the cell [22].

### **The structure and properties of NeuN/Fox-3 protein**

For a long time, the nucleotide sequence encoding the NeuN protein remained unknown. In 2009, a research team in the USA [23] carried out a mass spectrometry analysis of peptides derived from trypsinization of the protein, reacting with antibodies to NeuN (clone A60). As a result, the primary structure of the Fox-3 protein was established. The protein consists of 374 amino acids and can exist in four isoforms generated by alternative splicing of the mRNA. Kim *et al.* [23] demonstrated that the protein that reacts with antibodies to Fox-3 interacts with tissue antigens in the same way as known anti-NeuN antibodies. The character of intracellular structure staining upon reaction with anti-Fox-3 antibodies is completely identical to the results of an immunocytochemical reaction for NeuN. It was also shown that expression of the NeuN protein is tapered when using small hairpin RNAs (shRNA) against Fox-3. Finally, it turned out that Fox-3, similarly to NeuN, is expressed only in the nervous tissue. Based on these ex-

perimental data, the authors concluded that the NeuN protein is a product of the *Fox-3* gene, which belongs to the *Fox-1* gene family. This work [23] was performed at a high methodological level, using modern molecular-genetic, cytological, and histological methods and made a significant contribution to our understanding of the molecular nature of the antigenic determinant that binds A60 antibodies. Most authors, when investigating NeuN, share Kim's opinion on the identity of the NeuN antigen and Fox-3 protein, as evidenced by the numerous references to this work (89 references by December 2014) in the articles refereed in databases belonging to the Web of Science service (Thomson Reuters).

Importantly, the same research team [23] reported the detected cross-reactivity of A60 antibodies to the NeuN protein with synapsin I, a member of the neuron-specific phosphoprotein family associated with synaptic vesicles, which play a role in the synaptogenesis and modulation of neurotransmitter secretion. Cross-reactivity is apparently due to the presence of a fragment consisting of 14 homologous amino acid residues in Fox-3 and synapsin I. A part of this fragment is probably involved in the formation of the epitope recognized by A60 antibodies. Importantly, the cross-reactivity of the epitopes of synapsin and NeuN was observed only when using the immunoblotting method, while anti-NeuN antibodies did not bind to synapsin I in an immunocytochemical study on paraffin sections. This may be associated with both the masking of the antigenic determinant due to fixation in formaldehyde and the pouring of paraffin over the material and low affinity of anti-NeuN antibodies to the synapsin I epitope, which is compensated by the high concentration of synapsin in the material under study in immunoblotting [21, 23].

Sequencing and identification of the gene encoding the NeuN protein naturally led to an investigation of the NeuN/Fox-3 functions in nervous system cells. It was shown that this protein plays a role in neurospecific alternative splicing [24]. Subsequently, it has been experimentally established that regulated NeuN/Fox-3 splicing greatly contributes to the regulation of neuron differentiation in the nervous system of vertebrates [25]. In this regard, it is suggested that the functions of the Fox-3 protein in a cell should be taken into account when using NeuN-immunostaining as a convenient neuronal marker. [21].

### **Using NeuN protein as a neuromarker**

Although the structure of the antigenic determinant that binds A60 antibodies and the conditions of this binding are not fully understood, antibodies to the NeuN protein are widely used in scientific research and in histopathologic diagnosis. Thus, during the last

decade, the NeuN protein has been used as a universal neuron-specific marker for studying the differentiation of stem cells [7, 26–28]. The presence of some specific marker proteins, whose immunocytochemical detection allows for selective identification of cells belonging to the nervous system tissues, in postmitotic cells provides evidence of neuronal differentiation. Such proteins include, for example,  $\beta$ -tubulin III, MAP-2, doublecortin, synaptophysin, neurofilament proteins, neuron-specific enolase, the neural cell adhesion molecule, as well as the neurotransmitter synthesis enzymes (tyrosine hydroxylase, choline acetyl transferase), etc. [28–29]. The use of the NeuN protein as a neuronal differentiation marker has several advantages. Firstly, the NeuN protein is expressed exclusively in the nervous tissue, while other neuronal differentiation marker proteins are also found in other cells. For example, MAP-2 is expressed not only in neurons, but also in skeletal muscles, epithelial cells, etc. Astrocytes also give positive immunocytochemical reaction for neuron-specific enolase, and synaptophysin was found not only in neurons, but also in neuroendocrine cells [29]. Secondly, NeuN is not found in immature neural progenitor cells as long as they are not out of the cell cycle [15, 19, 30]. In this context, some markers are less convenient, as they detect both mature neurons and undifferentiated neuroepithelial cells (MAP-2), or only nerve cells at the late stages of differentiation (neurotransmitters synthesis marker enzymes) [31]. Finally, the NeuN protein is the only one of these markers whose expression is primarily associated with the cell nucleus. In connection to this, detection of this protein, in contrast to cytoplasmic markers, does not depend on a small volume of cytoplasm, which is typical of neuroblasts and small neurons. In addition, nuclear localization of this marker allows one to obtain discrete stained structures of specimens, which are available for binarization (image processing procedures required during the automated quantitative analysis of the objects) when being photographed.

The reaction for NeuN is also used in pathohistological diagnosis in neurooncology [9, 31]. There is evidence of NeuN expression in some cells of differentiated neuronal tumors (neurocytomas, gangliocytomas, medulloblastomas) [30, 31]. For example, Wolf *et al.* [30] revealed NeuN immunoreactivity in the nuclei of some glioma cells and absence of such immunoreactivity in oligodendroglial cells, which can be used for the differential morphologic diagnosis of cancer. Inclusion of this marker into an antibody panel used for the diagnosis of neurocytomas can result in improved reliability of diagnostics and differential diagnosis, at least in the case of central nervous system neuroblastomas [31].

Although NeuN is considered to be a convenient marker of postmitotic neurons and differentiated cells of neurogenic tumors, one should be careful when using the protein for identifying neural cells *in vitro*. As shown by Darlington *et al.* [32], NeuN immunoreactivity is present in the primary cell cultures of the murine, rat and human brain. But not only neurons are NeuN-immunopositive. It has been shown that some NeuN-immunopositive cells in these cultures express the glial fibrillary acidic protein (GFAP), an astrocyte marker. Moreover, NeuN is expressed by all GFAP-positive cells. The identified NeuN<sup>+</sup>/GFAP<sup>+</sup> cells demonstrate astrocyte morphology, do not proliferate (according to the results of BrdU labeling), and demonstrate no expression of other neuronal markers. Based on these data, we suggested that NeuN<sup>+</sup>/GFAP<sup>+</sup> cells identified *in vitro* are astrocytes rather than partially differentiated neuronal precursors at the stage of the beginning of synthesis of neuron-specific proteins as might have been expected as an alternative. Apart from astrocytes, one of the fibroblast cell lines (3T3) proved to be immunoreactive to NeuN *in vitro*. The reason for the NeuN immunoreactivity of non-neuronal cells observed in cultures remains not fully understood. When working with paraffin sections, it was found that NeuN immunoreactivity is affected by some methodological techniques [33–36]. It was noted that long-term fixation in formalin (for several months or years) reduces NeuN immunoreactivity as compared to the level observed after fixation of the same materials for several days or weeks. Furthermore, thermal unmasking of the antigen is usually required for A60 antibody binding [15, 36]. At the same time, decalcification of the objects in a formic acid solution does not lead to a deterioration of the reaction for NeuN [35]. Obviously, NeuN immunostaining involves specific protocols that are standardized for use with paraffin sections [29, 37, 38] but are likely to require further improvement and standardization in the case of *in vitro* studies.

Another application of anti-NeuN antibodies is associated with the identification of pathological changes in existing neuronal populations. Various pathological processes accompanied by a weakening or disappearance of NeuN immunoreactivity in neurons have been reported in several studies. Thus, complete disappearance of NeuN immunohistochemical staining of neuronal nuclei and cytoplasm at the area of ischemic damage to the striatum in a rat brain [39, 40] has been noticed. Termination of NeuN protein synthesis by certain striatal neurons in Huntington's disease has also been observed [41]. It has been shown that the NeuN nuclear protein disappears from damaged or dying pyramidal neurons in the hippocampus [42]. A decrease in

NeuN immunoreactivity in hypoxia and brain injury was also reported [43–45].

It is important to note that in some studies the loss of NeuN immunoreactivity was explained by neuronal death. Thus, Davoli *et al.* [44] compared NeuN-immunostaining with TUNEL staining in ischemia and found that NeuN immunoreactivity was significantly reduced 24 hours after exposure, which correlates with the increase in the number of apoptotic cells (detected by TUNEL). Based on these data, it was suggested that the decrease in NeuN immunostaining is associated with neuronal death in the damaged area of the brain. On the other hand, it was subsequently shown that the loss of NeuN-staining is not always associated with neuronal death and may be effected by other agents; for example, temporarily suspended synthesis of this protein by neurons due to damage (but without viability loss). When using a moderate ischemia model (30 min ischemia), it was found that neurons lose NeuN immunoreactivity 6 h after exposure, while retaining the integrity of the cell and intact nucleus; i.e., they do not exhibit typical signs of cell death [45]. According to the authors, the loss of immunoreactivity in this case is associated with the loss of the antigen's ability to bind anti-NeuN antibodies, rather than a reduction in NeuN protein synthesis in neurons. In contrast, in the case of axotomy, a sharp decrease in the amount of the NeuN protein in neurons was shown [20]. Therefore, the loss of neuronal NeuN immunoreactivity is indicative of damage, but it cannot be definitive evidence of neuronal death (expected or actual). This fact should be

borne in mind when interpreting the results of quantitative immunohistochemical studies.

### CONCLUSION

In conclusion, despite the many years of intensive studies of the NeuN protein, a number of issues related to its structure and functions remain open. Thus, antigenic determinants that bind anti-NeuN antibodies and the conditions required for effective interaction between antibodies and the antigen both *in vivo* and *in vitro* remain poorly studied. The entire range of functions of the NeuN protein in cells has not been determined. It is unclear what processes in cells lead to the changes in the intensity of the reaction for NeuN/Fox-3 or loss of NeuN immunoreactivity, as well as post-translational modifications in this protein, which are observed in some cases. Despite this, NeuN has been successfully used for more than 20 years as a reliable marker of postmitotic neurons in studies of neuronal differentiation and in the assessment of neuronal status both in norm and pathology. In recent years, there has been an increase in the number of studies aimed at investigating the properties of the NeuN/Fox-3 protein. New data should deepen our understanding of the structure and functions of this protein and facilitate the objective interpretation of research results using antibodies to the NeuN protein. ●

*This work was supported by the Russian Scientific Foundation (the project No 14-15-00014).*

### REFERENCES

- Ugrumov M.V. // *J Chem Neuroanat.* 2009. V. 38. № 4. P. 241–256.
- Ugrumov M., Taxi J., Pronina T., Kurina A., Sorokin A., Sapronova A., Calas A. // *Neuroscience.* 2014. V. 277. P. 45–54.
- Korzhevskii D. E., Grigoriev I. P., Kirik O. V., Sukhorukova E. G., Alekseyeva O. S. // *Journal of Evolutionary Biochemistry and Physiology.* 2014. V. 50. № 2. P. 177–180.
- Korzhevskii D.E., Petrova E.S., Kirik O.V., Otellin V.A. // *Neurosci Behav Physiol.* 2009. V. 39. № 6. P. 513–516.
- Petrova E. S., Isaeva E. N., Korzhevskii D. E. // *Neuroscience and Behavioral Physiology.* 2014. V. 44. № 4. P. 478–481.
- Petrova E.S., Isaeva E.N., Korzhevskii D.E. // *Bull of Exp Biol Med.* 2014. V.158. № 1. P. 123–126.
- Verdiev B.I., Poltavtseva R.A., Podgornyi O.V., Marei M.V., Zinovyeva R.D., Sukhikh G.T. Aleksandrova M.A. // *Bull Exp Biol Med.* 2009. V. 148. № 4. P. 697–704.
- Chan M.H., Kleinschmidt-Demasters B.K., Donson A.M., Birks D.K., Foreman N.K., Rush S.Z. // *Pediatr Blood Cancer.* 2012. V. 59. № 7. P. 1173–1179.
- You H., Kim Y.I., Im S.Y., Suh-Kim H., Paek S.H., Park S.H., Kim D.G., Jung H.W. // *J Neurooncol.* 2005. V. 74. № 1. P. 1–8.
- Hagel C., Treszl A., Fehlert J., Harder J., von Haxthausen F., Kern M., von Bueren A.O., Kordes U. // *J Neurooncol.* 2013. V. 112. № 2. P.191–197.
- Mullen R.J., Buck C.R., Smith A.M. // *Development.* 1992. V. 116. P. 201–211.
- Cannon J.R., Greenamyre J.T. // *Neurosci. Lett.* 2009. V. 464. № 1. P. 14–17.
- Sukhorukova E. G. // *Neuroscience and Behavioral Physiology.* 2014. V. 44. № 5. P. 539–541.
- Kumar S.S., Buckmaster P.S. // *Brain Research.* 2007. V. 1142. P. 54–60.
- Sarnat H.B., Noehlin D., Born D.E. // *Brain Dev.* 1998. V. 20. P. 88–94.
- Lind D., Franken S., Kappler J., Jankowski J., Schilling K. // *J Neurosci Res.* 2005. V. 79. P. 295–302.
- Dent M.A., Segura-Anaya E., Alva-Medina J., Aranda-Anzaldo A. // *FEBS Lett.* 2010. V. 584. № 13. P. 2767–2771.
- Darnell R.B. // *Annu Rev Neurosci.* 2013. V. 36. P. 243–270.
- Weyer A., Schilling K. // *J Neurosci Res.* 2003. V. 73. P. 400–409.
- McPhail L.T., McBride C.B., McGraw J., Steeves J.D., Tetzlaff W. // *Exp Neurol.* 2004. V. 185. P. 182–190.
- Maxeiner S., Glassmann A., Kao H.-T., Schilling K. // *Histochem. Cell Biol.* 2014. V. 141. P. 43–55.

## REVIEWS

22. Williamson M.P. // *Biochem J.* 1994. V. 297. P. 249–260.
23. Kim K.K., Adelstein R.S., Kawamoto S. // *J Biol Chem.* 2009. V. 284. P. 31052–31061.
24. Kim K.K., Kim Y.C., Adelstein R.S., Kawamoto S. // *Nucleic Acids Res.* 2011. V. 39. P. 3064–3078.
25. Kim K.K., Nam J., Mukoyama Y.S., Kawamoto S. // *J Cell Biol.* 2013. V. 200. P. 443–458.
26. Hess D.C., Hill W.D., Martin-Studdard A., Carroll J., Brailer J., Carothers J. // *Stroke.* 2002. V. 33. P. 1362–1368.
27. Tanvig M., Blaabjerg M., Andersen R.K., Villa A., Rosager A.M., Poulsen F.R., Martinez-Serrano A., Zimmer J., Meyer M. // *Brain Res.* 2009. V. 1295. P. 1–12.
28. Korzhevskii D.E., Petrova E.S., Kirik O.V., Beznin G.V., Sukhorukova E. G. // *Cell Transplantation and Tissue Engineering.* 2010. V. 5. № 3. P. 57–63.
29. Korzhevskii D.E., Kirik O.V., Petrova E.S., Karpenko M.N., Grigor'ev I.P., Sukhorukova E.G., Kolos E. A. Theoretical bases and practical application of the immunohistochemical methods. SPb: SpecLit, 2014. 119 p.
30. Wolf H.K., Buslei R., Schmidt-Kastner R., Schmidt-Kastner P.K., Pietsch T., Wiestler O.D. Blümcke I. // *J Histochem Cytochem.* 1996. V. 44. P. 1167–1171.
31. Soylemezoglu F., Onder S., Tezel G. G., Berker M. // *Pathol Res Pract.* 2003. V. 199. P. 463–468.
32. Darlington P.J., Goldman J. S., Cui Q.L., Antel J.P., Kennedy T.E. // *J Neurochem.* 2008. V. 104. P. 1201–1209.
33. Korzhevskii D.E., Gilerovich E.G., Zin'kova N.N., Grigor'ev I.P., Otellin V.A. // *Neurosci Behav Physiol.* 2006. V. 36. № 8. P. 857–859.
34. Korzhevskii D. E., Sukhorukova E. G., Gilerovich E. G., Petrova E. S., Kirik O. V., Grigor'ev I. P. // *Neuroscience and Behavioral Physiology.* 2014. V. 44. № 5. P. 542–545.
35. Kolos E. A., Korzhevskii D. E. // *Neuroscience and Behavioral Physiology.* 2014. V. 44. № 7. P. 790–792.
36. Gill S.K., Ishak M., Rylett R.J. // *J Neurosci Methods.* 2005. V. 148. P. 26–35.
37. Korzhevskii D.E., Gilyarov A. V. // *Neuroscience and Behavioral Physiology.* 2010. V. 40. № 1. P. 107–109.
38. Giliarov A.V., Kirik O.V., Korzhevskii D.E. // *Morfologiya.* 2010. V. 137. № 5. P. 59–64.
39. Kirik O.V., Sukhorukova E.G., Vlasov T.D., Korzhevskii D.E. // *Morfologiya.* 2009. V. 135. № 2. P. 80–82.
40. Korzhevskii D.E., Kirik O.V., Baisa A.E., Vlasov T.D. // *Bull Exp Biol Med.* 2009. V. 147. № 2. P. 255–256.
41. Tippett L.J., Waldvogel H.J., Thomas S.J., Hogg V.M., van Roon-Mom W., Synek B.J., Graybiel A.M., Faull R.L. // *Brain.* 2007. V. 130. P. 206–221.
42. Korzhevskii D. E., Khozhai L.I., Gilerovich E. G., Grigor'ev I. P., Gilyarov A. V., Otellin V.A. // In the conference abstract-book «Structural, functional and neurochemical regularities of the brain asymmetry and plasticity-2006». Proceedings of the All-Russian conference with international participation, Moscow, 2006. P. 139–142.
43. Igarashi T., Huang T.T., Noble L.J. // *Exp Neurol.* 2001. V. 172. P. 332–341.
44. Davoli M.A., Fourtounis J., Tam J., Xanthoudakis S., Nicholson D., Robertson G.S., Ng G.Y., Xu D. // *Neuroscience.* 2002. V. 115. P. 125–136.
45. Unal-Cevik I., Kiliç M., Gürsoy-Ozdemir Y., Gurer G., Dalkara T. // *Brain Res.* 2004. V. 1015. P. 169–174.

# *In Vitro* Mouse Ovarian Follicle Growth and Maturation in Alginate Hydrogel: Current State of the Art

M. A. Filatov\*, Y. V. Khranova, M. L. Semenova

Faculty of Biology, Lomonosov Moscow State University, Leninskie Gory, 1, bld. 12, Moscow, 119991, Russia

\*E-mail: maxfilat@yandex.ru

Received 18.11.2014

Revised manuscript received 06.03.2015

Copyright © 2015 Park-media, Ltd. This is an open access article distributed under the Creative Commons Attribution License, which permits unrestricted use, distribution, and reproduction in any medium, provided the original work is properly cited.

**ABSTRACT** This review describes the main factors affecting the *in vitro* development of mouse ovarian follicles under conditions of three-dimensional alginate hydrogel system. The factors discussed include concentration of alginate hydrogel, presence of additives (collagen, fibrin) influencing substrate rigidity; culture conditions; composition of culture media; substances that act like antioxidants (salts of ascorbic acid, glutathione) and contribute to the improvement of lipid metabolism (*L*-carnitine), hormones and growth factors. The methods for follicle group cultivation in alginate hydrogel and cocultivation of different cell populations with follicles encapsulated in alginate hydrogel are covered in the present article.

**KEYWORDS** alginate, hydrogel, follicle, ovary, mice.

**ABBREVIATIONS** 2D – two-dimensional; 3D – three-dimensional; FSH – follicle-stimulating hormone; hCG – human chorionic gonadotropin; LH – luteinizing hormone; BSA – bovine serum albumin; FCS – fetal calf serum; ITS – insulin, transferrin, selenium; EGF – epidermal growth factor.

## INTRODUCTION

Researchers show great interest in designing a system that would allow *in vitro* producing mature oocytes. For various reasons, a woman may require mature oocytes produced *in vitro* from ovarian tissue. For example, ovariectomy is used in hormone-dependent breast cancer to reduce secretion of sex hormones [1]. Radio- and chemotherapy are used to treat other cancer types and also have a negative effect on ovarian status. Chemotherapeutic agents make ovarian cells degrade via the apoptotic pathway. Both the stroma and the follicular ovarian systems are involved in this process [2] by decreasing the number of primordial follicles, reducing the ovarian reserve and causing infertility [3]. Ovarian tissue cryopreservation is currently offered to patients with an eye to returning this tissue to the organism after successful treatment [4]. This procedure is associated with a number of challenges, since both harvesting the ovarian tissue and autografting require surgical intervention and hormonal stimulation to initiate follicle growth and maturation. All these manipulations may have a negative effect on the debilitated condition of the female patient, including increasing the risk of cancer recurrence.

*In vitro* culturing of ovarian tissue followed by production of mature fertilizable oocytes that can be subjected to cryopreservation and subsequently used in

assisted reproductive technology programs is a way out of situations such as this one. The methods for *in vitro* culturing of ovarian tissue and individual follicles are currently being actively developed using various animal models, including dog [5] and rhesus macaque [6] models; however, mouse ovarian tissue is used most commonly [7–11]. Although encouraging results have recently been obtained [7, 8, 10], many questions regarding the regulation of follicle growth and oocyte maturation under *in vitro* conditions are far from being solved. Regulation of follicle growth and oocyte maturation *in vivo* depends on hormones secreted by the pituitary gland and ovarian cells, growth factors, as well as other substances whose role remains to be elucidated. Furthermore, follicle growth largely depends on the mechanical properties of the surrounding ovarian tissue. All these conditions need to be provided to successfully culture follicles *in vitro*.

Many researchers culture individual follicles isolated from the ovary either mechanically or enzymatically. A larger number of follicular cells (including theca cells) are preserved when the mechanical method is used, which contributes to better follicle growth *in vitro* [12, 13].

Individual follicles can be cultured in 2D (planar, two-dimensional) or 3D (spatial, three-dimensional) systems. 3D systems have a number of advantages



over 2D ones. The main drawback of 2D systems is that the microenvironment of the cultured fragment shows poor correlation to the *in vivo* conditions. In two-dimensional culturing, cells of the follicle and the surrounding stroma migrate within the plane, follicles lose their shape, and oocytes are deprived of the normal cellular environment. Functioning of 2D systems can be regulated only by varying concentrations of chemical agents (growth factors, hormones, etc.) in the culture medium, while 3D culturing technologies allow one to perform regulation by selecting the optimal physical parameters of 3D microenvironment of the explant.

Agarose, collagen, matrigel, or alginate derivatives are used as substrates when designing 3D culture systems [14]. Alginate hydrogels resulting from dissolution of alginic acid salts (alginates) are advantageous over other substances: it is sufficient to add a solution containing the binding agent ( $\text{Ca}^{2+}$  or  $\text{Mg}^{2+}$  ions) to induce their polymerization. Exposure to neither high temperatures nor UV radiation fatal to living cells is needed. Furthermore, alginates are of vegetative origin (they are derived from brown algae), so they can be employed in projects with the limitation to use only systems with animal-free components. *Figure 1* shows the scheme of formation of alginate hydrogel due to polymerization of sodium alginate induced by calcium ions. Hydrogels having different structures and densities and thus exhibiting different mechanical properties can be produced by varying concentrations of calcium and magnesium salts used in polymerization, alginate solution concentration, and polymerization duration.

### Mechanical environment surrounding the follicle

Mechanical strains emerging in follicular cells play a crucial role in normal follicle growth and oocyte maturation. Studies by several independent groups of researchers focused on gene expression in mouse ovarian follicles have demonstrated that cultivation of follicles in less concentrated, and therefore softer, alginate substrates better simulates the *in vivo* conditions of follicle growth and maturation than cultivation in more rigid alginate substrates [9, 15, 16].

The number of transcripts of the *Gdf9*, *Bmp15*, *Tcl1* and *Zp3* genes in oocytes increased as follicles were cultivated in the presence of 0.25% alginate hydrogels (0.25 g sodium alginate dissolved in 100 mL of the solution) as compared to 1.5% alginate hydrogel (1.5 g sodium alginate dissolved in 100 mL of the solution). The high expression level of these genes is typical of normal *in vivo* oogenesis. Furthermore, cultivation of follicles in softer alginate hydrogels (0.25%) significantly increased oocyte and follicle size compared to cultivation in more rigid alginate hydrogel (1.5%) [9].

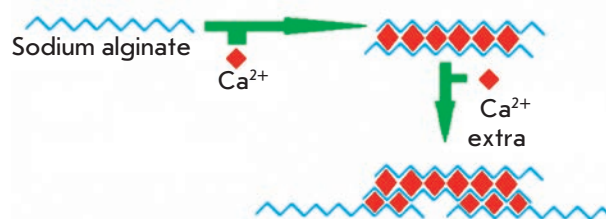
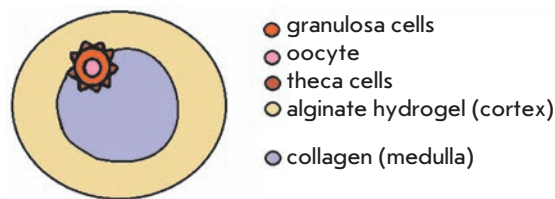


Fig. 1. Scheme of alginate hydrogel formation

A group of U.S. researchers have demonstrated that cultivation of follicles in rigid alginate hydrogels (1.5%) that reduce the follicle growth and development rates compared to cultivation in softer alginate hydrogels (0.5%) results in excessive expression of such genes as *Star* (regulating the extracellular transport of cholesterol required for sex hormone synthesis), *Cyp11a1* (responsible for conversion of cholesterol to pregnenolone), and *Hsd3b1* (encoding hydroxy- $\delta$ -5-steroid dehydrogenase). Moreover, the expression level of the *Lhcgr* gene, the gene encoding luteinizing hormone and chorionic gonadotropin, was enhanced by cultivation in 0.5% alginate hydrogel as compared to 1.5% hydrogel. The expression level of the *Cyp19a1* gene responsible for conversion of androstendione to estradiol also increased between day 0 and day 8 of follicle cultivation in granulosa cells. This process was more efficient in 0.5% alginate hydrogel: the *Cyp19a1* expression level increased 34-fold, cultivation in 1.5% hydrogel resulted in an only 15-fold rise. As a result, a considerably lower level of estradiol secretion was observed in follicles cultured using the more rigid substrates [15].

It is also of special interest to compare the levels of gene expression for ovarian follicles developed *in vivo* and cultured *in vitro* in alginate hydrogel [16]. Follicles containing two granulosa cell layers (double-layered follicles) were isolated from the ovaries of 12-day-old sexually immature mice, encapsulated in 0.25% alginate hydrogel and cultured for 4 days. The gene expression levels in follicular cells after cultivation in alginate hydrogel and in multilayered follicular cells isolated from the ovaries of 16-day-old mice were compared. The isolated follicles were 150–180  $\mu\text{m}$  in diameter and corresponded to the size of follicles cultured *in vitro*. It was found that ovarian follicles cultured in 0.25% alginate hydrogel and those developing *in vivo* had similar expression patterns, including expression of such genes as *Fshr* (encoding FSH receptor), *Inha* (responsible for the formation of inhibin  $\alpha$ -subunit), *Igf1* (insulin-like growth factor 1 having an effect on follicle growth), *Zp2* (encoding one of zona pellucida glycoproteins), and *Lhcgr*.



**Fig. 2.** Scheme of alginate–collagen system structure. Follicle is located in the transient zone of mechanical forces between the cortex (the more rigid region) and medulla (softer region). During development follicle transits into the medulla

Although soft alginate hydrogels provide better results for follicle cultivation than the more rigid microenvironment, cultivation in hydrogels with a low alginate concentration is associated with a number of technological challenges. Destruction of hydrogel drops occurs quicker in less concentrated solutions, since fewer cross-links are formed between alginate molecules and the structure is weaker. Alginate solutions with a low concentration show promise for cultivation technologies where follicle is encapsulated into the hydrogel and the culture medium is replaced in such a way that hydrogel is not damaged.

#### **In vitro reconstruction of the cortical-medullary structure of the ovary**

During *in vivo* growth, a follicle migrates from the rigid area of the ovary (cortex) to the less rigid area (medulla) [17]. Thus, mechanical strains are gradually reduced in follicular cells under natural conditions. Two different methods that use alginates and allow one to reconstruct the cortical-medullary structure for an individual follicle have been designed: cultivation in fibrin–alginate or alginate–collagen hydrogel.

In order to simulate the conditions of variable mechanical strains [17–20], methods for culturing follicles in fibrin–alginate hydrogel were developed; this hydrogel is formed by simultaneous polymerization of alginate and fibrin (alginate polymerization is induced by calcium ions ( $\text{Ca}^{2+}$ ), while fibrin polymerization is induced by thrombin and blood coagulation factor XIII). A growing follicle releases lytic enzymes (proteases) that destroy the polymerized fibrin. The mechanical strains existing around the follicle being cultured in fibrin–alginate hydrogel are reduced, resulting in a further increase in follicle size [18]. Fibrin–alginate hydrogel based on 0.25% alginate significantly enhances estradiol and progesterone secretion by follicles and oocyte size increases to a much greater extent than when the standard 0.25% alginate hydrogel without fibrin additive is used [20].

The alginate–collagen system is another way to provide a dynamic environment of the follicle characterized by different rigidity levels. This type of cultivation suggests that collagen is located in the center of a drop with a follicle encapsulated in it, while alginate hydrogel is present at the periphery. Collagen is a much softer substrate compared to alginate hydrogel; hence, the resulting system is heterogeneous in terms of its rigidity and imitates the follicular microenvironment in the ovary under *in vivo* conditions: the cortex is more rigid, while the medulla is softer [21]. *Figure 2* shows the scheme of alginate–collagen drop structure with an encapsulated follicle.

The method for follicle encapsulation in the double-layered alginate–collagen system using the microfluidics technology has recently been developed. This technology makes it possible to produce drops consisting of different substances taken at desired ratios due to the directed microflows of different fluids that are generated in a pre-made chip according to a particular scheme [22]. This technology can be used to produce drops of desired size, including those corresponding to the volume of an individual follicle, which simplifies the further cultivation stages [21].

*Table 1* lists the main types of follicle culture systems and parameters characterizing the efficiency of these systems, such as the survival rate and the percent of oocytes that reached metaphase II (MII). The best results were achieved by using follicles with an initial diameter of more than 130  $\mu\text{m}$ ; follicles less than 100  $\mu\text{m}$  in diameter are not used in these studies, although the number of follicles of this size in the ovary is sufficiently large. A certain minimal volume of cellular microenvironment seems to be needed for successful follicle growth and oocyte maturation in alginate hydrogels.

#### **Composition of follicle culture media**

A two-stage culture system is usually used to culture follicles encapsulated in alginate hydrogel. At the first stage, cultivation is carried out in the medium facilitating follicle growth, IVC (*In vitro culture medium*). At the second stage, follicles are placed into the *in vitro* maturation medium (IVM). *Table 2* shows the main types of media used to culture follicles encapsulated inside alginate hydrogels and their derivatives.

$\alpha$ -MEM complete medium supplemented with different additives is typically used for follicle growth and maturation. To stimulate follicle growth, the medium is supplemented with insulin, selenite, transferrin (ITS), bovine serum albumin (BSA) or fetal calf serum (FCS), and follicle-stimulating hormone (FSH). Substances exhibiting antioxidant properties (ascorbic acid) or enhancing lipid metabolism (L-carnitine) are sometimes added to the culture medium.

## REVIEWS

**Table 1.** Development of the procedures for cultivation of mouse ovarian follicles in alginate hydrogels of different compositions (according to [23] with modifications)

Hydrogel composition	Cultivation duration, days	Initial follicle size, $\mu\text{m}$	Survival rate, %	MII phase reached, %	Additional observations	Source
2% alginate (cortex), 0.5% alginate (core) vs 2% alginate (cortex), 0.5% type I collagen (core)	More than 9	100–130	No data available	No data available	The antral follicle stage is reached more often when collagen is used	[21]
Alginate, 0.25% vs 1.5%	8	130–150	No data available	86 vs 63.8	The expression levels of the main folliculogenesis genes are higher for softer substrates	[9]
0.25% alginate–fibrin	8	130–150	No data available	No data available	Follicle destroys fibrin by proteases, thus reducing mechanical strain	[18]
0.25% alginate–fibrin	12	No data available	75	88	Formation of 2-cell embryos after fertilization of oocytes derived from follicles <i>in vitro</i>	[20]
0.25% alginate	12	100–130	78	59	Investigation of gap junctions in follicular cells	[24]
Alginate, 1.5% vs 0.5%	2–8	150–180	82.7 vs 84.3	No data available	Soft substrate (0.5%) facilitates follicle growth as compared to the more rigid substrate (1.5%)	[15]
0.25% alginate–fibrin	12	100–130	77–81	75–82	No data available	[19]
Alginate, 0.7, 1.5, 3%	8–12	100–130 150–180	31–66 46–91	No data available	Investigation of estrogen secretion by follicles	[25]
Different culture systems (both individual alginate hydrogel and its complexes with various peptides): 1.5% alginate solution 1.5% alginate–type I collagen solution 1.5% alginate–fibronectin solution 1.5% solution of alginate with tripeptides (arginine, glycine, aspartic acid) 1.5% alginate–type IV collagen solution 1.5% alginate–laminin solution	8	100–130 vs 150–180	64 vs 69 65 vs 67 70 vs 72 72 vs 62 72 vs 48 63 vs 61	40 44 71 65 50 71	Cultivation in complexes of alginate with type I collagen and tripeptides resulted in follicle growth; the use of hydrogels containing fibronectin, tripeptides or laminin stimulated formation of oocytes at the MII phase	[26]
Alginate 1.5%	8	150–180	93	71	Birth of live pups after oocytes derived <i>in vitro</i> from follicles were fertilized	[27]
Alginate, 0.25, 0.5, 1, 1.5%	12	100–130	74–85	56–67	Investigation of the effects of substrate rigidity: softer substrates contribute to oocyte development	[28]

The oocyte maturation medium is always supplemented with human chorionic gonadotropin (hCG) to stimulate ovulation. Growth factors, including epidermal growth factor (EGF) facilitating normal meiosis, are also added to this medium in most studies [30].

No unified culturing procedure has been developed thus far, although most researchers use the two-stage culturing procedure, which allows one to stimulate follicle growth and subsequently induce oocyte maturation in them. The first-priority aim of further studies

focused on *in vitro* production of fertilizable oocytes is to investigate whether it is reasonable to supplement the two-stage culture systems with various additives capable of inducing follicle and oocyte growth and development or not.

### Regulation of lipid metabolism in folliculogenesis

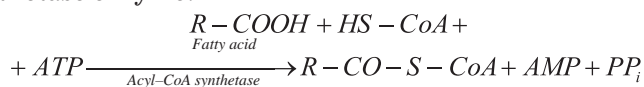
Significant attention during *in vitro* follicle culturing is typically given to carbohydrate metabolism. In most cases, carbohydrates are added to the medium as an

**Table 2.** Comparison of the media used to culture mouse follicles in alginate hydrogel

Composition of follicle growth medium	Composition of oocyte maturation medium	MII phase reached, %	Source
αMEM, 3 mg/mL BSA, 1 mg/mL fetuin, 10 mIU/mL FSH, 5 μg/mL insulin, 5 μg/mL transferrin, and 5 ng/mL selenite	Not used	No data available	[11]
αMEM, 3 mg/mL BSA, 1 mg/mL bovine fetuin, 5 μg/mL insulin, 5 μg/mL transferrin, ng/mL selenite (ITS), 0.01 IU/mL recombinant human FSH, 50 μg/mL sodium ascorbate	Not used	No data available	[29]
αMEM, GlutaMax (3 mM), penicillin and streptomycin (100 IE/mL), 5 mg/mL human serum albumin, insulin (5 μg/mL), transferrin (5 μg/mL), selenite (5 ng/mL), ascorbic acid (50 μg/mL), FSH (0.01 IE/mL)	Not used	No data available	[10]
αMEM, 5% ETS, 0.01 IU/mL LH, 0.1 IE/mL FSH, 1 mM L-carnitine	αMEM, 10% ETS, 1.5 IU/mL hCG	51	[7]
αMEM, 1% ETS	αMEM, 10% ETS, 1.5 IU/mL hCG, 5 ng/mL EGF	88	[20]
αMEM, 0.01 IU/mL recombinant FSH, 3 mg/mL BSA, 1 mg/mL bovine fetuin, 5 μg/mL insulin, 5 μg/mL transferrin, 5 ng/mL selenite	αMEM, 10% ETS, 1.5 IU/mL hCG, 5 ng/mL EGF	59	[24]
αMEM, 0.01 IU/mL recombinant FSH, 3 mg/mL BSA, 1 mg/mL bovine fetuin, 5 μg/mL insulin, 5 μg/mL transferrin, 5 ng/mL selenite	αMEM, 10% ETS, 1.5 IU/mL hCG, 5 ng/mL EGF	75–82	[19]
αMEM, 0.01 IU/mL recombinant FSH, 3 mg/mL BSA, 1 mg/mL bovine fetuin, 5 μg/mL insulin, 5 μg/mL transferrin, 5 ng/mL selenite	αMEM, 0.25 pg/mL EGF, 0.045 IU/mL hCG	No data available	[25]
αMEM, 0.01 IU/mL recombinant FSH, 3 mg/mL BSA, 5 μg/mL insulin, 5 μg/mL transferrin, 5 ng/mL selenite	αMEM, 1.5 IU/mL hCG, 5 ng/mL EGF	40–71	[26]

energy substrate: α-MEM containing sodium pyruvate is the main component of most follicle culture systems. Both the carbohydrate trophic pathway and the lipid β-oxidation pathway are essential for proper oocyte and embryo development. However, only sporadic studies focused on lipid metabolism during follicle and embryo cultivation [7, 31]. Lipid metabolism via the β-oxidation pathway requires carnitine, which facilitates lipid penetration into the mitochondria by being involved in the formation of the so-called carnitine tunnel [32].

ATP is formed during lipid metabolism in mitochondria due to β-oxidation of fatty acids. Fatty acids are activated on the outer surface of the mitochondrial membrane at the first stage of lipid metabolism. ATP, coenzyme A (HS-CoA), and Mg<sup>2+</sup> ions are involved in activation. The reaction is catalyzed by acyl-CoA synthetase enzyme:



The reaction yields acyl-CoA, which is the active form of the fatty acid. At the second stage of lipid metabolism, the activated fatty acid is supposed to penetrate into the mitochondria. Carnitine palmitoyltransferase I (CPT1B) is the key and simultaneously the limiting factor of this process; this enzyme requires carnitine for functioning [31]. The third stage of lipid

metabolism takes place in the mitochondrial matrix, where ATP molecules are synthesized via the citric acid cycle and the electron transport chain [31].

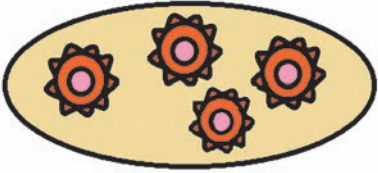
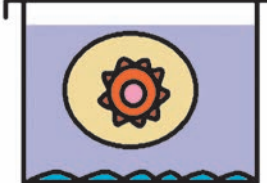
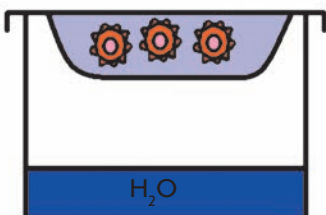
Inhibition of carnitine palmitoyltransferase I was shown to prevent normal meiotic division [31, 33]; hence, a conclusion can be drawn that L-carnitine must be used for normal oocyte development and maturation *in vitro*. The experiments involving mouse follicles cultured in alginate substrate [7] demonstrate that supplementation of oocyte maturation medium with L-carnitine increases the number of normally developing embryos produced by fertilizing oocytes grown *in vitro* using L-carnitine.

Activation of all the metabolic systems (both the carbohydrate and lipid ones) is crucial for stimulating oocyte maturation. Hence, one should expect that there will be further studies focused on the use of L-carnitine and other cofactors stimulating lipid metabolism and that new efficient procedures for follicle cultivation giving rise to mature oocytes will be developed.

### Effect of oxidative stress on follicle growth and maturation

Mammalian ovarian follicles are typically cultured in a conventional carbon dioxide incubator with a 5 vol. % CO<sub>2</sub>/air ratio. Thus, the culturing atmosphere is characterized by the following ratio between the gases (vol. %): 5 CO<sub>2</sub>, 20 O<sub>2</sub>, and 75 N<sub>2</sub> [34]. At this ratio between

**Table 3.** Main follicle coculture systems

Cocultivation type	Experimental scheme	Source
1. Non-contact cultivation of a large number of follicles	 <ul style="list-style-type: none"> <li>● granulosa cells</li> <li>● oocyte</li> <li>● theca cells</li> <li>● alginate hydrogel</li> </ul>	[8]
2. Follicles in the embryonic fibroblasts-conditioned medium	 <ul style="list-style-type: none"> <li>● granulosa cells</li> <li>● oocyte</li> <li>● theca cells</li> <li>● alginate hydrogel</li> <li>● embryonic fibroblasts</li> <li>● conditioned medium</li> </ul>	[43]
3. Follicles in the pre-conditioned medium	 <ul style="list-style-type: none"> <li>● granulosa cells</li> <li>● oocyte</li> <li>● theca cells</li> <li>● pre-conditioned medium</li> </ul>	[13]

the gases in the culturing atmosphere, the partial pressure of oxygen in tissues being cultured is approximately 140 mm Hg [6], while the partial pressure of oxygen in the peritoneal cavity is approximately 40 mm Hg [35], which corresponds to 5 vol. % O<sub>2</sub> in the atmosphere inside the culture incubator.

The viability of follicles cultured at reduced oxygen concentration increases due to the low level of reactive oxygen species (ROS) formed during cultivation. ROS are actively formed when mammalian ovarian follicles are cultured at increased partial pressure of oxygen, thus inducing oxidative stress in cells that has a negative effect on follicle growth and development [36].

It has been demonstrated in a number of studies [10, 37] that cultivation at low oxygen concentrations (5 vol. % compared to 20 vol. % O<sub>2</sub>) in an incubator atmosphere increases the viability and improves growth of mouse ovarian follicles.

Special attention should be paid to oxygen concentration in an incubator atmosphere at early stages of cultivation of follicles (primordial, primary, and early secondary ones). Under *in vivo* conditions, these follicles reside in the ovarian cortex, whose degree of vascularization is much lower than that in the medulla. As a result, early follicles actually exist under extreme hypoxic conditions. Similar conditions need to be reproduced to culture them *in vitro*. Thus, when early

secondary mouse follicles 100–120 μm in diameter are cultured in 2.5 vol. % oxygen atmosphere, their growth, survival rate, and production of vascular endothelial growth factor A (VEGFA), lactate, inhibin B, and anti-Müllerian hormone reliably increase as compared to cultivation in an atmosphere containing 20 vol. % O<sub>2</sub> [11].

On the other hand, it has been demonstrated that cultivation at elevated oxygen concentrations yields higher quality oocytes both during follicle cultivation [38] and when oocyte–cumulus complexes mature *in vitro* [39]. Low oxygen concentration may disturb activity of motor proteins, including dynein and dynactin, regulatory factors responsible for mitotic spindle formation, and proteins regulating the cell cycle in oocytes [38]. Furthermore, reduced oxygen concentration in the culture medium impairs mitochondrial function, which, in turn, reduces ATP production. This very process may result in impaired function of all the groups of proteins mentioned above. Follicle cultivation and maturation at low oxygen levels may also desynchronize nuclear and cytoplasmic maturation of oocytes [38].

The ambiguity of data on the optimal oxygen concentration in a culture atmosphere makes further research relevant, since quality of the embryos developing from oocytes depends on which conditions were selected. Multistage culture systems combining the use

of different oxygen concentrations at different culture stages might be developed. The three-stage culture system shows promise. Ultra-low oxygen concentrations should be used at the first stage (when culturing early follicles). At the second stage (when culturing later antral follicles), oxygen concentration in the incubator atmosphere should be increased. Oxygen concentration in the incubator atmosphere should probably be additionally increased at the third stage (when the oocyte-cumulus complexes isolated from the culture mature). However, the number of culturing stages and the percentage of oxygen in the culture medium at each stage have not been determined yet. It may also be possible that better results are achieved not by changing oxygen concentration in the culturing atmosphere stepwise but by gradually increasing it during the entire cultivation procedure.

The level of reactive oxygen species in follicles being cultured can also be reduced in a different way: by supplementing the culture medium with antioxidants. To reduce the level of formation of reactive oxygen species during follicle cultivation, the medium can be supplemented with various antioxidants, such as quercetin [40], ascorbic acid [29, 41], 7,8-dihydroxyflavone [42], and glutathione [29]. Meanwhile, it has been demonstrated that the positive effect of sodium ascorbate on follicle growth is caused by its ability to stimulate the formation of contacts between follicular cells and the extracellular matrix rather than by antioxidant properties of this substance. Cultivation of mouse follicles encapsulated in alginate hydrogel in the presence of glutathione increased neither their survival rate nor growth compared to the follicles cultured in the medium supplemented with sodium ascorbate. The antioxidant activity of both ascorbic acid and glutathione is most likely to have no significant effect on *in vitro* folliculogenesis [29].

### The use of coculture procedures

Natural conditions of follicle growth and maturation *in vitro* are imitated by supplementing the culture medium with hormones (FSH, hCG, LH), [7, 16, 17], growth factors [20, 25], and other components [7, 10, 29]. Nevertheless, *in vivo* follicle growth conditions cannot be imitated in a laboratory so far. In addition to hormones, follicle's granulosa and theca cells produce a large amount of growth factors so that a specific area locally enriched in hormones is formed. This area is most favorable for follicle growth and development and oocyte growth in them.

Some researchers use a fundamentally different approach (follicle group cocultivation) to produce a follicle culture medium supplemented with numerous growth factors and hormones. It is expected that ovarian com-

ponents during cocultivation of several follicles will stimulate mutual growth and development by enriching the environment in paracrine factors secreted at concentrations required to ensure normal growth of follicles. There are currently three main types of coculture: non-contact coculture of a large number of follicles within one drop of alginate hydrogel [8], coculture of follicles with embryonic fibroblasts [29, 43], and coculture of follicles in a conditioned medium [13, 43]. Table 3 lists the schemes of the most common follicle coculture systems.

When performing direct coculture, several follicles are placed in an alginate hydrogel drop; however, follicles do not contact with one another and some space for growth is left between them. Follicles 'communicate' by releasing paracrine factors into the environment surrounding the follicles. The best results were achieved by culturing 10 follicles per group [8].

Follicles are cocultured with embryonic fibroblasts as follows: follicles encapsulated in alginate hydrogel are placed onto a monolayer of inactivated mouse embryonic fibroblasts that condition the coculture medium by various paracrine factors. Follicles with smaller diameter (starting with 80–90  $\mu\text{m}$ ) can be grown under these conditions more successfully than in feeder layer-free culture systems, which support growth of follicles larger than 100  $\mu\text{m}$  in diameter.

When culturing follicles in a conditioned medium, various cell cultures (mouse embryonic fibroblasts, ovarian cell components) are grown preliminarily; the culture medium is then collected and follicles encapsulated in alginate hydrogel are placed in it. This medium contains various paracrine factors, including the required growth factors that diffuse into the hydrogel, thus forming favorable conditions for follicle growth.

Each of these three main methods has its own advantages and drawbacks. When using non-contact cocultivation of a large number of follicles, it is extremely difficult to control growth and maturation of each individual follicle. Death of a single follicle in the group will also reduce the growth rates of the remaining follicles. Meanwhile, the non-contact cocultivation of follicles is a technologically simple method that allows one to achieve rather good results during cultivation. There are a number of difficulties associated with using the feeder layer of inactivated embryonic fibroblasts to be cocultured with follicles. In particular, the optimal equilibrium between the compositions of culture media needs to be maintained, since the medium needs to contain various substances to ensure normal growth and development of follicles and embryonic fibroblasts. Furthermore, the applicability of this method in medical practice is also an open question, since fetal cells are used during cocultivation in this type of systems. Cul-

tivation of follicles in a pre-conditioned medium is also associated with technological challenges. This coculture system implies several stages, and contamination of the culture medium needs to be avoided at each stage. Furthermore, it is difficult to standardize the process of medium conditioning by proliferating cell population as each batch of the conditioned medium may contain different concentrations of active substances.

## CONCLUSIONS

The technologies for cultivation of mammalian ovarian tissue become more and more advanced and better correlate with *in vivo* conditions. Taking into account the significant number of various aspects, researchers have successfully achieved better cultivation results: the produced oocytes mature in most cases and follicle growth until later stages is observed more often. New components for supplementing culture media to

ensure better growth and maturation of follicles are likely to be discovered in future. Further research will also focus on *in vitro* ovarian reconstruction, which will allow one to culture follicles under optimal conditions. A high-performance follicle culture system can be designed with allowance for numerous factors (mechanical strain, follicular metabolism, gas concentration in the culture environment, hormonal background, effect of paracrine factors, etc.). Hence, studies using a combination of all the factors required for normal follicle growth and development can be expected in the near future; these conditions will allow one to produce oocytes characterized by fertilizability and developmental competency. ●

*This study was supported by the Russian Science Foundation (project № 14-50-00029).*

## REFERENCES

- Di Leva G., Piovani C., Gasparini P., Ngankeu A., Taccioli C., Briskin D., Cheung D.G., Bolon B., Anderlucci L., Alder H., et al. // *PLoS Genet.* 2013. V. 9. № 3. e1003311.
- Verga Falzacappa C., Timperi E., Bucci B., Amendola D., Piergrossi P., D'Amico D., Santaguida M.G., Centanni M., Misiti S. // *J. Endocrinol.* 2012. V. 215. № 2. P. 281–289.
- Oktem O., Oktay K. // *Cancer Res.* 2007. V. 67. № 21. P. 10159–10162.
- Meirow D., Baum M., Yaron R., Levron J., Hardan I., Schiff E., Nagler A., Yehuda D.B., Raanani H., Hourvitz A., Dor J. // *Leuk. Lymphoma.* 2007. V. 48. № 8. P. 1569–1576.
- Songsasen N., Woodruff T.K., Wildt D.E. // *Reproduction.* 2011. V. 142. № 1. P. 113–122.
- Xu J., Lawson M.S., Yeoman R.R., Pau K.Y., Barrett S.L., Zelinski M.B., Stouffer R.L. // *Hum. Reprod.* 2011. V. 26. № 5. P. 1061–1072.
- Dunning K.R., Akison L.K., Russell D.L., Norman R.J., Robker R.L. // *Biol. Reprod.* 2011. V. 85. № 3. P. 548–555.
- Hornick J.E., Duncan F.E., Shea L.D., Woodruff T.K. // *Reproduction.* 2013. V. 145. № 1. P. 19–32.
- Jiao Z.X., Woodruff T.K. // *Fertil. Steril.* 2013. V. 99. № 5. P. 1453–1459.
- Gook D.A., Edgar D.H., Lewis K., Sheedy J.R., Gardner D.K. // *Mol. Hum. Reprod.* 2014. V. 20. № 1. P. 31–41.
- Makanji Y., Tagler D., Pahnke J., Shea L.D., Woodruff T.K. // *Am. J. Physiol. Endocrinol. Metab.* 2014. V. 15. № 306(8). e893–903.
- Figueiredo J.R., Hulshof S.C., Van den Hurk R., Ectors F.J., Fontes R.S., Nusgens B., Bevers M.M., Beckers J.F. // *Theriogenology.* 1993. V. 40. № 4. P. 789–799.
- Choi J.K., Agarwal P., He X. // *Tissue Eng. Part. A.* 2013. V. 19. № 23–24. P. 2626–2637.
- West E.R., Shea L.D., Woodruff T.K. // *Semin. Reprod. Med.* 2007. V. 25. № 4. P. 287–299.
- West-Farrell E.R., Xu M., Gomberg M.A., Chow Y.H., Woodruff T.K., Shea L.D. // *Biol. Reprod.* 2009. V. 80. № 3. P. 432–439.
- Parrish E.M., Siletz A., Xu M., Woodruff T.K., Shea L.D. // *Reproduction.* 2011. V. 142. № 2. P. 309–318.
- Xu J., Lawson M.S., Yeoman R.R., Molskness T.A., Ting A.Y., Stouffer R.L., Zelinski M.B. // *Hum. Reprod.* 2013. V. 28. № 8. P. 2187–2200.
- Shikanov A., Xu M., Woodruff T.K., Shea L.D. // *J. Vis. Exp.* 2011. V. 15. № 49. P. 2695.
- Shikanov A., Xu M., Woodruff T.K., Shea L.D. // *Biomaterials.* 2009. V. 30. № 29. P. 5476–5485.
- Jin S.Y., Lei L., Shikanov A., Shea L.D., Woodruff T.K. // *Fertil. Steril.* 2010. V. 93. № 8. P. 2633–2639.
- Choi J.K., Agarwal P., Huang H., Zhao S., He X. // *Biomaterials.* 2014. V. 35. № 19. P. 5122–5128.
- Streets A.M., Huang Y. // *Curr. Opin. Biotechnol.* 2014. № 25. P. 69–77.
- Desai N., Alex A., AbdelHafez F., Calabro A., Goldfarb J., Fleischman A., Falcone T. // *Reprod. Biol. Endocrinol.* 2010. V. 14. № 8. P. 119.
- Xu M., Banc A., Woodruff T.K., Shea L.D. // *Biotechnol. Bioeng.* 2009. V. 103. № 2. P. 378–386.
- West E.R., Xu M., Woodruff T.K., Shea L.D. // *Biomaterials.* 2007. V. 28. № 30. P. 4439–4448.
- Kreeger P.K., Deck J.W., Woodruff T.K., Shea L.D. // *Biomaterials.* 2006. V. 27. № 5. P. 714–723.
- Xu M., Kreeger P.K., Shea L.D., Woodruff T.K. // *Tissue Eng.* 2006. V. 12. № 10. P. 2739–2746.
- Xu M., West E., Shea L.D., Woodruff T.K. // *Biol. Reprod.* 2006. V. 75. № 6. P. 916–923.
- Tagler D., Makanji Y., Tu T., Bernabé B.P., Lee R., Zhu J., Kniazeva E., Hornick J.E., Woodruff T.K., Shea L.D. // *Biotechnol. Bioeng.* 2014. V. 111. № 7. P. 1417–1429.
- Conti M., Hsieh M., Park J.Y., Su Y.Q. // *Mol. Endocrinol.* 2006. V. 20. № 4. P. 715–723.
- Dunning K.R., Cashman K., Russell D.L., Thompson J.G., Norman R.J., Robker R.L. // *Biol. Reprod.* 2010. V. 83. № 6. P. 909–918.
- Montjean D., Entezami F., Lichtblau I., Belloc S., Gurgan T., Menezo Y. // *J. Assist. Reprod. Genet.* 2012. V. 29. № 11. P. 1221–1225.
- Downs S.M., Mosey J.L., Klinger J. // *Mol. Reprod. Dev.* 2009. V. 76. № 9. P. 844–853.
- Xu J., Bernuci M.P., Lawson M.S., Yeoman R.R., Fisher

## REVIEWS

- T.E., Zelinski M.B., Stouffer R.L. // *Reproduction*. 2010. V. 140. P. 685–697.
35. Tsai A.G., Friesenecker B., Mazzoni M.C., Kerger H., Buerk D.G., Johnson P.C., Intaglietta M. // *Proc. Natl. Acad. Sci. USA*. 1998. V. 95. P. 6590–6595.
36. Silva A.E., Rodriguez P., Cavalcante L.F., Rodrigues B.A., Rodrigues J.L. // *Reprod. Domest. Anim.* 2009. V. 44. Suppl 2. P. 259–262.
37. Adam A.A., Takahashi Y., Katagiri S., Nagano M. // *Jpn. J. Vet. Res.* 2004. V. 52. № 2. P. 77–84.
38. Hu Y., Betzendahl I., Cortvrindt R., Smitz J., Eichenlaub-Ritter U. // *Hum. Reprod.* 2001. V. 16. № 4. P. 737–748.
39. Banwell K.M., Lane M., Russell D.L., Kind K.L., Thompson J.G. // *Hum. Reprod.* 2007. V. 22. № 10. P. 2768–2775.
40. Kang J.T., Kwon D.K., Park S.J., Kim S.J., Moon J.H., Koo O.J., Jang G., Lee B.C. // *J. Vet. Sci.* 2013. V. 14. № 1. P. 15–20.
41. Kere M., Siriboon C., Lo N.W., Nguyen N.T., Ju J.C. // *J. Reprod. Dev.* 2013. V. 59. № 1. P. 78–84.
42. Choi J.Y., Kang J.T., Park S.J., Kim S.J., Moon J.H., Saadeldin I.M., Jang G., Lee B.C. // *J. Reprod. Dev.* 2013. V. 59. № 5. P. 450–456.
43. Tagler D., Tu T., Smith R.M., Anderson N.R., Tinggen C.M., Woodruff T.K., Shea L.D. // *Tissue Eng. Part. A*. 2012. V. 18. № 11–12. P. 1229–1238.



# Search for Human Lactate Dehydrogenase A Inhibitors Using Structure-Based Modeling

D. K. Nilov<sup>1,2\*</sup>, E. A. Prokhorova<sup>2</sup>, V. K. Švedas<sup>1,2</sup>

<sup>1</sup>Belozersky Institute of Physico-Chemical Biology, Lomonosov Moscow State University, Leninskie Gory 1, bldg. 40, 119991 Moscow, Russia

<sup>2</sup>Faculty of Bioengineering and Bioinformatics, Lomonosov Moscow State University, Leninskie Gory 1, bldg. 73, 119991, Moscow, Russia

\*E-mail: nilov@belozersky.msu.ru

Received 10.12.2014

Copyright © 2015 Park-media, Ltd. This is an open access article distributed under the Creative Commons Attribution License, which permits unrestricted use, distribution, and reproduction in any medium, provided the original work is properly cited.

**ABSTRACT** The human lactate dehydrogenase isoform A plays an important role in the anaerobic metabolism of tumour cells and therefore constitutes an attractive target in the oncology field. Full-atom models of lactate dehydrogenase A (in complex with NADH and in the apo form) have been generated to enable structure-based design of novel inhibitors competing with pyruvate and NADH. The structural criteria for the selection of potential inhibitors were established, and virtual screening of a library of low-molecular-weight compounds was performed. A potential inhibitor, STK381370, was identified whose docking pose was stabilized through additional interactions with the loop 96-111 providing for the transition from the open to the closed conformation.

**KEYWORDS** Docking, inhibitor, lactate dehydrogenase, molecular modeling.

**ABBREVIATIONS** LDH – lactate dehydrogenase, LDH-A – lactate dehydrogenase isoform A, 88N - inhibitor name presented in the 4ajp crystal structure.

## INTRODUCTION

Lactate dehydrogenase (LDH) catalyzes the NADH-driven conversion of pyruvate to lactate at the final stage of anaerobic glycolysis. In view of tumor energy metabolism, involving glycolysis activation and inhibition of respiratory chain activity (known as the Warburg effect) [1], human LDH has emerged as a promising tumor promoting factor and a therapeutic target. Glycolic rates in tumor cells could be elevated by an increased level of lactate dehydrogenase isoform A (LDH-A) [2, 3]. Thus, selective inhibition of LDH-A can arrest ATP production and promote tumor cell death [4–6]. Another point to bear in mind is distinguishing between LDH-A and LDH-B (heart muscle LDH) that exhibit high structural similarity [7]. Available X-ray structures of human LDH-A, as well as knowledge of the active site configuration and the catalytic mechanism, provide a means for discovery and structural optimization of inhibitors.

LDH-A is comprised of four subunits, each of which has an active site. Initial binding of the coenzyme NADH by subunit is followed by binding of pyruvate. This is mediated by the Arg168 side chain that forms twin hydrogen bonds with the carboxyl group of pyruvate [8]. In the reaction mechanism hydride ion is transferred to the carbonyl carbon of pyruvate from

NADH and proton is donated to the carbonyl oxygen from His192. The loop 96-111 is essential for catalysis, closing over the active site of LDH-A after the coenzyme and substrate are bound. Being the rate-limiting step, loop closure favors hydrogen bond formation between pyruvate and Arg105 to stabilize the transition state [9]. The structure of human LDH-A crystallized as a ternary complex in the presence of NADH and oxamate (PDB ID 1i10) shows that transition of the loop 96-111 from the open to the closed form may not necessarily occur following substrate binding [7]. Two of the eight subunits remain in the open conformation in the asymmetric units (D and G). A recent study of the crystal structures of the apo form and NADH binary complexes of human LDH-A (PDB ID 4l4r and 4l4s, respectively) demonstrated that the binding of NADH only induces small-scale local changes in the loop structure [10].

Despite a great deal of research into the structural and physico-chemical properties of LDH-A, only a few classes of LDH-A inhibitors have been described, with most compounds having low potencies [11]. The reference substrate-like inhibitor of LDH is oxamate, with a dissociation constant of 26  $\mu$ M against human LDH-A [12]. N-substituted oxamates also inhibit different LDH isoforms in the micromolar range [13, 14]. Recently,

AstraZeneca and ARIAD Pharmaceuticals unveiled new LDH-A inhibitors: derivatives of malonic and nicotinic acids [15, 16]. These compounds were obtained by linking of molecular fragments recognized by the substrate-binding and coenzyme-binding sites. These fragments were identified using high-throughput screening of compound databases, involving molecular modeling at certain points. A crystal structure of human LDH-A in complex with one of the most efficient inhibitors (PDB ID 4ajp) was determined, with the loop 96–111 in the closed conformation. Interestingly, the effective binding does not require loop transition to the closed form, since several enzyme-inhibitor complexes of LDH-A were solved with the loop in the open configuration [17–19].

Virtual screening and molecular modeling of protein interactions may assist in the identification of putative inhibitors in large compound libraries. However, such a modeling should take into account the mobility of the loop 96–111 that can affect binding efficiency. The objective of this study was to select an appropriate crystal structure of LDH-A, build the full-atom model on its basis, and verify the validity of the model for structure-based inhibitor screening and design.

## EXPERIMENTAL SECTION

Human LDH-A models have been constructed based on the crystal structure 1i10 [7] using the AmberTools 1.2 and Amber 10 packages (<http://ambermd.org>) [20]. Hydrogen atoms were added to the protein and ligands, and then the protein molecule was solvated in a TIP3P water box with a minimum distance of 12 Å between the solute and the box edge (crystallographically resolved water molecules were retained). Chloride ions were added to charge neutrality. The energy minimization of the obtained system was performed using 2,500 steps of the steepest descent, followed by 2,500 steps of conjugate gradient, with positional restraints of 2 kcal/(mol × Å<sup>2</sup>) on heavy atoms of protein and ligands. To describe the protein molecule, the *ff99SB* force field was employed [21]. The parameters for NADH were obtained from the AMBER parameter database [22]; for oxamate the parameters of the *GAFF* force field were used [23]. Water molecules and chloride ions were removed from the optimized structure to produce the Model 0 of LDH-A. Models 1 and 2 for docking simulation were obtained by removing oxamate and oxamate with NADH from Model 0, respectively.

The structures of pyruvate and known inhibitors of LDH were modeled using the ACD/ChemSketch 8.17 software [24]. Virtual screening for LDH-A inhibitors was performed among low-molecular-weight compounds from the Vitas-M library [25]. Compounds were protonated using OpenBabel 2.3.0 [26], and their 3D

structures were generated with CORINA 3.4 [27]. Using the ACD/Spectrus DB 14.0 software [28], pyruvate and oxamate derivatives conforming to the Lipinski's rule of five [29] were retrieved from the library.

Molecular docking into the active site of Models 1 and 2 with fixed amino acid coordinates was done using Lead Finder 1.1.15 [30]. The energy grid maps were computed for subunit A to overlap the binding site of oxamate (Model 1) or both binding sites of oxamate and NADH (Model 2). Minimum grid box was created around mentioned ligands (whose coordinates were derived from Model 0), and then the sides were moved away from the box center by a value of 6 Å to include neighbourhood area. The energy of ligand binding was estimated accounting for van der Waals interactions, hydrogen bonding, electrostatics, and entropy changes due to desolvation and restriction of torsion angles. Docking runs were performed in the XP (extra precision) mode. RMS deviation values of the docking poses of inhibitors were calculated using reference coordinates obtained from the 1i10 and 4ajp structures (subunit A). An automated structural filtration was applied to modeled complexes to sort out ones exceeding the distance of 4.5 Å between the carboxyl carbon of the ligand and the guanidinium carbon of Arg168.

Visualization, superimposition, and analysis of structures were performed using VMD 1.8.6 [31] and Swiss-PdbViewer 4.1.0 [32].

## RESULTS AND DISCUSSION

### Crystal structure selection

The Protein Data Bank contains the following human LDH-A structures: the apo form (PDB ID 4l4r), the binary complex with NADH (4l4s), and complexes with inhibitors in the open (4jnk, 4m49, 4qo7, 4qo8) and closed (1i10, 4ajp) conformational states. To analyze the conformational space of the flexible loop 96–111, we superimposed individual subunits of these structures onto the subunit A of the 1i10 structure using C<sup>α</sup>-atoms. The analysis shows that in the open conformation state the loop can be variously arranged, even within one tetramer (*Fig. 1A*). The superimposition of the subunits of the apo form 4l4r yielded a RMS deviation value of 2.09 Å for the C<sup>α</sup>-atoms of the loop. By contrast, in the closed state the loop appears to be stabilized in a unique configuration, with a slight shift in the subunit E of the 1i10 complex (*Fig. 1B*).

The conformational variability of the loop 96–111 in the open state complicates the choice of an appropriate structure for modeling and virtual screening. Recent work on LDH-A conformations advocated the use of ensemble docking, whereby the pose of a putative inhibitor is calculated for various protein structures, fol-

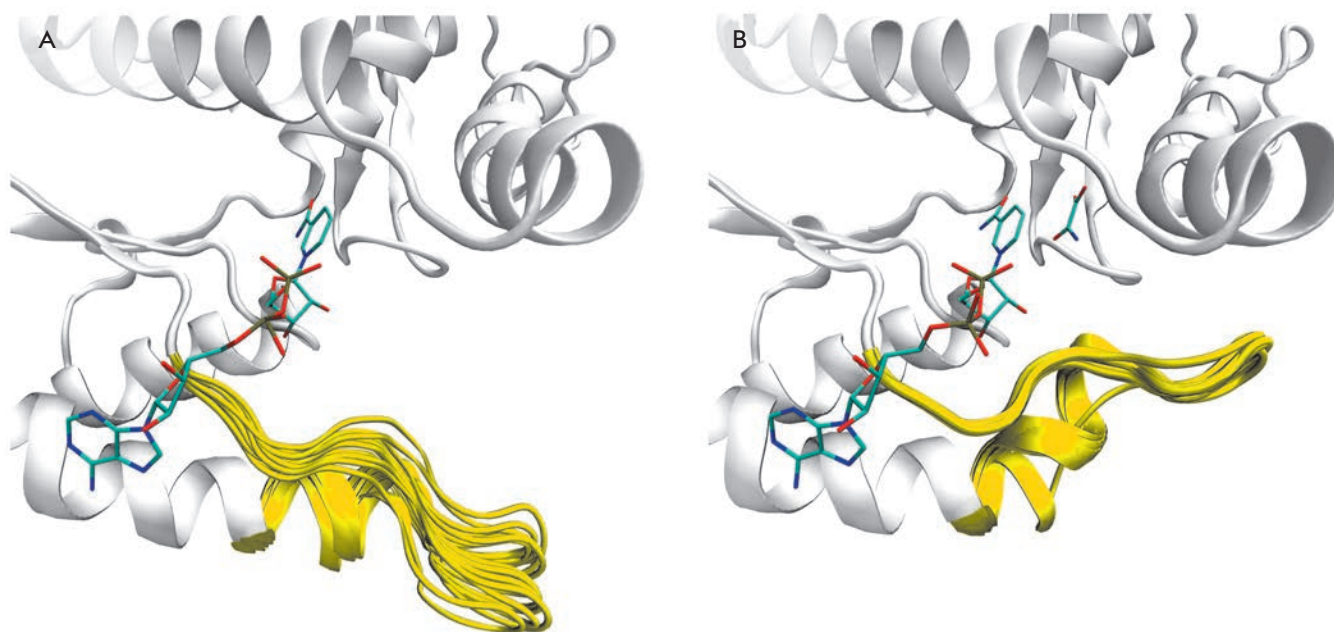


**Fig. 1.** Open (A) and closed (B) conformations of human LDH-A according to X-ray crystallography. The loop 96–111 is colored yellow, and the positions of NADH and oxamate are colored by atom types. The ensemble of open conformations of the loop 96–111 was obtained by superimposition of separate subunits of the structures 4jnk (A, C, D), 4m49 (A–D), 4l4r (A, H), 4l4s (A, H), 4qo7 (A, C, D), 4qo8 (A, C, D) using the C $\alpha$ -atoms. The ensemble of closed conformations was generated by superimposing subunits of the structures 1i10 (A–C, E, F, H) and 4ajp (A–D)

lowed by an analysis of the generated complexes [33]. However, this approach processes large datasets and complicates the establishing criteria for the selection of potential inhibitors.

At the same time, the closed conformation of LDH-A favors structure-based inhibitor design due to the well-defined position of the loop 96–111. The prediction accuracy of closed-state models could be tested by docking substrates and known inhibitors. Therefore, the closed structures of human LDH-A 1i10 and 4ajp were of concern. The 1i10 structure at 2.30 Å resolution is complexed with NADH and oxamate, and the 4ajp structure at 2.38 Å resolution is complexed with the highly potent inhibitor 88N occupying the substrate- and coenzyme-binding sites. The 1i10 structure was chosen for further modeling due to high resolution and the presence of coordinates of all residues within the tetramer.

#### Construction of full-atom enzyme models

Hydrogen atoms were added to the tetrameric LDH-A molecule derived from 1i10. The His192 residue was protonated on the N $\delta^1$  and N $\epsilon^2$ -atoms of the imidazole ring, whereas other ionizable residues in the active site (Arg98, Arg105, Arg168) were modeled in the standard charged form. Energy minimization of the

solvated system was performed to adjust the positions of the added hydrogens. Following the removal of the bound ligands (NADH and/or oxamate) and water molecules, two LDH-A models were generated for docking simulations. Model 1 with NADH in the active site is designed for docking of compounds that compete with pyruvate, and Model 2 in its free form can be used for docking of compound competing with both pyruvate and NADH.

The models were validated by docking human LDH-A inhibitors for which complex's structure is known (Fig. 2). Oxamate, a substrate-like inhibitor, was docked into the active site of Model 1. The RMS deviation value of the predicted pose of oxamate from that of the 1i10 structure was 0.24 Å (Fig. 3A). The docking simulations of substrate binding demonstrated that the pose of pyruvate is similar to that of oxamate, providing catalytically important interactions with Arg105, Arg168, His192, and the NADH nicotinamide ring. Docking of inhibitor 88N into the active site of Model 2 yielded a 1.65-Å deviation from the crystallographic position in 4ajp (Fig. 3B). Known LDH-A inhibitors were correctly oriented in the model active site with a RMS deviation value of within 2 Å with regard to the reference pose, which lends credence to the use of the docking algorithm applied.

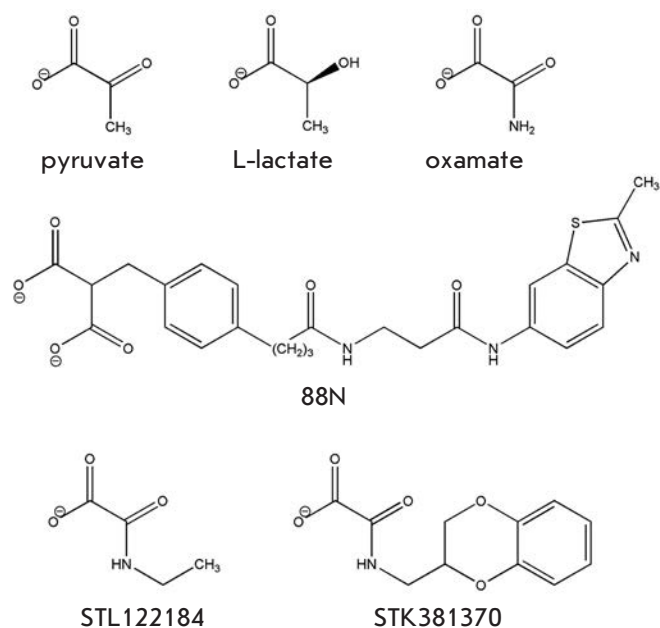


Fig. 2. Substrates and inhibitors of human LDH-A

### Accounting for loop 96–111 interactions

Computer-aided screening with the generated LDH-A models should take into consideration interactions between substrates/inhibitors and the loop 96–111, which stabilized the closed conformation state. To identify hydrogen bonding and hydrophobic interactions that are formed upon loop closure, we compared structures of the apo form 4l4r and those of the enzyme-inhibitor complexes 1i10 and 4ajp.

In the complex 1i10, oxamate, a competitive analogue of pyruvate, forms hydrogen bonds with the Arg105 guanidinium group. This interaction with the loop is well known, since it plays an essential role in stabilizing the transition state during substrate conversion. There is also another hydrogen bond between the 3'-OH-group of the NADH nicotinamide and the backbone oxygen of Ala97; hydrophobic contact between the C2'- and C3'-atoms of the NADH nicotinamide and the side-chain C<sup>β</sup>-atom of Arg98; electrostatic interaction between the pyrophosphate of NADH and the guanidinium group of Arg98 (*see Table*). In the complex 4ajp, the carboxyl groups of inhibitor 88N interact with Arg105 in the same fashion as oxamate. In addition, one carboxyl group is hydrogen-bonded to the side chain of Gln99. The C21-atom of the methylene group and the C27-atom of the benzene ring form hydrophobic contact with the C<sup>β</sup>-atom of Arg98. Interestingly, no short-range interaction between the polar groups of the inhibitor and the guanidinium group of Arg98 is

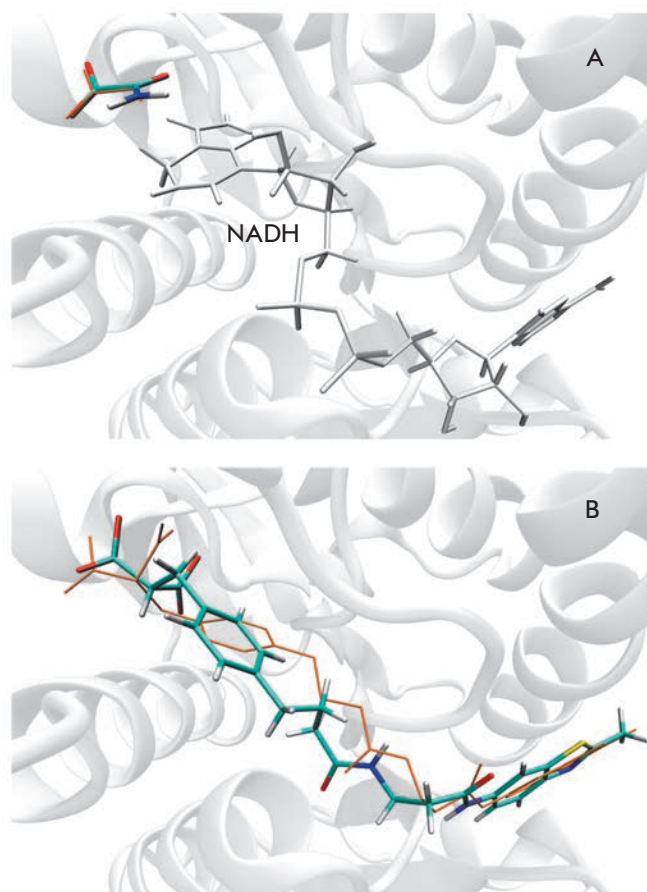
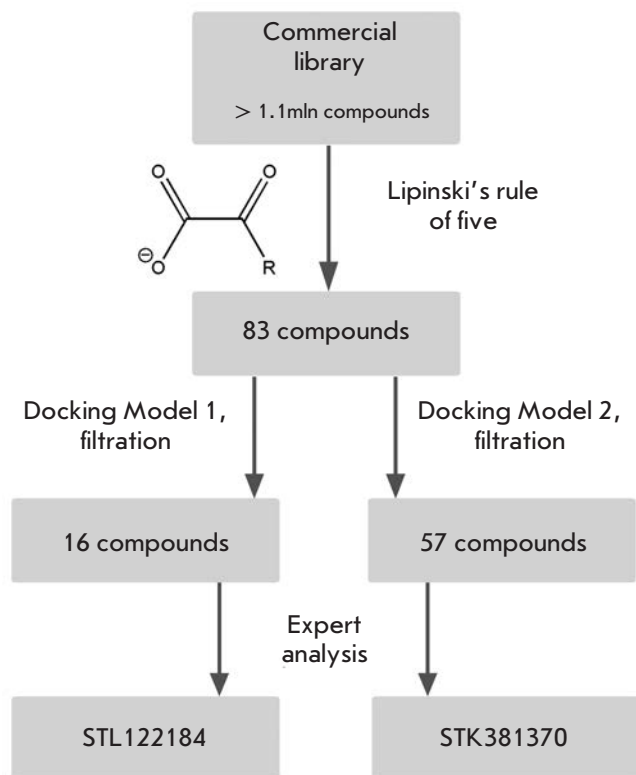


Fig. 3. Poses of known inhibitors in the active site of human LDH-A as predicted by molecular docking. (A) The docking pose of oxamate in Model 1 containing NADH,  $\Delta G^{\text{calc}} = -4.8$  kcal/mol. (B) The docking pose of 88N in Model 2,  $\Delta G^{\text{calc}} = -9.6$  kcal/mol. Orange denotes the coordinates of compounds in the crystal structures 1i10 and 4ajp

observed. The above-listed hydrogen bonds, electrostatic contacts, and hydrophobic interactions with the loop 96–111 are present in modeled complexes with pyruvate, oxamate, and inhibitor 88N and could be used as structural criteria for the selection of potential LDH-A inhibitors among screened compounds.

### Virtual screening for inhibitors

The LDH-A models were evaluated by screening 83 pyruvate and oxamate derivatives ( $\alpha$ -keto acids and their salts) retrieved from Vitas-M library using the Lipinski's rule. This rule defines physico-chemical parameter ranges associated with drug-like compounds (molecular weight  $\leq 500$ ,  $\log P \leq 5$ , hydrogen bond donors  $\leq 5$ , hydrogen bond acceptors  $\leq 10$ ). When docked into the active site of Models 1 and 2, compounds were



**Fig. 4.** Flow-chart of virtual screening of a low-molecular-weight compound library against human LDH-A

additionally filtered to sort out ones that do not form twin hydrogen bonds with Arg168 of the active site (this strong two-point interaction is involved in the binding of pyruvate and oxamate and should be common to substrate-like inhibitors). Via an expert analysis of modeled complexes, compounds capable of forming additional interactions with the protein (hydrogen bonds and hydrophobic contacts) were then selected. At this point, structural criteria for potential LDH-A inhibitor were at least one (for Model 1) or two (for Model 2) interactions with the loop 96–111 listed in Table. Two compounds were eventually selected: STL122184 ( $\Delta G^{\text{calc}} = -4.9$  kcal/mol) and STK381370 ( $\Delta G^{\text{calc}} = -7.9$  kcal/mol) for Model 1 and 2, respectively (Fig. 2, 4).

STL122184 (N-ethyloxamic acid) was recently shown to compete with pyruvate for binding to LDH-A from mouse skeletal muscle ( $K_i = 140$   $\mu\text{M}$ ) [34]. When docked, STL122184 forms twin hydrogen-bonded contacts with the guanidine group of Arg168, hydrogen bonds with Arg105, and forms a hydrophobic contact between the ethyl moiety and the Ile241 side chain (Fig. 5A). Interestingly, STK499896 (N-isopropyllox-

**Table.** Interactions of the loop 96–111 with nicotinamide of NADH, oxamate (OXM), and inhibitor 88N in the closed conformation. Distances to NADH and oxamate are averaged over subunits A–C,F,H of the 1i10 structure, distances to the 88N inhibitor are averaged over subunits A–D of the 4ajp structure

Interaction	Distance, Å	
	1i10	4ajp
Ala97:O ... NADH:O3'	2.88	
Arg98:CB ... NADH:C2'	3.71	
Arg98:CB ... NADH:C3'	3.56	
Arg98:NH1 ... NADH:P	4.0	
Arg105:NH2 ... OXM:O <sub>carboxyl</sub>	2.86	
Arg105:NE ... OXM:O <sub>carbonyl</sub>	2.93	
Arg98:CB ... 88N:C21		4.38
Arg98:CB ... 88N:C27		4.45
Gln99:NE2 ... 88N:O <sub>carboxyl2</sub>		2.72
Arg105:NH2 ... 88N:O <sub>carboxyl1</sub>		3.14
Arg105:NE ... 88N:O <sub>carboxyl2</sub>		3.04

amic acid) and STK501930 (N-propyloxamic acid), close structural analogs of STL122184, were discarded because of no hydrogen bonding with Arg168 and an unfavourable interaction of hydrophobic substituent with the backbone of Thr247, respectively. Experimental testing of these compounds against mouse LDH-A also showed low inhibitory potencies [34, 35].

STK381370 remains yet to be tested for inhibitory activity. This putative inhibitor of LDH-A forms all the necessary interactions listed for Model 2: twin hydrogen-bonded contact with Arg168, hydrogen bonds with Arg105, and a hydrophobic contact with the side chain of Arg98 (Fig. 5B). In addition, the polycyclic moiety of STK381370 may form hydrogen bond with the side-chain of Asn137 and a hydrophobic contact with Val30.

## CONCLUSIONS

The flexibility of the loop 96–111, which forms part of the active site of human LDH-A, dramatically contributes to substrate binding. An analysis of X-ray crystal structures revealed the conformational variability of the loop in the open state. After LDH-A proceeds to the closed state, the loop conformation is stabilized

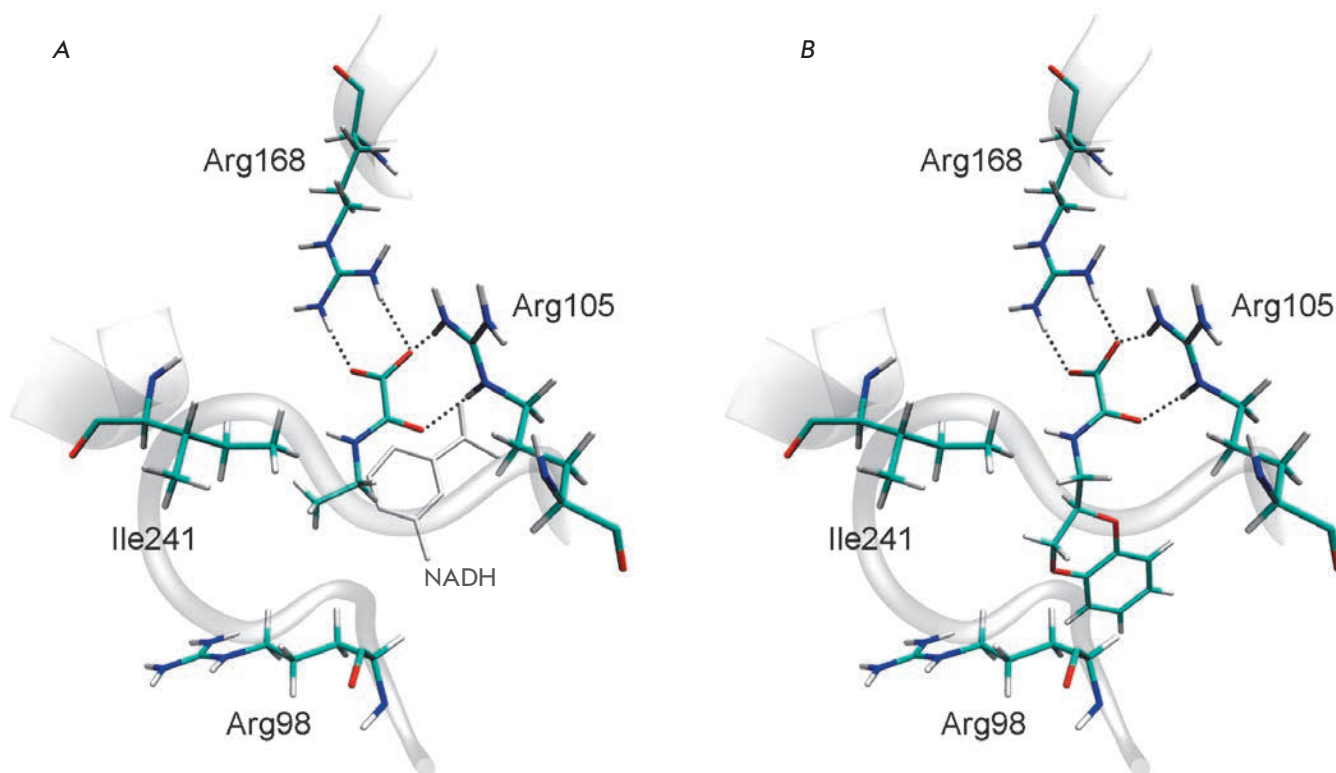


**Fig. 5.** Positions of potential inhibitors in the active site of human LDH-A revealed by virtual screening of a commercial compound library. (A) The docking pose of STL122184 in Model 1. (B) The docking pose of STK381370 in Model 2. The Arg98 and Arg105 residues of the mobile loop 96-111 are shown

by hydrogen bonds and hydrophobic contacts formed by Ala97, Arg98, Gln99, and Arg105 with bound substrates and inhibitors.

On the basis of the crystal tetrameric structure 1i10, we constructed full-atom models of human LDH-A (in complex with NADH and in the apo form) that showed promise in virtual screening of a low-molecular-weight compound library. The established criteria for the se-

lection of putative inhibitors were hydrogen bonds and hydrophobic contacts with the loop 96-111. They enabled us to identify a potential inhibitor, STK381370, whose docking pose was stabilized through additional interactions with Arg105 and Arg98. ●

*This work was supported by RFBR  
(grant № 14-08-01251).*

#### REFERENCES

- Warburg O. // *Science*. 1956. V. 124. P. 269–270.
- Goldman R.D., Kaplan N.O., Hall T.C. // *Cancer Res*. 1964. V. 24. P. 389–399.
- Koukourakis M.I., Giatromanolaki A., Sivridis E., Bougioukas G., Didilis V., Gatter K.C., Harris A.L. // *Br. J. Cancer*. 2003. V. 89. P. 877–885.
- Fantin V.R., St-Pierre J., Leder P. // *Cancer Cell*. 2006. V. 9. P. 425–434.
- Le A., Cooper C.R., Gouw A.M., Dinavahi R., Maitra A., Deck L.M., Royer R.E., Vander Jagt D.L., Semenza G.L., Dang C.V. // *Proc. Natl. Acad. Sci. USA*. 2010. V. 107. P. 2037–2042.
- Miao P., Sheng S., Sun X., Liu J., Huang G. // *IUBMB Life*. 2013. V. 65. P. 904–910.
- Read J.A., Winter V.J., Eszes C.M., Sessions R.B., Brady R.L. // *Proteins*. 2001. V. 43. P. 175–185.
- Dunn C.R., Wilks H.M., Halsall D.J., Atkinson T., Clarke A.R., Muirhead H., Holbrook J.J. // *Philos. Trans. R. Soc. Lond. B Biol. Sci*. 1997. V. 332. P. 177–184.
- Gerstein M., Chothia C. // *J. Mol. Biol*. 1991. V. 220. P. 133–149.
- Dempster S., Harper S., Moses J.E., Dreveny I. // *Acta Crystallogr. D Biol. Crystallogr*. 2014. V. 70. P. 1484–1490.
- Granchi C., Bertini S., Macchia M., Minutolo F. // *Curr. Med. Chem*. 2010. V. 17. P. 672–697.
- Eszes C.M., Sessions R.B., Clarke A.R., Moreton K.M., Holbrook J.J. // *FEBS Lett*. 1996. V. 399. P. 193–197.
- Yu Y., Deck J.A., Hunsaker L.A., Deck L.M., Royer R.E., Goldberg E., Vander Jagt D.L. // *Biochem. Pharmacol*. 2001. V. 62. P. 81–89.

## RESEARCH ARTICLES

14. Choi S.R., Beeler A.B., Pradhan A., Watkins E.B., Rimoldi J.M., Tekwani B., Avery M.A. // *J. Comb. Chem.* 2007. V. 9. P. 292–300.
15. Ward R.A., Brassington C., Breeze A.L., Caputo A., Critchlow S., Davies G., Goodwin L., Hassall G., Greenwood R., Holdgate G.A., et al. // *J. Med. Chem.* 2012. V. 55. P. 3285–3306.
16. Kohlmann A., Zech S.G., Li F., Zhou T., Squillace R.M., Commodore L., Greenfield M.T., Lu X., Miller D.P., Huang W.S., et al. // *J. Med. Chem.* 2013. V. 56. P. 1023–1040.
17. Dragovich P.S., Fauber B.P., Corson L.B., Ding C.Z., Eigenbrot C., Ge H., Giannetti A.M., Hunsaker T., Labadie S., Liu Y., et al. // *Bioorg. Med. Chem. Lett.* 2013. V. 23. P. 3186–3194.
18. Fauber B.P., Dragovich P.S., Chen J., Corson L.B., Ding C.Z., Eigenbrot C., Giannetti A.M., Hunsaker T., Labadie S., Liu Y., et al. // *Bioorg. Med. Chem. Lett.* 2013. V. 23. P. 5533–5539.
19. Dragovich P.S., Fauber B.P., Boggs J., Chen J., Corson L.B., Ding C.Z., Eigenbrot C., Ge H., Giannetti A.M., Hunsaker T., et al. // *Bioorg. Med. Chem. Lett.* 2014. V. 24. P. 3764–3771.
20. Case D.A., Darden T.A., Cheatham T.E., III, Simmerling C.L., Wang J., Duke R.E., Luo R., Crowley M., Walker R.C., Zhang W., et al. // *AMBER 10*. University of California, San Francisco. 2008.
21. Hornak V., Abel R., Okur A., Strockbine B., Roitberg A., Simmerling, C. // *Proteins*. 2006. V. 65. P. 712–725.
22. Walker R.C., de Souza M.M., Mercer I.P., Gould I.R., Klug D.R. // *J. Phys. Chem. B*. 2002. V. 106. P. 11658–11665.
23. Wang J., Wolf R.M., Caldwell J.W., Kollman P.A., Case D.A. // *J. Comput. Chem.* 2004. V. 25. P. 1157–1174.
24. ACD/ChemSketch Freeware, version 8.17. Advanced Chemistry Development, Inc., [www.acdlabs.com](http://www.acdlabs.com). 2005.
25. ST(K/L) collection. Vitas-M Laboratory, Ltd, [www.vitasmlab.com](http://www.vitasmlab.com). 2012.
26. O’Boyle N.M., Banck M., James C.A., Morley C., Vandermeersch T., Hutchison G.R. // *J. Cheminform.* 2011. V. 3. P. 33.
27. Sadowski J., Gasteiger J., Klebe G. // *J. Chem. Inf. Comput. Sci.* 1994. V. 34. P. 1000–1008.
28. ACD/Spectrus DB, version 14.01. Advanced Chemistry Development, Inc., [www.acdlabs.com](http://www.acdlabs.com). 2012.
29. Lipinski C.A. // *Drug Discov. Today Technol.* 2004. V. 1. P. 337–341.
30. Stroganov O.V., Novikov F.N., Stroylov V.S., Kulkov V., Chilov G.G. // *J. Chem. Inf. Model.* 2008. V. 48. P. 2371–2385.
31. Humphrey W., Dalke A., Schulten K. // *J. Mol. Graphics.* 1996. V. 14. № 1. P. 33–38.
32. Guex N., Peitsch M.C. // *Electrophoresis*. 1997. V. 18. P. 2714–2723.
33. Buonfiglio R., Ferraro M., Falchi F., Cavalli A., Masetti M., Recanatini M. // *J. Chem. Inf. Model.* 2013. V. 53. P. 2792–2797.
34. Rodríguez-Páez L., Chena-Taboada M.A., Cabrera-Hernández A., Cordero-Martínez J., Wong C. // *J. Enzyme Inhib. Med. Chem.* 2011. V. 26. P. 579–586.
35. Wong C., Rodríguez-Páez L., Noguera B., Pérez A., Baeza I. // *Biochim. Biophys. Acta.* 1997. V. 1343. P. 16–22.

# Modified Method of rRNA Structure Analysis Reveals Novel Characteristics of Box C/D RNA Analogues

J. A. Filippova<sup>1,2\*</sup>, G. A. Stepanov<sup>1</sup>, D. V. Semenov<sup>1</sup>, O. A. Koval<sup>1,2</sup>, E. V. Kuligina<sup>1</sup>, I. V. Rabinov<sup>1</sup>, V. A. Richter<sup>1</sup>

<sup>1</sup>Institute of Chemical Biology and Fundamental Medicine, Siberian Branch of the Russian Academy of Sciences, Lavrentiev Ave., 8, Novosibirsk, 630090, Russia

<sup>2</sup>Novosibirsk State University, Pirogova Str., 2, Novosibirsk, 630090, Russia

\*E-mail: filippova@niboch.nsc.ru

Received 04.08.2014

Copyright © 2015 Park-media, Ltd. This is an open access article distributed under the Creative Commons Attribution License, which permits unrestricted use, distribution, and reproduction in any medium, provided the original work is properly cited.

**ABSTRACT** Ribosomal RNA (rRNA) maturation is a complex process that involves chemical modifications of the bases or sugar residues of specific nucleotides. One of the most abundant types of rRNA modifications, ribose 2'-O-methylation, is guided by ribonucleoprotein complexes containing small nucleolar box C/D RNAs. Since the majority of 2'-O-methylated nucleotides are located in the most conserved regions of rRNA that comprise functionally important centers of the ribosome, an alteration in a 2'-O-methylation profile can affect ribosome assembly and function. One of the key approaches for localization of 2'-O-methylated nucleotides in long RNAs is a method based on the termination of reverse transcription. The current study presents an adaptation of this method for the use of fluorescently labeled primers and analysis of termination products by capillary gel electrophoresis on an automated genetic analyzer. The developed approach allowed us to analyze the influence of the synthetic analogues of box C/D RNAs on post-transcriptional modifications of human 28S rRNA in MCF-7 cells. It has been established that the transfection of MCF-7 cells with a box C/D RNA analogue leads to an enhanced modification level of certain native sites of 2'-O-methylation in the target rRNA. The observed effect of synthetic RNAs on the 2'-O-methylation of rRNA in human cells demonstrates a path towards targeted regulation of rRNA post-transcriptional maturation. The described approach can be applied in the development of novel diagnostic methods for detecting diseases in humans.

**KEYWORDS** small nucleolar box C/D RNAs, RNA post-transcriptional modifications, RNA 2'-O-methylation, reverse transcription termination.

**ABBREVIATIONS** rRNA – ribosomal RNA; PTC – peptidyl transferase center; snoRNA – small nucleolar RNA; snoRNP –small nucleolar ribonucleoprotein; FAM – 5(6)-carboxyfluorescein; M-MLV – Moloney murine leukemia virus; dNTP – deoxynucleoside triphosphates; RT – reverse transcription; PAGE – polyacrylamide gel electrophoresis; pre-rRNA – precursor of ribosomal RNA.

## INTRODUCTION

The RNAs of all living organisms undergo post-transcriptional modifications and contain not only the canonical, but also the modified nucleotides necessary for the proper functioning of sophisticated biological complexes. Post-transcriptional modifications significantly influence the formation of the RNA secondary structure and function [1, 2].

One of the most abundant types of non-coding RNA modifications in mammals is the 2'-O-ribose methylation of nucleotides [3]. The position of many 2'-O-methylation sites in rRNA is conserved, and the majority of the modifications have been found in most evolutionary-conserved and functionally important regions of rRNA that play the key role in different stages of

translation [4]. A change in the overall pattern of rRNA methylation and the lack of modified nucleotides can result in aberrations in ribosome assembly and function [5, 6]. For instance, it has been demonstrated that the blockage of nucleotide modification in the ribosomal peptidyl transferase center (PTC) causes changes in the secondary structure of 25S rRNA in yeast, impairs the translational activity of ribosomes and, in some cases, enhances cellular sensitivity to translational inhibitors [2, 7].

Modifications are considered to promote the stabilization of the rRNA functional structure due to the influence on inter- and intramolecular interactions [2]. So far, the main function of modifications is believed to be participation in ribosome maturation and assembly:



rRNA modification may serve to some extent as an additional quality criterion of newly synthesized rRNA, contributing to the selection of only “proper” rRNAs for integration into ribosomes [8].

Ribose 2'-O-methylation of rRNAs and small nuclear RNAs in mammalian cells is known to be performed by ribonucleoprotein complexes containing a small nucleolar box C/D RNA (snoRNPs) [9]. Furthermore, box C/D RNA, being complementary to the region of the target RNA, is directly involved in the process of recognition of the target nucleotide for 2'-O-methylation; the fifth nucleotide from the box D is subjected to modification (*Fig. 1*) [10, 11].

It has been recently shown that several types of cancer cells exhibit enhanced expression of box C/D RNAs, as well as of fibrillarin, the key protein of snoRNPs, which functions as a methyltransferase [12, 13]. It has been established that various types of breast cancer cells can differ in the methylation level of several rRNA nucleotides [14]. Differences in the expression of certain box C/D RNAs have been detected in various types of leukemia [15]. It has been mentioned earlier that aberrations in rRNA maturation and ribosomal protein synthesis in human cells can result in pathological changes [16, 17]. Thus, snoRNAs are able to participate in oncogenesis, and the change in the rRNA 2'-O-methylation profile may have a diagnostic value. Therefore, the development of novel approaches for the analysis of rRNA and other long cellular RNA structures that enable a quantitative evaluation of the modification level of certain nucleotides in such RNAs is of great interest.

The current paper presents an adaptation of the method for the determination of 2'-O-methylated

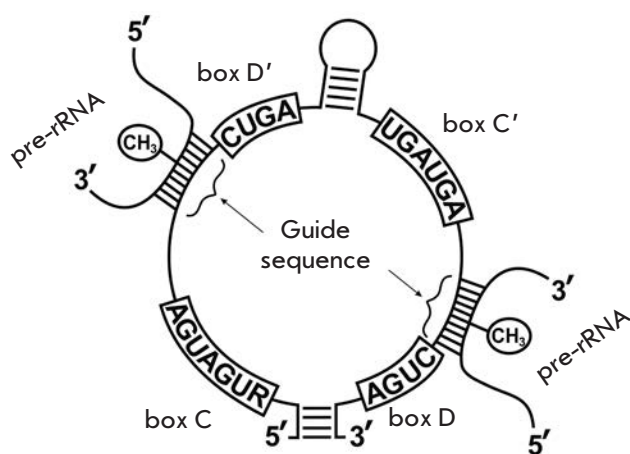


**Fig. 1.** Structure of box C/D RNA and its interaction with a target pre-rRNA

nucleotides in RNA to the use of 5'-fluorescently labeled primers with further analysis of reverse transcription (RT) termination products on an automated DNA-analyzer. Using the proposed approach, we have analyzed the influence of synthetic box C/D RNAs on the changes in the 2'-O-methylation profile of rRNA in human cells. It has been established that transfection of human breast adenocarcinoma MCF-7 cells with 28S rRNA-directed synthetic box C/D RNAs leads to an increase in the 2'-O-methylation level of certain nucleotides within the target RNA.

## EXPERIMENTAL

### Analysis of human 18S and 28S rRNA

#### 2'-O-methylation profiles

Nucleotide numbers of human rRNAs are presented according to GenBank: U13369 (7935–12969 nt) for 28S rRNA and X03205 for 18S rRNA.

Reverse transcription was carried out with primers containing 5'-terminal [<sup>32</sup>P] or 5(6)-carboxyfluorescein (FAM) label: 18-2 – 5'-TAATGATCCTTCCGCAG-GTTC-3' (complementary to the region 1849–1869 nt of 18S rRNA); FAM-28-2.2 – 5'-ATTGGCTCCTCAGC-CAAGCA-3' (4608–4627 nt of 28S rRNA) and FAM-4491 – 5'-GACGGTCTAAACCCAGCTCA-3' (4491–4510 nt of 28S rRNA). A reagent mixture containing 3.0 µg of total cellular RNA and 1.4 pmol of primer was incubated at 70°C for 3 min and cooled to 4°C; then reverse transcription buffer containing 50 mM KCl, 50 mM Tris-HCl (pH 8.3), 4 mM MgCl<sub>2</sub>, and 10 mM DTT, and also 3 AU/µl of M-MLV reverse transcriptase (Biosan, Novosibirsk, Russia) was added to the solution. The mix of dNTP was added separately to a final concentration of 2.0, 1.0, 0.1, or 0.04 mM. The reaction mixture was incubated at 40°C for 2 h. The RT products were precipitated with 75% ethanol, dried, and dissolved in deionized water.

The sequencing of the 18S rRNA region was conducted using the method of reverse transcription in the presence of ddNTP. In order to do this, 3.0 µg of total cellular RNA and 1.4 pmol of primer 18-2 were incubated at 70°C for 3 min and cooled to 4°C. One type of ddNTP was then added to the reaction mixture: ddATP to a final concentration of 5.0 µM, ddCTP – 2.5 µM, ddGTP – 5.0 µM or dTTP – 5.0 µM. The final concentration of the dNTP corresponding to the type of ddNTP in the solution was 25 µM; the concentration of the other dNTP – 100 µM. The obtained solution was mixed with reverse transcription buffer (see above), 2.0 mM MnCl<sub>2</sub>, 10 mM DTT and 3 AU/µl of M-MLV reverse transcriptase. The mixture was incubated at 40°C for 90 min.

### Analysis of the products of reverse transcription of human ribosomal RNA

The separation of fluorescently labeled products of the reverse transcription of rRNA was performed on an ABI3100 Genetic Analyzer (Applied Biosystems, Genomics Core Facility, Siberian Branch of the Russian Academy of Sciences). The data were analyzed using Peak Scanner Software version 1.0 (Applied Biosystems, USA). The relative change in the yield of RT products was determined on the basis of the peak area normalized to the total area of the peaks with relative intensities changing within the limits of 20%. The presented data are the average results of at least three independent experiments.

### Synthesis of artificial box C/D RNAs

The analogues of box C/D RNAs were obtained via *in vitro* transcription according to [18, 19]:

28A4518 (98 nt)

5' - GACUCAGCAUGCGUGUCAUGCU-AUGAUGAAAAGUCAACUUAGGCGUGGUU-GUGGCCUAAAACUAACCUGUCUCUGAUG-GCAGAGGCAUGCUGAGUC-3';

RNA3 (77 nt)

5' - GGGUGCAGAUGAUGUAAAUAAGCGAC-GGGCGGUGCUGAGAGAUGGUGAUGAACGGU-CUAAAACCCAGCUGAUGCACCC-3';

RNA5 (77 nt)

5' - GGGUGCAGAUGAUGUAAAUAAGCGACGGGCG-GUGCUGAGAGAUGGUGAUGAACGACGGUCU-AAACCCUGAUGCACCC-3';

RNA5mC (77 nt)

5' - GGGUGCAGACAGCACAAAUAAGCGACGGGCG-GUGCUGAGAGAUGGCAGCAGACGACGGUCU-AAACCCUGAUGCACCC-3';

RNA5D/N (77 nt)

5' - GGGUGCAGAUGAUGUAAAUAAGCGACGGGCG-GUGAAAAGAGAUGGUGAUGAACGACGGUCU-AAACCAAAAUGCACCC-3';

RNA5mD (77 nt)

5' - GGGUGCAGAUGAUGUAAAUAAGCGACGGGCG-GUGAAAAGAGAUGGUGAUGAACGACGGUCU-AAACCAAAAUGCACCC-3'.

Ribosomal RNA recognition motifs are underlined; conserved elements (boxes C and D) are in bold.

### Transfection of MCF-7 cells with synthetic RNAs. Isolation of total cellular RNA

MCF-7 cells (from the Russian cell culture collection of vertebrates, Institute of Cytology, Russian Acade-

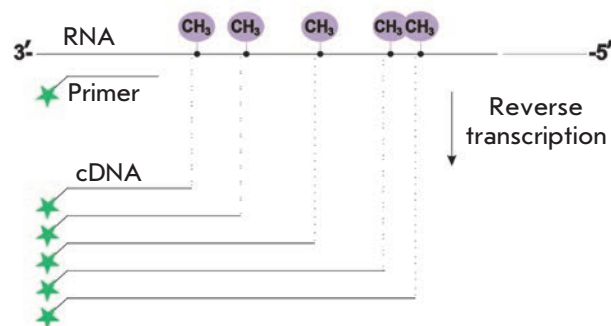


Fig. 2. Method of reverse transcription termination

my of Sciences, St. Petersburg) were cultured in MDM medium with 10 mM L-glutamine and 40 µg/ml of gentamicin in the presence of 10% fetal bovine serum in 5% CO<sub>2</sub> at 37°C.

Synthetic analogues of box C/D RNAs (10<sup>-6</sup> M) were pre-incubated with Lipofectamine (Invitrogen, USA) at a concentration of 0.06 mg/ml at 20°C for 15 min. MCF-7 cells were transfected with the RNA/lipofectamine complex (the final concentration of RNA in the medium was 7 × 10<sup>-8</sup> M). Control cells were incubated in the medium with Lipofectamine (6 µg/ml) only. After 24 h of incubation, total cellular RNA was isolated using Trizol Reagent (Invitrogen, USA) according to the manufacturer's protocol. The integrity of total RNA was assessed by electrophoresis using the Lab-on-chip platform for nucleic acid analysis (Agilent Bioanalyzer), and the samples with RIN values not less than 8.0 were further used in the experiments. The 2'-O-methylation profile of rRNA was analyzed as described above.

## RESULTS AND DISCUSSION

### Modification of the method of reverse transcription termination

The method of reverse transcription termination is based on the ability of 2'-O-methylated nucleotides to cause the arrest of reverse transcriptase at dNTP concentrations less than 1 mM [20]. The location of 2'-O-methylated nucleotides in the analyzed RNA can be excluded from the length of RT termination products [21] (Fig. 2). Unlike the conventional technique, which assumes the reaction of reverse transcription with the radioactively labeled primer and separation of cDNA products in a polyacrylamide gel with further autoradiography, the approach we have developed is based on the use of fluorescently labeled primers and analysis of cDNA by capillary gel electrophoresis on an automated genetic analyzer.

The possibility of applying such an approach in the determination of 2'-O-methylated sites in RNA has

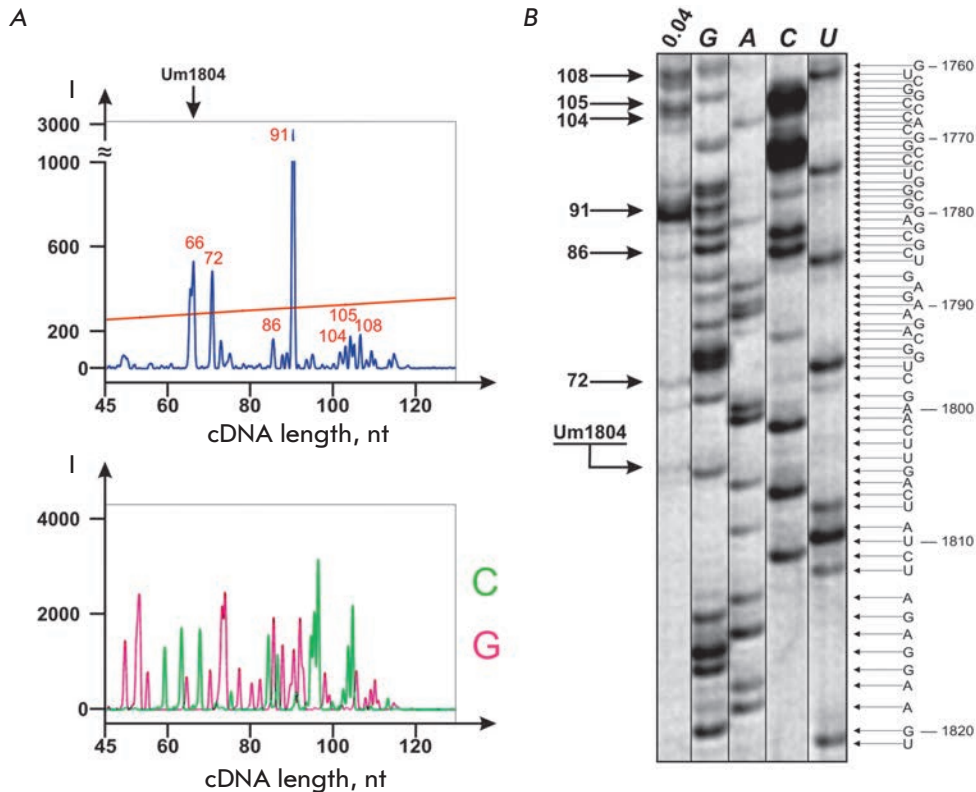


**Fig. 3.** Comparison of the products of 18S rRNA reverse transcription termination with 5'-[<sup>32</sup>P]-labeled or 5'-FAM-labeled primer 18-2 (0.04 mM dNTP). **A** – 5'-FAM-labeled products of RT termination separated by capillary gel electrophoresis on an automated DNA analyzer (*upper insertion*); products of 18S rRNA RT with ddGTP and ddCTP (*lower insertion*). **B** – 5'-[<sup>32</sup>P]-labeled products of RT separated on 12% denaturing PAGE. Lane 0.04 – products of RT termination at 0.04 mM dNTP. Lanes G, A, C and U – RT of 18S rRNA with ddCTP, dTTP, ddGTP and ddATP, respectively

been studied by conducting the reverse transcription of 18S and 28S rRNA from MCF-7 cells with [5'-<sup>32</sup>P]- or 5'-FAM-labeled primers. *Figure 3* depicts the comparison between the typical results of the conventional method utilizing radioactively labeled primers and the method adapted to the analysis of fluorescently labeled cDNA products on an automated genetic analyzer. It can be seen from *fig. 3A,B* that the sets of cDNA products are in good agreement with each other in length and relative yield.

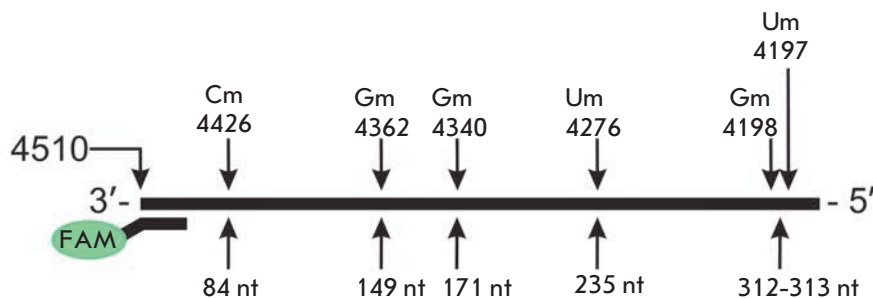
In order to determine precisely whether there is a correspondence between the detected products of RT termination and the location of specific nucleotides in the RNA template, we separated Sanger sequencing products of the 18S rRNA region (*Fig. 3A, lower insertion*).

Reproducibility of the results was assessed by using the data of three independent experiments of total cellular RNA reverse transcription with primers specific to various regions of 18S and 28S rRNAs, followed by separation of the cDNA products on a genetic analyzer. It has been established in a series of experiments that the main products of RT termination of the same regions of the rRNA template correspond to each other in the retention time ( $\pm 1$  nt) and intensities of cDNA signals ( $\pm 10\%$ ) (data not shown).

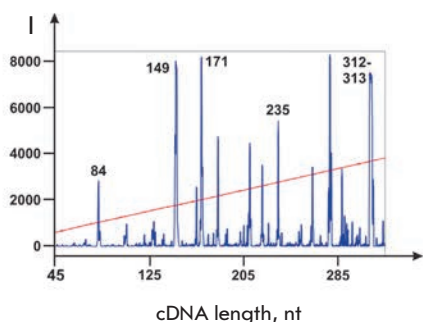
Using the proposed method, we analyzed the sets of human 28S rRNA RT termination products at different concentrations of monomers in the reaction mixture. In addition to conventional conditions of the RT experiment that utilizes low dNTP concentrations (0.001–0.1 mM) in the reaction mixture [21], we also conducted the reaction at a high concentration of monomers (2.0 mM). *Figure 4* demonstrates that decreased dNTP concentrations in the reaction mixture lead to a higher yield of cDNA products 84, 149, 171, and 235 nt in length that correspond to known sites of 2'-O-methylation: Cm4426, Gm4362, Gm4340, and Um4276, respectively (*Fig. 4B,C*). The reverse transcriptase terminates directly at a modified nucleotide (Gm4362, Gm4340 and Um4276) or at the 3' neighboring nucleotide to the 2'-O-methylated (Cm4426). Moreover, it has been established that specificity of termination at 2'-O-methylated nucleotides can be achieved upon increasing dNTP concentration to 2.0 mM. For instance, at 2.0 mM of dNTP, the yield of the termination products that do not correspond to the 2'-O-methylated nucleotides of the RNA template decreases substantially compared to a reaction conducted at 0.1 mM dNTP (*Fig. 4B,D*).

The advantage of the new approach is the possibility of quantitatively assessing the yield of RT termination products. Furthermore, the separation of termination

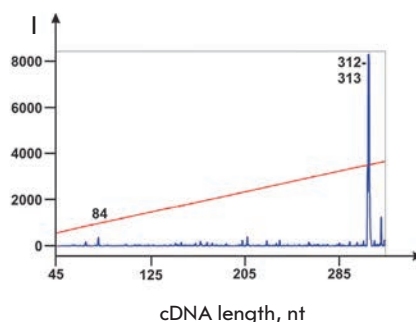
A



B



C



D

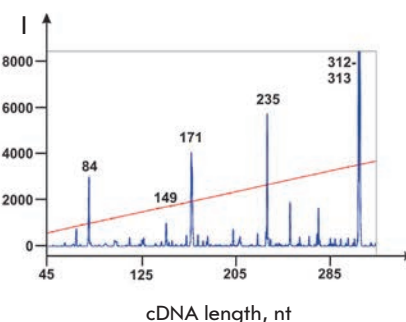


**Fig. 4.** Analysis of cDNA products corresponding to the native sites of 2'-O-methylation in 28S rRNA. A – 2'-O-methylated nucleotides in 28S rRNA and lengths of corresponding termination products of RT with primer FAM-4491. B–D – analysis of FAM-labeled products of RT termination separated on an automated DNA analyzer. RT of 28S rRNA isolated from MCF-7 cells was conducted with the following concentrations of dNTP in the reaction mixture: B – 0.1 mM, C – 1.0 mM, D – 2.0 mM

products on an automated genetic analyzer enables to obtain more complete information on the location of termination sites in the RNA template due to the analysis of longer RNA regions compared to the conventional separation of cDNA in denaturing PAGE. The proposed approach can be applied for the identification of modified nucleotides in native RNAs, verification of the location of modification sites in synthetic RNAs, and for solving other tasks related to the analysis of the structures of long RNA molecules by the reverse transcription method as well.

#### The influence of box C/D RNA analogues on the profile of 2'-O-methylation in human rRNA

The approach we have proposed can be used to study the influence of small nucleolar box C/D RNA analogues on the processing of target rRNAs in human cells. Earlier, J. Cavaille *et al.* demonstrated the possibility of directing 2'-O-methylation of rRNA using DNA constructs encoding box C/D RNAs [22]. We have designed and obtained synthetic analogues of human small nucleolar box C/D RNAs containing altered guide sequences (Fig. 1). We chose human rRNA nucleotides located within or in close vicinity to ribosomal

PTC: G4499, U4502 and A4518 of 28S rRNA [23–25] as the targets for artificial box C/D RNAs. The analogues of small nucleolar box C/D RNAs were constructed to contain all the necessary components for directing 2'-O-methylation in a defined target nucleotide: conserved regions of boxes C and D (snoRNP protein recognition domains) and a sequence complementary to a region within the target rRNA (Fig. 5).

The box C/D RNA analogue named 28A4518 has a structure appropriate for guiding 2'-O-methylation of A4518 of 28S rRNA. Figure 6C demonstrates that transfection of RNA 28A4518 into human MCF-7 cells does not lead to the formation of a new termination product, 109-nt-long cDNA, corresponding to the target nucleotide. The absence of a nucleotide modification in the target rRNA has been discussed by us previously [18]. In particular, we assume that the observed absence of target nucleotide 2'-O-methylation may be an indication of the low content of the modified rRNA in cells due to its robust degradation. As shown in the studies by B. Liu and M.J. Fournier *et al.*, 2'-O-methylation of several nucleotides that comprise ribosome active centers in yeast induces degradation of target rRNAs and impedes cell growth [23, 27, 28].

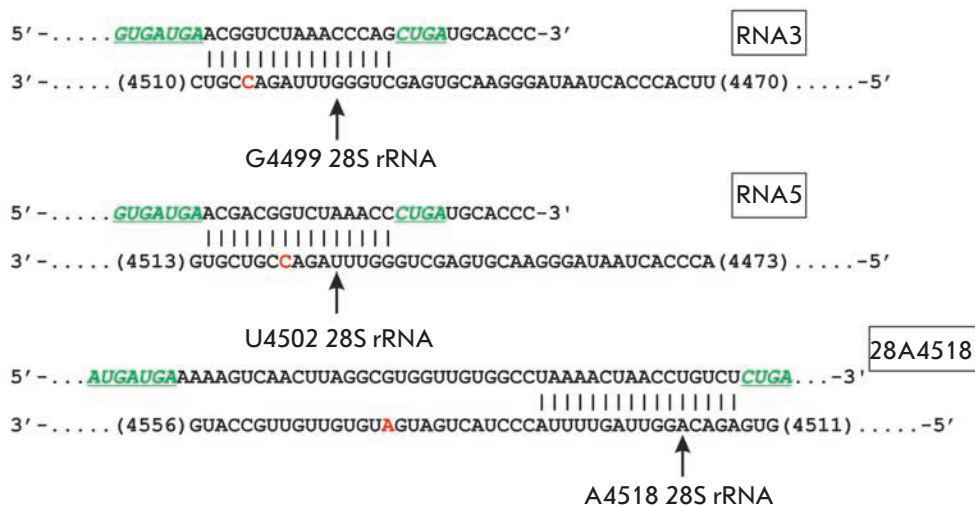


**Fig. 5.** Design of the artificial analogues of box C/D RNAs. Conserved elements of snoRNA analogues – boxes C (C') and D (D') – are colored in green. Target nucleotides in rRNA are arrowed with the number of a nucleotide denoted according to [26]. Known sites of 2'-O-methylation in 28S rRNA are colored in red. The rectangles contain the designation of box C/D RNA analogues complementary to a specific region in the corresponding rRNA

Despite the absence of termination at the target nucleotide for RNA 28A4518, the transfection of cells with the synthetic analogue led to changes in the level of 2'-O-methylation of known sites of modification. *Figure 6B,C* demonstrates the increase in the yield of termination products that correspond to 2'-O-methylated Gm4362, Gm4198, and Um4197. A comparison of the cDNA product intensities has shown that the transfection of cells with RNA 28A4518 causes a 1.5-fold increase in the termination efficacy at Gm4362, while the yield of the 428-429-nt-long product (Gm4198 and Um4197) increases 2.2 times. The increase in the yield of RT products corresponding to the arrest of reverse transcriptase at 2'-O-methylated nucleotides indicates a higher modification level of these nucleotides in transfected cells.

A change in the modification level of rRNA nucleotides can be associated with an increase in the local concentration of the components of the complexes that perform 2'-O-methylation of nucleotides during the maturation of the rRNA nucleolar precursor (pre-rRNA). Gm4362, Gm4198, and Um4197 nucleotides of 28S rRNA are located at a considerable distance (more than 150 nt away) from the sequence complementary to the box C/D RNA (*Fig. 5*). An increase in the 2'-O-methylation level of the mentioned nucleotides can be associated with their spatial proximity in the structure of pre-rRNA with the nucleotide targets of box C/D RNA and migration of the methyltransferase complex components from the box-C/D-RNA/rRNA duplex to the nearest rRNA nucleotides. The possible influence of synthetic RNAs on the secondary structure of rRNA and interaction with independent trans-factors, such as helicases, that control the stages of rRNA maturation in eukaryotic cells, also cannot be excluded [29].

We have also observed an increase in RT termination at known sites of 2'-O-methylation when studying the influence of other box C/D RNA analogues on human cells. In particular, the analogues RNA3 and RNA5 have been designed to direct 2'-O-methylation of G4499 and U4502 of 28S rRNA, respectively. The transfection of MCF-7 cells with RNA3 or RNA5 did not induce the modification of the target nucleotide but enhanced the 2'-O-methylation level of Cm4506 of 28S rRNA (*Fig. 7C,D*). The data shown in *fig. 7* and *table* indicate a 40- and 7-fold increase in the yield of the 121-nt-long cDNA product after transfection of MCF-7 cells with synthetic RNA3 and RNA5, respectively. This cDNA product forms as a result of M-MLV revertase termination at 2'-O-methylated Cm4506 of 28S rRNA during the elongation of primer FAM-28-2.2. The detected increase in the yield of the termination product indicates an enhanced 2'-O-methylation level of Cm4506.

In order to determine the structural features of box C/D RNA analogues that influence the level of native 2'-O-methylation of rRNA, we obtained the analogues of box C/D RNA5 with substitutions in box C(C') or D(D') sequences: RNA5mC, RNA5D/N, and RNA5mD. All the listed analogues had the same guide sequence targeted to U4502 of 28S rRNA (*Fig. 5, Table*). In RNA5mC, the sequences of boxes C (AUGAUGU) and C' (GUGAUGA) had been substituted with (ACAGCAC) and (GCAGCAG), respectively. RNA5D/N contained the only substitution in box D structure (AGUC), while RNA5mC had both the D and D' sequences (CUGA) changed to (AAAA).

It has been established that the substitutions in the structures of boxes D and C substantially decrease the efficacy of box C/D RNA analogue action. For instance,

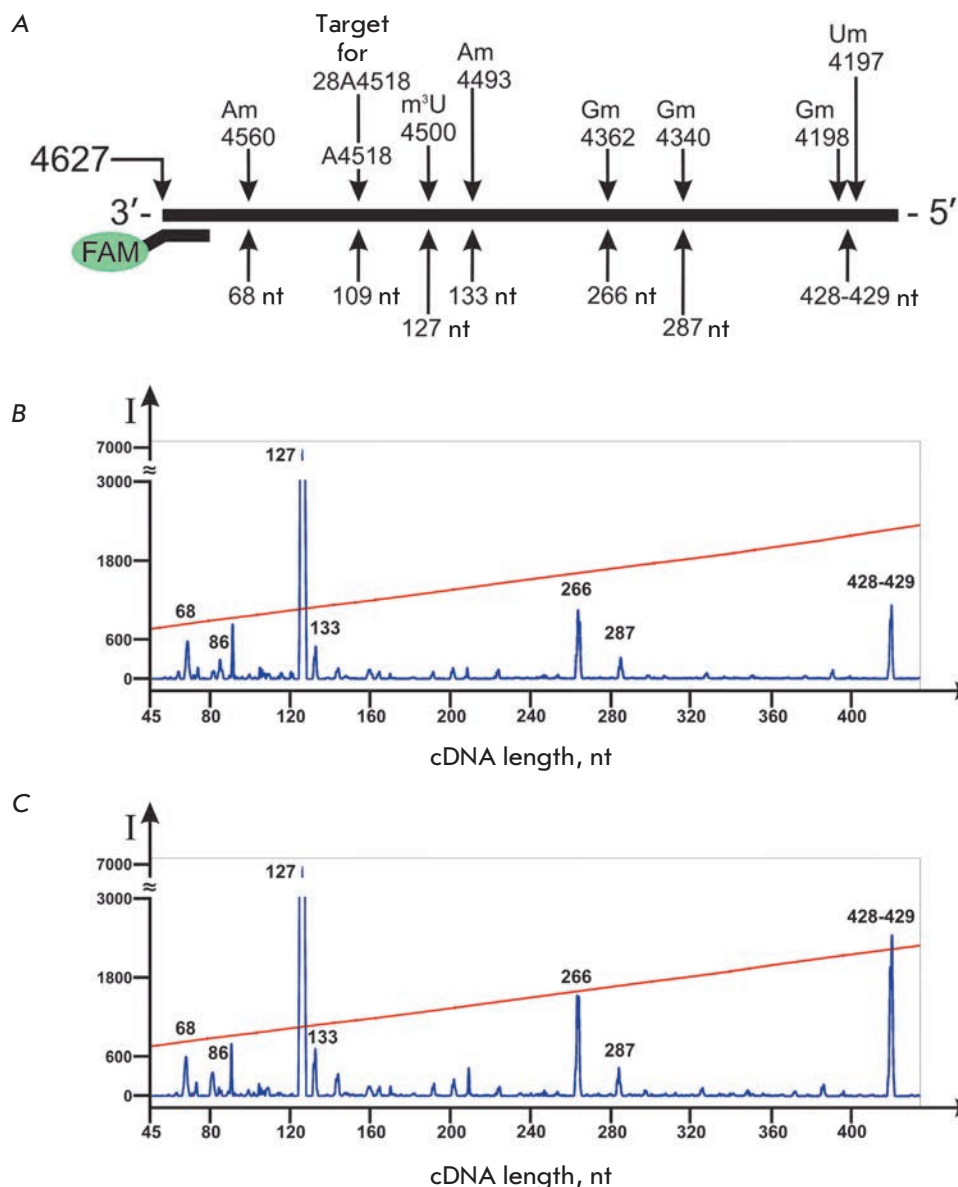


**Fig. 6.** Influence of artificial box C/D RNA analogues on the yield of rRNA RT termination products. A – 2'-O-methylated nucleotides in 28S rRNA and lengths of corresponding termination products of RT with primer FAM-28-2.2. RT products of rRNA isolated from control MCF-7 cells (B) and from MCF-7 cells transfected with analogue 28A4518 (C). RT was conducted at 0.04 mM dNTP

a substitution of only the box D sequence in the structure of RNA5 led to a 2-fold decrease in the relative yield of the termination product, while simultaneous substitution of both D and D' boxes or both the C and C' boxes decreased the yield to the level of the control cells (Fig. 7D–G, Table). The obtained data led us to assume that boxes C and D are the key elements in the structure of artificial box C/D RNAs that influence the level of rRNA 2'-O-methylation when transfected into human cells. A single pair of boxes C/D in the structure of synthetic RNA is sufficient to influence rRNA modification. Elimination of the functional elements – boxes C and D – abolishes the action of snoRNA analogues on the structure of rRNA in transfected cells (Fig. 7, Table).

The obtained data enabled us to conclude that box C/D RNA analogues influence post-transcriptional processing of ribosomal RNAs when penetrating into human cells. Despite the fact that transfection of box C/D RNA analogues into MCF-7 cells did not cause *de novo* 2'-O-methylation of rRNA target nucleotides, the analogues enhanced the level of native 2'-O-methylation in 28S rRNA.

It has been recently shown that in a series of tumor cell lines an increase in the level of several box C/D RNAs is accompanied by an increase in fibrillarin, the key component of the nucleolar methyltransferase complex [12]. Moreover, the 2'-O-methylation profile of rRNA can vary in cancer cells of different origins [14]. In this regard, it is suggested that the regulation

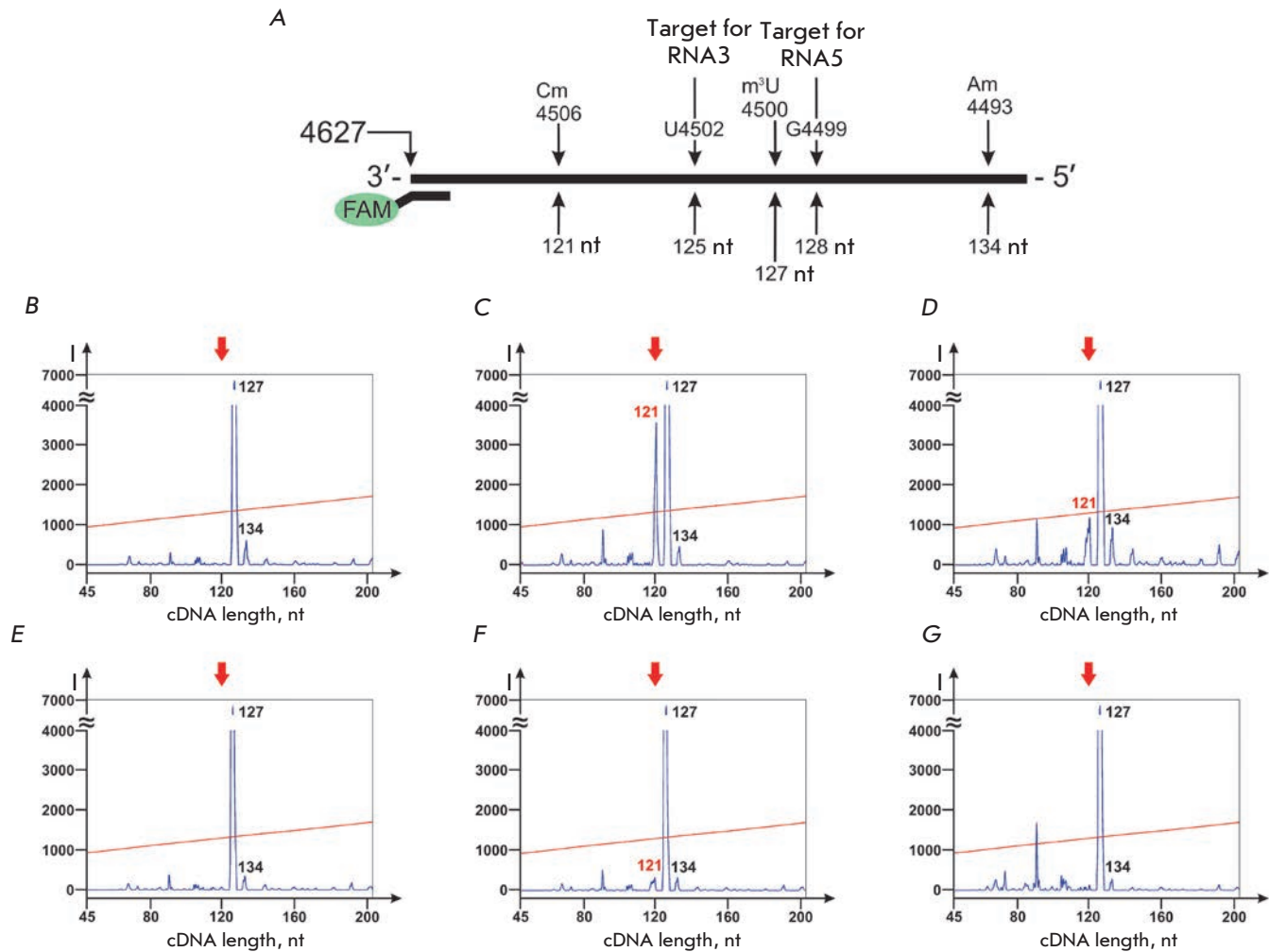


**Fig. 7.** Influence of artificial box C/D RNA analogues on the 2'-O-methylation level of Cm4506 of 28S rRNA in human cells. **A** – location of primer FAM-28-2.2, 2'-O-methylated nucleotides in 28S rRNA and target nucleotides for box C/D RNA analogues. (**B–G**) – 5'-FAM-labeled products of 28S rRNA RT termination (0.04 mM dNTP) isolated from control MCF-7 cells (**B**) and MCF-7 cells transfected with RNA3 (**C**), RNA5 (**D**), RNA5mC (**E**), RNA5D/N (**F**), and RNA5mD (**G**). Red arrow points to the location of the RT termination product that corresponds to Cm4506 of 28S rRNA. The 127-nt-long product of RT termination corresponds to m<sup>3</sup>U4500 of 28S rRNA

of ribosomal RNA maturation can affect oncogenic transformation of cells and be implicated in the control of cancer cell life cycle [30, 31]. Therefore, the observed effect of synthetic RNAs on 2'-O-methylation of rRNAs in human cells sheds light on perspectives for developing systems for the regulation of rRNA post-transcriptional maturation that can lay the groundwork for the development of novel therapeutic approaches. The proposed approach for the analysis of 2'-O-methylated nucleotides in RNAs can be used both to detect artificially directed RNA modifications and search for diagnostically significant differences in the profile of RNA modifications in human cells.

## CONCLUSIONS

This paper presents an adaptation of the reverse transcription termination method for determination of the location of 2'-O-methylated nucleotides in RNA and analysis of 5'-fluorescently labeled cDNA products by capillary gel electrophoresis on an automated DNA-analyzer. Using the proposed approach, we have analyzed the influence of synthetic analogues of small nucleolar box C/D RNAs on the 2'-O-methylation profile of human 28S rRNA in MCF-7 cells. It has been demonstrated that the transfection of cells with synthetic analogues of box C/D RNAs leads to enhanced RT termination at known 2'-O-methylation sites of

## Yields of the RT termination product corresponding to Cm4506 of 28S rRNA in MCF-7 cells transfected with box C/D RNA analogues

Name of box C/D RNA analogue	Alteration in box C/D RNA structure compared to RNA5	Yield of the RT termination product corresponding to Cm4506 28S rRNA**	Relative yield of the RT termination product ***, %
RNA5	–	1100 ± 154	100
RNA3	3-nucleotide shift to the 5'-end of rRNA in the complementary region	6500 ± 780	590
RNA5mC	box C (AUGAUGU) → (ACAGCAC); box C' (GUGAUGA) → (GCAGCAG)	170 ± 25	15
RNA5D/N	box D (CUGA) → (AGUC)	570 ± 86	50
RNA5mD	Boxes D and D' (CUGA) → (AAAA)	150 ± 25	13
Control*	–	150 ± 25	13

\* Control cells were incubated with lipofectamine alone.

\*\* Values of peak areas normalized to the total area of the peaks of RT termination products (± SD).

\*\*\* Relative yields of the RT termination product corresponding to Cm4506 28S rRNA compared to the yield of the same product of the RT of 28S rRNA isolated from MCF-7 cells transfected with RNA5.

rRNAs, indicating a significant increase in the modification level of certain nucleotides within the target rRNAs. Moreover, the conserved elements in the structure of snoRNAs – boxes C and D – play the key role in the action of synthetic RNAs.

Today it is believed that post-transcriptional modifications of different nucleotides in rRNA are independent processes. For instance, directed 2'-O-methylation of unmodified nucleotides of rRNA does not affect the modification outcome of other nucleotides [28, 32]. Our data demonstrate that box C/D RNAs that contain a guide sequence targeted to a defined nucleotide and do not induce 2'-O-methylation of the target nucleotide can influence the modification level of other nucleo-

tides of rRNA. It is possible that the effect we observed reflects the functioning of a novel, native mechanism of coherent regulation of rRNA post-transcriptional modification. The implementation of such a mechanism can help modulate the 2'-O-methylation level of some nucleotides while affecting the modification of others that are brought together in the spatial structure of the nucleolar precursor of rRNA. ●

*This work was supported by the Russian Foundation for Basic Research (grants № 13-04-01058 and 14-04-31468) and the Interdisciplinary Integration Project of SB RAS № 84 (2012–2014).*

## REFERENCES

- Lapeyre B. // Top. Curr. Genet. 2005. V. 12. P. 85–91.
- Baxter-Roshek J.L., Petrov A.N., Dinman J.D. // PLoS One. 2007. V. 2. № 1. e174.
- Piekna-Przybylska D., Decatur W.A., Fournier M.J. // Nucl. Acids Res. 2008. V. 36. D178–183.
- Decatur W.A., Fournier M.J. // Trends Biochem. Sci. 2002. V. 27. № 7. P. 344–351.
- Liang X.H., Liu Q., Fournier M.J. // Mol. Cell. 2007. V. 28. № 6. P. 965–977.
- Esguerra J., Warringer J., Blomberg A. // RNA. 2008. V. 14. № 4. P. 649–656.
- Liang X.H., Liu Q., Fournier M.J. // RNA. 2009. V. 15. № 9. P. 1716–1728.
- Song X., Nazar R.N. // FEBS Lett. 2002. V. 523. № 1–3. P. 182–186.
- Kiss-Laszlo Z., Henry Y., Bachellerie J.P., Caizergues-Ferrer M., Kiss T. // Cell. 1996. V. 85. № 7. P. 1077–1088.
- Makarova J.A., Kramerov D.A. // Molekulyarnaya Biologiya (Mosk.). 2007. V. 41. № 2. P. 246–259.
- Reichow S.L., Hama T., Ferre-D'Amare A.R., Varani G. // Nucl. Acids Res. 2007. V. 35. № 5. P. 1452–1464.
- Su H., Xu T., Ganapathy S., Shadfan M., Long M., Huang T.H., Thompson I., Yuan Z.M. // Oncogene. 2014. V. 33. № 11. P. 1348–1358.
- Marcel V., Ghayad S.E., Belin S., Therizols G., Morel A.-P., et al. // Cell. 2013. V. 24. № 3. P. 318–330.
- Belin S., Beghin A., Solano-Gonzalez E., Bezin L., Brunet-Manquat S., et al. // PLoS One. 2009. V. 4. № 9. e7147.
- Teittinen K.J., Laiho A., Uusimaki A., Pursiheimo J.P., Gyenesei A., Lohi O. // Cell. Oncol. (Dordr). 2013. V. 36. № 1. P. 55–63.
- Montanaro L., Trere D., Derenzini M. // Am. J. Pathol. 2008. V. 173. № 2. P. 301–310.
- Freed E.F., Bleichert F., Dutca L.M., Baserga S.J. // Mol. Biosyst. 2010. V. 6. № 3. P. 481–493.
- Stepanov G.A., Semenov D.V., Kuligina E.V., Koval O.A., Rabinov I.V., Kit Y.Y., Richter V.A. // Acta Naturae. 2012. V. 4. № 1 (12). P. 34–43.
- Stepanov G.A., Semenov D.V., Savelyeva A.V., Koval O.A., Kuligina E.V., Rabinov I.V., Richter V.A. // Biomed. Res. Int. 2013. ID:656158.
- Maden B.E., Corbett M.E., Heeney P.A., Pugh K., Ajuh P.M. // Biochimie. 1995. V. 77. № 1–2. P. 22–29.



## RESEARCH ARTICLES

21. Maden B.E. // *Methods*. 2001. V. 25. № 3. P. 374–382.
22. Cavaille J., Nicoloso M., Bachelier J.P. // *Nature*. 1996. V. 383. № 6602. P. 732–735.
23. Liu B., Fournier M.J. // *RNA*. 2004. V. 10. № 7. P. 1130–1141.
24. Graifer D., Molotkov M., Styazhkina V., Demeshkina N., Bulygin K., Eremina A., Ivanov A., Laletina E., Venyaminova A., Karpova G. // *Nucl. Acids Res.* 2004. V. 32. № 11. P. 3282–3293.
25. Bulygin K., Malygin A., Hountondji C., Graifer D., Karpova G. // *Biochimie*. 2013. V. 95. № 2. P. 195–203.
26. Lestrade L., Weber M.J. // *Nucl. Acids Res.* 2006. V. 34. D158–162.
27. Liu B., Ni J., Fournier M. J. // *Methods*. 2001. V. 23. № 3. P. 276–286.
28. Liu B., Liang X.H., Piekna-Przybylska D., Liu Q., Fournier M.J. // *RNA Biol.* 2008. V. 5. № 4. P. 249–254.
29. Rodriguez-Galan O., Garcia-Gomez J.J., de la Cruz J. // *Biochim. Biophys. Acta*. 2013. V. 1829. № 8. P. 775–790.
30. Williams G.T., Farzaneh F. // *Nat. Rev. Cancer*. 2012. V. 12. № 2. P. 84–88.
31. Mannoer K., Liao J., Jiang F. // *Biochim. Biophys. Acta*. 2012. V. 1826. № 1. P. 121–128.
32. Qu G., van Nues R.W., Watkins N.J., Maxwell E.S. // *Mol. Cell. Biol.* 2011. V. 31. № 2. P. 365–374.

# Specific Depletion of Myelin-Reactive B Cells via BCR-Targeting

A. V. Stepanov<sup>1,2\*</sup>, A. A. Belogurov Jr.<sup>1,2,3</sup>, P. Kothapalli<sup>4</sup>, O. G. Shamborant<sup>1</sup>, V. D. Knorre<sup>1</sup>, G. B. Telegin<sup>1</sup>, A. A. Ovsepyan<sup>1</sup>, N. A. Ponomarenko<sup>1</sup>, S. M. Deyev<sup>1</sup>, S. V. Kaveri<sup>4</sup>, A. G. Gabibov<sup>1,2,3</sup>

<sup>1</sup>M.M. Shemyakin and Yu.A. Ovchinnikov Institute of Bioorganic Chemistry, Miklukho-Maklaya Str., 16/10, Russian Academy of Sciences, 117997, Moscow, Russia

<sup>2</sup>Kazan Federal University, Kremlevskaya Str., 18, 420008, Kazan, Republic of Tatarstan, Russia

<sup>3</sup>Institute of Gene Biology, Russian Academy of Sciences, Vavilova Str., 34/5, 119334, Moscow, Russia

<sup>4</sup>Centre de Recherche des Cordeliers, Université Pierre et Marie Curie, UMR S 1138, F-75006, Paris, France

\*E-mail: stepanov.aleksei.v@gmail.com

Received 05.05.2015

Copyright © 2015 Park-media, Ltd. This is an open access article distributed under the Creative Commons Attribution License, which permits unrestricted use, distribution, and reproduction in any medium, provided the original work is properly cited.

**ABSTRACT** B cells play a crucial role in the development and pathogenesis of systemic and organ-specific autoimmune diseases. Autoreactive B cells not only produce antibodies, but also secrete pro-inflammatory cytokines and present specific autoantigens to T cells. The treatment of autoimmune diseases via the elimination of the majority of B cells using the monoclonal anti-CD19/20 antibody (Rituximab) causes systemic side effects and, thus, requires a major revision. Therapeutic intervention directed towards selective elimination of pathogenic autoreactive B cells has the potential to become a universal approach to the treatment of various autoimmune abnormalities. Here, we developed a recombinant immunotoxin based on the immunodominant peptide of the myelin basic protein (MBP), fused to the antibody Fc domain. We showed that the obtained immunotoxin provides selective *in vivo* elimination of autoreactive B cells in mice with experimental autoimmune encephalomyelitis. The proposed conception may be further used for the development of new therapeutics for a targeted treatment of multiple sclerosis and other autoimmune disorders.

**KEYWORDS** multiple sclerosis, autoantigens, B cells, immunoglobulins, immunotoxins.

**ABBREVIATIONS** MBP – myelin basic protein; MS – multiple sclerosis; EAE – experimental autoimmune encephalomyelitis; CFA – complete Freund's adjuvant; ELISA – enzyme-linked immunosorbent assay.

## INTRODUCTION

Multiple sclerosis (MS) is a chronic autoimmune neurodegenerative disease that affects the central nervous system, in which the major autoantigens are proteins of the myelin sheath of nerve fibers [1]. More than 200,000 people are affected by multiple sclerosis in the Russian Federation [2]. Despite the advances in the treatment of MS made in recent years, the existing therapeutics do not provide full recovery to the patient [3]. Modern approaches to the treatment of MS, including the introduction of recombinant antibodies and other low-molecular-weight agents specifically acting on components of the immune system, are prohibitively expensive for the budgets of developed countries and, taking into account the need for long-term care, endanger the entire rehabilitation system. Furthermore, the levels of disability of patients do not provide expectations for a positive prognosis in the social sphere. It

is important to note that the current methods used in MS include primarily nonselective immunosuppressive drugs, which often cause systemic complications [4].

It has been considered for a long time that CD4<sup>+</sup> T cells play a crucial role in the pathogenesis of MS. However now it is obvious that the B cell response undoubtedly plays an important role in the disease's development. Autoreactive B cells not only produce autoantibodies, but they are also able to effectively function as antigen-presenting cells that in turn activate T cells [5]. In addition, B cells can secrete proinflammatory cytokines and enhance pathological self-destructive processes [6]. Therapy directed at a specific population of lymphocytes is, in the long term, a versatile remedy for a wide range of B cell disorders. Currently, elimination of autoreactive B cells is accomplished by administration of the monoclonal anti-CD19/20 antibody, Rituximab (Rituxan, MabThera), which is extensively used

in the therapy of lymphomas and autoimmune diseases [7–12]. Clinical use of this drug is limited to a great extent and occurs in exceptional circumstances, since it leads to the elimination of most B cells in the body and, consequently, a wide range of side effects [13]. In this regard, the problem of developing drugs for specific therapy of multiple sclerosis and other autoimmune diseases remains rather topical.

The main approach to the treatment of multiple sclerosis is based on subcutaneous injection of an immunomodulating drug, glatiramer acetate (GA). GA is a polypeptide of 40–100 amino acid residues, comprising a random combination of alanine, lysine, glutamate, and tyrosine in a ratio of 4.5 : 3.6 : 1.5 : 1, respectively. The GA structure mimics one of the major autoantigens in MS, the highly positively charged myelin basic protein (MBP). The GA action presumably includes competition with fragments of the myelin basic protein for binding to MHC class II DR molecules, as well as induction of regulatory T cells (Th2/3 type) secreting anti-inflammatory IL-4 and IL-10 cytokines and the brain-derived neurotrophic factor [14]. It should be noted that the extent of GA therapy efficacy is highly fluctuant, up to full patient resistance to drug therapy [14].

In this paper, we suggest and successfully implement an approach to the development of recombinant polypeptides capable of specific depletion of abnormal lymphocytes *in vivo*. As a target for precise delivery of cytotoxic agents, we chose the surface immunoglobulin of autoreactive B cells (B cell receptor, BCR), which is a unique receptor that differentiates a certain, clonally homogeneous population of B cells from other cells of the organism. A number of studies have already demonstrated the high efficacy of targeted elimination of lymphocytes by BCR-specific immunotoxins *in vitro* [15, 16]. A high titer of autoantibodies specific for MBP has been previously shown in the serum of MS patients [17–19]. One of the most appropriate animal model of multiple sclerosis is experimental autoimmune encephalomyelitis (EAE) induced in SJL/J strain mice [20, 21]. Upon developing EAE in SJL/J mice, MBP-specific autoantibodies are also produced. Based on a previously generated library of recombinant MBP epitopes and using the enzyme-linked immunosorbent assay (ELISA), a comparative analysis of the specificity of the serum autoantibodies derived from MS patients and various EAE animals for different epitopes of the autoantigen was performed [22]. Based on the obtained data, the [QDENPVVHFFKNIVTPRTPPPSQ] MBP<sub>82–105</sub> immunodominant fragment was chosen as a highly specific ligand for surface BCRs of autoreactive B cells. Further, we developed a chimeric protein consisting of the MBP<sub>82–105</sub> sequence fused to the antibody constant

fragment that exhibits good pharmacodynamic parameters and, at the same time, can effectively induce the mechanisms of antibody-dependent cytotoxicity. In the present study, the therapeutic potential of the generated killer protein was studied in terms of selective depletion of autoreactive MBP-specific B cells *in vivo* in SJL/J strain mice with induced EAE.

## EXPERIMENTAL

### Development of the genetic construct encoding the immunoglobulin constant fragment fused with MBP<sub>82–105</sub>

The nucleotide sequence encoding the MBP<sub>82–105</sub> fragment was produced by PCR amplification with the mutually overlapping outer and inner primers 5'ATTAGGTACCCAAGATGAAAACCCCGTAGTCCACTTCTTCAAGA3', 5'CGTAGTCCACTTCTTCAAGAACATTGTGACGCCTCGCACACC3', and 5'TAATGTCGACTCCCTGCGACGGGGGTGGTGTGCGAGGCGTCACA3'. The PCR product was treated with the restriction endonucleases EcoRI and BgIII and then ligated with the similarly prepared pFUSE vector.

### Generation of clones producing recombinant molecules

To generate a stable line of CHO cells producing the recombinant MBP<sub>82–105</sub>-Fc (pFUSE-MBP<sub>82–105</sub>-Fc) and Fc (pFUSE-Fc) molecules, CHO cells were transfected with appropriate genetic constructs. For this purpose, a day before transfection, CHO cells were split into wells of a six-well plate (Nunc) at a concentration of 0.5 million/mL. Upon reaching 80% confluency, the cells were transfected by lipofection using a Lipofectamine LTX kit (Invitrogen) according to the manufacturer's recommendations. After 72 h, a medium with a selective antibiotic zeocin was added to the cells. The antibiotic-resistant cells were transferred to 96-well plates (Corning). The resulting clones were tested for the production of recombinant molecules by ELISA using monoclonal anti-Fc-antibodies.

### Isolation of Fc and MBP<sub>82–105</sub>-Fc molecules

Isolation of killer proteins containing the Fc-fragment of a class IgG2a antibody was carried out as follows. Initially, the supernatant of CHO cells transfected with plasmids containing the nucleotide sequences encoding the antibody constant fragment fused with a peptide sequence was collected. The collected supernatant was centrifuged at 13,000 rpm for 10 min. After centrifugation supernatant was applied to an affinity chromatography column with the immobilized G protein (HiTrap Protein-G Sepharose, Amersham, USA) in PBS at a flow rate of 0.5 mL/min. The column was

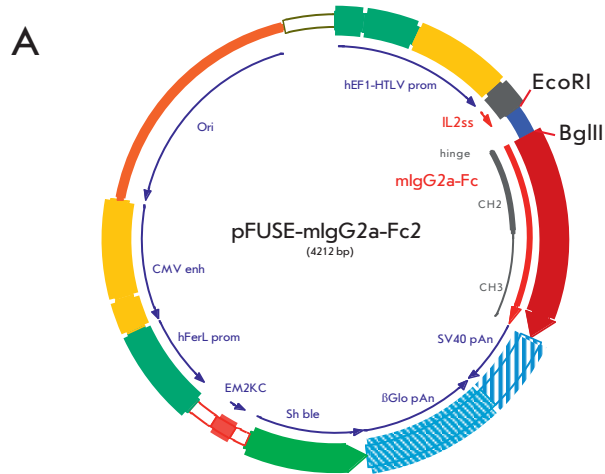
then washed with 80–100 PBS volumes at a speed of 2.5 mL/min to elute non-specifically adsorbed proteins. The fraction was eluted from the column with a 100 mM Glycine-HCl solution (pH 2.5) and immediately neutralized with a 2 M Tris base solution to pH 7.3–7.7. All chromatographic isolation stages were carried out on a DuoFlow BioRad system. Identification of Fc and MBP<sub>82–105</sub>-Fc samples and assessment of their purity were performed using denaturing polyacrylamide gel electrophoresis, followed by silver staining and an enzyme-linked immunoassay.

### Induction and therapy of EAE in SJL strain mice.

The experiments were carried out at the Research and Production Department of the Branch of the Shemyakin-Ovchinnikov Institute of Bioorganic Chemistry, the Nursery for Laboratory Animals “Pushchino” (Russia, Pushchino), and at the Centre de Recherche des Cordeliers de Jussieu (CRC) (France, Paris) in compliance with all ethical standards. EAE was induced in SJL female mice at the age of 6 to 8 weeks with the SPF (specified pathogen free) status in accordance with the protocol [23] by a double injection of 100 µg of a mouse spinal cord homogenate (MSCH) in complete Freund’s adjuvant (CFA) containing tuberculin at a concentration of 4 mg/mL. On day 1, MSCH was injected subcutaneously into two points along the spinal column and, on the 3rd day, into the sole of hind feet. Additionally, on the day of MSCH in PAF injections, the mice were intravenously administered with a solution of the pertussis toxin (Calbiochem, USA) at a dose of 500 ng/mouse. Mice induced with EAE were divided into four groups of 10 animals, each: without injection (group without treatment); animals with a single injection of 200 µg of GA (Teva); animals in the groups Fc and MBP<sub>82–105</sub>-Fc were intravenously injected with 50 µg of the drug on days 5 and 10 after EAE induction. The severity of the autoimmune disease was evaluated on a daily basis according to the following scale: 0 – norm; 1 – loss of tail tone; 2 – weakness or paralysis of the hind legs; 3 – strong limb paralysis; 4 – complete paralysis (inability to move); and 5 – death.

### Flow cytometry

The spleen was isolated from the SJL/J mice of each experimental group. Next, the spleen was transferred to a Petri dish and homogenized to obtain a splenocyte suspension. The isolated splenocytes were resuspended in a DMEM medium, and 1 million cells were centrifuged at 400 g for 10 min, then the precipitate was washed twice with PBS. The cells were added with a solution of the biotinylated MBP peptides (7-TQDENPVVHFFKNIIVTPRTPPPS or 12-DAQGTLISKIFKLGGRDSRSGSPMARR) in phosphate buffer containing



### B

#### QDENPVVHFFKNIIVTPRTPPPSQG - MBP<sub>82-105</sub>

ASQKRPSQRHGSKYLATASTMDHARHGFLPRHRDTG  
ILDSIGRFFGGDRGAPKRGSKDSHHPARTAHYGSL  
PQKSHGRT**QDENPVVHFFKNIIVTPRTPPPSQG**KGRG  
LLSLSRFSWGAEGQRPFGFYGGGRASDYKSAHKGFKGV  
DAQGTLISKIFKLGGRDSRSGSPMARR

**Fig. 1.** A map of the pFUSE-Fc vector, a plasmid containing cDNA coding for IgG2a Fc. (A) Amino acid sequences of full-size MBP and the MBP<sub>82–105</sub> fragment (shown in bold) integrated into the pFUSE-Fc vector (B)

1% BSA. The cells were incubated at +4 °C for 40 min, centrifuged (400 g, 10 min), and resuspended in physiological buffer. The cell suspension was supplemented with the anti-B220-APC antibodies (eBioscience, USA) and Streptavidin-Pacific Blue™ conjugate, incubated (+4 °C, 40 min), centrifuged (400 g, 10 min), resuspended in FACS buffer (0.1% BSA, 0.02% sodium azide, 50 µg/mL propidium iodide in phosphate buffer), and analyzed on a FACSDiva flow cytometer (Becton Dickinson, USA).

## RESULTS AND DISCUSSION

### Development of the genetic construct encoding the immunoglobulin constant fragment fused to the MBP peptide

To develop highly selective cytotoxic proteins capable of targeted elimination of a population of autoreactive B cells with known specificity, we generated a genetic construct encoding the mouse antibody constant fragment (Fc) fused with the MBP<sub>82–105</sub> fragment. For this

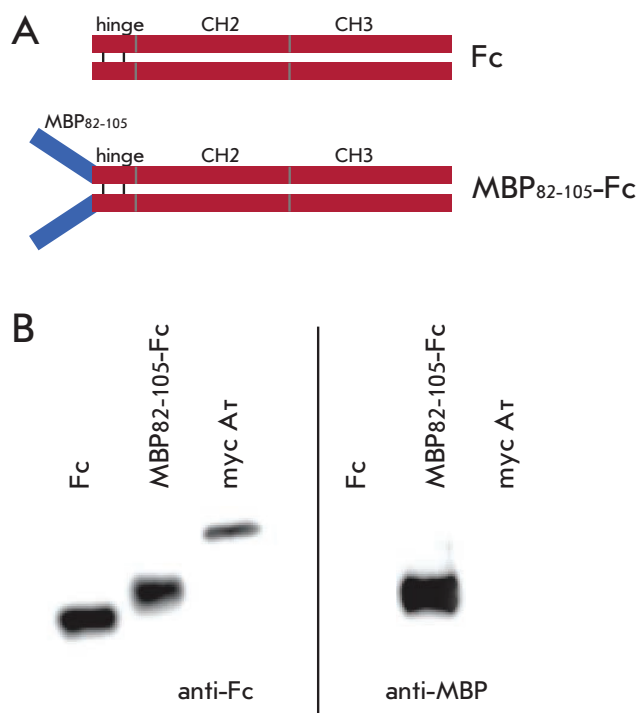


**Fig. 2.** Schematic representation of the developed recombinant Fc and MBP<sub>82-105</sub>-Fc proteins (A). WB analysis of recombinant Fc and MBP<sub>82-105</sub>-Fc using anti-Fc and anti-MBP antibodies

purpose, the commercially available pFUSE plasmid vector containing the gene coding for the constant fragment of mouse IgG2a immunoglobulin (Invivogen) (Fig. 1) was used. The nucleotide sequence encoding the MBP<sub>82-105</sub> (QDENPVVHFFKNIIVTPRTPPPSQG) fragment was amplified by PCR with overlapping primers. The resulting DNA fragments were inserted into the pFUSE-mIgG2a plasmid vector at the EcoRI and BgIII restriction sites.

To generate a stable CHO cell line producing the recombinant MBP<sub>82-105</sub>-Fc (pFUSE-MBP<sub>82-105</sub>-Fc) and Fc (pFUSE-Fc) proteins, CHO cell lines were transfected with the appropriate genetic constructs using lipofec-

tion. The transfected cells were selected on a medium supplemented with the zeocin antibiotic. The antibiotic-resistant cells were cloned. The resulting clones were tested for the production of recombinant proteins by ELISA. The selected producer clones were used for preparative production of a protein in 125 cm<sup>2</sup> flasks for 9 days. The Fc-containing proteins were successively purified from the growth medium by affinity chromatography on a sorbent with the immobilized G protein and on a Superdex200 gel filtration column. According to the electrophoretic analysis, the sample's homogeneity was beyond 95%. The presence of the MBP fragment in the isolated recombinant proteins was evaluated by Western blotting using the anti-MBP (Fig. 2B) and anti-Fc (Fig. 2A) antibodies. Hybridization with anti-MBP antibodies confirmed that the fusion MBP<sub>82-105</sub>-Fc protein contained the immunodominant MBP fragment, whereas the control Fc lacked this fragment.

### Depletion of autoreactive B cells in SJL mice with induced EAE

Experimental autoimmune encephalomyelitis was induced in SJL strain mice to generate a population of autoreactive B cells specific for MBP. For this purpose, animals received two subcutaneous injections of a mouse spinal cord homogenate in a complete Freund's adjuvant emulsion. Additionally, on the same days, the animals were intravenously injected with a pertussis toxin solution to enhance the development of EAE. Group (1), which included non-immunized mice, was used as a negative control. Further, mice with induced EAE were divided into four experimental groups of 10 animals each: (2) without treatment; (3) animals with a single injection of 200 µg of GA (Teva) (GA group); animals in two groups were intravenously injected twice with Fc (4) and MBP<sub>82-105</sub>-Fc (5) (table).

The development of EAE symptoms in all groups was evaluated on a five-grade scale, starting with the seventh day after EAE induction and until the end of the experiment.

EAE symptoms in mice of all groups began to develop on days 14–15 after induction, and the disease

**Table.** Experimental groups

Group	Number of mice	EAE	Injections	Number of injections	Day of injection	Dose µg/mouse
1	5	–	–	–	–	–
2	10	+	–	–	–	–
3	10	+	GA	1	1	200
4	10	+	Fc	2	5 and 10	50
5	10	+	MBP <sub>82-105</sub> -Fc	2	5 and 10	50

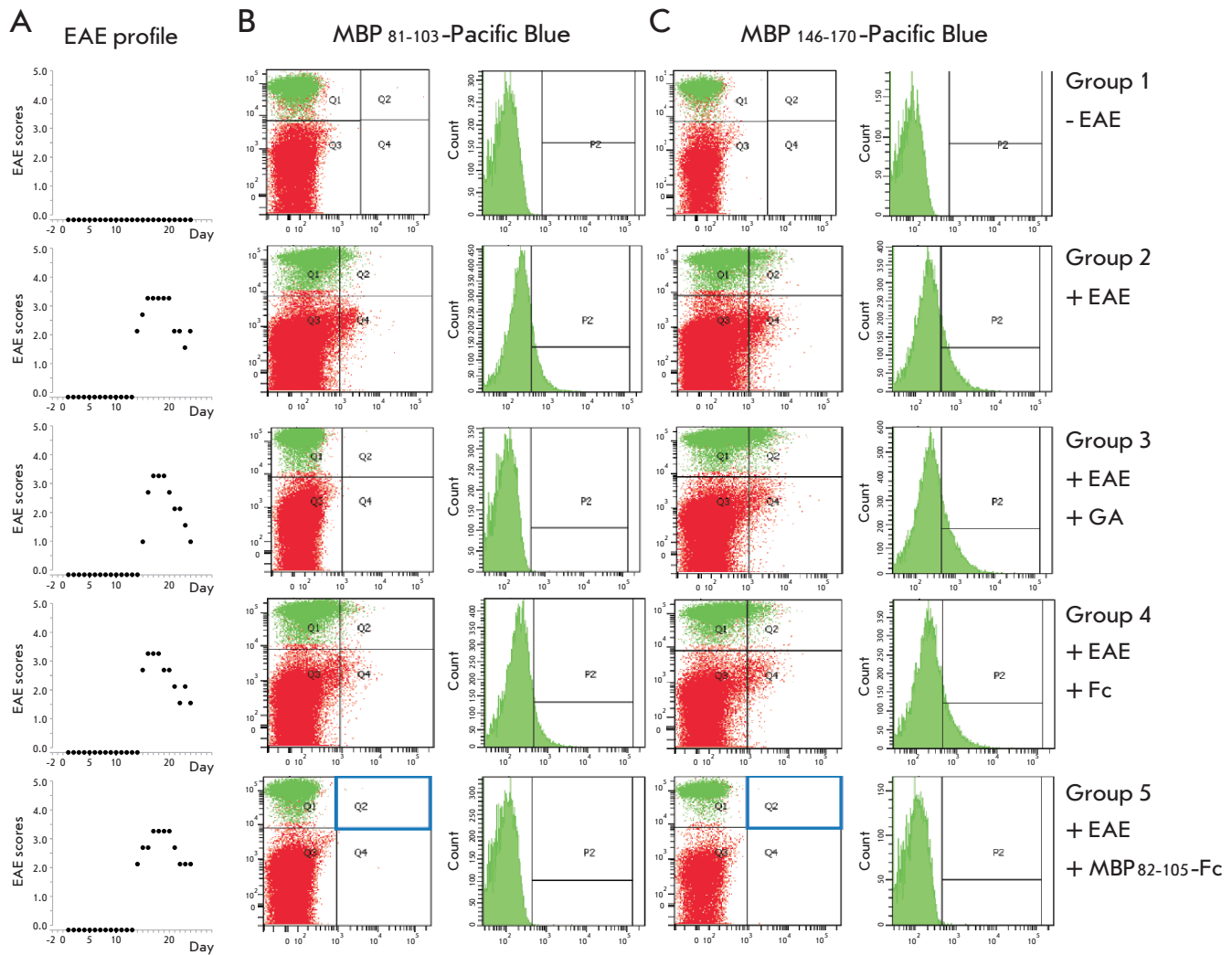


**Fig. 3.** Plots representing the EAE development scores in mice from all experimental groups (A). FC analysis of isolated splenocytes for the presence of B cells specific for the fragments MBP<sub>81-103</sub> (B) and MBP<sub>146-170</sub> (C)

peaked on days 17–19. On day 23, SJL mice with identical EAE clinical scores were selected from each experimental group (Fig. 3A). The splenocyte cultures derived from these mice were analyzed for B cells specific for the immunodominant and C-terminal MBP fragments. For this purpose, the cells were incubated with the MBP<sub>81-103</sub> and MBP<sub>146-170</sub> peptides conjugated with biotin. A conjugate of anti-B220-antibodies with the APC fluorophore (eBioscience) was used to visualize B cells. In turn, the biotinylated MBP peptides bound to the surface BCRs were detected by adding the conjugate of streptavidin with the Pacific Blue™ fluorophore (eBioscience). Samples were analyzed by flow cytometry on the FACSDiva device (BD). As can be seen from Fig. 3B, C, a mouse from the control group lacked a population of B cells specific for MBP, whereas a significant

population of B cells specific for both MBP peptides was detected in the culture of splenocytes obtained from an animal from the group without treatment. As expected, intravenous injections of control Fc without MBP peptides did not lead to any change in the population of MBP-reactive B cells. In the case of a single GA injection, the population specific for MBP<sub>81-103</sub> disappeared in the cell culture but there was a population of B cells with surface BCR specific for the C-terminal MBP<sub>146-170</sub> fragment. This observation once again confirms that the therapeutic effect of GA is aimed at the population of B cells specific for the immunodominant MBP<sub>81-103</sub> epitope [24]. Administration of the fusion MBP<sub>81-103</sub>-Fc protein resulted in the complete depletion of B cells specific not only for the MBP<sub>81-103</sub> fragment, which is a part of the administered immunotoxin, but

also for the MBP<sub>146-170</sub> fragment. Therefore, the profile of the population of B cells specific for MBP in the splenocytes culture of mice subjected to MBP<sub>81-103</sub>-Fc protein therapy coincided with the profile of healthy animals. The obtained results suggest that the MBP<sub>81-103</sub>-Fc immunotoxin, along with the selective depletion of B cells specific for the immunodominant MBP<sub>81-103</sub> fragment, also inhibits the formation of B cells specific for the MBP<sub>146-170</sub> fragment.

## CONCLUSIONS

In the last decade, antigen-specific therapy has gained increasing relevance in the development of drugs for the treatment of patients with multiple sclerosis and other autoimmune diseases. By the animal model, we tested one of the most topical current approaches to

the treatment of multiple sclerosis – the selective depletion of autoreactive B cells. A highly selective B cell killer protein was generated on the basis of the immunoglobulin constant fragment fused with the immunodominant MBP sequence. Administration of this recombinant immunotoxin to SJL/J mice with induced EAE led to complete elimination of the population of B cells specific for MBP fragments. These findings lead to the conclusion that the suggested concept could be successfully implemented in the development of drugs for targeted therapy of multiple sclerosis and other autoimmune disorders. ●

*This work was supported by the Russian Ministry of Education (project №RFMEFI60714X0061).*

## REFERENCES

- Nylander A., Hafler D.A. // J. Clin. Invest. 2012. V. 122. P. 1180–1188.
- Kingwell E., Marriott J.J., Jette N., Pringsheim T., Makhani N., Morrow S.A., Fisk J.D., Evans C., Beland S.G., Kulaga S. // BMC Neurol. 2013. V. 13. P. 128.
- Ransohoff R.M., Hafler D.A., Lucchinetti C.F. // Nat. Rev. Neurol. 2015. V. 11. P. 134–142.
- Sorensen P.S. // Curr. Opin. Neurol. 2014. V. 27. P. 246–259.
- Krumbholz M., Derfuss T., Hohlfeld R., Meinl E. // Nat. Rev. Neurol. 2012. V. 8. P. 613–623.
- Marino E., Grey S.T. // Autoimmunity. 2012. V. 45. P. 377–387.
- Arkfeld D.G. // Rheumatol. Int. 2008. V. 28. P. 205–215.
- Wang M., Fowler N., Wagner-Bartak N., Feng L., Romaguera J., Neelapu S.S., Hagemester F., Fanale M., Oki Y., Pro B. // Leukemia. 2013. V. 27. P. 1902–1909.
- Ransohoff R.M., Zamvil S.S. // Neurotherapeutics. 2007. V. 4. P. 569–570.
- Cross A.H., Stark J.L., Lauber J., Ramsbottom M.J., Lyons J.A. // J. Neuroimmunol. 2006. V. 180. P. 63–70.
- Deyev S.M., Lebedenko E.N. // Acta Naturae. 2009. No. 1. P. 32–50.
- Deyev S.M., Lebedenko E.N., Petrovskaya L.E., Dolgikh D.A., Gabibov A.G., Kirpichnikov M.P. // Russian chemical reviews. 2015. V. 84. No. 1. P. 1–26.
- Castillo-Trivino T., Braithwaite D., Bacchetti P., Waubant E. // PLoS One. 2013. V. 8. P. e66308.
- Sela M., Mozes E. // Proc. Natl. Acad. Sci. USA. 2004. V. 101. P. 14586–14592.
- Stepanov A.V., Belogurov A.A. Jr., Ponomarenko N.A., Stremovskiy O.A., Kozlov L.V., Bichucher A.M., Dmitriev S.E., Smirnov I.V., Shamborant O.G., Balabashin D.S., et al. // PLoS One. 2011. V. 6 (6). P. e20991.
- Zocher M., Baeuerle PA, Dreier T., Iglesias A. // Int Immunol. 2003. V.15 (7). P. 789–796.
- Johnson A.B., Dal Canto M.C. // Nature. 1976. V. 264. P. 453–454.
- Abramsky O., Lisak R.P., Silberberg D.H., Pleasure D.E. // New Engl. J. Med. 1978. V. 298. P. 743.
- Ponomarenko N.A., Durova O.M., Vorobiev I.I., Belogurov A.A. Jr., Kurkova I.N., Petrenko A.G., Telegin G.B., Suchkov S.V., Kiselev S.L., Lagarkova M.A., et al. // Proc. Natl. Acad. Sci. USA. 2006. V. 103. № 2. P. 281–286.
- Miller S.D., Karpus W.J., Davidson T.S. // Curr. Protoc. Immunol. 2010. Ch. 15. V. 15. P. 11.
- Stromnes I.M., Goverman J.M. // Nat. Protoc. 2006. V. 1. P. 1810–1819.
- Belogurov A.A. Jr., Kurkova I.N., Friboulet A., Thomas D., Misikov V.K., Zakharova M.Y., Suchkov S.V., Kotov S.V., Alehin A.I., Avalle B., et al. // J. Immunol. 2008. V. 180. P. 1258–1267.
- Yasuda T., Tsumita T., Nagai Y., Mitsuzawa E., Ohtani S. // Japan J. Exp. Med. 1975. V. 45. P. 423–427.
- Sela M., Teitelbaum D. // Expert Opin. Pharmacother. 2001. V. 2. P. 1149–1165.

# Determination of Alkali-Sensing Parts of the Insulin Receptor-Related Receptor Using the Bioinformatic Approach

I. E. Deyev\*, N. V. Popova, A. G. Petrenko

Laboratory of Receptor Cell Biology, Shemyakin–Ovchinnikov Institute of Bioorganic Chemistry, Russian Academy of Sciences, Miklukho-Maklaya Str., 16/10, 117997, Moscow, Russia

\*E-mail: deyevie@gmail.com

Received 09.12.2014

Copyright © 2015 Park-media, Ltd. This is an open access article distributed under the Creative Commons Attribution License, which permits unrestricted use, distribution, and reproduction in any medium, provided the original work is properly cited.

**ABSTRACT** IRR (insulin receptor-related receptor) is a receptor tyrosine kinase belonging to the insulin receptor family, which also includes insulin receptor and IGF-IR receptor. We have previously shown that IRR is activated by extracellular fluid with pH > 7.9 and regulates excess alkali excretion in the body. We performed a bioinformatic analysis of the pH-sensitive potential of all three members of the insulin receptor family of various animal species (from frog to man) and their chimeras with swapping of different domains in the extracellular region. An analysis using the AcalPred program showed that insulin receptor family proteins are divided into two classes: one class with the optimal working pH in the acidic medium (virtually all insulin receptor and insulin-like growth factor receptor orthologs, except for the IGF-IR ortholog from *Xenopus laevis*) and the second class with the optimal working pH in the alkaline medium (all IRR orthologs). The program had predicted that the most noticeable effect on the pH-sensitive property of IRR would be caused by the replacement of the L1 and C domains in its extracellular region, as well as the replacement of the second and third fibronectin repeats. It had also been assumed that replacement of the L2 domain would have the least significant effect on the alkaline sensitivity of IRR. To test the *in silico* predictions, we obtained three constructs with swapping of the L1C domains, the third L2 domain, and all three domains L1CL2 of IRR with similar domains of the insulin-like growth factor receptor. We found that replacement of the L1C and L1CL2 domains reduces the receptor's ability to be activated with alkaline pH, thus increasing the half-maximal effective concentration by about 100%. Replacement of the L2 domain increased the half-maximal effective concentration by 40%. Thus, our results indicate the high predictive potential of the AcalPred algorithm, not only for the pH-sensitive enzymes, but also for pH-sensitive receptors.

**KEYWORDS** receptor, alkaline pH, phosphorylation.

## INTRODUCTION

The insulin receptor (IR) family consists of IR, insulin-like growth factor receptor (IGF-IR), and the insulin receptor-related receptor (IRR). All three receptors are highly homologous receptor tyrosine kinases with a single transmembrane segment, which exist as homologous dimers linked via cystine bridges [1, 2]. This property makes the members of the IR family different than other tyrosine kinase receptors, which form non-covalent dimers only after activation. As they mature, both monomers are proteolyzed in the near-membrane zone of the extracellular portion. As a result, a receptor molecule consists of two pairs of covalently bound alpha and beta subunits.

All three receptors contain the leucine-rich L1 and L2 domains in the extracellular N-terminal portion of the alpha subunit with the C domain (furin-like cyste-

ine-rich region) located between them. These domains are followed by three fibronectin repeats: FnIII-1, FnIII-2, and FnIII-3 [3]. The tyrosine kinase domain is located in the cytoplasmic portion of the beta subunit. The degree of homology between IGF-IR and IRR is somewhat higher than that between IR and IRR [2]; hence, it is believed that duplication and separation of the genes encoding IGF-IR and IRR were evolutionarily later processes compared to separation of the insulin receptor gene [2].

Since receptors are pre-dimerized, binding of the peptide ligand to the extracellular portion of IR or IGF-IR causes changes in conformation, which result in autophosphorylation of the tyrosine residues located in the cytoplasmic tyrosine kinase domain. As opposed to its homologs, IRR has no ligands of peptide or protein nature. Meanwhile, we found that IRR is activated at



pH of the extracellular fluid higher than 7.9 [4, 5]. *In vivo* experiments using mice with IRR gene knockout demonstrated that this receptor is involved in the regulation of renal excretion of excess alkali in the form of bicarbonate [6, 7]. Mapping of the regions determining the pH sensitivity of IRR has shown that several extracellular domains are responsible for receptor activation [5, 8], which ensures positive cooperation in activation (the Hill's coefficient being ~ 2.4) [5, 9].

The following question is of obvious fundamental interest: what is the reason for such striking differences between the functions of IR and IGF-IR receptors, on the one hand, and IRR, on the other hand. In this study, we used the bioinformatic approach to perform a comparative analysis of the pH sensitivity of IRR receptor and other receptors belonging to the insulin receptor family. The AcalPred program [10], which was designed to predict pH values (either acidic or alkaline) that would be optimal for enzyme function based on its primary structure, allowed us to divide the IR family into two types: the “acid-dependent” proteins (almost all IR and IGF-IR orthologs) and the “base-dependent” proteins (all IRR orthologs). This approach has made it possible to estimate the relative contribution of individual domains in the extracellular portion of IRR. The predicted properties of IRR chimeras and the IGF-IR receptor were verified *in vitro* by determining their pH sensitivity.

## EXPERIMENTAL

### The sequences of insulin family receptors

All the sequences of ectodomains of the insulin family *Bos taurus* (BosTau), *Canis familiaris* (CanFam), *Cavia porcellus* (CavPor), *Coturnix japonica* (CotJap), *Danio rerio* (DanRer), *Equus caballus* (EquCab), *Felis catus* (FelCat), *Gallus gallus* (GalGal), *Gasterosteus aculeatus* (GasAcu), *Homo sapiens* (HomSap), *Macaca mulatta* (MacMul), *Microcebus murinus* (MicMur), *Monodelphis domestica* (MonDom), *Mus musculus* (MusMus), *Ochotonas princeps* (OchPri), *Oryctolagus cuniculus* (OryCun), *Pan troglodytes* (PanTro), *Rattus norvegicus* (RatNor), *Scophthalmus maximus* (ScoMax), *Sus scrofa* (SusScr), and *Xenopus laevis* (XenLae) were taken from the material accompanying this article [11]. Since the genes of the IR and IGF-IR receptors in *Danio rerio* are duplicated, additional symbols, either a or b, were used for them.

### Production of chimeric receptors

The sequences encoding human chimeric receptors were produced by polymerase chain reaction using the following primers: for L1C(IGF-IR) IRR-HA, 5'-CATCCCTTGTGAAGGTCCTTGCCCTAAA-

GAGTGCAAGGTAGGC and 5'-cccGGtACcTGT-CACCTCCTCCAGTCGGTA, then 5'-gggGGTAC-CGAATTCATGAAGTCTGGCTCCGGAGGAG; for L2(IGF-IR) IRR-HA, 5'-CACAAAGTGCAGGGGCT-GTGCCCCAAGGTCTGTGAGGAAGAAA and 5'-cccGG-TACCCGTCACCTCCTCCATGCGGTAA, then 5'-ggg-GGTACCGAATTCATGGCAGTGCCTAGTCTGTGG. The correct sequences of the resulting constructs was verified by sequencing.

### Transfection of eukaryotic cells and receptor activation

HEK293 cells were grown on a DMEM medium containing 10% of a fetal bovine serum, 1% of penicillin/streptomycin and 2 mM L-glutamine under standard conditions (37°C and 5% CO<sub>2</sub>). The cells were transfected with pcDNA3.1 plasmids encoding IRR-HA or chimeric receptors using Unifectin-56 (UnifectGroup) according to the manufacturer's recommendations. In 36-40 hours after transfection, the cells were left in a serum-free growth medium for 2-3 h under standard conditions. In order to test receptor activation and plot the activation curves, the receptor-expressing HEK293 cells after “starvation” in the serum-free medium were incubated in phosphate-buffered saline containing 60 mM Tris-HCl with the target pH value for 10 min at room temperature. The buffer was subsequently removed, and the cells were immediately lysed in 1× SDS-PAGE buffer.

### Western blot and construction of activation curves

SDS-PAGE (8%) and Western blot analysis were carried out using the standard protocol described in [12]. The total amount of receptors was determined using rabbit serum against the cytoplasmic portion of IRR (anti-IR/IRR); rabbit serum against phosphorylated IRR (anti-pIR/IRR) was used to detect the phosphorylated form. Anti-IRR antibodies were produced and characterized at our laboratory [5]. HRP-conjugated goat anti-rabbit antibodies (Jackson ImmunoResearch) were used as secondary antibodies. The resulting blots were scanned; specific signals were processed using the ImageJ software. The signal transmitted from antibodies to phosphorylated IRR was normalized with respect to the signal transmitted from the antibody against the C-terminal portion of the IRR receptor. The normalized signals for each pH value ( $n \geq 3$ ) were further processed in the GraphPad Prism 5 software using Hill's equation (One site – Specific binding with Hill slope analysis). As a result of the interpolation analysis, the Hill's coefficient and the half-maximal effective concentration of hydroxyl ions for the activation curve of chimeric proteins were calculated using the GraphPad Prism 5 software.

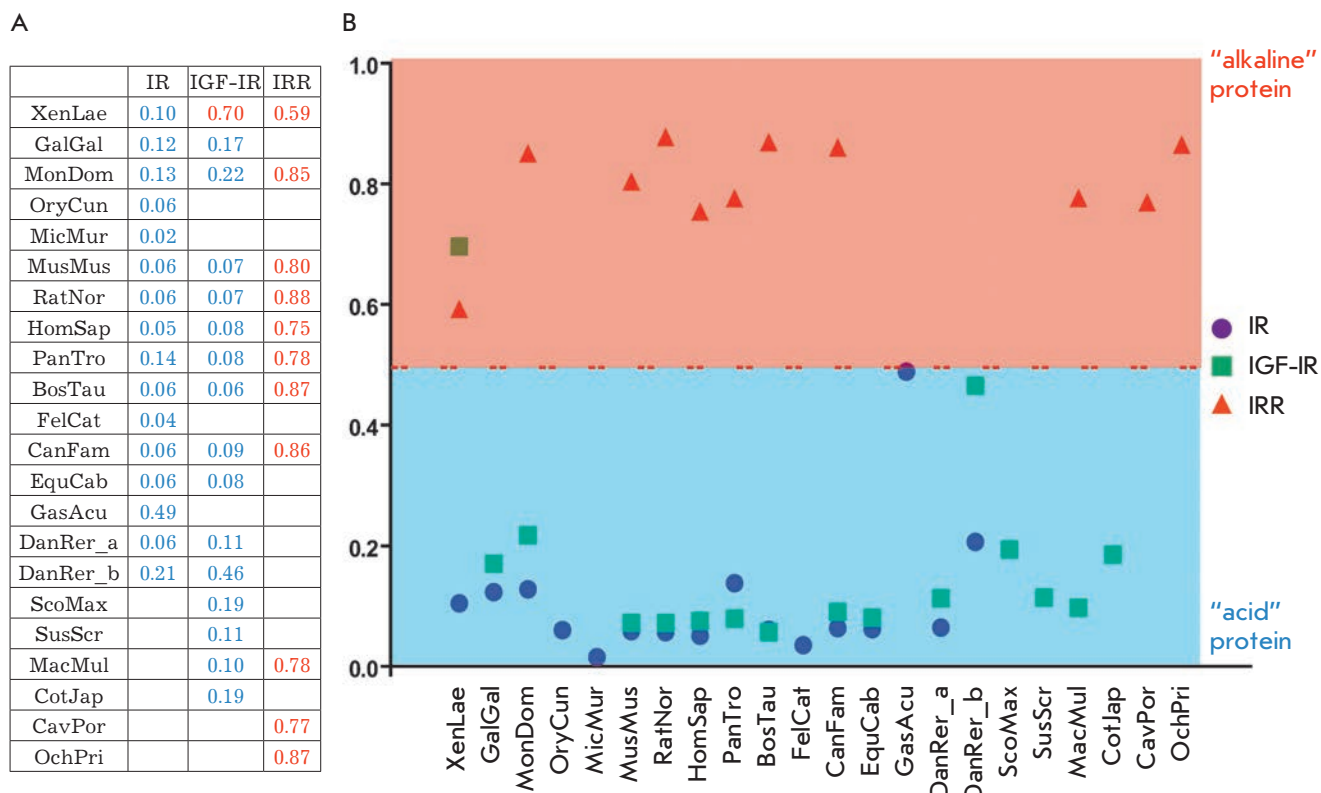


**Fig. 1.** A – Sequence analysis of insulin receptor family ectodomains using the AcalPred program. The relative probabilities of activation of insulin receptor family ectodomains from various species at alkaline pH are shown in table. Full names of the species are given in the Experimental section. B – The graphical representation of the aforescribed probabilities. The red line highlights the notional boundary value prediction – 0.5. Proteins with a predicted probability of alkaline sensitivity greater than 0.5 are shown as “alkaline” (in the red zone), and proteins with the probability less than 0.5 are indicated as “acidic” proteins (in the blue zone)

## RESULTS AND DISCUSSION

Receptor tyrosine kinase IRR exhibits a unique property to be activated in an alkaline extracellular medium. This property makes IRR stand out both among other members of the insulin receptor family and among most tyrosine kinase receptors that are activated by peptides or proteins. We wondered whether it was possible to predict this unique property of the IRR receptor using modern bioinformatic approaches. The recently described AcalPred program was originally developed for predicting pH values (either acidic or alkaline) that would be optimal for enzyme functioning based on its sequence. This program is now available online and is the most reliable option among the previously reported algorithms for predicting pH values optimal for enzyme functioning [10]. As a result, the relative probability of the fact that the protein “prefers” to function either in an alkaline or acidic medium was determined; the overall probability is equal to 1. This

algorithm was developed for soluble enzymes: therefore, we used sequences of the ectodomains of IR family receptors from about 20 various organisms, from frog to man, and analyzed them using the AcalPred software (complete names of the organisms and their abbreviations are given in the Experimental section). We provide the results of an analysis of ectodomains of the human insulin receptor family as an example. Thus, human IR was classified as an “acidic” protein with a probability of 0.95 and as an “alkaline” protein, with a probability of 0.05. Human IGF-IR belongs to “acidic” proteins with a probability of 0.92 and to “alkaline” proteins with a probability of 0.08. Finally, there is a probability of 0.25 that human IRR is an “acidic” protein and 0.75 that it is an “alkaline” protein.

Figure 1A shows the estimated probability that a protein is classified as an “alkaline” one for the rest of the ectodomains from different organisms. Figure 1B provides a graphic interpretation of this table; separa-

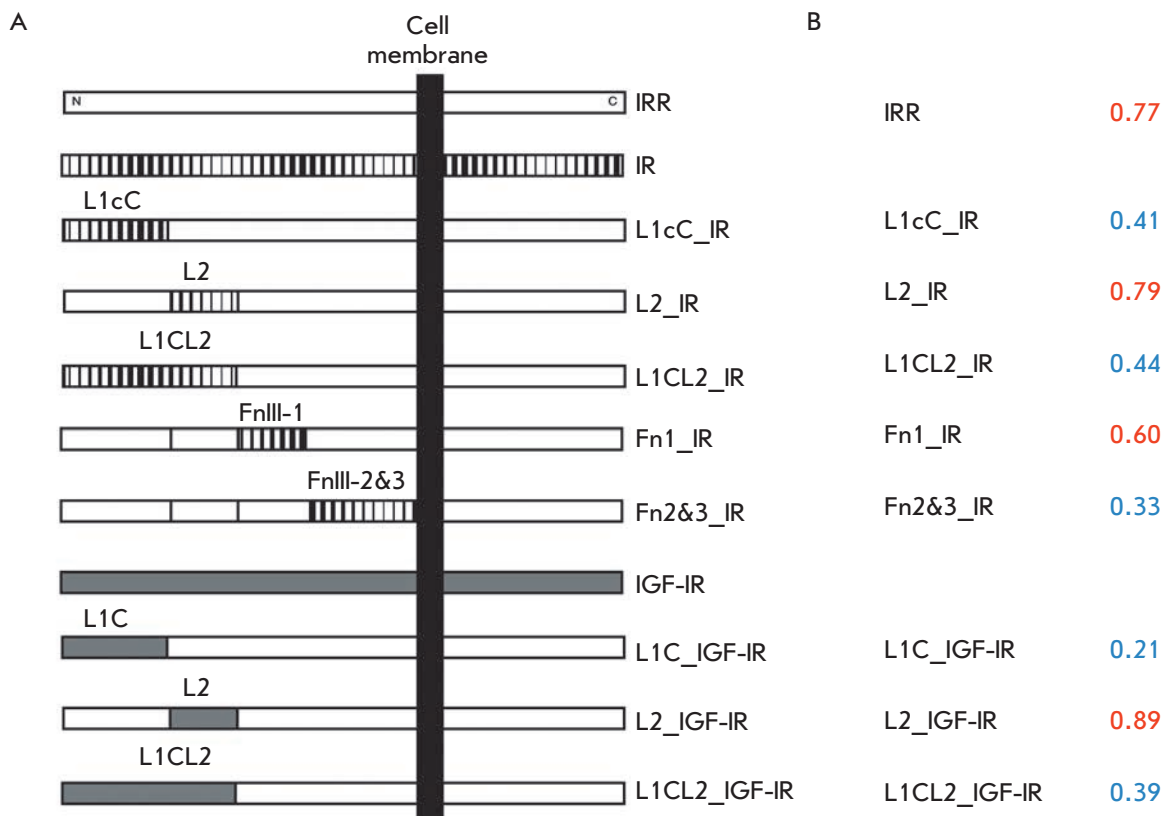


**Fig. 2.** A – Schematic representation of the resulting chimeric proteins. IRR domains are shown in white; IR, in striped; and IGF-IR domains, in gray. L1 and L2 – L-domains, C – furin-like cysteine-rich domain, FnIII-1 and FnIII 2 & 3 – the first or second and third fibronectin repeats. B – Sequence analysis of the ectodomains of the chimeric receptors described above using the AcalPred program. The relative predicted probabilities that the ectodomain is an “alkaline” protein are shown in table. Predicted probability values above 0.5 are shown in red (“alkaline” proteins), and those less than 0.5 are shown in blue (“acidic” proteins)

tion is made at a probability of 0.5 (“alkaline” proteins are placed above the line, while the “acidic” proteins are shown below the line). It is an interesting fact that the insulin receptor family is subdivided into two classes: a) IR and IGF-IR (except for frog IGF-IR), which are supposed to be “acidic” proteins; b) IRR orthologs, which are “alkaline” proteins. These results indicate that the AcalPred program can have a broader application than just analyzing the pH dependence of enzymes and can be used to predict alkaline activation and regulation of tyrosine kinase receptors. In particular, it is possible that the frog IGF-IR receptor, which was classified as an “alkaline” protein, can potentially be sensitive to a weakly alkaline environment.

To evaluate the applicability of the AcalPred program for the analysis of the pH-sensitive properties of receptor tyrosine kinases, we experimentally compared certain properties of previously produced chimeric human IR and IRR proteins with replacement of some

domains of the extracellular portion (*Fig. 2A*) [8, 9, 13]. Chimeric sequences were produced by replacing the first two L1C domains, the third L2 domain, all three L1CL2 domains, and the first fibronectin repeat FnIII-1 or the second and third fibronectin repeats in the IRR ectodomains with identical regions of the IR receptor.

An analysis of these sequences using the AcalPred program has demonstrated that replacement of the first two L1C domains or the second and third fibronectin repeats FnIII-2 and FnIII-3 is crucial for protein “alkalinity” (*Fig. 2B*). Replacement of the first fibronectin repeat FnIII-1 has a weaker effect; and replacement of the third L2 domain does not worsen the expected sensitivity to alkaline pH (*Fig. 2B*). These data show overall agreement with our experimental findings. Thus, it has been demonstrated that the substitutions with the strongest effect are the ones in the first two L1C domains or the second and the third fibronectin repeats FnIII-2 and FnIII, which are believed to form

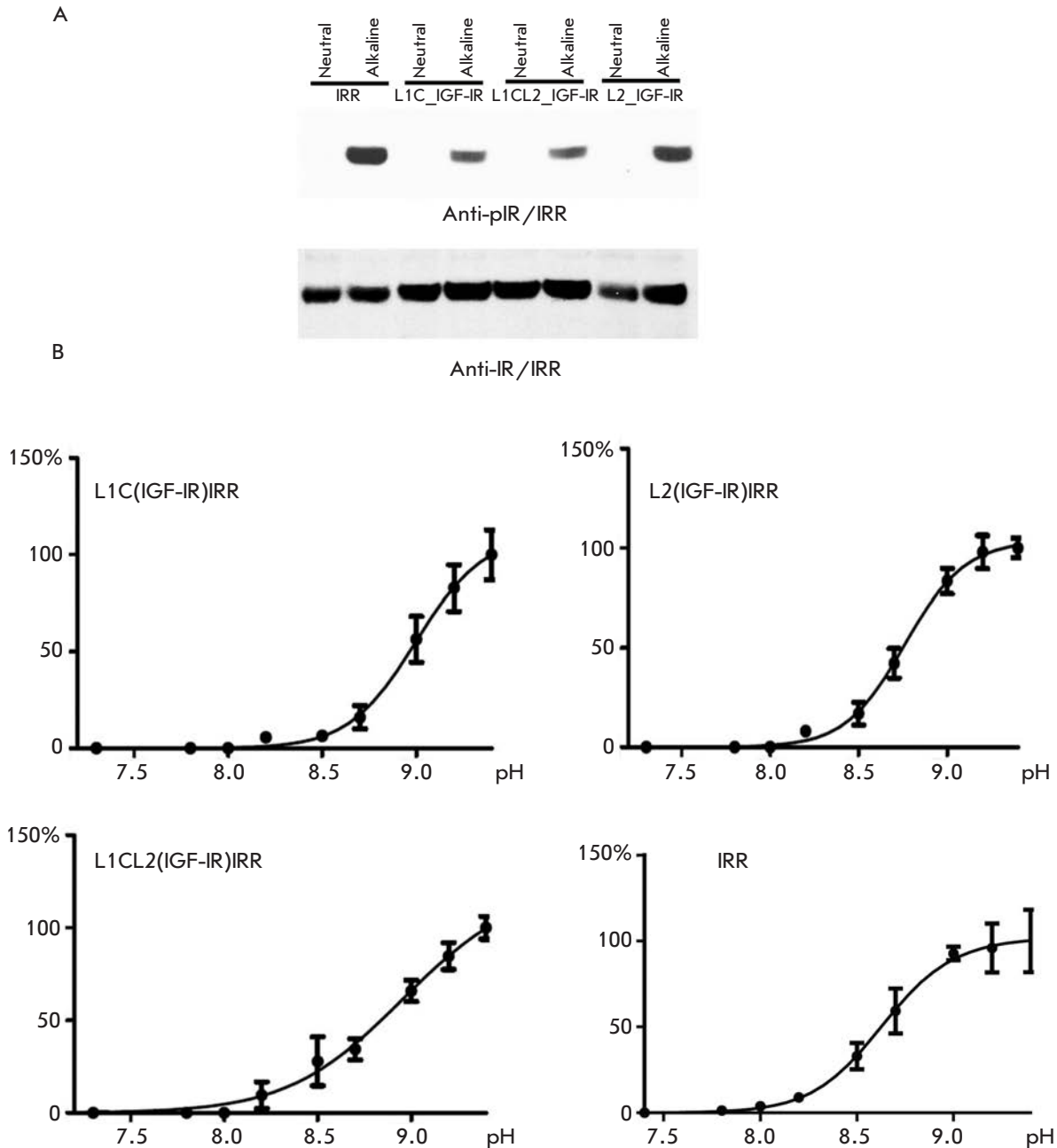


**Fig. 3.** A – Activation of chimeric receptors at alkaline pH. HEK293 cells after expression of chimeric proteins were treated with 60 mM Tris-HCl buffers with pH 7.3 or 9.0, then lysed, and the proteins were separated by SDS-PAGE and transferred onto nitrocellulose membranes for Western blot analysis. An antibody to the phosphorylated IRR was used to detect phosphorylated receptors; the beta subunit was detected with an antibody against the C-terminal part of the IRR. B – pH-dependent activation curves of IRR and chimeric receptors. HEK293 cells after expression of chimeric proteins were treated with a buffer with pH ranging from 7.3 to 9.4 (7.3; 7.8; 8.0; 8.2; 8.5; 8.7; 9.0; 9.2; 9.4); the cells were then lysed, and the proteins were separated by SDS-PAGE and transferred onto a nitrocellulose membrane for Western blot analysis. Antibody to the phosphorylated IRR was used for detecting phosphorylated receptors; the beta-subunit was detected with an antibody against the C-terminal part of the IRR. The phosphorylated receptor was normalized to the total amount of the receptor (signal from beta-receptor subunits) for each pH value. The normalized signals for each pH ( $n \geq 3$ ) were calculated using the GraphPad Prism 5 software with One site – Specific binding with Hill slope interpolation. On each plot, the Y axis shows the percentage of the maximum average activation at pH 9.4

Hill's coefficient (H) and half effect of hydroxyl ions ( $EC_{50}$ ) for the designated receptors

Receptor	Hill's coefficient, H	Half effect, $EC_{50}$ , $\mu\text{M}$
IRR	$2.4 \pm 0.4$	$4.1 \pm 0.4$
L1C_IGF-IR	$2.4 \pm 0.6$	$9.9 \pm 1.5$
L2_IGF-IR	$2.5 \pm 0.4$	$5.8 \pm 0.5$
L1CL2_IGF-IR	$1.6 \pm 0.3$	$9.8 \pm 2.6$

the main site of pH sensitivity in the IRR receptor [13]. The substitution of the L2 domain in IRR for an identical sequence from IR had a small but still noticeable effect on the sensitivity of IRR to alkaline pH [9], while no changes were predicted by AcalPred. The substitution of the first fibronectin repeat FnIII-1 for an identical IR fragment resulted in an effect stronger than that of the replacement of the L2 domain, comparable to the effect of L1C substitution but weaker than the effect of a replacement of the second and third fibronectin repeats FnIII-2 and FnIII-3 [9, 13], which showed agreement with the result predicted by the program. We can conclude that the AcalPred program has a predictive potential in analyzing chimeric receptors; however, it should be taken into account that the resulting parameters describe the probability rather than provide an accurate assessment of the pH dependence. In other words, the results are qualitative rather than quantitative.

In evolutionary terms, IRR is structurally more similar to the IGF-IR receptor than to insulin receptor. Hence, in addition to analyzed IRR receptor where the L1CL2 domains were substituted for identical regions of the IGF-IR receptor [8], we produced two chimeric proteins where the L1C or L2 IRR domains were replaced with the corresponding domains of the IGF-IR receptor (Fig. 2A). Next, we checked the response of the resulting receptors to increased pH of the extracellular medium. These proteins were expressed in HEK293 eukaryotic cells. The cells expressing chimeric receptors were treated with a buffer with pH 7.3 or 9.0. Same as IRR, L1C\_IGF-IR, L1CL2\_IGF-IR, and L2\_IGF-IR chimeras were activated in response to alkaline pH (Fig. 3A).

We plotted the curve showing the degree of activation of each chimeric receptor as a function of pH in a range from 7.3 to 9.4. The activation curves were recorded for all three chimeric proteins: L1C\_IGF-IR, L1CL2\_IGF-IR, and L2\_IGF-IR (Fig. 3B). The Hill's

coefficient (H) and half effect of hydroxyl ions ( $EC_{50}$ ) were calculated for each receptor using the GraphPad Prism 5 software, which allows one to estimate the pH sensitivity of various chimeric receptors and cooperation of their interaction with an agonist. An analysis of the curves has demonstrated that when two L1C domains or one L2 domain are replaced, the Hill's coefficient remains virtually unchanged. Thus, the Hill's coefficient for L1C\_IGF-IR was  $2.4 \pm 0.6$  and  $2.5 \pm 0.4$  for L2\_IGF-IR and L2\_IGF-IR, respectively, while  $2.4 \pm 0.4$  for IRR. Meanwhile, replacement of the L1C domain increased the  $EC_{50}$  value by more than 100%, while substitution of the L2 domain increased it by approximately 40% (Fig. 3B and table). Replacement of all three L1CL2 domains in the chimeric construct resulted in the strongest effect: the Hill's coefficient decreased to  $1.6 \pm 0.3$ , while  $EC_{50}$  rose by more than 100%, up to  $9.8 \pm 2.6 \mu\text{M}$  (almost identically to the values in the chimeric construct with the first two L1C domains replaced) (table) [8]. Such a decline in the Hill's coefficient may be associated with the change in structure and mutual arrangement of pH-sensitive sites inside the ectodomain as the first three domains are replaced. Interestingly, replacement of the L1C and L2 domains in chimeric IRR receptors for the corresponding domains of insulin receptors led to more significant negative changes than insertion of IGF-IR domains [9]. Thus, replacement of L1C portions had the greatest negative effect, while the least effect was observed when the L2 domain was substituted.

## CONCLUSIONS

In this study, we used the bioinformatic approach to the analysis of the pH-sensitivity of the IRR receptor. The AcalPred algorithm elaborated to predict the optimal pH for the activity of soluble enzymes can also be used to describe the pH-sensitive properties of the members of the insulin receptor family. Moreover, this program can be employed to predict the contribution of individual structural fragments of the receptor to its pH-sensing function. It should be mentioned that the program mostly provides a qualitative result, while the quantitative conclusions may not be accurate enough. ●

*This study was supported by the Russian Science Foundation (14-14-01195), Presidium of the Russian Academy of Sciences "Molecular and Cellular Biology" and "Fundamental Sciences for Medicine," and the Russian Foundation for Basic Research (grants № 13-04-01359A, 14-04-01736A, 12-04-91054, 13-04-90481).*

## REFERENCES

1. Kurachi H., Jobo K., Ohta M., Kawasaki T., Itoh N. // *Biochem. Biophys. Res. Commun.* 1992. V. 187. P. 934–939.
2. Hernandez-Sanchez C., Mansilla A., de Pablo F., Zardoya R. // *Mol. Biol. Evolution.* 2008. V. 25. P. 1043–1053.
3. De Meyts P. // *Trends Biochem. Sci.* 2008. V. 33. P. 376–384.
4. Deev I.E., Vasilenko K.P., Kurmangaliev E., Serova O.V., Popova N.V., Galagan Y.S., Burova E.B., Zozulya S.A., Nikol'skii N.N., Petrenko A.G. // *Dokl. Biochem. Biophys.* 2006. V. 408. P. 184–187.
5. Deyev I.E., Sohet F., Vassilenko K.P., Serova O.V., Popova N.V., Zozulya S.A., Burova E.B., Houillier P., Rzhovsky D.I., Berchatova A.A., et al. // *Cell Metabolism.* 2011. V. 13. P. 679–689.
6. Deyev I.E., Rzhovsky D.I., Berchatova A.A., Serova O.V., Popova N.V., Murashev A.N., Petrenko A.G. // *Acta Naturae.* 2011. V. 3. P. 114–117.
7. Petrenko A.G., Zozulya S.A., Deyev I.E., Eladari D. // *Biochim. Biophys. Acta.* 2013. V. 1834. P. 2170–2175.
8. Popova N.V., Deyev I.E., Petrenko A.G. // *Dokl. Biochem. Biophys.* 2013. V. 450. P. 160–163.
9. Deyev I.E., Mitrofanova A.V., Zhevlenov E.S., Radionov N., Berchatova A.A., Popova N.V., Serova O.V., Petrenko A.G. // *J. Biol. Chem.* 2013. V. 288. P. 33884–33893.
10. Lin H., Chen W., Ding H. // *PLoS One.* 2013. V. 8. e75726.
11. Renteria M.E., Gandhi N.S., Vinuesa P., Helmerhorst E., Mancera R.L. // *PLoS One.* 2008. V. 3. e3667.
12. Deyev I.E., Petrenko A.G. // *Biochimie.* 2010. V. 92. P. 418–422.
13. Deyev I.E., Chachina N.A., Shayahmetova D.M., Serova O.V., Petrenko A.G. // *Biochimie.* 2015. V. 92. P. 1–9.

# Detection of T-Cadherin Expression in Mouse Embryos

K. A. Rubina<sup>1\*</sup>, V. A. Smutova<sup>1</sup>, M. L. Semenova<sup>2</sup>, A. A. Poliakov<sup>3</sup>, S. Gerety<sup>4</sup>, D. Wilkinson<sup>3</sup>, E. I. Surkova<sup>1</sup>, E. V. Semina<sup>1</sup>, V. Yu. Sysoeva<sup>1</sup>, V. A. Tkachuk<sup>1</sup>

<sup>1</sup>Department of Biochemistry and Molecular Medicine, Faculty of Fundamental Medicine, Lomonosov Moscow State University, Lomonosovskiy Prosp., 31/5, 119192, Moscow, Russia

<sup>2</sup>Department of Embryology, Biology Faculty, Lomonosov Moscow State University, Leninskie Gory, 1/12, 119234, Moscow, Russia

<sup>3</sup>Division of Developmental Neurobiology, MRC National Institute for Medical Research, The Ridgeway, Mill Hill, London NW7 1AA, UK

<sup>4</sup>Wellcome Trust Sanger Institute, Wellcome Trust Genome Campus, Hinxton, Cambridge CB10 1SA, UK

\*E-mail: rkseiniya@mail.ru

Received 31.10.2014

Revised manuscript received 20.02.2015

Copyright © 2015 Park-media, Ltd. This is an open access article distributed under the Creative Commons Attribution License, which permits unrestricted use, distribution, and reproduction in any medium, provided the original work is properly cited.

**ABSTRACT** The aim of the present study was to evaluate T-cadherin expression at the early developmental stages of the mouse embryo. Using *in situ* hybridization and immunofluorescent staining of whole embryos in combination with confocal microscopy, we found that T-cadherin expression is detected in the developing brain, starting with the E8.75 stage, and in the heart, starting with the E11.5 stage. These data suggest a possible involvement of T-cadherin in the formation of blood vessels during embryogenesis.

**KEYWORDS** T-cadherin; embryogenesis; angiogenesis; *in situ* hybridization.

**ABBREVIATIONS** T-cad – T-cadherin; PBS – phosphate-buffered saline.

## INTRODUCTION

T-cadherin was first discovered in a chick embryo brain over 20 years ago [1]. In early studies, Ranscht demonstrated [1] that expression of T-cadherin in developing somites correlates with migration of neural crest cells from the neural tube. Neural crest cells are the transient multipotent population of cells that further give rise to a variety of tissues, including craniofacial bones and cartilages, smooth muscle cells, melanocytes, peripheral neurons, glia, etc. More recent studies by the same laboratory have revealed that migratory neural crest cells and motor neuron axons growing to their targets choose their pathway through the rostral part of the somites, avoiding, along their pathway, the caudal part of the somites where cells express T-cadherin. *In vitro* experiments, using soluble T-cadherin or T-cadherin as a substrate, demonstrated that T-cadherin inhibits the development of neurites and growth of motor neuron axons. This suggested that T-cadherin functions as a guidance molecule for growing axons and migrating neural crest cells [2, 3]. Like other guidance molecules, ephrins and their receptors [4], T-cadherin in the developing nervous system acts as a “repulsive molecule” and negatively regulates axon growth and cell migration.

It should be noted that the T-cadherin expression level in an adult brain is higher than that in an embryonic brain [5]. Our laboratory found that T-cadherin in an adult organism is expressed not only in the nervous system, but also in the cardiovascular system [6, 7]. Immunohistochemical staining of aorta sections revealed the presence of T-cadherin in all layers of the vascular wall (intima, media, and adventitia), endothelium, smooth muscle cells, and pericytes. A high level of T-cadherin in the adventitia was detected in the *vasa vasorum* walls [6]. We also observed elevated T-cadherin expression in blood vessels in various pathologies: upon development of atherosclerotic lesions and post-angioplasty restenosis, which are conditions associated with pathological angiogenesis in humans [6, 7]. Furthermore, overexpression of T-cadherin in the arterial wall after balloon angioplasty in rats was found to correlate with late stages of the neointima formation and to coincide with the phase of active migration and proliferation of vascular cells. Expression of T-cadherin in the *vasa vasorum* of the adventitia of damaged blood vessels suggests its involvement in the regulation of angiogenesis or repair of vascular wall damage [7].

The formation of the nervous and cardiovascular systems during embryogenesis is known to occur in

parallel, whereby nerves and blood vessels are often located in close proximity to each other. Nerve and vascular cells secrete neurotrophic and angiogenic factors, respectively, which promote their survival and determine the direction of growth and migration [8]. The regulatory mechanisms of directed axonal growth and nerve cell migration are well studied [4, 9, 10], while there is much less data on the factors and mechanisms regulating directed growth of blood vessels. Guidance molecules that are involved in the regulation of the formation of the nervous and vascular systems include proteins such as semaphorins and their receptors (plexins and neuropilins), netrins and their receptors (DCC/neogenin and Unc5), slit ligands and their receptors (Robo), and some other proteins [10]. Data on the expression of T-cadherin in the cardiovascular system during embryogenesis have yet to be reported. It is unknown whether T-cadherin is expressed in the developing heart and blood vessels during embryogenesis, or whether its role is limited to the regulation of the trajectory of axon growth and migration of neural crest cells.

In this regard, we analyzed the expression of T-cadherin at different stages of a mouse's development using *in situ* hybridization and immunofluorescent staining of whole embryos in combination with confocal microscopy. Expression of the T-cadherin mRNA was detected starting with the E8.75 stage in the developing brain and starting with the E11.5 stage in the heart, which coincides with the processes of active growth and formation of blood vessels due to vasculogenesis and angiogenesis in the cardiovascular system and brain.

## EXPERIMENTAL

### Production of dated pregnancy in mice

Mouse embryos derived from F1 CBA/C57Bl6 hybrids were used in this study. Mice were maintained under standard, 14-hour light conditions. In the evening hours, males were introduced to females, and, the next morning, mated mice were detected by the presence of vaginal plugs. The day of vaginal plug detection was considered as half of the first pregnancy day.

### Generation of mouse embryos at the postimplantation stages of development

Postimplantation embryos were recovered according to a standard protocol described by Monk [11]. Females were sacrificed by cervical dislocation. The abdominal cavity was opened, and the uterus with deciduomas was removed and placed in a Petri dish with cold phosphate buffered saline (PBS, Sigma-Aldrich). Next, the uterine horns were incised along the antimesometri-

al edge, exposing the decidual capsules with embryos and separating them from the mesometrial wall. The deciduomas were transferred into a clean Petri dish containing cold PBS. The decidual capsule was incised, capturing its mesometrial end, and the embryo was gently pushed into the solution. After that, the embryo was released from the amniotic sac by preparation needles and transferred to a clean Petri dish with PBS for washing. Embryos were fixed in 4% formaldehyde (PRS Panreac) in PBS at +4 °C overnight.

### Immunofluorescent staining of mouse embryos with antibodies to T-cadherin

After fixation, embryos were washed 5 times for 20 min each in PBS containing a 0.2% Triton X-100 detergent (Sigma-Aldrich). To prevent nonspecific staining, the samples were placed into 1 : 10 normal goat non-immune serum (Sigma-Aldrich) and incubated at +4 °C on a shaker overnight. Then, the embryos were incubated in a 1 : 25 solution of the rabbit monoclonal antibody to mouse T-cadherin (BioDesign). As a control, non-immune rabbit IgG immunoglobulins (Abd Serotec) were used in a concentration equivalent to the concentration of specific antibodies. Incubation was carried out at room temperature under constant shaking for a day. Antibodies were washed in a 0.2% solution of Triton X-100 in PBS (three times for 20 min each at room temperature) and following that (in the fourth change of solution) on a shaker at +4 °C overnight. After washing, the embryos were placed in a solution of goat secondary antibodies conjugated with a fluorochrome Alexa Fluor® 594 where they were kept on a shaker at room temperature for a day. Cell nuclei were additionally stained with a fluorescent dye DAPI (Sigma-Aldrich) in 1 : 1000 dilution for 30 min, then washed 3 times for 20 min each in 0.2% Triton X-100 in PBS, and left in the same solution at +4 °C on a shaker overnight. The next day, the embryos were mounted on a Aqua-Poly/Mount medium (Polysciences). The prepared samples were analyzed using a Leica SP5 confocal multiphoton microscope and Leica Application Suite Advanced Fluorescence 2.2.0 software (Leica Microsystems).

### Purification of plasmids for *in situ* hybridization

Purification and isolation of plasmids were performed using a commercial EndoFree® Plasmid Maxi Kit (Qiagen) according to the manufacturer's protocol.

### Linearization of plasmids for *in situ* hybridization

*In situ* hybridization with RNA probes to T-cadherin (sense and antisense) and Krox20 was performed on mouse embryos according to the previously developed technique [12].



To identify the expression of the T-cadherin mRNA in mouse embryos by *in situ* hybridization, the pFL-CI plasmid (ImaGenes, Germany) with the inserted EST-sequence (expressed sequence tag) of the T-cadherin cDNA was used. The Bluescript KS plasmid with the inserted EST sequence of the Krox20 cDNA was used as a positive control. ESTs are short cDNAs used for detection of gene expression and are available in the GenBank database.

For the linearization, the plasmid DNA was treated with restriction enzymes: Not1 (Fermentas) for Krox20 and BamH1 (Fermentas) for T-cadherin. The composition of a linearization reaction mixture was as follows: 10× buffer, deionized water (Sintol), the plasmid (4 µg), and a restriction enzyme (Not1 or BamH1). The mixture was incubated at +37 °C for 12 h. After incubation, DNA was purified using a commercial GFX PCR DNA kit and a Gel Purification Kit (GE Healthcare) according to the manufacturer's protocol. Linearized and non-linearized plasmids were analyzed by electrophoresis in 1.2% agarose gel.

#### Synthesis of a RNA-containing probe for *in situ* hybridization

The reaction mixture for the synthesis of a digoxigenin-labeled RNA-containing probe included: 5× transcription buffer, RNase free deionized water, a linearized plasmid, a mixture of nucleotides labeled with DIG (10 mM ATP, 10 mM CTP, 10 mM GTP, 6.5 mM UTP, 3.5 mM DIG-11-UTP, pH 7.5, Roche), a RNase inhibitor (Merck Biosciences), and RNA polymerase. The mixture was incubated at +37 °C for 2 h. T3 RNA polymerase (Fermentas) was used to synthesize a RNA-containing probe from a linearized plasmid containing the Krox20 sequence. T7 RNA polymerase (Promega) was used to synthesize the RNA probe for the T-cadherin sense sequence (negative control) from the linearized plasmid, and T3 RNA polymerase (Fermentas) was used to synthesize the antisense RNA probe for detection of the T-cadherin mRNA. The resulting RNA probes were purified on a commercial RNAspin Mini column (GE Healthcare) according to the manufacturer's protocol.

#### Hybridization of mouse embryos *in situ*

Hybridization of mouse embryos was performed with the RNA probe (antisense) synthesized on the T-cadherin gene template. The antisense RNA probe (reverse sequence) enables detection of expression at the transcriptional level. The sense probe (direct sequence) does not bind to the mRNA in the cell, since it is non-complementary to the mRNA and is used as a negative control. The RNA probe synthesized on the *Krox20* gene template, whose expression level is high in the central

nervous system cells of mouse embryos at these stages of development, was used as a positive control.

Hybridization was performed in E8.75, E9.5 and E10.5 mouse embryos.

Embryos were fixed in 4% formaldehyde (PRS Panreac) in PBS, which also contained 1% Tween-20 (Sigma-Aldrich), at +4 °C overnight, then washed (2 × 5 min) with cold PBS, and fixed sequentially in solutions of increasing concentrations of methanol (25, 50, 75, and twice with 100%). After that, the embryos were frozen and stored for subsequent studies at -20 °C. Immediately prior to hybridization, the embryos were rehydrated in solutions of decreasing concentrations of methanol (75, 50, and 25%), washed three times in PBS, and treated with proteinase K at room temperature (Qiagen, at a concentration of 10 µg/mL in PBS). Then, the embryos were washed in PBS, fixed in 4% formaldehyde (PRS Panreac) in PBS for 20 min, and washed twice for 5 min in PBS. Next, the embryos were gradually transferred into a hybridization buffer containing 50% formamide (Sigma-Aldrich), 5× SSC buffer (stock solution: 20× SSC buffer containing 3 M NaCl, 0.3 M sodium citrate, pH 7.0), 0.1% Triton X-100 (DiaEm), 50 µg/mL heparin (Sigma-Aldrich), 1 mg/mL RNA from type IV yeast (Sigma-Aldrich), 5 mM EDTA (Applichem), 2% blocking solution (Roche), and 0.1% CHAPS (3-[(3-cholamidopropyl)-dimethylammonio]-1-propanesulfonate) (Sigma-Aldrich). The embryos were incubated at room temperature in a (1 : 1) mixture of a hybridization buffer and PBS and then in the hybridization buffer. The embryos were left in the hybridization buffer at +65 °C overnight. In the morning, the embryos were placed in a fresh hybridization buffer, added with a RNA probe (0.5 µg of the probe per 1 mL of buffer), and incubated at +65 °C for 24 h. After that, the embryos were washed in the hybridization buffer (3 times for 30 min at +65 °C) and then in a (1 : 1) mixture of the hybridization buffer and a MABT buffer at +65 °C for 30 min. The MABT buffer composition: 100 mM maleic acid (Sigma-Aldrich), pH 7.5, 150 mM NaCl, and 0.1% Tween-20 (Sigma-Aldrich). Next, the embryos were washed 3 times with the MABT buffer for 10 min at room temperature, placed in a blocking solution (2% blocking solution (Roche) containing 20% sheep serum (Abd Serotec) and MABT) at room temperature for 2 h, and then incubated in a 10% sheep serum solution containing 1 : 200 diluted anti-digoxigenin antibodies conjugated with alkaline phosphatase (Roche) at +4 °C for 12 h. After incubation with antibodies, the embryos were washed in MABT at room temperature and then in an NTMT buffer until staining. The composition of the NTMT buffer (per 1 mL): 100 mM Tris-HCl (Sigma-Aldrich), pH 9.5, 50 mM MgCl<sub>2</sub> (Sigma-Aldrich), 100 mM NaCl, 0.1%

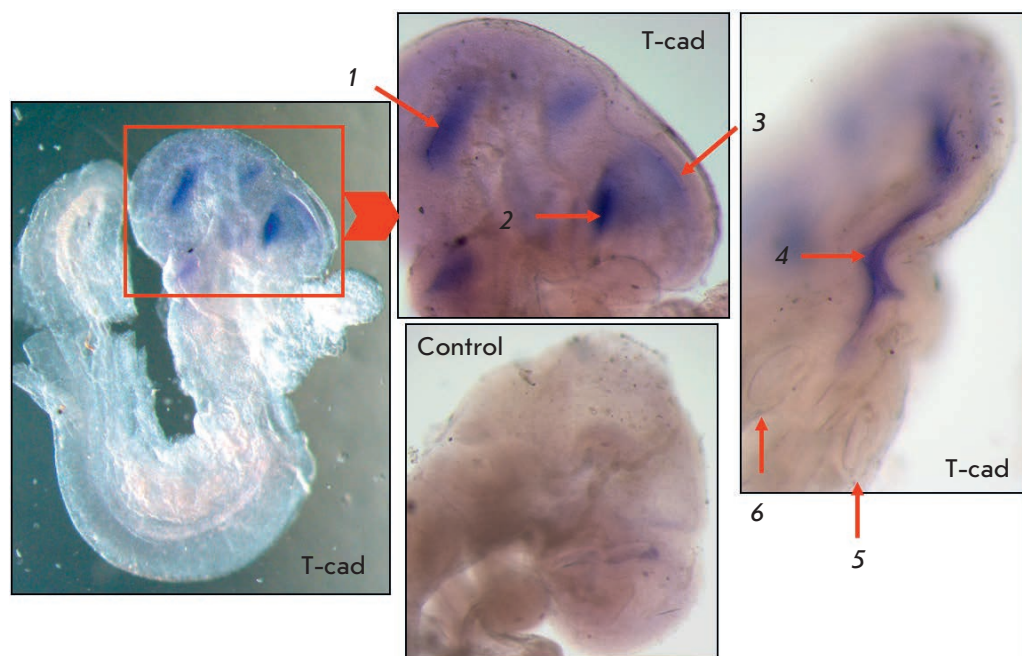


**Fig. 1.** *In situ* hybridization of mouse embryos at the of E8.75 stage. Expression of T-cadherin mRNA (T-cad): 1 – in the mesencephalon region; 2 – in the base of the developing optic vesicle; 3 – in the inner lining of the telencephalon; 4 – in the myelencephalon; 5, 6 – in the optic vesicles. No specific staining in the negative control (control). Magnification of 3.2, 5, and 6×

Tween-20 (Sigma-Aldrich), 4.5  $\mu$ L of NBT (4-nitro-blue tetrasodium chloride, Vector Laboratories), and 3.5  $\mu$ L of BCIP (5-bromo-4-chloro-3-indolylphosphate, Vector Laboratories). The staining reaction was stopped by repeated washing in PBS. Then, the embryos were fixed in 4% formaldehyde (PRS Panreac) in PBS at room temperature for 2 h. Images of the embryos were produced using a stereomicroscope (Olympus SZX 16, AxioCam HRc camera, Carl Zeiss) and the Axio Vision 3.1 software.

## RESULTS

We evaluated the expression of T-cadherin at the E8.75–E11.5 stages of early embryonic mouse development using *in situ* hybridization and immunofluorescent staining of whole embryos in combination with confocal microscopy.

### Expression of T-cadherin in the embryonic mouse brain

Expression of T-cadherin mRNA was detected in the developing brain, starting with the E8.75 stage, in particular, in the diencephalon and prosencephalon – in the inner lining of the telencephalon cavity (*Fig. 1*). The T-cadherin mRNA was also detected in the region of optic vesicles, at the transition of the diencephalon to the developing thalamencephalon. In the negative control (sense probe), nonspecific diffuse background staining in the prosencephalon was observed that was different from specific staining using the positive control and the antisense probe for T-cadherin.

At the E9.5 stage, expression of the T-cadherin mRNA was detected in the prosencephalon, thickening olfactory placode, base of the optic vesicles, parietal bend region, and at the transition of the myelencephalon to the spinal cord (in the occipital bend region) (*Fig. 2*).

At the E10.5 stage, expression of T-cadherin mRNA was observed in the mesencephalon and developing ependymal roof of the diencephalon and its lateral parts (*Figs. 3 and 4*). Specific staining was also found in the choroid plexus of the telencephalon (*Fig. 3*).

No specific staining was found in the negative control. The specific staining pattern typical of the *Krox20* gene was observed in the positive control (*Figs. 3 and 4*).

The T-cadherin protein was detected by immunofluorescent staining with anti-T-cadherin antibodies in whole mouse embryos in combination with confocal microscopy. T-cadherin was detected starting with the E9.5 stage, with specific staining being observed in the linings of the developing brain (*Fig. 5*), including the base of the developing optic vesicles.

The T-cadherin expression level in the inner lining of the brain was high, starting with the E11.5 stage: intense specific staining was observed in the diencephalon region, developing eyecup, as well as in the mesencephalon and metencephalon region (*Fig. 6*).

Therefore, these data indicate that T-cadherin expression at the mRNA level begins with the E8.75 stage and is detected in different parts of the embryonic brain. The T-cadherin protein is detected in embryos, starting with the E9.5 stage. The maximum intensity of

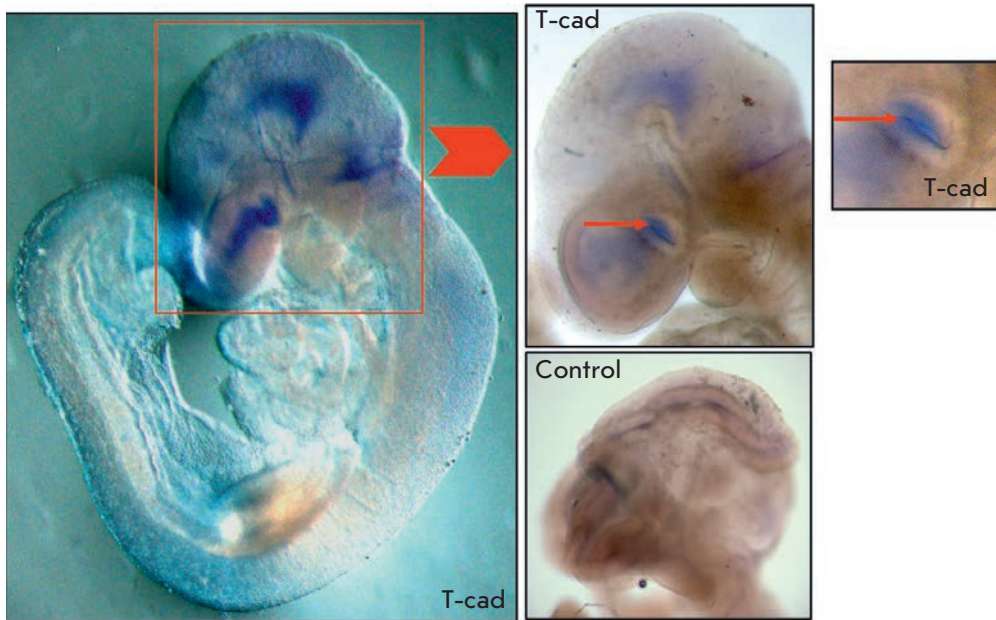


**Fig. 2.** *In situ* hybridization of mouse embryos at the E9.5 stage. Staining of brain regions corresponds to the localization of T-cadherin mRNA (T-cad). Expression is observed in the base of the developing optic vesicles, in the parietal and occipital bend regions. Small arrows indicate the base of the developing optic vesicle. Control – the negative control. Magnification of 3.2, 5, and 6 $\times$

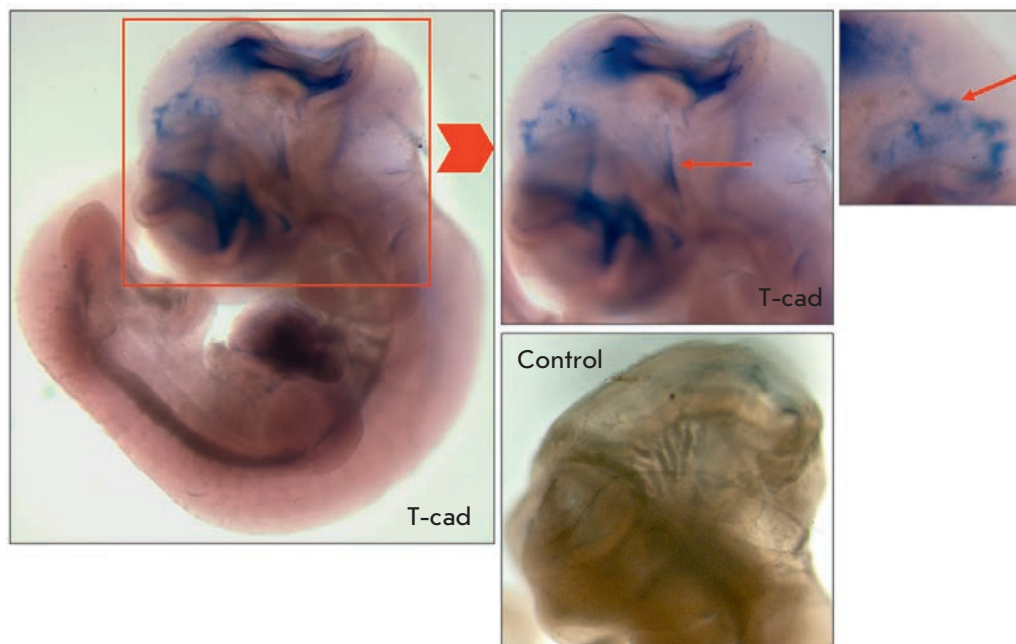


**Fig. 3.** *In situ* hybridization of mouse embryos at the E10.5 stage. Intense expression of T-cadherin (T-cad) in the developing tectum and the lateral regions of the diencephalon. The arrow indicates specific staining of the choroid plexus in the telencephalon region. No specific staining in the negative control (control). Magnification of 3.2, 5, and 6 $\times$

T-cadherin expression was detected in the inner lining of the brain.

#### Expression of T-cadherin in the embryonic heart

In the mouse embryo heart, T-cadherin is expressed starting with the E11.5 stage (*Fig. 7*). No expression of either T-cadherin mRNA or T-cadherin in the developing heart was detected at the E8.75, E9.5 and E10.5 stages (*Fig. 8*).

#### DISCUSSION

The obtained data indicate that T-cadherin mRNA in the developing brain is expressed starting with the E8.75 stage – in the inner lining of the telencephalon cavity and diencephalon. No expression of T-cadherin was detected until this stage. Active formation and growth of blood vessels are known to occur in the brain bend regions at the early developmental stages [13]. Probably, expression of T-cadherin at the E9.5 stage

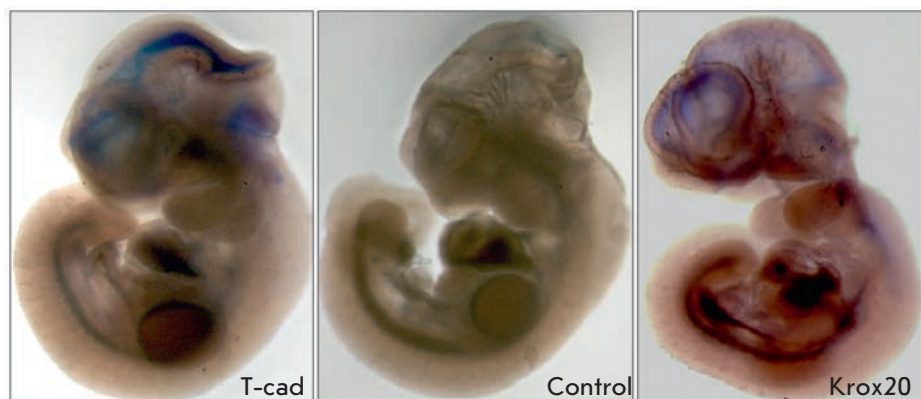


**Fig. 4.** *In situ* hybridization of mouse embryos at the E10.5 stage. T-cad – specific staining of T-cadherin in the tectum (in the occipital bend region) and inner lining of the telencephalon; control – no specific staining in the negative control; Krox20 – staining of central nervous system structures in the positive control. Magnification of 3.2×

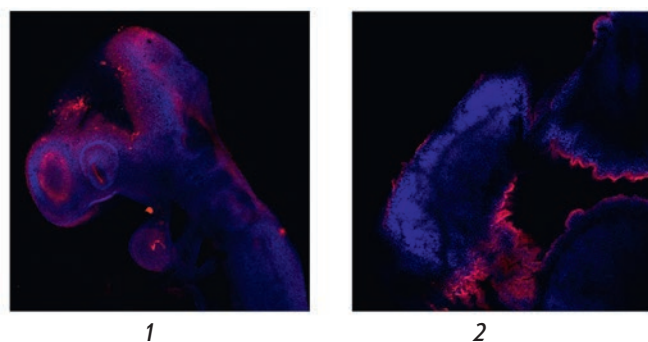


**Fig. 5.** Immunofluorescent staining of mouse embryos at the E9.5 (-1-) and E12.5 (-2-) stages. Specific staining (red fluorescence) corresponds to T-cadherin expression in the linings of the brain at both stages; expression of T-cadherin in the developing optic vesicle in the E9.5 embryo. Blue fluorescence corresponds to nuclei additionally stained with DAPI. Magnification of 5×

in these regions of the developing brain is associated with intensive angiogenesis and potential involvement of this protein in the regulation of directional growth of blood vessels in the same manner as it occurs during the growth of motoneuronal axons to their targets in the nervous system.

Later, at the E9.5 stage, the T-cadherin mRNA was identified in the prosencephalon, olfactory placode, base of the optic vesicles, and region of the parietal and occipital bends. The active formation and growth of blood vessels are known to occur in the brain bend regions at this stage, which suggests possible involvement of T-cadherin in vascularization of these structures [13]. Noteworthy, T-cadherin expression at the mRNA level in the optic vesicle region was detected at the E8.75 stage. We suppose that expression of T-cadherin at the base of the developing optic vesicles is associated with the epithelialization of the structures of

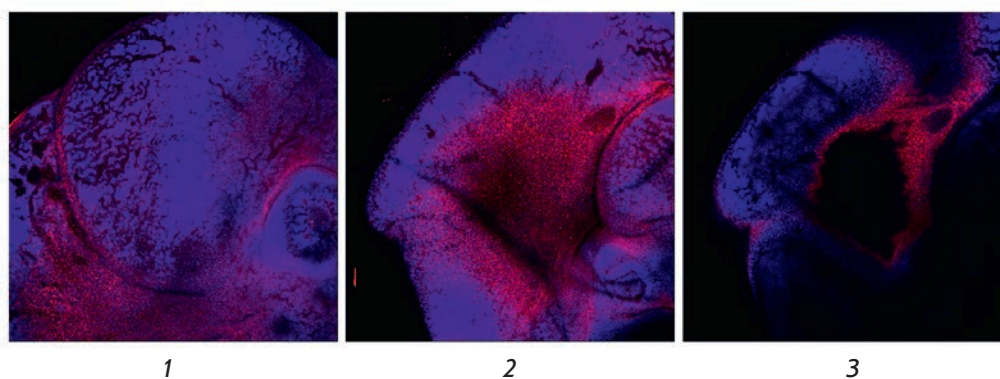


**Fig. 6.** Immunofluorescent staining of mouse embryos at the E11.5 stage. Specific staining (red fluorescence) corresponds to expression of the T-cadherin protein. Blue fluorescence corresponds to nuclei additionally stained with DAPI. 1 – specific staining in the diencephalon region, as well as in the region of the developing eyecup; 2 – specific staining in the mesencephalon and metencephalon region; 3 – the same region as in 2 – at another optical plane level. Magnification of 5×

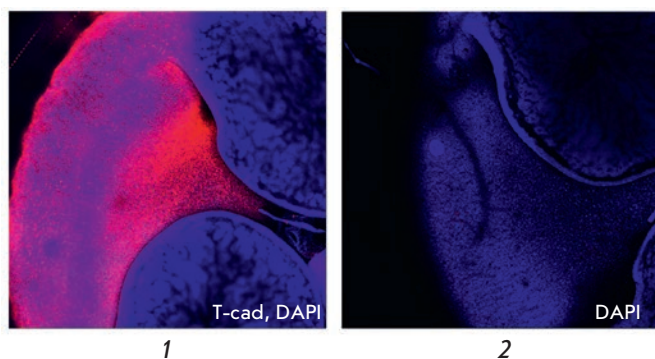


**Fig. 7.** Immunofluorescent staining of mouse embryos at the E11.5 stage. Specific staining (red fluorescence) corresponds to expression of the T-cadherin protein (T-cad). Blue fluorescence corresponds to nuclei additionally stained with DAPI. 1 – specific staining reflecting T-cadherin expression in the heart region; 2 – control staining with antibodies to immunoglobulin G. Magnification of 5×

the future eyecups; otherwise, T-cadherin could be involved in the choroid formation. However, further research is necessary to exactly determine the role of T-cadherin in the formation of these structures.

Later, at the E10.5 stage, intense staining corresponding to T-cadherin mRNA was detected in the mesencephalon, developing ependymal roof of the diencephalon, and its lateral parts. Specific staining was also found in the region of the choroid plexus of the telencephalon. The stained areas morphologically corresponded to the areas of the choroid plexus formation in the walls of the developing brain ventricular system.

The *in situ* hybridization results of T-cadherin expression detection at the protein level were confirmed

by immunofluorescent staining of whole mouse embryos. Confocal microscopy combined with an image analysis enabled us to detect the T-cadherin protein in the linings of the developing brain, starting with the E9.5 stage. Expression of T-cadherin was also identified at the base of the developing optic vesicles, which corresponds to the *in situ* hybridization data. T-cadherin expression in the developing eyecups indicates the possible involvement of this protein in the choroid development.

Antibody staining of embryos revealed intense expression of T-cadherin in the inner lining of the brain, starting with the E11.5 stage. In particular, intense specific staining was observed in the diencephalon region, developing optic eyecup, as well as in the mesencephalon and metencephalon region. We suppose that T-cadherin is involved in the formation of the brain ventricular system, more specifically the choroid plexus in the ventricular walls, since the active formation of brain vessels is known to occur at this stage of embryonic development [13].

Therefore, the use of *in situ* hybridization and immunofluorescent staining in combination with confocal microscopy enabled us for the first time to detect T-cadherin in mouse embryos and identify the stage at which T-cadherin expression at the mRNA and protein level starts, as well as the morphological regions where the protein is expressed. In different parts of the developing brain T-cadherin expression at the mRNA level was detected starting from the E8.75 stage. Expression of the T-cadherin protein was detected starting from the E9.5 stage. The highest T-cadherin expression was observed in the inner lining of the brain, which suggests a possible involvement of T-cadherin in the formation of the choroid plexus in the ventricular walls of the developing brain.



**Fig. 8.** Lack of T-cadherin mRNA in the developing heart of mouse embryos at the E8.75–E10.5 stages (1, 2, 3). Arrows and the selected area indicate the developing heart region. Magnification of 5× (1, 2) and 6× (3)

*In situ* hybridization and immunofluorescent staining of whole mouse embryos revealed T-cadherin expression at the protein level in the heart, starting with the E11.5 stage. No expression of either T-cadherin mRNA or T-cadherin protein in the developing heart was observed at the E8.75, E9.5 and E10.5 stages.

Expression of T-cadherin in the embryonic heart, which was first identified at the E11.5 stage, reflects apparently the active formation and growth of the heart and its parts, as well as its vascularization [14].

Presumably, T-cadherin mRNA synthesis is activated between the E10.5–E11.5 stages of mouse embryo development; then, rapid and intense accumulation of the T-cadherin protein occurs. It is likely that T-cadherin is also involved in the formation of synaptic contacts in the developing cardiac conduction system.

Earlier, T-cadherin deficient mice were generated in the Ranscht laboratory [15]. These mice were viable and fertile, which typical for a wide range of knockout animals and indicates possible compensatory mechanisms implemented in embryogenesis. However, based on experiments in various animal models reproducing human cardiovascular diseases, T-cadherin was found to play an important role in the restoration of blood supply upon injury. By using an ischemia-reperfusion model, T-cadherin was demonstrated to perform the cardioprotective function, since the infarction size in the control mice was significantly less than that in T-cadherin-deficient animals [16, 17]. Based on a hindlimb ischemia model in these mice, T-cadherin was found to be necessary for a complete revascu-

larization of ischemic muscles [18]. The present study suggests the role of T-cadherin as a guidance molecule regulating vascular growth during embryogenesis and is consistent with the results obtained in experimental animal models.

## CONCLUSIONS

The data on T-cadherin in the developing mouse brain and heart indicate that the onset of T-cadherin expression coincides with active formation and growth of blood vessels due to vasculogenesis and angiogenesis in the cardiovascular system and the brain [19]. These results suggest a role for T-cadherin as a molecule regulating the formation and directional growth of blood vessels during embryogenesis. As it was previously demonstrated, the mechanism by which T-cadherin regulates neuronal growth in the developing nervous system is based on homophilic recognition between T-cadherins on the contacting cells and their subsequent “repulsion” [2, 3]. Earlier, using *in vivo* and *in vitro* angiogenic models we had found that the same mechanism of homophilic interaction is used for the regulation of blood vessels growth [20]. We suggest that a similar mechanism involving T-cadherin could be utilized for the regulation of blood vessels growth in embryogenesis. ●

*This work was supported by a grant from the Russian Science Foundation (project № 14-24-00086) and conducted using equipment purchased with funds from the Moscow University Development Program.*

## REFERENCES

- Ranscht B., Dours-Zimmermann M.T. // *Neuron*. 1991. V. 7. № 3. P. 391–402.
- Fredette B.J., Ranscht B. // *J. Neurosci*. 1994. V. 14. P. 7331–7346.
- Fredette B.J., Miller J., Ranscht B. // *Development*. 1996. V.122. P. 3163–3171.
- Eichmann A., Makinen T., Alitalo K. // *Genes & development*. 2005. V. 19. № 9. P. 1013–1021.
- Takeuchi T., Misaki A., Liang S.B., Tachibana A., Hayashi N., Sonobe H., Ohtsuki Y. // *J. Neurochem*. 2000. V.74. P. 1489–1497.
- Ivanov D., Philippova M., Antropova J., Gubaeva F., Iljinskaya O., Tararak E., Bochkov V., Erne P., Resink T., Tkachuk V. // *Histochem. Cell. Biol*. 2001. V.115. P. 231–242.
- Kudrjashova E., Bashtrikov P., Bochkov V., Parfyonova Ye., Tkachuk V., Antropova J., Iljinskaya O., Tararak E., Erne P., Ivanov D. et al. // *Histochemistry and cell biology*. 2002. V. 118. № 4. P. 281–290.
- Carmeliet P. // *Nature Reviews Genetics*. 2003. V. 4. № 9. P. 710–720.
- Poliakov A., Cotrina M., Wilkinson D. // *Developmental cell*. 2004. V. 7. № 4. P. 465–480.
- Weinstein B.M. Vessels and nerves: matching to the same tune // *Cell*. 2005. V.120. P. 299–302.
- Monk M. *Mammalian development. A practical approach*. Oxford ; Washington, (DC): IRL Press; 1987. P. 313.
- Wilkinson D. *In situ hybridization: a practical approach*. Oxford.: Oxford University Press, 1998. P. 212.
- Vasudevan A., Bhide P. // *Cell adhesion & migration*. 2008. V. 2, № 3. P. 167–169.
- Burggren W., Keller B. *Development of cardiovascular systems*. Cambridge, UK.: Cambridge University Press, 1997. P. 360.
- Hebbard L.W., Garlatti M., Young L.J.T., Cardiff R.D., Oshima R.G., Ranscht B. // *Cancer Res*. 2008. V. 68. № 5. P. 1407–1416.
- Denzel M., Scimia M., Zumstein P., Walsh K., Ruiz-Lozano P., Ranscht B. // *J. Clin. Invest*. 2010. V. 120. № 12. P. 4342–4352.
- Parker-Duffen J., Walsh K. // *Best Pract. Res. Clin. Endocrinol. Metab*. 2014. V. 28. № 1. P. 81–91.
- Parker-Duffen J., Nakamura K., Silver M., Zuriaga M.A., MacLauchlan S., Aprahamian T.R., Walsh K. // *Biol. Chem*. 2013. V. 288. № 34. P. 24886–24897.
- Gilbert S.F. *Developmental Biology*. Sunderland (MA): Sinauer Associates, 2006. P. 817.
- Rubina K., Kalinina N., Potekhina A., Efimenko A., Semina E., Poliakov A., Wilkinson D.G., Parfyonova Y., Tkachuk V. // *Angiogenesis*. 2007. V.10. № 3. P. 183–195.

# The Effect of Hydrophobic Monoamines on Acid-Sensing Ion Channels ASIC1B

E. I. Nagaeva\*, N. N. Potapieva, D. B. Tikhonov

Sechenov Institute of Evolutionary Physiology and Biochemistry, Russian Academy of Sciences,  
Prosp. Toreza, 44, 194223, St.Petersburg, Russia

\*E-mail: eline00111@gmail.com

Received 11.11.2014

Revised manuscript received 04.04.2015

Copyright © 2015 Park-media, Ltd. This is an open access article distributed under the Creative Commons Attribution License, which permits unrestricted use, distribution, and reproduction in any medium, provided the original work is properly cited.

**ABSTRACT** Acid-sensing ion channels (ASICs) are widely distributed in both the central and peripheral nervous systems of vertebrates. The pharmacology of these receptors remains poorly investigated, while the search for new ASIC modulators is very important. Recently, we found that some monoamines, which are blockers of NMDA receptors, inhibit and/or potentiate acid-sensing ion channels, depending on the subunit composition of the channels. The effect of 9-aminoacridine, IEM-1921, IEM-2117, and memantine both on native receptors and on recombinant ASIC1a, ASIC2a, and ASIC3 homomers was studied. In the present study, we have investigated the effect of these four compounds on homomeric ASIC1b channels. Experiments were performed on recombinant receptors expressed in CHO cells using the whole-cell patch clamp technique. Only two compounds, 9-aminoacridine and memantine, inhibited ASIC1b channels. IEM-1921 and IEM-2117 were inactive even at a 1000  $\mu\text{M}$  concentration. In most aspects, the effect of the compounds on ASIC1b was similar to their effect on ASIC1a. The distinguishing feature of homomeric ASIC1b channels is a steep activation-dependence, indicating cooperative activation by protons. In our experiments, the curve of the concentration dependence of ASIC1b inhibition by 9-aminoacridine also had a slope (Hill coefficient) of 3.8, unlike ASIC1a homomers, for which the Hill coefficient was close to 1. This finding indicates that the inhibitory effect of 9-aminoacridine is associated with changes in the activation properties of acid-sensing ion channels.

**KEYWORDS** ion channels; ASIC; 9-aminoacridine; memantine; patch clamp; potentiation; inhibition.

**ABBREVIATIONS** ASIC – acid-sensing ion channel; CNS – central nervous system; PNS – peripheral nervous system; GFP – green fluorescent protein;  $\text{IC}_{50}$  – half maximal inhibitory concentration.

## INTRODUCTION

A proton is the simplest neurotransmitter [1]; its effect is mediated by acid-sensing ion channels (ASICs). ASICs are voltage-insensitive channels that belong to the superfamily of degenerin/epithelial sodium channels (DEG/ENaC) and are activated in response to acidification of an extracellular medium. Currently, four genes (*accn1-4*) encoding six different ASIC subunits are known: ASIC1a and ASIC1b, which are products of alternative splicing of the *accn2* gene; ASIC2a and ASIC2b, which are products of alternative splicing of the *accn1* gene; as well as the ASIC3 and ASIC4 subunits [2]. A functionally active channel can be both homo- and heterotrimeric [3], with only the ASIC1a, ASIC1b, ASIC2a, and ASIC3 subunits being able to form functioning homomeric channels.

In the central nervous system, the ASIC1a, ASIC2a, and ASIC2b subunits are mainly expressed in the hippocampus, amygdala, cerebellum, striatum, cerebral cortex, and olfactory bulbs [4–10]. In the peripheral

nervous system, the ASIC1b and ASIC3 subunits predominate. They can be found in the sensory neurons of the spinal cord dorsal roots and trigeminal and vagus nerves. It is worth noting that only ASIC3 can produce a sustained current in response to decrease in pH. This subtype of proton-activated channels, as well as ASIC1b, is responsible for the perception of pain stimuli accompanying an inflammation, fractures, tumors, hematomas, and postoperative wounds, and it is also involved in mechanosensation [11, 12]. In the central nervous system, ASICs are involved in important physiological processes such as synaptic transmission, synaptic plasticity, memory, learning [13], anxiety and depression [14], drug addiction [15], and chemosensation [16].

Despite the widespread occurrence of proton-activated channels in CNS and PNS, the pharmacology of these receptors remains little-studied. For example, it is known that only ASIC1a and ASIC3 homomers can be specifically inhibited by psalmotoxin-1 (PcTx1), a

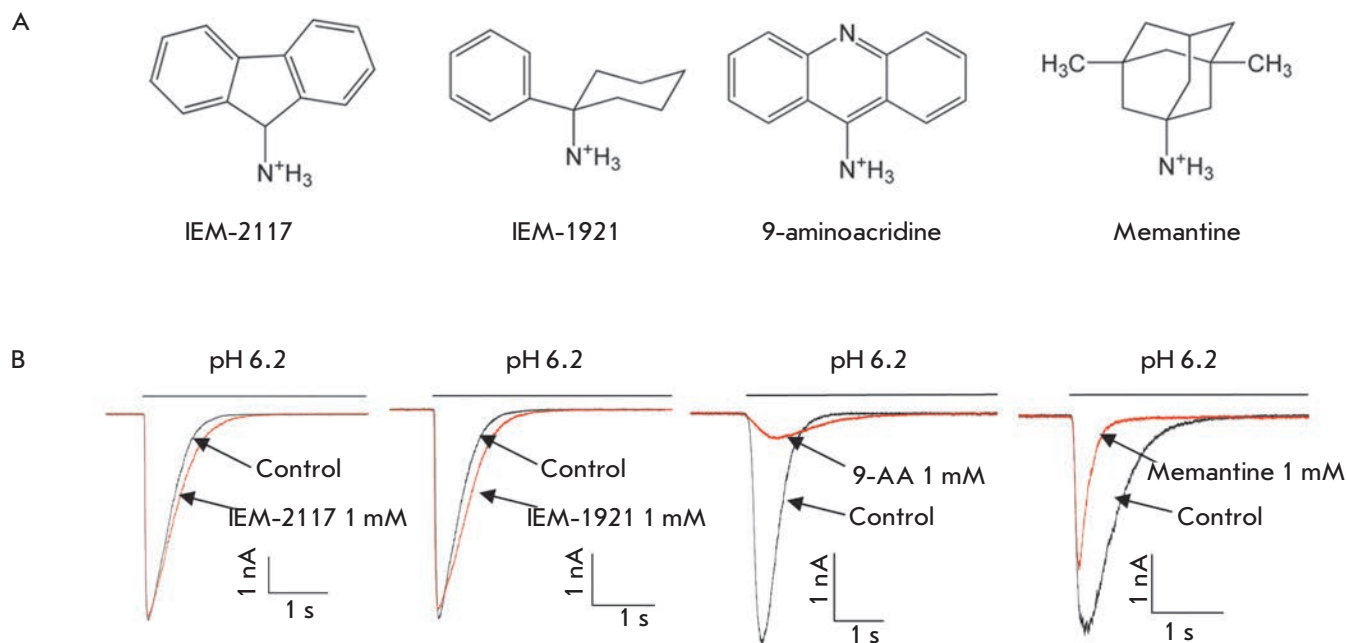


**Fig. 1.** Effect of hydrophobic monoamines on ASIC1b. **A**, chemical structures of the tested compounds. **B**, representative examples of currents in the control (black) and in the presence of 1000  $\mu\text{M}$  tested compounds (red)

toxin from the venom of the South American tarantula *Psalmopoeus cambridgei* [17], and the APETx2 toxin from the venom of the sea anemone *Anthopleura elegantissima* [18], respectively. The psalmotoxin-1 specificity is lost as its concentration increases: at concentrations above 3 nM, it can also inhibit ASIC1a/2b heteromers, and at concentrations greater than 100 nM, it causes potentiation of ASIC1b [19]. The most known blocker of acid-sensing ion channels, amiloride [20], affects all types of ASICs, as well as other sodium channels of the DEG/ENaC family [21]. All attempts to synthesize more specific amiloride-based structures with one or two amidine groups have not yielded the desired results [22, 23]. Synthetic compound, 2-guanidine-4-methylquinazoline (GMQ) is able to activate selectively ASIC3 homomers via interaction with a ligand-binding domain, which differs from the proton-binding domain [24]. Thus, to date there are a few pharmacological tools differentiating subtypes of proton-activated ion channels, and the search for new, specific inhibitors/activators is the actual problem.

Recently, we have demonstrated that four blockers of NMDA-receptors (*Fig. 1A*) (9-aminoacridine [25], IEM-1921 [26, 27], memantine [28], and IEM-2117 [29, 30]) can differently modulate acid-sensing ion channels, depending on their subunit composition [31]. For example, 9-aminoacridine (9AA), IEM-2117, and memantine inhibited, to varying degrees, ASIC1a homomers,

while IEM-1921 had no effect even at a concentration of 1000  $\mu\text{M}$ . The responses of ASIC2a, on the contrary, were potentiated by IEM-1921, IEM-2117, and memantine and were unaffected by 9AA. The effect of the tested compounds on ASIC3 was more complex because currents through these channels have peak and sustained components. IEM-1921 and 9-aminoacridine potentiated the sustained component but inhibited the peak component. IEM-2117 and memantine potentiated both components of the response. In this case, IEM-2117 was the most active potentiator and it also activated ASIC3 channels in a neutral pH (7.4), causing a sustained current.

In the present work, we studied the effect of four compounds mentioned above on a homomeric channel formed by the ASIC1b subunit, which is a product of alternative splicing of the *accn2* gene. This channel is interesting because of its very specific activation curve with a high Hill coefficient ( $n_H$ ) equal to 4.8 [32]. Analysis of the effects of potentiators/inhibitors on this receptor may help test the hypothesis of a possible mechanism of ligand action via increasing/reducing affinity of protons for the proton binding site of ASICs. We have demonstrated that the effect of hydrophobic monoamines on ASIC1b is similar to their effect on ASIC1a, except that the concentration-dependent inhibition curve of 9AA has a much greater Hill coefficient compared to that for ASIC1a.



## EXPERIMENTAL

CHO cells (Chinese hamster ovarian epithelial cell culture) were cultured in a CO<sub>2</sub> incubator at 37 °C and 5% CO<sub>2</sub>. The cell growth medium consisted of a DMEM/F12 (Dulbecco's Modified Eagle's Medium) solution supplemented with 10% fetal bovine serum and 1% streptomycin/penicillin. Transfection of cells with plasmids was performed using the Lipofectamine 2000 reagent (Invitrogen, USA) according to the manufacturer's protocol. The plasmid carrying the rASIC1b-pECFP-C1 construct was courtesy of A. Starushchenko. CHO cells were seeded on glasses with an area not exceeding 25 mm<sup>2</sup> and uniformly distributed on the bottom of a Petri dish with a diameter of 35 mm. For the expression of homomeric ASIC1b channels, the cells were transfected with the plasmid (0.5 µg) carrying the *ASIC1b* gene, together with the plasmid (0.5 µg) encoding the fluorescent protein GFP. Electrophysiological experiments were performed 36–72 h after transfection. Transfected cells were detected by green luminescence using a Leica DM IL microscope (Leica Microsystems, Germany).

The currents caused by fast acidification of the medium were recorded using the whole cell patch clamp technique. For this purpose, an EPC-8 amplifier (HEKA Electronics, Germany) was used; the signal was filtered in the frequency band of 0–5 kHz, digitized at the sampling rate of 1 kHz and recorded on a personal computer using the Patchmaster software from the same manufacturer (HEKA Electronics, Germany). All experiments were performed at room tempera-

ture (23–25 °C). The micropipette solution contained 100 mM CsF, 40 mM CsCl, 5 mM NaCl, 0.5 mM CaCl<sub>2</sub>, 5 mM EGTA, and 10 mM HEPES (pH was adjusted to 7.2 by adding CsOH). The extracellular solution contained 143 mM NaCl, 5 mM KCl, 2.5 mM CaCl<sub>2</sub>, 10 mM D-glucose, 10 mM HEPES, and 10 mM MES (pH was adjusted to 7.35 by adding NaOH). All solutions were filtered through micropore cellulose membranes using a vacuum glass filter (Sartorius AG, Germany).

Solutions with low pH values, which were used to activate channels, were prepared from the extracellular stock solution by adding HCl. The monoamines were synthesized earlier, under a request from our laboratory, by V.E. Gmiro at the St. Petersburg Institute of Experimental Medicine. To prepare a stock solution with a monoamine concentration of  $5 \times 10^{-2}$  M, a sample weight of its crystalline form was dissolved in bidistilled water. Further, the required volume of the stock solution was added to working solutions with different pH values. When preparing monoamine solutions, the pH of the resulting mixture was checked for each preparation. If a shift was detected, then the pH was adjusted to the required value using a 0.1 N HCl solution or a 0.2 N NaOH solution. For fast drug application the ALA-VM8 manifold system (ALA Scientific Instruments, USA) was used. The interval between test applications was 60 s.

All data are presented as a “mean ± standard deviation” calculated from at least five experiments. The statistical significance of the effects was evaluated using the paired *t*-test with *p* = 0.05 (the value of the re-

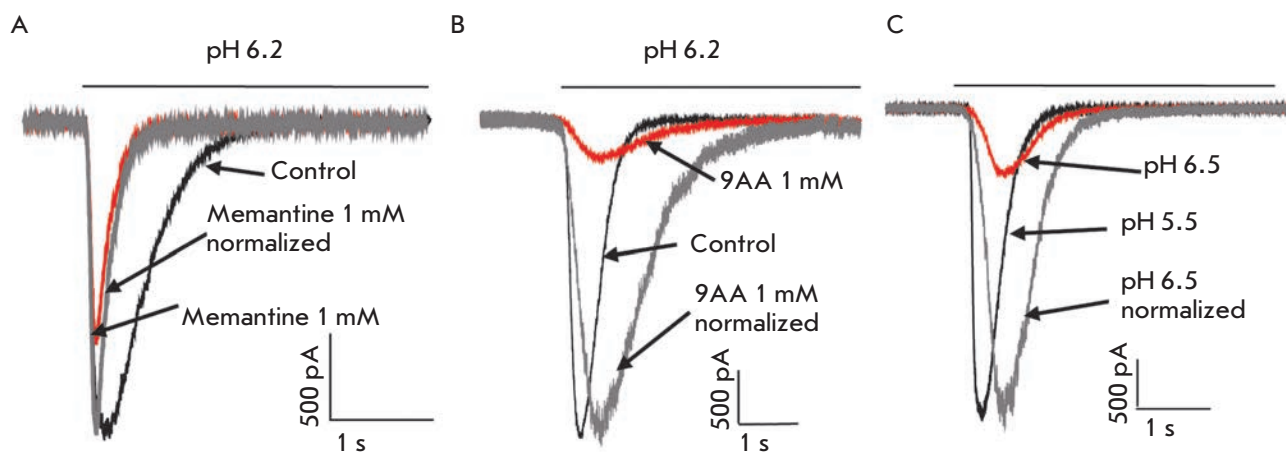


**Fig. 2.** Changes in the response kinetics in the presence of 1000 µM memantine (**A**) and 1000 µM 9AA (**B**). The gray trace shows the response in the presence of an inhibitor. The response is normalized by the amplitude to the control level. Memantine, a weak inhibitor, increases the rate of desensitization. Contrary, 9AA broadens the response. **C**, examples of the currents evoked by modest (red) and strong (black) acidifications. As in the presence of 9AA (**B**), response to modest acidification has a low amplitude and slow kinetics

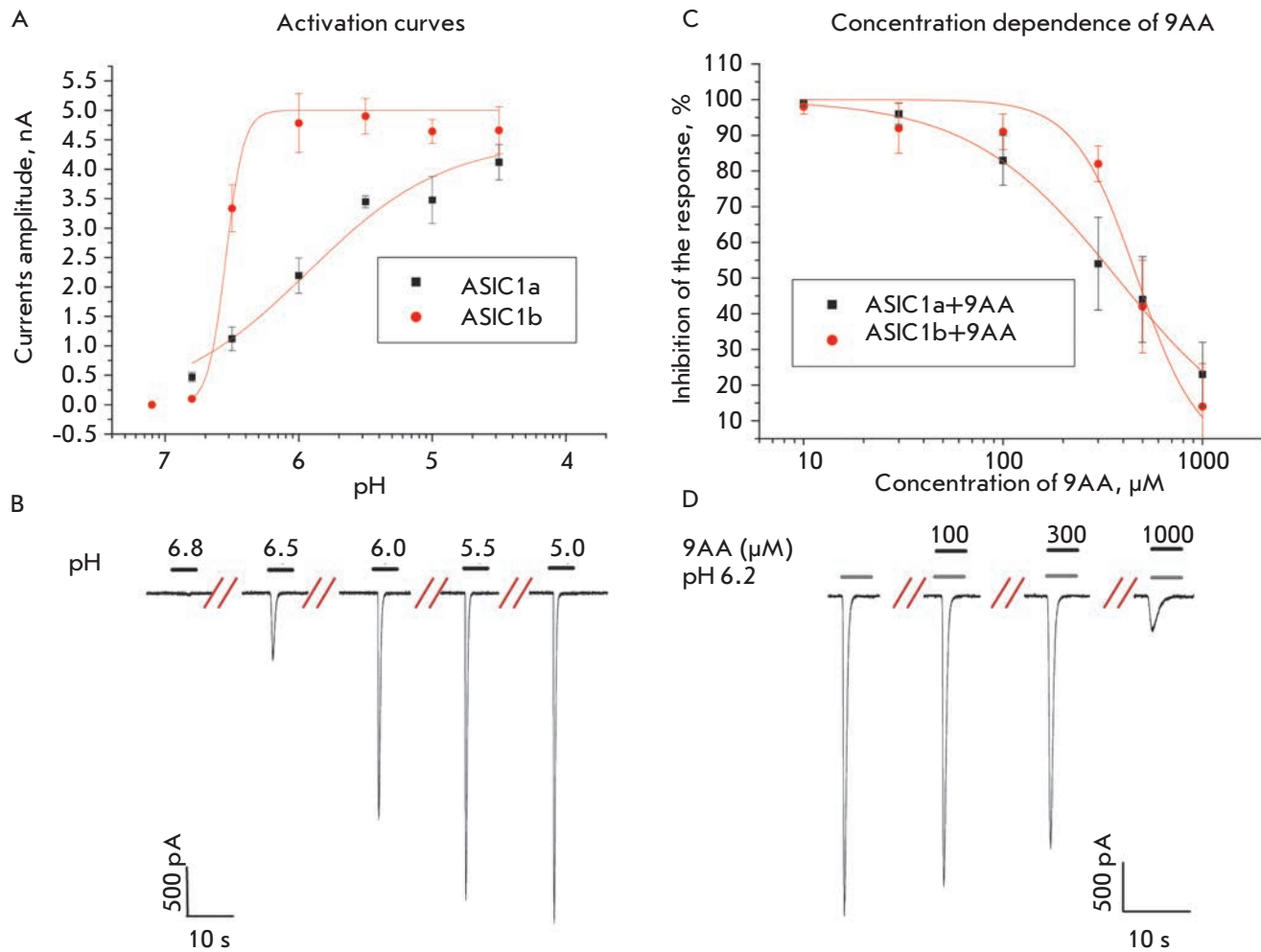


**Fig. 3.** Correlation between the activation properties of ASIC1a and ASIC1b and their inhibition by 9AA. **A**, pH-dependencies of the response amplitude for ASIC1a (black dots) and ASIC1b (red dots) activation. **B**, representative examples of ASIC1b channel currents evoked by different pHs. The interval between applications is 60 s. **C**, concentration dependencies of ASIC1a (black dots) and ASIC1b (red dots) inhibition by 9AA. **D**, representative examples of ASIC1b currents at pH=6.2 in the presence of different 9AA concentrations

sponse amplitude in the presence of a test compound relative to the control). The response shape was analyzed by measuring the current rise time from 10 to 90% of the maximum amplitude and calculating the response decay time constant using a least squares exponential fitting.

To simplify evaluation of the changes in the response kinetics under the influence of the test compounds, the currents were normalized by the amplitude (Fig. 2). For this, the ratio of the control current in response to pH and the current in the presence of a test compound was calculated. The current with the smaller amplitude was multiplied by the obtained ratio, thereby producing responses with equal amplitudes.

## RESULTS

Reducing the pH of the extracellular medium from the initial level of 7.35 resulted in transient currents in cells carrying the ASIC1b plasmid. Threshold currents exceeding the noise level by more than 2 times (40–100 pA) were observed for a solution with pH= 6.8. When the solution pH was reduced to 6.5 (Fig. 3A, B), currents up to 1 nA were detected. This sharp increase in the response is related to the high slope of the activation curve ( $n_H = 4.9 \pm 0.2$ ;  $pH_{50} = 6.3 \pm 0.2$ ,  $n = 5$ ) (Fig. 3A). These results are consistent with previously published data [32]. The classical blocker of acid-sensing ion channels, amiloride, (30 μM) blocked  $53 \pm 7\%$  ( $n = 6$ ) of the currents evoked by application of a solution with

pH=6.2. The kinetics of the response decay due to receptor desensitization ( $\tau = 0.67 \pm 0.12$  s,  $n = 5$ ) was also consistent with the previously published data.

None of the four tested compounds caused currents in the neutral medium even at high concentrations (data are not shown).

#### IEM-1921 and IEM-2117

Since ASIC1b and ASIC1a are two alternative splice variants of the same *accn2* gene, it can be assumed that the effect of the compounds on ASIC1b will be similar to those on ASIC1a. However, this assumption was correct only for some of the compounds. As in the case of ASIC1a, a phenylcyclohexyl derivative IEM-1921 exhibited no activity on ASIC1b channels at concentrations ranging from 10 to 1000  $\mu$ M. The effect of IEM-2117 was the same (Fig. 1B), although, in the case of ASIC1a, it acted as a weak inhibitor: 1000  $\mu$ M of the compound caused  $34 \pm 10\%$  ( $n = 7$ ) decrease of the response.

#### Memantine

The only clinically used blocker of NMDA receptors [33], memantine, had no effect on ASIC1b homomers at concentrations below 100  $\mu$ M. However, at higher concentrations, memantine behaved as a weak inhibitor. Thus, memantine at a concentration of 300  $\mu$ M inhibited  $19 \pm 6\%$  ( $n = 5$ ) of the current, and application of 1000  $\mu$ M resulted in  $44 \pm 16\%$  ( $n = 5$ ) decrease in the response amplitude (Fig. 1B). Since a saturating concentration of the compound was not achieved, it was impossible to measure the  $IC_{50}$  parameter. Apart from the inhibitory effect, 1000  $\mu$ M memantine induced a decrease in the response decay time constant from  $0.50 \pm 0.12$  s ( $n = 6$ ) to  $0.15 \pm 0.02$  s ( $n = 5$ ) (Fig. 2A). Earlier, we had observed a similar change in the response shape for ASIC1a homomers.

#### 9-Aminoacridine

9AA was the most potent inhibitor of ASIC1b channels. 1000  $\mu$ M 9AA reduced the response amplitude by  $86 \pm 10\%$  ( $n = 7$ ) upon simultaneous application with a solution with pH 6.2 (Fig. 1B).  $IC_{50}$  was  $440 \pm 20$   $\mu$ M ( $n = 7$ ) (Fig. 3C). An interesting feature of the 9AA effect on ASIC1b channels was a sharp increase in the inhibitory effect upon a slight increase in the compound concentration; i.e., the Hill coefficient was high ( $3.8 \pm 0.5$ ,  $n = 5$ ) (Fig. 3C). The curve of ASIC1b sensitivity to the agonist is also characterized by a high Hill coefficient (see above). On the contrary the curves of ASIC1a activation and its inhibition by 9-aminoacridine had a Hill coefficient of  $1.2 \pm 0.3$  ( $n = 5$ ) and  $1.3 \pm 0.3$  ( $n = 5$ ), respectively.

9AA significantly changed the shape of the ASIC1b response to acidification (Fig. 2B). In the

presence of 1000  $\mu$ M 9AA, the response kinetics became slower and the current rise time increased from  $0.15 \pm 0.02$  s ( $n = 5$ ) in the control to  $0.48 \pm 0.12$  s ( $n = 5$ ). The response decay time constant also increased significantly ( $\tau = 0.67 \pm 0.12$  s,  $n = 5$  in the control and  $\tau = 1.2 \pm 0.2$  s,  $n = 5$  in the presence of 9AA). This effect may be caused by asynchronous activation of channels, which is typical of the action of low agonist concentrations. Indeed, a similar difference was observed upon ASIC1b activation by acidification to pH 6.5 and 5.5 (Fig. 2C); i.e., it may be proposed that channel affinity for protons decreases in the presence of 9AA. Therefore, in the presence of 9AA, the amplitude and shape of the response to the solution with pH 6.2 become similar to those of the response to the solution with pH 6.5.

Since the effect of 9-aminoacridine on ASIC1a homomers was previously characterized by a pronounced pH-dependence (weakening of inhibition as the activating pH value decreased), we decided to analyze this effect on ASIC1b channels, too. Under conditions of a relatively low proton concentration (pH 6.5), an almost complete response inhibition ( $92 \pm 3\%$ ,  $n = 7$ ) was observed. Upon stronger acidification (pH 5.0), the effect decreased to  $28 \pm 8\%$  ( $n = 5$ ) (Fig. 4). This fact agrees with the hypothesis of reduction of proton affinity for the receptor as a possible mechanism of 9AA action.

#### DISCUSSION

As it might be expected, the effect of hydrophobic monoamines on ASIC1b homomers largely resembles their effect on ASIC1a homomers. The phenylcyclohexyl derivative IEM-1921 had no effect on the activity of both channels. Memantine and 9AA exerted a pronounced inhibitory effect upon simultaneous application with an acidic solution. Similar to the case of ASIC1a, memantine not only reduced the response amplitude, but also greatly decreased the current decay time constant. 9AA was found to be the most potent inhibitor: at a concentration of 1000  $\mu$ M, it caused  $86 \pm 10\%$  ( $n = 7$ ) of the response via ASIC1b and  $77 \pm 9\%$  ( $n = 6$ ) of the response via ASIC1a. The effect of 9AA was characterized by a pronounced pH-dependence in both cases: the inhibitory effect considerably decreased at the saturating agonist concentration. Only IEM-2117 exhibited some subunit specificity and did not inhibit ASIC1b homomers. Despite the small differences in the effect of the tested compounds on the two related homomers, it may be concluded that alternative splicing has no direct effect on the action of hydrophobic monoamines.

At this stage, it is impossible to draw definitive conclusions about the action mechanism of the studied compounds on ASIC channels. Probably, there are differences in the action mechanisms between memantine

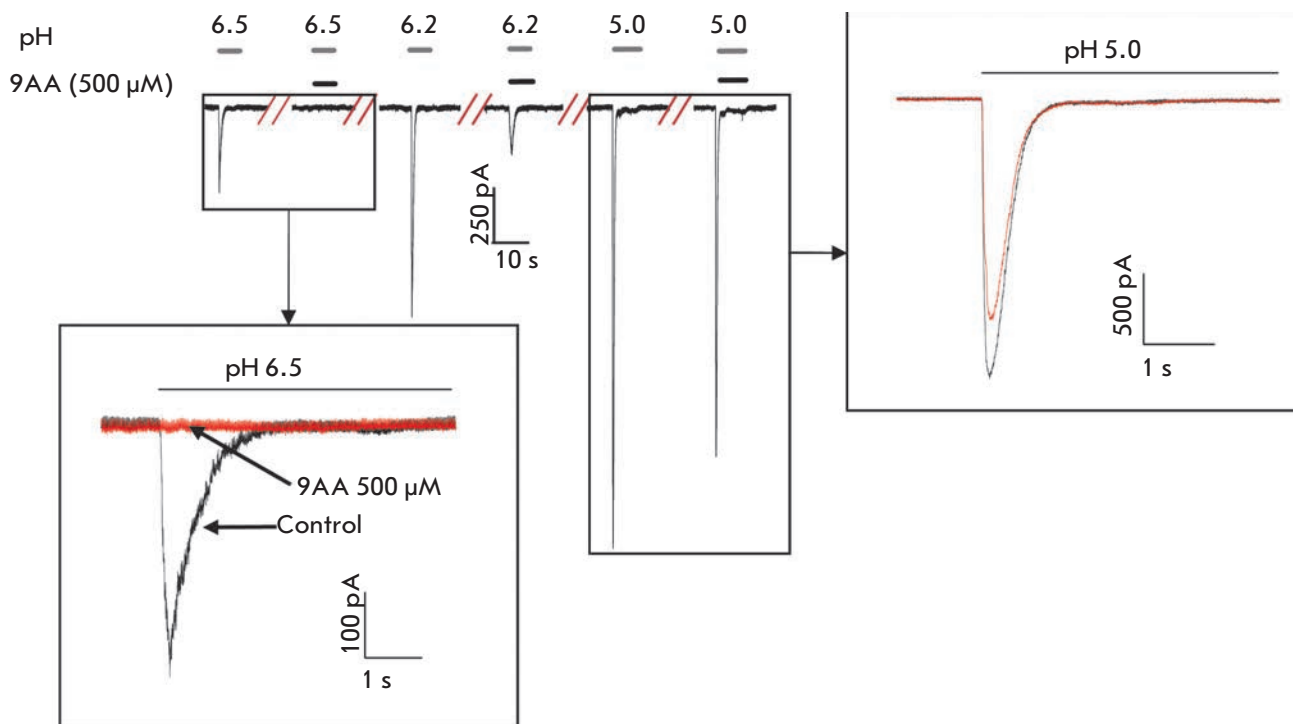


**Fig. 4.** Dependence of the 9AA effect on the ASIC1b activation level. Representative examples of currents through ASIC1b are shown for different pH values in the presence and absence of 500  $\mu\text{M}$  9AA. Insets show superimposed currents at a larger scale. At pH=6.5 (lower inset), inhibition is almost complete. At more acidic pH, which causes strong ASIC activation (right inset), inhibition becomes modest

and 9AA, since these compounds differently change the shape of the response to acidification (Fig. 2A, B). The effect of memantine (decrease in the decay time constant) resembles the effect of open channel blockers or desensitization promoters. The effect of 9AA is probably associated with a change in the affinity for protons. The arguments in favor of this hypothesis are (1) the correlation between the Hill coefficients for activation of channels and their inhibition by 9AA (Fig. 3A, C) and (2) the analogy between the change in the response shape in the presence of 9AA and upon channel activation by slight acidification (Fig. 2B, C). More exact conclusions about the mechanisms and sites of the binding of hydrophobic monoamines to ASICs require further research.

## CONCLUSIONS

In this paper, in addition to earlier results, we have demonstrated that classical blockers of NMDA receptors can modulate the activity of all functionally active ASIC homomers and that the specificity of the effect depends on the subunit composition of a receptor. Importantly, all the tested compounds have very simple chemical structure comprising one amino group and

a hydrophobic “core.” This structure differs from the amidine-containing derivatives of amiloride and other known modulators of acid-sensing ion channels. This fact makes it possible to assign hydrophobic monoamines to a new class of ASIC ligands. Furthermore, it suggests that ASICs can serve as targets for many clinically used drugs (e.g., tricyclic antidepressants and some psychotropic compounds), as well as endogenous monoamines and their derivatives. The latter suggestion is crucial in understanding the physiological role of proton-activated ion channels in the CNS. As mentioned above, ASICs have a high expression level in all of the most vital parts of the brain. However, the range of pH where these channels are activated is atypical of normal physiological processes. Therefore, there is a high probability of existence of endogenous activators/modulators of these channels. The search for those endogenous amines seems promising. ●

*This work was supported by the Russian Foundation for Basic Research (grants № 14-04-31861 mol\_a and 13-04-00724) and the program of the Presidium of the Russian Academy of Sciences “Molecular and Cell Biology.”*

## REFERENCES

1. Du J., Reznikov L.R., Price M.P., Zha X.M., Lu Y., Moninger T.O., Wemmie J.A., Welsh M.J. // *Proc. Natl. Acad. Sci. U. S. A.* 2014. V. 111. № 24. P. 8961–8966.
2. Deval E., Gasull X., Noël J., Salinas M., Baron A., Diochot S., Lingueglia E. // *Pharmacol. Ther.* 2010. V. 128. № 3. P. 549–558.
3. Jasti J., Furukawa H., Gonzales E.B., Gouaux E. // *Nature.* 2007. V. 449. № 7160. P. 316–323.
4. Alvarez de la Rosa D., Zhang P., Shao D., White F., Canessa C.M. // *Proc. Natl. Acad. Sci. U. S. A.* 2002. V. 99. № 4. P. 2326–2331.
5. Baron A., Waldmann R., Lazdunski M. // *J. Physiol.* 2002. V. 539. № 2. P. 485–494.
6. Bolshakov K.V., Essin K. V., Buldakova S.L., Dorofeeva N.A., Skatchkov S.N., Eaton M.J., Tikhonov D.B., Magazanik L.G. // *Neuroscience.* 2002. V. 110. № 4. P. 723–730.
7. García-Añoveros J., Derfler B., Neville-Golden J., Hyman B.T., Corey D.P. // *Proc. Natl. Acad. Sci. U. S. A.* 1997. V. 94. № 4. P. 1459–1464.
8. Lingueglia E., de Weille J.R., Bassilana F., Heurteaux C., Sakai H., Waldmann R., Lazdunski M. // *J. Biol. Chem.* 1997. V. 272. № 47. P. 29778–29783.
9. Price M.P., Snyder P.M., Welsh M.J. // *J. Biol. Chem.* 1996. V. 271. № 14. P. 7879–7882.
10. Wemmie J.A., Askwith C.C., Lamani E., Cassell M.D., Freeman J.H., Welsh M.J. // *J. Neurosci.* 2003. V. 23. № 13. P. 5496–5502.
11. Price M.P., Lewin G.R., McIlwrath S.L., Cheng C., Xie J., Heppenstall P.A., Stucky C.L., Mannsfeldt A.G., Brennan T.J., Drummond H.A., et al. // *Nature.* 2000. V. 407. № 6807. P. 1007–1011.
12. Wemmie J.A., Price M.P., Welsh M.J. // *Trends Neurosci.* 2006. V. 29. № 10. P. 578–586.
13. Wemmie J.A., Chen J., Askwith C.C., Hruska-Hageman A.M., Price M.P., Nolan B.C., Yoder P.G., Lamani E., Hoshi T., Freeman J.H., et al. // *Neuron.* 2002. V. 34. № 3. P. 463–477.
14. Wemmie J.A., Coryell M.W., Askwith C.C., Lamani E., Leonard A.S., Sigmund C.D., Welsh M.J. // *Proc. Natl. Acad. Sci. U. S. A.* 2004. V. 101. № 10. P. 3621–3626.
15. Kreple C.J., Lu Y., Taugher R.J., Schwager-Gutman A.L., Du J., Stump M., Wang Y., Ghobbeh A., Fan R., Cosme C.V., et al. // *Nat. Neurosci.* 2014. V. 17. № 8. P. 1083–1091.
16. Ziemann A.E., Allen J.E., Dahdaleh N.S., Drebot I.I., Coryell M.W., Wunsch A.M., Lynch C.M., Faraci F.M., Howard M. A., Welsh M.J., et al. // *Cell.* 2009. V. 139. № 5. P. 1012–1021.
17. Escoubas P., De Weille J.R., Lecoq a, Diochot S., Waldmann R., Champigny G., Moinier D., Ménez A., Lazdunski M. // *J. Biol. Chem.* 2000. V. 275. № 33. P. 25116–25121.
18. Diochot S., Baron A., Rash L.D., Deval E., Escoubas P., Scarzello S., Salinas M., Lazdunski M. // *EMBO J.* 2004. V. 23. № 7. P. 1516–1525.
19. Baron A., Diochot S., Salinas M., Deval E., Noël J., Lingueglia E. // *Toxicol.* 2013. V. 75. P. 187–204.
20. Waldmann R., Champigny G., Bassilana F. // *Nature.* 1997. V. 386. № 6621. P. 173–177.
21. Kellenberger S., Schild L. // *Physiol. Rev.* 2002. V. 82. № 3. P. 735–767.
22. Chen X., Orser B.A., MacDonald J.F. // *Eur. J. Pharmacol.* 2010. V. 648. № 1–3. P. 15–23.
23. Kuduk S.D., Chang R.K., Wai J.M.-C., Di Marco C.N., Cofre V., DiPardo R.M., Cook S.P., Cato M.J., Jovanovska A., Urban M.O., et al. // *Bioorg. Med. Chem. Lett.* 2009. V. 19. № 15. P. 4059–4063.
24. Yu Y., Chen Z., Li W., Cao H., Feng E., Yu F., Liu H., Jiang H., Xu T. // *Neuron.* 2010. V. 68. P. 61–72.
25. Benveniste M., Mayer M.L. // *J. Physiol.* 1995. V. 483. № 2. P. 367–384.
26. Rogawski M.A., Thurkauf A., Yamaguchi S., Rice K.C., Jacobson A.E., Mattson M.V. // *J. Pharmacol. Exp. Ther.* 1989. V. 249. № 3. P. 708–712.
27. Bolshakov K. V., Kim K.H., Potapjeva N.N., Gmiro V.E., Tikhonov D.B., Usherwood P.N.R., Mellor I.R., Magazanik L.G. // *Neuropharmacology.* 2005. V. 49. № 2. P. 144–155.
28. Bormann J. // *Eur. J. Pharmacol.* 1989. V. 166. № 3. P. 591–592.
29. Barygin O.I., Gmiro V.E., Kim K., Magazanik L.G., Tikhonov D.B. // *Neurosci. Lett.* 2009. V. 451. № 1. P. 29–33.
30. Bolshakov K.V., Gmiro V.E., Tikhonov D.B., Magazanik L.G. // *J. Neurochem.* 2003. V. 87. № 1. P. 56–65.
31. Tikhonova T.B., Nagaeva E.I., Barygin O.I., Potapieva N.N., Bolshakov K. V., Tikhonov D.B. // *Neuropharmacology.* 2014. V. 89. P. 1–10.
32. Hesselager M., Timmermann D.B., Ahring P.K. // *J. Biol. Chem.* 2004. V. 279. № 12. P. 11006–11015.
33. Chen H.S.V., Pellegrini J.W., Aggarwal S.K., Lei S.Z., Warach S., Jensen F.E., Lipton S.A. // *J. Neurosci.* 1992. V. 12. № 11. P. 4427–4436.

# Thio Derivatives of 2(5H)-Furanone As Inhibitors against *Bacillus subtilis* Biofilms

E. Yu. Trizna<sup>1\*</sup>, E. N. Khakimullina<sup>1</sup>, L. Z. Latypova<sup>1</sup>, A. R. Kurbangalieva<sup>1</sup>, I. S. Sharafutdinov<sup>1</sup>, V. G. Evtyugin<sup>1</sup>, E. V. Babynin<sup>1</sup>, M. I. Bogachev<sup>2</sup>, A. R. Kayumov<sup>1</sup>

<sup>1</sup>Kazan (Volga Region) Federal University, Kremlevskaya Str., 18, 420008, Kazan, Russia

<sup>2</sup>St. Petersburg State Electrotechnical University, Prof. Popova Str., 5, 197376, St. Petersburg, Russia

\*E-mail: trizna91@mail.ru

Received 18.11.2014

Revised manuscript received 09.02.2015

Copyright © 2015 Park-media, Ltd. This is an open access article distributed under the Creative Commons Attribution License, which permits unrestricted use, distribution, and reproduction in any medium, provided the original work is properly cited.

**ABSTRACT** Gram-positive bacteria cause a wide spectrum of infectious diseases, including nosocomial infections. While in the biofilm, bacteria exhibit increased resistance to antibiotics and the human immune system, causing difficulties in treatment. Thus, the development of biofilm formation inhibitors is a great challenge in pharmacology. The gram-positive bacterium *Bacillus subtilis* is widely used as a model organism for studying biofilm formation. Here, we report on the effect of new synthesized 2(5H)-furanones on the biofilm formation by *B. subtilis* cells. Among 57 compounds tested, sulfur-containing derivatives of 2(5H)-furanone (F12, F15, and F94) repressed biofilm formation at a concentration of 10 µg/ml. Derivatives F12 and F94 were found to inhibit the biosynthesis of GFP from the promoter of the *eps* operon encoding genes of the biofilm exopolysaccharide synthesis (EPS). Using the differential fluorescence staining of alive/dead cells, we demonstrated an increased bacterial sensitivity to antibiotics (kanamycin and chloramphenicol) in the presence of F12, F15, and F94, with F12 being the most efficient one. The derivative F15 was capable of disrupting an already formed biofilm and thereby increasing the efficiency of antibiotics.

**KEYWORDS** antibacterial activity, biofilms; 2(5H)-furanones; *Bacillus subtilis*.

**ABBREVIATIONS** MIC – minimum inhibitory concentration; MBIC – minimum biofilm inhibitory concentration.

## INTRODUCTION

It has now been established that in nature most bacteria exist in the form of specifically organized biofilms. Biofilms are a community of differentiated microbial cells tightly adhered to a substrate that are embedded in a polysaccharide matrix (EPS). This form of existence provides bacteria with a series of advantages under the influence of negative environmental factors and of the host organism. This leads, on one hand, to an increased efficiency of biotechnological processes and, on the other hand, to enhanced resistance to antimicrobial agents, antiseptics and disinfectants, and refractoriness to treatment, which results in an increased incidence of nosocomial infections and creates difficulties in microbiological diagnostics of infectious diseases [1–3]. Therefore, biofilms represent a serious problem and require the development of drugs that disrupt bacterial biofilms and inhibit their formation on medical devices. *Bacilli*, gram-positive spore-forming rods, e.g., *Bacillus anthracis* and *Bacillus cereus*, which cause anthrax and severe foodborne toxicoinfections, also form biofilms on

various surfaces [1]. *B. subtilis* cells are widely used as a model for studying bacillus biofilms [1].

Nowadays, bacterial biofilms are treated by coating surfaces with silver particles, immobilized enzymes disrupting the biofilm matrix, as well as various low-molecular weight substances that act as inhibitors of biofilm formation genes [4]. Among these substances, a special place belongs to compounds of the 2(5H)-furanone series [5] that were firstly isolated from the red alga *Delisea pulchra*. Furanone derivatives have been shown to possess antimicrobial activity against a great number of gram-positive and gram-negative bacteria and inhibit biofilm formation [5, 6].

## EXPERIMENTAL

### Furanones

Figure 1 depicts the structures of the studied compounds: F12 – 5-hydroxy-4-[(4-methylphenyl)sulfonyl]-3-chloro-2(5H)-furanone [7], F15 – 4-benzyl-sulfonyl-5-hydroxy-3-chloro-2(5H)-furanone [8], and

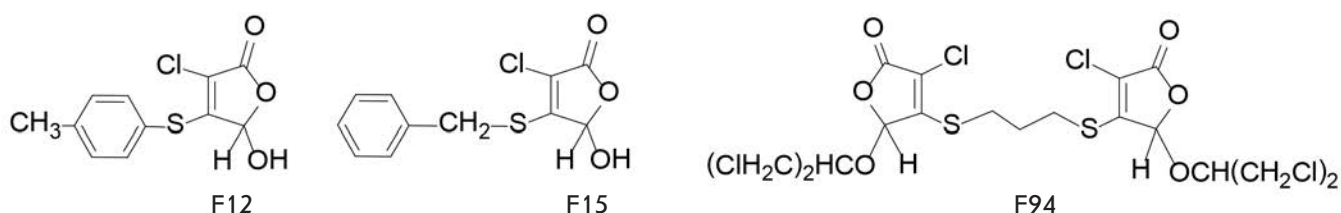


Fig. 1. Structures of furanones that inhibit *B. subtilis* biofilm formation at a concentration of 10 µg/ml

Table 1. Minimum furanone concentrations inhibiting *B. subtilis* 168 growth and biofilm formation; cyto- and genotoxic properties of the compounds

Furanone	Minimum inhibitory concentration (MIC), µg/ml	Minimum biofilm inhibitory concentration (MBIC), µg/ml	CC <sub>50</sub> for MCF-7 cells, µg/ml	Genotoxicity of compounds (excess over the control, times/cell number)	
				Ames test*	SOS chromotest*
F12	25	10	36.9	2.4 (109 ± 25.2)	0.69
F15	25	10	65.7	3.1 (133 ± 25.4)	0.61
F94	50	10	83.9	0.9 (41 ± 4.4)	1.09
Control**	–	–	–	1.0 (45 ± 3.5)	1.00
Positive control***	–	–	–	8.2 (369 ± 15.6)	22.71

\*Genotoxicity was evaluated at a 10 µg/ml concentration of furanones (corresponds to their MBIC values).

\*\*Amount of dimethyl sulfoxide added in the form of a furanone solution.

\*\*\*Sodium azide (3 µg/ml) and mytomycin C (0.1 µg/ml) were used in the Ames test and SOS chromotest, respectively.

Table 2. The effect of furanones on the thickness of a *B. subtilis* biofilm

Furanone	Biofilm thickness, µm	
	Cultivation with preliminary added furanones, 96 h	Addition of furanones to the formed biofilm with further incubation for 24 h
Control	10 ± 1.6	10 ± 1.3
F12	4 ± 0.4	6 ± 0.3
F15	2 ± 0.3	4 ± 0.2
F94	4 ± 0.6	8 ± 0.7

F94 – 1,3-bis[3-chloro-5-(1,3-dichloropropane-2-yl)oxy)-2(5H)-furanone-4-ylsulfonyl]propane [9]; the compounds were synthesized according to the known techniques.

### Strains and culture conditions

The following strains were used in the study: *B. subtilis* 168 [10]; *B. subtilis* K511 [11] carrying the *gfp* gene under the control of the promoter of the *epsA* gene, which is active during biofilm formation in *B. subtilis*.

The strains *Salmonella typhimurium* TA100 (*HisG46*, *rfa*, *wvr*-, *pkm* 101, *bio*-) [12] and *S. typhimu-*

*rium* TA1535/pSK1002 [13] were used to test the compounds for mutagenicity.

All the bacterial strains were maintained and cultured in a LB medium (1.0 g/L of tripton; 0.5 g/L of yeast extract; 0.5 g/L of NaCl; pH 8.5) [14]. Biofilm formation was determined using a BM medium (Basal medium), which is a modified SMM medium [15] supplemented with peptone to a final concentration of 7 g/L.

### Biofilm staining with crystal violet

Biofilm formation was assessed in 96-well plastic plates (Cellstar Grenier bio-one No. 655 180) by stain-

ing with crystal violet. Bacteria were cultured in BM at 37 °C without shaking in wells containing 200 µl of the bacterial culture with an initial density of  $3 \times 10^7$  CFU/ml. After 72 h of incubation, the culture liquid was removed and the plates were washed once with phosphate-buffered saline (PBS) pH 7.4 and dried for 20 min. Then, 150 µl of a 0.1% crystal violet solution (Sigma–Aldrich) in 96% ethanol was added per well and the plates were further incubated for 20 min. The unbound dye was washed off with PBS. The bound dye was eluted in 150 µl of 96% ethanol, and the absorbance at 570 nm was measured on a Tecan Infinite 200 Pro microplate reader (Switzerland). Cell-free wells that were subjected to all staining manipulations were used as a control.

#### Determination of the minimum inhibitory concentration

The minimum inhibitory concentration (MIC) of furanones was determined by broth microdilution method in the BM medium in 96-well plastic plates. The concentrations of furanones after serial dilutions were in the range of 0.1–500 µg/µl. The wells were seeded with 200 µl of the bacterial culture ( $3 \times 10^7$  CFU/ml) in the BM medium and incubated at 37 °C. The minimum inhibitory concentration was determined as the lowest concentration of furanone for which no visible bacterial growth was observed after 24 h of incubation. The minimum biofilm inhibitory concentration (MBIC) was determined as the lowest concentration of furanone that completely inhibited biofilm formation after 72 h of growth.

#### Determination of the geno- and cytotoxicity of furanones

The mutagenicity of furanones at the MBIC concentration was evaluated in the Ames test [12]. We used the dimethyl sulfoxide (DMSO) solvent as a negative control and sodium azide ( $\text{NaN}_3$ ) as a positive control. A tested compound was considered to be mutagenic if the number of revertant colonies in the experiment was more than 2 times higher than that in the control (solvent). The DNA-damaging activity of the compounds was evaluated in the SOS chromotest using the *S. typhimurium* TA1535/pSK1002 strain [13]. The overnight bacterial culture was diluted 10 times with a LB medium and grown in the presence of the study compounds for 4 h. Next, the cells were collected by centrifuging and the β-galactosidase activity was determined according to [16]. Cytotoxicity of the compounds was determined using the MTS test (Promega) on MCF-7 cells, and the median cytotoxicity concentration  $\text{CC}_{50}$  (the concentration required to reduce cell activity by 50%) was calculated.

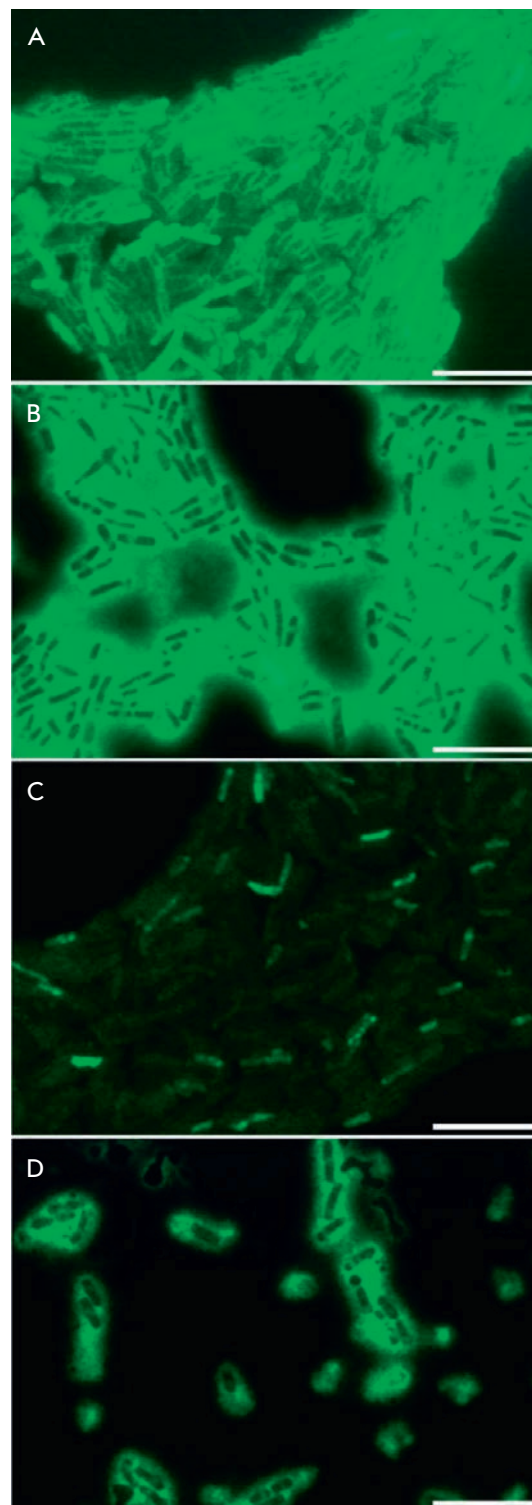


**Fig. 2.** The effect of furanones on the fluorescence intensity of GFP expressed from the *eps* operon promoter in *B. subtilis* K511 cells. Cells were grown in the presence of F12 (B), F15 (C), and F94 (D) at a concentration of 10 µg/ml (corresponds to MBIC) for 72 h. Cells grown in the absence of furanones were used as a control (A). The scale bar is 10 µm



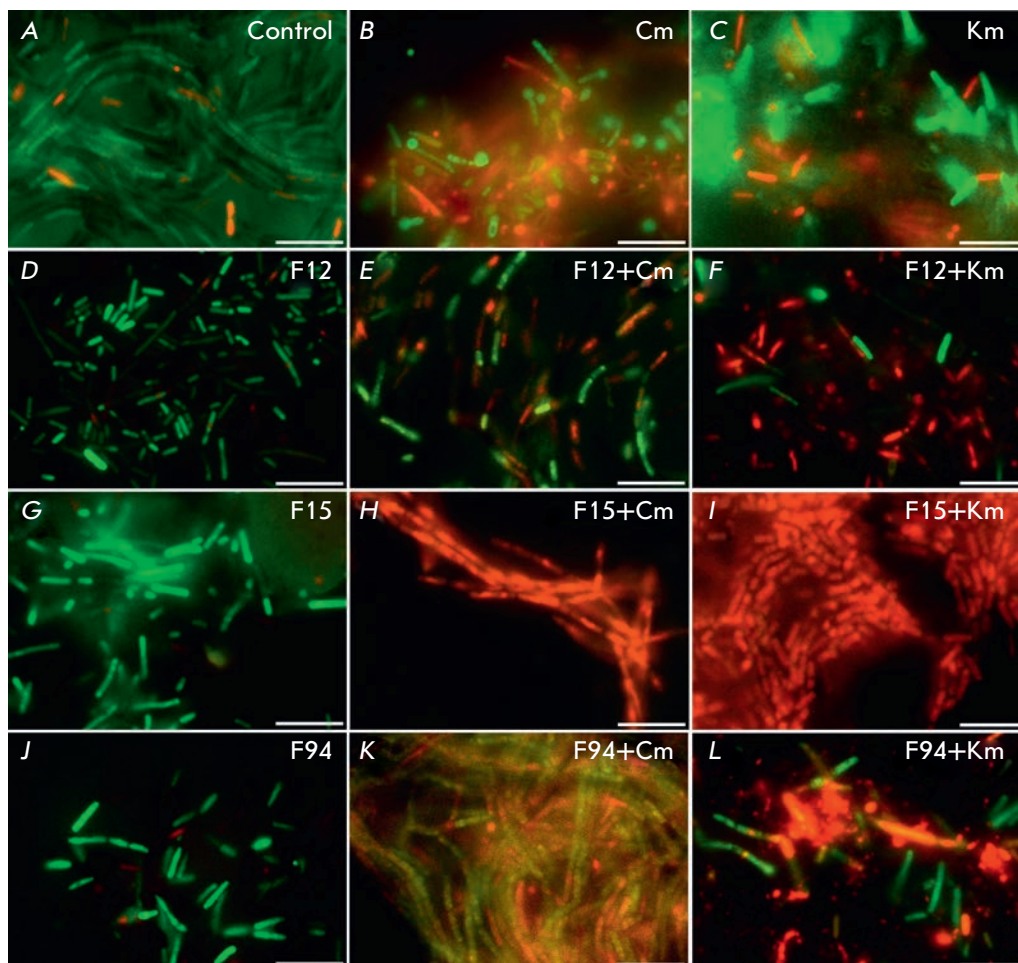


**Fig. 3.** The effect of furanones on biofilm formation by *B. subtilis* cells and the sensitivity of *B. subtilis* cells adhered to the culture plate surface to antibiotics. *B. subtilis* 168 cells were grown for 72 h to form a biofilm in the absence (A, B, C) or presence of furanones (D, G, J) at a concentration of 10  $\mu\text{g}/\text{ml}$  (corresponds to MBIC). Then, chloramphenicol (Cm) (E, H, K) or kanamycin (Km) (F, I, L) was added. After 24 h of incubation with an antibiotic, the number of viable cells was analyzed by staining the cells with propidium iodide and fluorescein diacetate. The scale bar is 10  $\mu\text{m}$

## RESULTS AND DISCUSSION

Earlier, we identified halogen- and sulfur-containing derivatives of 2(5*H*)-furanone that inhibited *B. subtilis* biofilm formation [6]. Additional screening of 56 substances enabled the identification of two more furanones (F15 and F94) inhibiting the biofilm formation at a concentration of 10  $\mu\text{g}/\text{ml}$  (Table 1). F2 and F8 (5-hydroxy-4-[(4-methylphenyl)sulfonyl]-3-chloro-2(5*H*)-furanone and 3,4-dichloro-5-[(1,3-dichloropropane-2-yl)oxy]-2(5*H*)-furanone, respectively), which were characterized in reference [6], increased the activity of the genetic competence system of *B. subtilis* and were not included in further research. F15 and F94 did not increase the activity of the transcription factor ComA, which activates the system of genetic competence development in *Bacilli* (not shown).

In order to establish the influence of furanones on the expression level of the *eps* operon encoding biofilm EPS synthesis genes, *B. subtilis* K511 cells carrying the *gfp* gene under control of the *epsA* gene

promoter were grown in a BM medium in the presence/absence of furanones for 72 h and analyzed using a fluorescent microscope (Fig. 2). Detection of GFP in the cells in the absence of furanones indicated expression of the *eps* operon and production of EPS, which is the biofilm matrix basis (Fig. 2A). GFP was not identified in the presence of furanones F12 and F94, suggesting the repression of EPS production and, as a consequence, the repression of biofilm formation in the presence of these compounds (Fig. 2B, D). Apparently, the molecular targets for these compounds are the regulatory pathways of organism adaptation to stress conditions. Indeed, F12 was demonstrated to inhibit the activity of the transcription factors Spo0A and TnrA [6]. On the contrary, GFP was also detected in the presence of F15, although in substantially lower amounts compared to the control; therefore, no suppression of the *eps* operon occurred. It is possible that F15 inhibits the biofilm formation through a different pathway, without involvement of the *eps* operon regulation.

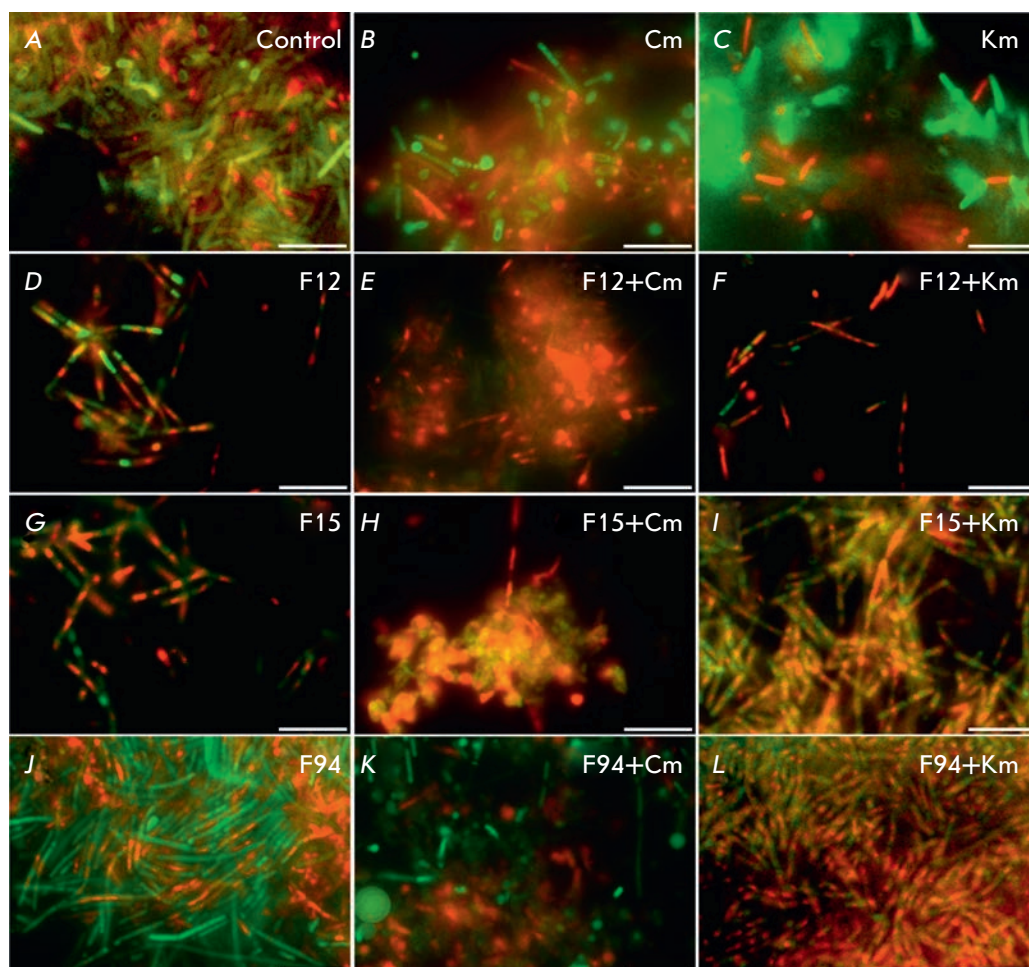


**Fig. 4.** Furanones disrupt a biofilm and increase the efficiency of antibiotics against biofilm-embedded *B. subtilis* cells. *B. subtilis* cells were cultured for 72 h to form a biofilm (A, B, C). Then, furanones were added to a final concentration of 30  $\mu\text{g}/\text{ml}$  (threefold excess of MBIC) (D, G, J) in the presence of chloramphenicol (Cm) (E, H, K) or kanamycin (Km) (F, I, L). After 24 h of incubation with an antibiotic, the number of viable cells was analyzed by staining the cells with propidium iodide and fluorescein diacetate. The scale bar is 10  $\mu\text{m}$

### Furanones increase the sensitivity of adhered cells to antibiotics

Antimicrobial agents are known to be ineffective against bacteria in the biofilm mode of existence. Presumably, the repression of biofilm formation should increase the efficiency of antimicrobial agents. Potential synergism between furanones and antibiotics was studied using the chessboard method, where the furanone and antibiotic (kanamycin and chloramphenicol) concentrations were varied from 0.1 to 2.0 MIC [17]. However, no compound exhibited synergism with antimicrobial agents with respect to plankton cells ( $\text{FIC} = 1.2 \pm 0.21$ ).

In order to investigate whether furanones increase the sensitivity of surface-adhered bacteria to antibiotics, *Bacilli* were grown in a BM medium in the presence of furanones at a 10  $\mu\text{g}/\text{ml}$  concentration (MBIC) for 72 h, then antibiotics (chloramphenicol and kanamycin) were added to a final concentration of 10  $\mu\text{g}/\text{ml}$  (established MIC values were 2.5  $\mu\text{g}/\text{ml}$ ). After 24 h of cultivation, the culture liquid was removed, the biofilm

was washed once with PBS, and differential fluorescent staining with propidium iodide and fluorescein diacetate was performed to identify dead and alive cells, respectively, in the layer of microbial cells adhered to the culture plate surface. The obtained specimens were analyzed using a Carl Zeiss Axio Imager 2.0 fluorescent microscope (Fig. 3).

The formation of a biofilm up to 10  $\mu\text{m}$  thick was observed in the control sample (Fig. 3A, Table 2). In this case, addition of chloramphenicol (Fig. 3B) or kanamycin (Fig. 3C) resulted in the death of only a small fraction of the adhered cells. In contrast, in the culture grown in the presence of F15 (10  $\mu\text{g}/\text{ml}$ ), the biofilm thickness was 2  $\mu\text{m}$ , and addition of an antibiotic resulted in almost complete death of bacilli (Fig. 3H, I), while furanone itself had no bactericidal effect (Fig. 3G). In case of F12 and F94 at the concentration of 10  $\mu\text{g}/\text{ml}$ , the effect was less pronounced. Thus, the presence of furanones in the culture medium inhibited biofilm formation on the culture dish surface and increased the efficiency of the antibiotics, apparently due

to a longer exposure of bacterial cells to antimicrobial agents.

The possibility of bacterial biofilm disruption in the presence of furanones was also studied. For this purpose, we grew *B. subtilis* cells in a BM medium for 72 h, removed the culture liquid, and added a pure BM medium supplemented with furanones (30 µg/ml), kanamycin, and chloramphenicol. After 24 h, the residual biofilm was washed with PBS and differential fluorescent staining was performed (Fig. 4).

As in the previous experiment, antibiotics in the absence of furanones were found to be ineffective against the cells embedded in the biofilm matrix (Fig. 4B, C). Supplementation with F12 (30 µg/ml) caused significant biofilm disruption after 24 h (Table 2), and addition of antibiotics caused the death of the vast majority of cells (Fig. 4D–F). In this case, the effect of F15 was less pronounced, while F94 caused almost no increase in the sensitivity of the cells to the antibiotics and did not lead to biofilm disruption (Fig. 3G–L).

#### Cyto- and genotoxic properties of compounds F12, F15, and F94

Determination of the cytotoxicity of F12, F15, and F94 showed that their  $CC_{50}$  values were 7 times higher than the concentrations necessary to inhibit biofilm formation (Table 1). Although the SOS chromotest did not

detect the DNA damaging activity of the compounds, the Ames test data indicated potential mutagenicity of F12 and F15.

#### CONCLUSIONS

Thus, the thio-containing compounds F12 and F15 may be of interest for further development of furanone-based inhibitors of bacterial biofilms. However, the potential mutagenicity of these furanones revealed in the Ames test serves as a contraindication for their direct application and requires further modification of their structure. ●

*The research was performed using the equipment of Interdisciplinary center for collective use of Kazan Federal University supported by Ministry of Education of Russia (ID RFMEFI59414X0003)*

*This work was supported by the Governmental Program on Improvement of Competitiveness of the Kazan (Volga Region) Federal University among the world's leading research and education centers, the Ministry of Education and Science of the Russian Federation (contract № 2014/187), and by the Russian Foundation for Basic Research (grant № 14-04-31635 mol\_a).*

#### REFERENCES

- Vlamakis H., Chai, Y., Beauregard P., Losick R., Kolter R. // *Nat. Rev. Microbiol.* 2013. № 11. P. 15–168.
- Kayumov A.R., Balaban N.P., Mardanov A.M., Kostrov S.V., Sharipova M.R. // *Microbiology.* 2006. V. 75. № 5. P. 557–563.
- Schmidt T., Ziganshin A.M., Nikolausz M., Scholwin F., Nelles M., Kleinstaub S., Pröter J. // *Biomass Bioenergy.* 2014. V. 69. P. 241–248.
- Ma Y., Xu Y., Yestrepky B.D., Sorenson R.J., Chen M., Larsen S.D., Sun H. // *PLoS One.* 2012. P. 1–10.
- Lonn-Stensrud J., Landin M.A., Benneche T., Petersen F.C., Scheiel A.A. // *J. Antimicrobial Chemotherapy.* 2009. № 63. P. 309–316.
- Kayumov A.R., Khakimullina E., Sharafutdinov I., Trizna E., Latypova L., Hoang L., Margulis A., Bogachev M., Kurbangaliev A. // *J. Antibiotics.* 2014. № 143. doi:10.1038/ja.2014.143 (epub ahead of print)
- Kurbangaliev A.R., Devyatova N.F., Bogdanov A.V., Berdnikov E.A., Mannafov T.G., Krivolapov D.B., Litvinov I.A., Chmutova G.A. // *Phosphorus, Sulfur, Silicon, Relat. Elem.* 2007. V. 182. № 3. P. 607–630.
- Latypova L.Z., Saygitbatalova E.Sh., Chulakova D.R., Lodochnikova O.A., Kurbangaliev A.R., Berdnikov E.A., Chmutova G.A. // *Rus. J. Org. Chem.* 2014. V. 50. Is. 4. P. 532–545.
- Khoang T.L., Khaziev R.M., Zaripova A.R., Kurbangaliev A.R., Chmutova G.A. // *Book of Abstracts of the III All-Russian Scientific Conference “Progress in Synthesis and Complex Formation”.* Moscow, April 21–25, 2014. Moscow: RUDN, 2014. P. 205.
- Kayumov A., Heinrich A., Sharipova M., Iljinskaya O., Forchhammer K. // *Microbiology.* 2008. V. 154. P. 2348–2355.
- Kobayashi K. // *Mol. Microbiol.* 2008. № 69. P. 1399–1410.
- Ames B.N., McCann J. // *Ann. N.Y. Acad. Sci.* 1976. № 271. P. 5–13.
- Oda Y., Nakamura S., Oki I., Kato T., Shinagawa H. // *Mutat Res.* 1985. № 147. P. 219–229.
- Sambrook J., Fritsch E.F., Maniatis T. *Molecular cloning. A laboratory manual.* N.Y.: Cold Spring Harbor Lab. Press, 1989. P. 4–16.
- Kayumov A., Heinrich A., Sharipova M., Iljinskaya O., Forchhammer K. // *Microbiology.* 2008. V. 154. P. 2348–2355.
- Fedorova K., Kayumov A., Woyda K., Ilinskaja O., Forchhammer K. // *FEBS Lett.* 2013. V. 587. P. 1293–1298.
- Prichard M.N., Jr. Shipman C. // *Antiviral Res.* 1990. № 14. P. 181–206.

# The Use of Atomic Force Microscopy for 3D Analysis of Nucleic Acid Hybridization on Microarrays

E. V. Dubrovin<sup>1\*</sup>, G. V. Presnova<sup>2</sup>, M. Yu. Rubtsova<sup>2</sup>, A. M. Egorov<sup>2,3</sup>, V. G. Grigorenko<sup>2</sup>, I. V. Yaminsky<sup>1,2</sup>

<sup>1</sup>Department of Physics, Lomonosov Moscow State University, Leninskie gory, 1/2, 119991, Moscow, Russia

<sup>2</sup>Department of Chemistry, Lomonosov Moscow State University, Leninskie gory, 1/3, 119991, Moscow, Russia

<sup>3</sup>Russian Medical Academy of Postgraduate Education, Barrikadnaya, 2/1, 125993, Moscow, Russia

\*E-mail: dubrovin@polly.phys.msu.ru

Received 20.09.2014

Revised manuscript received 25.02.2015

Copyright © 2015 Park-media, Ltd. This is an open access article distributed under the Creative Commons Attribution License, which permits unrestricted use, distribution, and reproduction in any medium, provided the original work is properly cited.

**ABSTRACT** Oligonucleotide microarrays are considered today to be one of the most efficient methods of gene diagnostics. The capability of atomic force microscopy (AFM) to characterize the three-dimensional morphology of single molecules on a surface allows one to use it as an effective tool for the 3D analysis of a microarray for the detection of nucleic acids. The high resolution of AFM offers ways to decrease the detection threshold of target DNA and increase the signal-to-noise ratio. In this work, we suggest an approach to the evaluation of the results of hybridization of gold nanoparticle-labeled nucleic acids on silicon microarrays based on an AFM analysis of the surface both in air and in liquid which takes into account of their three-dimensional structure. We suggest a quantitative measure of the hybridization results which is based on the fraction of the surface area occupied by the nanoparticles.

**KEYWORDS** DNA; oligonucleotide microarrays; hybridization; atomic force microscopy; gold nanoparticles; CTX-M type  $\beta$ -lactamases.

**ABBREVIATIONS** SEM – scanning electron microscopy; AFM – atomic force microscopy; EDTA – ethylenediaminetetraacetic acid; GPTMS –  $\gamma$ -glycidylxypropyl trimethoxysilane; PCR – polymerase chain reaction.

## INTRODUCTION

The oligonucleotide microarray technology is a relatively new method which appeared in the mid-1990s and is based on hybridization of oligonucleotide probes with target nucleic acids [1]. This method allows a simultaneous analysis of a large number of nucleic acids sequences and is a powerful tool for clinical diagnosis [2], assessment of drug sensitivity [3], and toxicological studies [4]. It is also used in other scientific and practical fields of biology and medicine [5].

A DNA microarray is composed of a solid support with a large number of immobilized oligonucleotide probes with known sequences. These probes are capable of hybridizing with the complementary DNA or RNA fragments from a test sample. The use of fluorescent dyes is the most common method to detect the result of hybridization of the probes with the target DNA [6]. Radioisotopes [7], enzymes [8], and gold nanopar-

ticles [9] are also used as labels in the microarray technology. Along with optical and fluorescence detection, electrochemical detection [10] and surface plasmon resonance [11] are used. Over recent years, the microarray surface has extensively been studied by high-resolution microscopy. Scanning electron microscopy (SEM) was used to examine the surface of glass microarrays with biotin-labeled oligonucleotide probes that were detected using streptavidin-peroxidase polymers and silver reduction enhancement [12]. It was shown that the silver nanoparticles formed during amplification are adsorbed on the surface and are clearly distinguishable on the surface using this method. Scanning electron microscopy was used to record sandwich hybridization of a model single-stranded DNA composed of 46 nucleotides. For that purpose, first-type oligonucleotide probes were immobilized on a support and DNA was detected using second-type oligonucleotide probes

labeled with gold nanoparticles [13]. A simple method of counting the number of particles per unit area was suggested, which provided high sensitivity and a better signal-to-noise ratio compared to those obtained with a fluorescent probe.

Atomic force microscopy (AFM), which is based on the operating principle of a profilometer, an instrument used to measure surface irregularities, has approximately the same lateral resolution as SEM, but considerably surpasses SEM in vertical resolution. Furthermore, AFM does not require a vacuum environment for sample examination and, thus, allows one to study samples under various conditions both in air and in liquid.

It should be noted that atomic force microscopy has gained considerable currency in the analysis of adsorbed DNA and RNA molecules without the use of labels [14–16]. A number of studies have used AFM as a tool for imaging and analyzing biospecific interactions, such as binding of bacterial cell fragments to antibodies in solution [17], binding of bacteriophages to the host cell [18], and other receptor-ligand interactions [19]. The use of AFM to analyze the surface topography of DNA microarrays has been reported. It facilitated the optimization of their preparation technology [20, 21]. The advantages of this method include the fact that there is no need for special preparation of the microarray surface and the relatively simple connection of a microarray to a microscope for further analysis (e.g., in most cases, one has to simply attach a support to a special magnetic disk). AFM analysis of the surfaces of DNA microarrays after their exposure to a sample solution led to a conclusion about hybridization of the probes with the complementary target DNAs [22] or gold nanoparticles incorporated therein [23]. In a number of studies, AFM made possible the development of quantitative criteria for the evaluation of target DNA hybridization on a microarray surface. A quantitative approach to an AFM analysis of DNA microarrays is extremely important, since it allows a quantitative comparison of the hybridization efficiency, in particular under significantly lower (compared to conventional detection methods) concentrations of the target. For example, the layer height on the biochip surface evaluated using AFM-nanolithography was used as a quantitative criterion [24]. In the cases where hybridized targets are morphologically distinguishable on the surface, the amount of bound DNA targets [25] or the nanoparticles associated with them [26] per unit surface area may serve this criterion. In this work, we developed an AFM-based approach to study silicon oligonucleotide microarray surfaces after hybridization, with the possibility of a quantitative analysis of its results. Allowance for the total area occupied by the

targets (the nanoparticles associated with them) bound to the microarray surface is a special feature of the developed approach.

We assumed that the unique capability of AFM to visualize single targets (nanoparticles) on the microarray surface and provide information on their height and other sizes will provide an additional morphology-based criterion for the selection of “true” targets and, thus, lower the threshold for the detection of targets, increase the signal-to-noise ratio, and also reduce the amount of material required to produce microarrays. Nucleic acids encoding bacterial CTX-M type  $\beta$ -lactamases, which are responsible for the development of resistance to cephalosporins in Gram-negative bacteria (causative agents of infectious diseases), were used as model DNAs [27, 28].

## EXPERIMENTAL

Gold nanoparticles were prepared according to the Frens method based on the reduction of chloroauric acid with sodium citrate [29]. The size of the gold nanoparticles was assessed by SEM using a Supra-40 scanning electron microscope (Carl Zeiss, Germany) equipped with an InLens secondary electron detector built in the microscope column.

Streptavidin (2 mg in 200  $\mu$ l of 10 mM K-phosphate buffer, pH 7.2) was modified with 3.2 mg of mercaptosuccinic acid in the presence of 3 mg of carbodiimide at +4°C overnight to obtain streptavidin conjugated to gold nanoparticles. Thereafter, 10  $\mu$ l of 10 mM EDTA was added, the mixture was stirred at room temperature for 30 min, and the resulting solution was dialyzed against phosphate buffer with EDTA. The colloidal gold solution pH was adjusted to 7.0 using a freshly prepared Na<sub>2</sub>CO<sub>3</sub> solution, and then streptavidin modified with mercaptosuccinic acid was added. After incubation at room temperature for 1 h, the solution was centrifuged (30 min, 11,000 rpm, 4°C). The supernatant was then removed, and the precipitate was dissolved in 10 mM K-phosphate buffer with pH 7.2.

The 5'-TTTTTTTTTTTTTTT-ATATCGCGGT-GATCTGGCC-3' probe was used to identify nucleic acids encoding CTX-M type  $\beta$ -lactamases. The 5'-TTTTTTTTTTTTTTT-CTAGACAGCCACTCATA-3' probe was used to control non-specific hybridization. These probes were modified with an amino group at the 5'-end.

Amplification of CTX-M type  $\beta$ -lactamase genes of 870 bp with simultaneous inclusion of biotin was performed by PCR as described in [30].

The surface of silicon plates was purified with oxygen plasma using a RDE-300 reactive ion-etching instrument (Alcatel, France) for 30 min. Then, it was chemically modified [31]: silicon was treated with

a 10 mM solution of 3-glycidyloxypropyl trimethoxysilane (GPTMS) in dry toluene at 80°C for 12 h then washed and heated at 100°C for 10 min. The surface of the modified silicon was covered by oligonucleotide probes with the 5'-end amino group using 20 pmol/ $\mu$ l solutions in 0.25 M Na-phosphate buffer containing 0.3 M Na<sub>2</sub>SO<sub>4</sub>. After immobilization, free protein binding sites on the silicon surface were blocked in a solution of 1% BSA and 1% casein in 10 mM K-phosphate buffer, pH 7.2, containing 0.15 M NaCl. Hybridization of 1 nM of biotin-labeled DNA was performed on an oligonucleotide microarray in buffer containing 0.05 M NaH<sub>2</sub>PO<sub>4</sub>, 0.5 M NaCl, and 0.005 M EDTA (pH 7.4) at a temperature of 45°C for 2 h. Washing was performed with 10 mM K-phosphate buffer (pH 7.2) containing 0.15 M NaCl and 0.1% Tween 20. The microarray was then incubated with a solution of streptavidin conjugated with gold nanoparticles with a protein concentration of 40 ng/ml at 37°C for 45 min and then washed.

In this work, we used a Nanoscope IIIa atomic force microscope (Digital Instruments, USA) in the tapping mode. Scanning was performed in air using fpN10 commercial cantilevers (Mikromash, Estonia) and in liquid using NP-S1 cantilevers (Veeco, USA) with a scanning frequency of 2.1 Hz, 512  $\times$  512 dots. Processing and analysis of images were performed using the Femto-Scan Online software (Advanced Technologies Center, Russia).

## RESULTS AND DISCUSSION

The hybridization analysis on silicon microarrays was performed using oligonucleotide probes immobilized on a silicon surface modified with  $\gamma$ -glycidyloxypropyl trimethoxysilane (GPTMS). The structure of the oligonucleotide probe used to detect nucleic acids encoding CTX-M type  $\beta$ -lactamases and the structure of the control probe are provided in the Experimental section. The hybridization reaction was carried out using a target DNA of 870 bp to which biotin molecules were incorporated during PCR. Biotin molecules in duplexes formed on the surface were detected using streptavidin conjugated with gold nanoparticles. We used spherical gold nanoparticles with a size of  $27 \pm 3$  nm. After hybridization and detection of the duplexes using streptavidin conjugated with gold nanoparticles, the microarray surface was examined by AFM.

Figure 1 shows the AFM images of the microarray surface obtained in a buffer before and after hybridization with gold nanoparticle-labeled nucleic acids encoding CTX-M-3  $\beta$ -lactamases. The microarray surface with DNA duplexes is morphologically composed of tightly packed globules 5–10 nm in diameter that consist of silicon modified by  $\gamma$ -GPTMS and oligonucleotides. Similar structures were previously observed

in the case of other oligonucleotide microarrays on silicon [22]. After hybridization with labeled DNA, nanoparticles, which are markers of hybridization products, appear on this surface. Their height is 30–50 nm (Fig. 1B). Images of the nanoparticles in a liquid medium are unstable, blurred, and replete with numerous scan failures, which is manifested in the appearance of light bands. This is likely due to weak fixation of DNA-bound nanoparticles on the surface, since only a small portion of the nucleic acid (18 nucleotides of 870) is involved in hybridization. Due to the weak adhesion of nanoparticles to the surface, the nanoparticle height measured by AFM exceeded the value of  $27 \pm 3$  nm obtained for these particles by SEM. Detection of gold nanoparticles, which are part of DNA duplexes, on the microarray surface is an important result, as it proves *in situ* binding of oligonucleotides to complementary DNA sites. It is advisable to perform a quantitative evaluation of DNA hybridization results after drying the microarray surface, to increase the stability of AFM images of gold nanoparticles.

Typical AFM images and the oligonucleotide microarray surface profile prior to hybridization, which were obtained in air, are shown in Fig. 2A–C. In this case, the microarray has a uniform surface consisting of globules of up to 10 nm in height, on which there are randomly shaped objects up to 330 nm in height (white

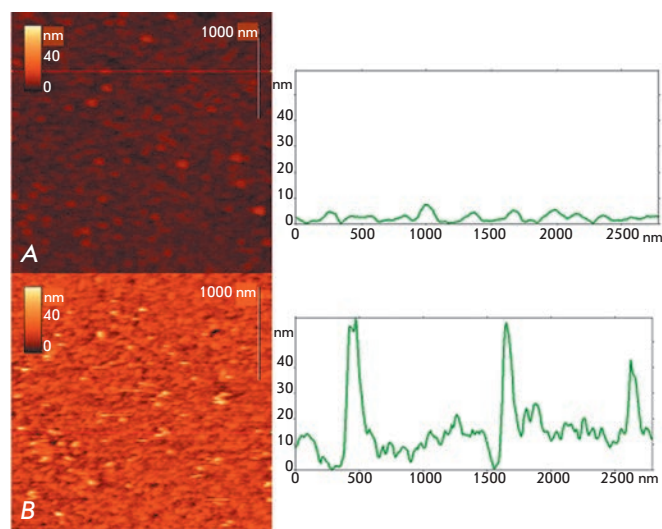
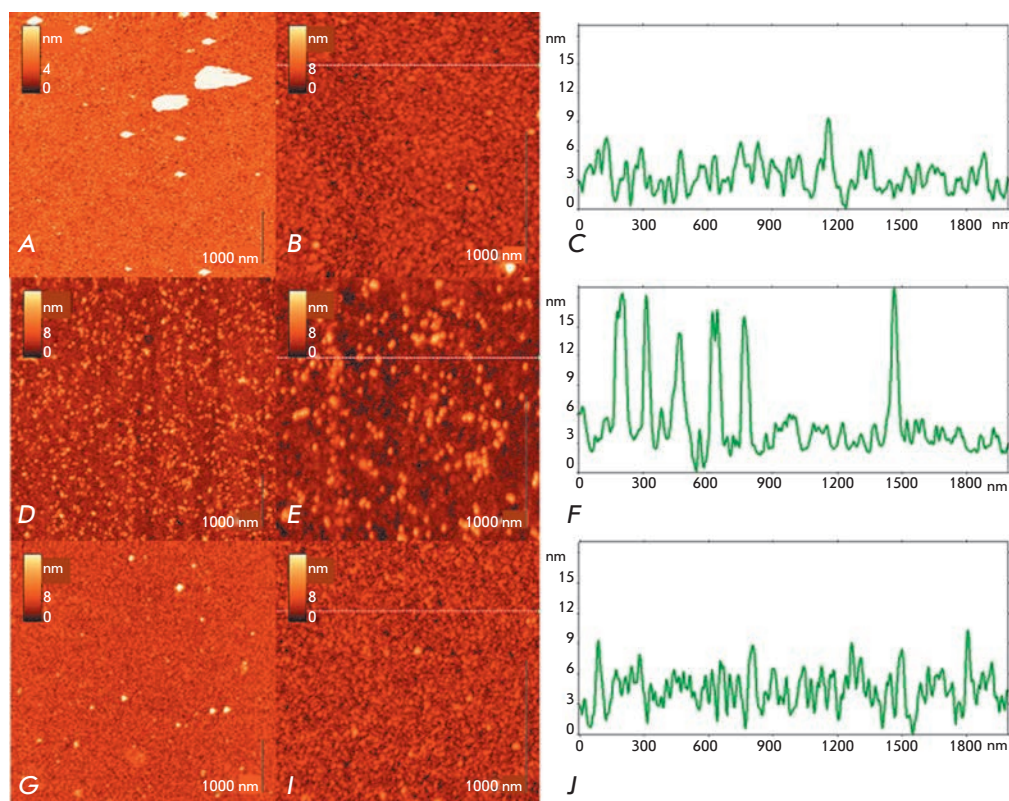


Fig. 1. AFM images of microarray surfaces obtained in buffer before (A) and after (B) hybridization with the biotin labeled target DNA and interaction with streptavidin conjugated to gold nanoparticles. On the right, vertical profiles of the microarray surfaces are shown along the line drawn in the corresponding image on the left



**Fig. 2.** AFM images and vertical profiles of the silicon microarray surface: (A–C) – immobilized oligonucleotide probes on  $\gamma$ -GPTMS modified silicon before exposure to an analyzed solution, (D–F) – after exposure to the analyzed solution of the target DNA and incorporation of nanoparticles into the duplexes, (G–I) – microarray areas without oligonucleotide probes on the surface, after their exposure to the analyzed solution of the target DNA and streptavidin conjugated to gold nanoparticles

structures in *Fig. 2A*). The globular surface in general reproduces the surface pattern observed in buffer (*Fig. 1A*). In this case, the high objects are probably impurities from buffer solutions and contaminants from the air, and they appear randomly during microarray preparation and DNA identification. AFM allows direct control of the total area of these structures, which is small compared to the microarray working surface.

Microarray surface images with DNA duplexes labeled with gold nanoparticles are shown in *Fig. 2D–F*. They demonstrate a large number of individual spherical particles 10–30 nm in height and their small aggregates composed of 10–15 particles. With allowance for the diameter of the used gold nanoparticles ( $27 \pm 3$  nm) and the possibility of their partial immersion into the oligonucleotide matrix during the hybridization of probes with target DNAs, the spherical particles observed in AFM images may be interpreted as gold nanoparticles, which are markers of hybridized DNA molecules.

*Figure 2G–I* shows AFM images and the surface profile of the microarray control region not covered with oligonucleotide probes, with hybridization with the DNA target followed by incorporation of gold nanoparticles being performed by the standard procedure, to control the hybridization specificity. In these imag-

es, a small amount (compared to *Fig. 2D–F*) of differently sized objects is observed on the background of  $\gamma$ -GPTMS modified silicon.

In order to interpret the results of the hybridization of probes with targets containing gold nanoparticles as labels, we developed a method for the quantitative analysis of AFM images of the microarray surface. It is based on the 3D-analysis of the microarray surface, i.e. on allowance for the heights and areas of the objects detected on the substrate surface after completion of all stages of the analysis. AFM provides information on the object's height with a high accuracy of up to a tenth of a nanometer, which allows one to range the objects observed on the microarray surface according to their height. Thus, it becomes possible to detect the results of complementary hybridization based on the height of the nanoparticles used as labels. In this case, we can disregard the objects non-specifically bound to the microarray surface, which have a smaller height.

All of the observed objects were selected for the analysis of the AFM images shown in *Fig. 2A D, G*. The mathematical algorithm of this selection was a search for the zero background level in a histogram as the most probable height distribution of all  $512 \times 512$  dots in an AFM image and construction of the threshold plane above which all parts of the surface were

taken as objects. This algorithm is integrated into the semi-automatic function of the software used for image processing (see the method). All selected objects are characterized by a number of easily computed geometric characteristics, such as the height, area, volume, perimeter, form factor reflecting the object shape, etc. *Figure 3* shows an example of automatic selection of objects in an AFM image containing gold nanoparticles.

The height range, within which the selected objects will be considered as labels, is selected individually in each task based on information on the used labels and the structural features of the microarray. We used the values 10 and 30 nm as the lower and upper limits of this filter. Selection of the upper limit (30 nm) was related to the known gold nanoparticle diameter distribution of  $27 \pm 3$  nm obtained by SEM. Due to the fact that objects higher than 30 nm were rarely observed in AFM images of microarrays after hybridization with DNA targets labeled with gold nanoparticles, we did not consider the possibility of a “vertical” arrangement of nanoparticle aggregates on the surface. Since the AFM-measured object height may be underestimated (due to surface deformation by cantilever) and also taking into account the possible partial immersion of a gold nanoparticle into the oligonucleotide (and GPTMS) matrix, the lower limit (10 nm) of the range was selected empirically based on the analysis of the lower limit of the gold nanoparticle height distribution in the corresponding AFM image. In principle, an algorithm can be developed for this step (selection of the height range filter) by selecting a threshold value for the fraction of objects observed within a given range with respect to the total number of objects observed on the surface. On surfaces with a small amount of impurities, this threshold value will be close to one; i.e., most of the observed objects will represent nanoparticles (the selected range corresponds to a threshold value of 0.9).

Histograms of the object’s height distribution in the selected range are shown in *Fig. 4* for the microarray working surface prior to hybridization (*Fig. 4A*), after hybridization (*Fig. 4B*), and also for the control surface of microarrays without immobilized probes, which is exposed to a solution with the target DNA under the same experimental conditions (*Fig. 4C*). The histograms summarize data obtained from AFM images in three different fragments of each surface. For clarity, the histograms are shown on the same scale. The total area of the objects, which were selected based on their heights ( $s_i$ ), normalized to the total area of the AFM image  $S_i:k = \sum s_i/S$  and expressed as a percentage was used for a quantitative comparison of the hybridization efficiency. In this way, accounting of nanoparticle aggregates will be more effective, because their area is proportional to the number of aggregated particles. The

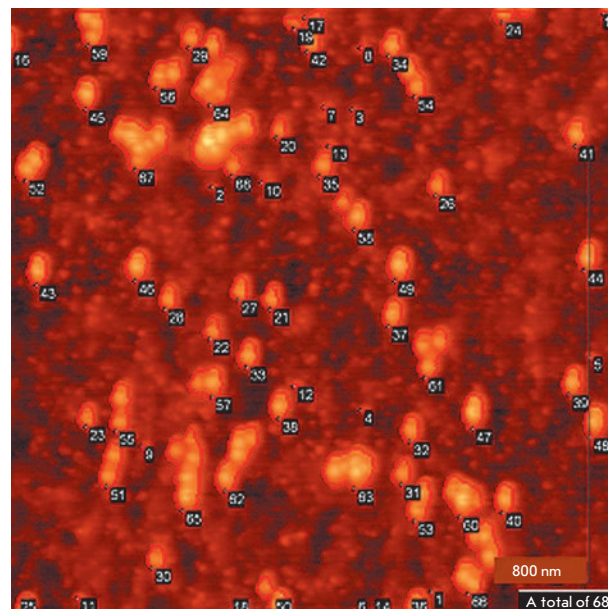


**Fig. 3.** Algorithm for object selection in the AFM image. Selected objects are outlined

parameter  $k$  reflects the fraction of the area occupied by nanoparticle labels with respect to the total microarray surface. In connection with the effect of broadening protruding objects by a cantilever of an atomic force microscope, it should be borne in mind that the  $k$  parameter is an upper estimate for the fraction of the area occupied by nanoparticles. *Figure 5* shows  $k$  values and their related errors for the experiments. The fraction of the area occupied by gold nanoparticles upon complementary hybridization was estimated to be 8%; in the absence of complementary binding – 0.5%, whereas the background particle surface area did not exceed 0.2%. In this case, the signal-to-noise ratio was 16 and 40, respectively. For reference, the signal-to-noise ratio for fluorescence detection was 10 (for a target concentration of 1 nM) [13].

Our approach allows the use of a quantitative criterion to assess the hybridization of oligonucleotide probes with target DNA and makes it possible to compare the efficiency of DNA identification on various microarrays. An important difference between our approach and conventional methods for detecting hybridization of a probe with the target DNA, as described in Introduction (e.g., fluorescence and optical detection), is the possibility to visualize single target binding events. Due to this fact, the detection threshold for target DNAs can be significantly reduced compared to conventional methods, which require the presence of simultaneous signals from a large number of bound targets. For ex-



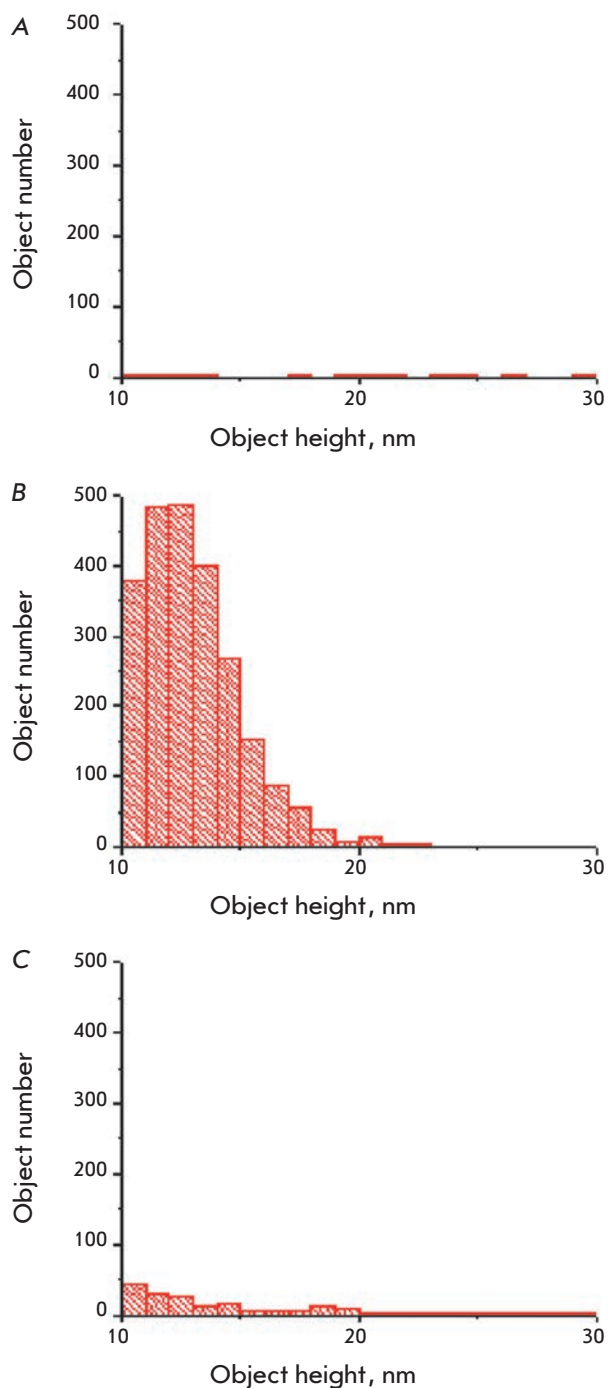


**Fig. 4.** Histograms for objects height distribution in the range of 10–30 nm observed in AFM images of the microarray surface before (A) and after (B) hybridization with the target DNA and streptavidin conjugated to gold nanoparticles and also for the control surface without oligonucleotide probes after exposure to the analyzed DNA target solution (C). Data for each histogram are summarized over three AFM images sized  $5 \times 5 \mu\text{m}$

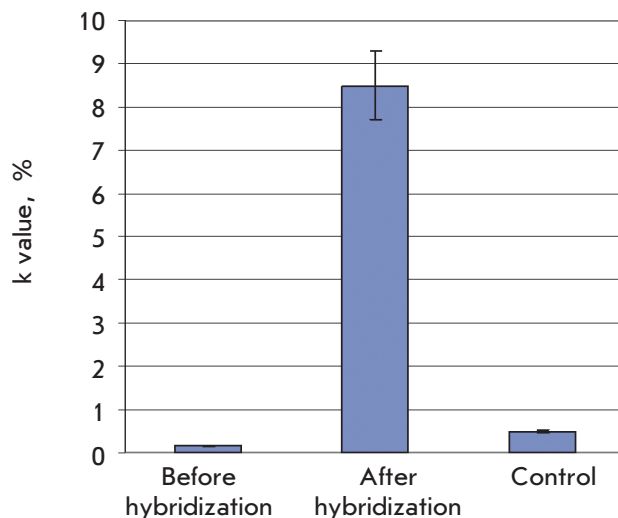


**Fig. 5.** *k* value (in %) for the microarray surface before and after hybridization with the target DNA and streptavidin conjugated to gold nanoparticles and also for the control surface without oligonucleotide probes after exposure to the analyzed DNA target solution. The parameter was calculated based on three AFM images sized  $5 \times 5 \mu\text{m}$

ample, in reference [13], where the hybridization efficiency was assessed by direct counting of nanoparticles in SEM images, the minimum detection threshold was achieved by detection of one nanoparticle per square micrometer, on average, with the minimum detectable concentration being 1,000 times lower compared to that for detection using fluorescent labels.

It should be emphasized that the use of our approach (and the *k* parameter) is not limited to systems using nanoparticles as DNA markers. This approach can be applied to the detection of molecules or other targets without the use of labels. In this case, the *k* parameter (or its equivalent, where the numerator is the sum of volumes rather than areas) will characterize the amount of bound material (target).

## CONCLUSIONS

In this work, the AFM method was used to study oligonucleotide microarrays for the identification of DNAs encoding bacterial CTX-M type  $\beta$ -lactamases. Incorporation of gold nanoparticles into DNA duplexes allows the use of AFM for effective detection of the hybridization of target DNA with oligonucleotide probes both in air and in liquid. In order to quantify the nucleic acid hybridization processes, we developed an approach to evaluate the results of hybridization using a three-dimensional analysis of AFM images of the microarray surface, which accounts for the height and area of the

gold nanoparticles used as labels. This method allows one to ignore particles that are non-specifically bound to the surface and differ from labels in height, as well as to take into account aggregates of target nanoparticles, which increases the detection efficiency. In the case of the silicon microarrays studied in this work, the parameter  $k$ , corresponding to the fraction of the area occupied by nanoparticles after hybridization with labeled specific DNA, was equal to 8%, while the control values did not exceed 0.5%. The main advantage of AFM over other methods for detection of binding on oligonucleotide microarrays is its capability to gain the

three-dimensional morphology of individual hybridized DNA molecules. The obtained information on the three-dimensional structure of an object allows the use of more accurate morphological criteria for the detection of hybridized DNA molecules. ●

*This work was supported by the Russian Foundation for Basic Research (project № 15-04-07678) and partially supported by the grant program of the President of the Russian Federation for young scientists (MK-312.2013.2).*

## REFERENCES

- Schena M., Shalon D., Davis R.W., Brown P.O. // *Science*. 1995. V. 270. P. 467–470.
- Yoo S.M., Choi J.H., Lee S.Y., Yoo N.C. // *J. Microbiol. Biotechnol.* 2009. V. 19. № 7. P. 635–646.
- Behr M.A., Wilson M.A., Gill W.P., Salamon H., Schoolnik G.K., Rane S., Small P.M. // *Science*. 1999. V. 284. P. 1520–1523.
- Nuwaysir E.F., Bittner M., Trent J., Barnett J.C., Afshari C.A. // *Mol. Carcinog.* 1999. V. 24. P. 153–159.
- Iida K., Nishimura I. // *Crit. Rev. Oral Biol. Med.* 2002. V. 13. P. 35–50.
- Sassolas A., Leca-Bouvier B.D., Blum L.J. // *Chem. Rev.* 2008. V. 108. P. 109–139.
- Herwig R., Aanstad P., Clark M., Lehrach H. // *Nucl. Acids Res.* 2001. V. 29. e117.
- Ryan O., Smyth M.R., Fagain C.O. // *Essays Biochem.* 1994. V. 28. P. 129–146.
- Lytton-Jean A.K., Han M.S., Mirkin C.A. // *Anal. Chem.* 2007. V. 79. P. 6037–6041.
- Liao J.C., Mastali M., Gau V., Suchard M.A., Møller A.K., Bruckner D.A., Babbitt J.T., Li Y., Gornbein J., Landaw E.M., et al. // *J. Clin. Microbiol.* 2006. V. 44. P. 561–570.
- Malic L., Cui B., Veres T., Tabrizian M. // *Opt. Lett.* 2007. V. 32. P. 3092–3094.
- Hering K.K., Moller R., Fritzsche W., Popp J. // *ChemPhysChem.* 2008. V. 9. P. 867–872.
- Kim H., Takei H., Yasuda K. // *Sens. Actuators. B.* 2010. V. 144. P. 6–10.
- Adamcik J., Klinov D.V., Witz G., Sekatskii S.K., Dietler G. // *FEBS Lett.* 2006. V. 580. P. 5671–5675.
- Dubrovin E.V., Staritsyn S.N., Yakovenko S.A., Yaminsky I.V. // *Biomacromolecules.* 2007. V. 8. P. 2258–2261.
- Dubrovin E.V., Gerritsen J.W., Zivkovic J., Yaminsky I.V., Speller S. // *Colloids Surf. B.* 2010. V. 76. P. 63–69.
- Dubrovin E.V., Fedyukina G.N., Kraevsky S.V., Ignatyuk T.E., Yaminsky I.V., Ignatov S.G. // *Open Microbiol. J.* 2012. V. 6. P. 22–28.
- Dubrovin E.V., Popova A.V., Kraevskiy S.V., Ignatov S.G., Ignatyuk T.E., Yaminsky I.V., Volozhantsev N.V. // *PLoS One.* 2012. V. 7. № 10. e47348.
- Dupres V., Verbelen C., Dufrêne Y.F. // *Biomaterials.* 2007. V. 28. P. 2393–2402.
- Oh S.J., Cho S.J., Kim C.O., Park J.W. // *Langmuir.* 2002. V. 18. P. 1764–1769.
- Legay G., Finot E., Meunier-Prest R., Cherkaoui-Malki M., Latruffe N., Dereux A. // *Biosens. Bioelectron.* 2005. V. 21. P. 627–636.
- Lenigk R., Carles M., Ip N.Y., Sucher N.J. // *Langmuir.* 2001. V. 17. P. 2497–2501.
- Festag G., Steinbruck A., Wolff A., Csaki A., Moller R., Fritzsche W. // *J. Fluoresc.* 2005. V. 15. P. 161–170.
- Han W.H., Liao J.-M., Chen K.-L., Wu S.-M., Chiang Y.-W., Lo S.-T., Chen C.-L., Chiang C.-M. // *Anal. Chem.* 2010. V. 82. P. 2395–2400.
- Cook M.A., Chan C.-K., Jorgensen P., Ketela T., So D., Tyers M., Ho C.-Y. // *PLoS One.* 2008. V. 3. e154.
- Lavalley V., Chaudouët P., Stambouli V. // *Surf. Sci.* 2007. V. 601. P. 5424–5432.
- Bush K. // *Ann. N.Y. Acad. Sci.* 2013. V. 1277. P. 84–90.
- Rubtsova M.Yu., Ulyashova M.M., Bachmann T.T., Schmid R.D., Egorov A.M. // *Biochemistry (Mosc).* 2010. V. 75. P. 1628–1649.
- Frens G. // *Nat. Phys. Sci.* 1973. V. 241. P. 20–22.
- Rubtsova M.Yu., Ulyashova M.M., Edelstein M.V., Egorov A.M. // *Biosens. Bioelectron.* 2010. V. 26. № 4. P. 1252–1260.
- Lamtire J.B., Beattie K.L., Burke B.E., Eggers M.D., Ehrlich D.J., Fowler R., Hollis M.A., Kosicki B.B., Reich R.K., Smith S.R., et al. // *Nucl. Acids Res.* 1994. V. 22. P. 2121–2125.

# Redistribution of Free- and Cell-Surface-Bound DNA in Blood of Benign and Malignant Prostate Tumor Patients

O. E. Bryzgunova<sup>1#</sup>, S. N. Tamkovich<sup>1,2\*#</sup>, A. V. Cherepanova<sup>1</sup>, S. V. Yarmoshchuk<sup>3</sup>,  
V. I. Permyakova<sup>1</sup>, O. Y. Anykeeva<sup>3</sup>, P. P. Laktionov<sup>1,3</sup>

<sup>1</sup>Institute of Chemical Biology and Fundamental Medicine, Siberian Branch of the Russian Academy of Sciences, Prosp. Lavrentieva, 8, 630090, Novosibirsk, Russia

<sup>2</sup>Novosibirsk State University, Pirogova Str., 2, 630090, Novosibirsk, Russia

<sup>3</sup>Meshalkin Novosibirsk State Research Institute of Circulation Pathology, Rechkunovskaya Str., 15, 630055, Novosibirsk, Russia

\*E-mail: s.tamk@niboch.nsc.ru

#First two authors contributed equally to this work

Received 03.12.2014

Revised manuscript received 19.03.2015

Copyright © 2015 Park-media, Ltd. This is an open access article distributed under the Creative Commons Attribution License, which permits unrestricted use, distribution, and reproduction in any medium, provided the original work is properly cited.

**ABSTRACT** A direct correlation between the concentration of cell-free and cell-surface-bound circulating DNA (cfDNA and csbDNA, respectively) was demonstrated. Based on an inverse correlation between blood plasma DNase activity and the cfDNA concentration, blood DNases are supposed to regulate the cfDNA concentration. However, no correlation was found between the DNase activity in blood plasma and the csbDNA concentration, indicating that blood DNases are not involved in csbDNA dissociation from the cell surface. The possibility of DNA redistribution between cfDNA and csbDNA indicates that the total pool of circulating DNA (cfDNA + csbDNA) should be used for a correct analysis of marker DNA concentrations and data standardization.

**KEYWORDS** plasma, circulating DNA; DNase activity; prostate cancer.

**ABBREVIATIONS** cfDNA – cell free DNA; csbDNA – cell-surface-bound circulating DNA; PC – prostate cancer; PBS-EDTA – 10 mM phosphate buffer (pH 7.5) with 0.15M NaCl and 5 mM EDTA.

## INTRODUCTION

The blood of healthy donors and cancer patients is known to contain constantly circulating extracellular DNAs. These circulating DNAs are found both in apoptotic bodies, nucleosomes, and the macromolecular protein complexes of plasma [1, 2] and on the surface of blood cells [1]. Previously, we demonstrated that the development of oncologic diseases such as breast cancer [3, 4] and lung cancer [5] is accompanied by an increase in the cfDNA concentration and a decrease in the csbDNA concentration. The relationships between these pools of circulating DNAs were not studied.

This article presents a study of the distribution of circulating DNAs between plasma and the surface of blood cells in prostate cancers.

## EXPERIMENTAL

Blood samples of healthy males ( $n = 40$ ) at the age of 37–71 ( $47.4 \pm 1.3$ ) years, containing the prostate-specific antigen (PSA) at the concentration corresponding to the clinical norm (not exceeding 2.8 ng/mL), were

received from the Central Clinical Hospital of the Siberian Branch of the Russian Academy of Sciences. Blood samples of newly admitted patients with prostate cancers at the age of 45–84 ( $70.2 \pm 1.4$ ) years were received from Municipal Clinical Hospital No.1; the PSA concentrations in a group of patients with benign hyperplasia ( $n = 25$ ) and prostate cancer ( $n = 16$ ) were 0–31.7 and 0–103.1 ng/mL, respectively (increased in 36 and 81% of cases). The study was conducted in compliance with the principles of voluntarism and confidentiality, according to the Fundamentals of Health Protection of Citizens in the Russian Federation. The disease stage was determined according to the TNM classification.

Collection and processing of blood and extraction of cfDNA from plasma, csbDNA from a PBS-EDTA eluate, and csbDNA from a trypsin eluate from the surface of blood cells were performed according to reference [5]. The extracellular DNA concentration was determined using an intercalating fluorescent dye PicoGreen [5]. The detection limits for DNA calculated to the initial blood volume were 0.4 ng/mL of blood in

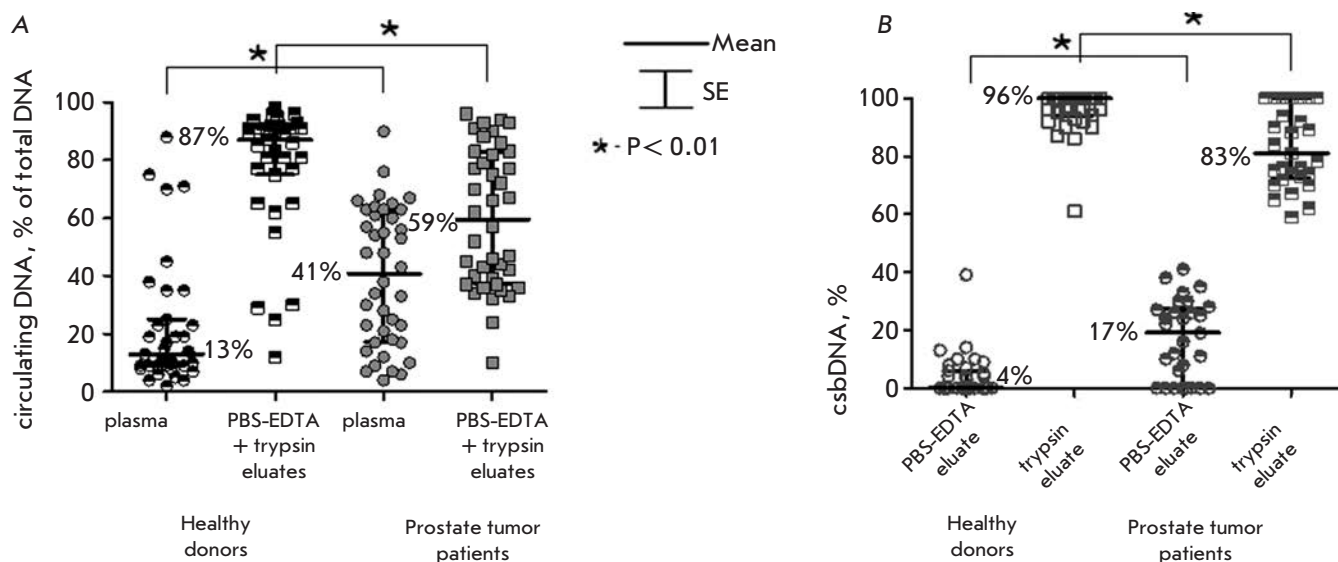


**Fig. 1.** Relative amounts of cfDNA and csbDNA (A) and csbDNA (B) in the blood of healthy donors and PC patients

plasma, 2 ng/mL of blood in the PBS-EDTA eluate, and 20 ng/mL of blood in the trypsin eluate. The integral DNase activity in the blood plasma of healthy donors and patients was determined by an enzyme-linked immunosorbent assay (ELISA) as described in reference [6]. The ELISA sensitivity, defined as the minimal, statistically significantly determined activity of DNase 1 in a sample, was 0.004 U/mL of a sample. The variation coefficient at each point was not more than 4%.

Results were processed by the GraphPad Prism 5 software using the non-parametric Mann-Whitney test and the Spearman correlation coefficient.

## RESULTS AND DISCUSSION

Previously, we demonstrated that the blood of healthy donors, as well as that of patients with lung cancer [5] and stomach and colon cancers [7], contains constantly circulating DNAs that occur not only in blood plasma, but also in complexes bound to the surface of blood cells. A portion of csbDNA dissociates after the treatment of cells with PBS-EDTA buffer and is apparently bound to phospholipids and other anions of the cell membrane through bridges of divalent metal ions [8] or low-affinity interactions and is eluted with 9 buffer volumes (compared to the plasma volume); another csbDNA portion is removed from the cell surface by treating cells with a 0.125% trypsin solution and, apparently, is a part of the complexes with surface proteins of the blood cells [1].

The present study investigates correlation relationships between the blood concentration of cfDNA and csbDNA in the norm and in prostate cancers (PCs).

Since the cfDNA and csbDNA concentrations in patients with benign prostatic hyperplasia did not differ statistically significantly from their concentrations in the blood of prostate cancer patients (data are not shown), these groups of patients were combined into one group of patients with PCs. The ratio of cfDNA concentration to total circulating DNA (cf + csbDNA) concentration revealed a statistically significant ( $P < 0.01$ ) increase in the fraction of cfDNA in PCs ( $40 \pm 4\%$ ) compared to the norm ( $22 \pm 4\%$ ) (Fig. 1A).

The PBS-EDTA eluate from the surface of the blood cells (i.e., weakly bound csbDNAs) of healthy donors and PC patients was found to contain  $4 \pm 1$  and  $17 \pm 3\%$  of the total amount of circulating DNAs bound to blood cells, respectively (Fig. 1B), and these differences between healthy and sick males were statistically significant ( $P < 0.01$ ).

The observed decrease in the csbDNA fraction and the simultaneous increase in the cfDNA fraction in the blood of PC patients may be due to the hydrolysis of csbDNAs by blood deoxyribonucleases. The data on DNase capability to hydrolyze nucleic acids bound to the cell surface are contradictory. Some authors believe that DNases can hydrolyze csbDNA [9], and according to others, DNases have little effect on the csbDNA concentration [8, 10].

The blood DNase activity was determined using a previously developed enzyme-linked immunosorbent assay based on the hydrolysis of a DNA PCR fragment modified with fluorescein and biotin moieties [6]. An analysis of the cfDNA concentration and DNase activity in blood plasma from healthy donors and can-

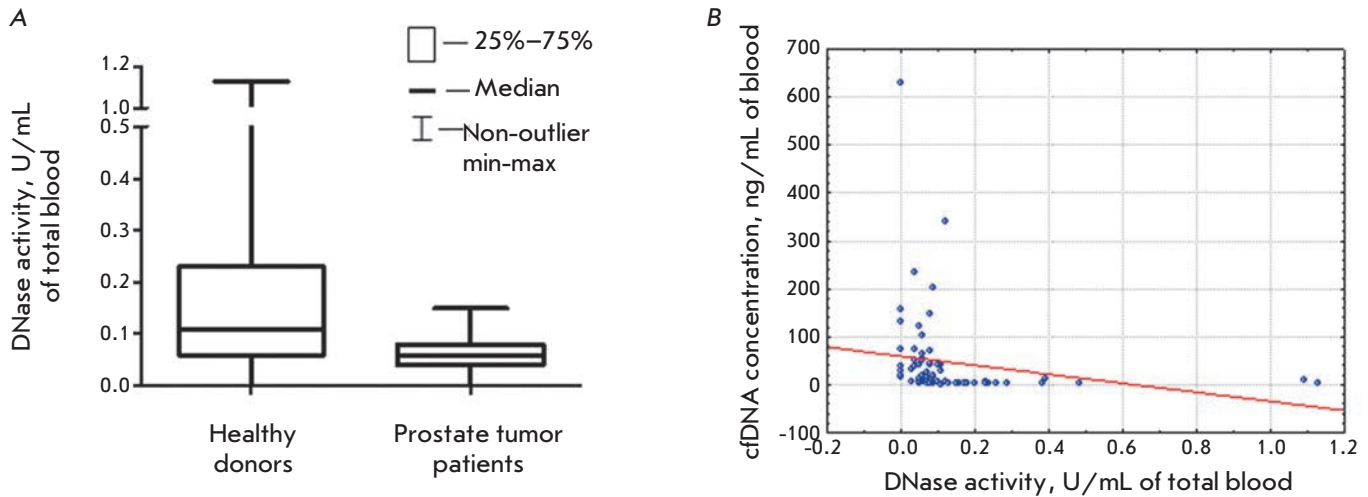


Fig. 2. DNase activity in the blood plasma of healthy donors and PC patients (A); dependence of the cfDNA concentration on DNase activity in the blood plasma of healthy donors and PC patients (B)

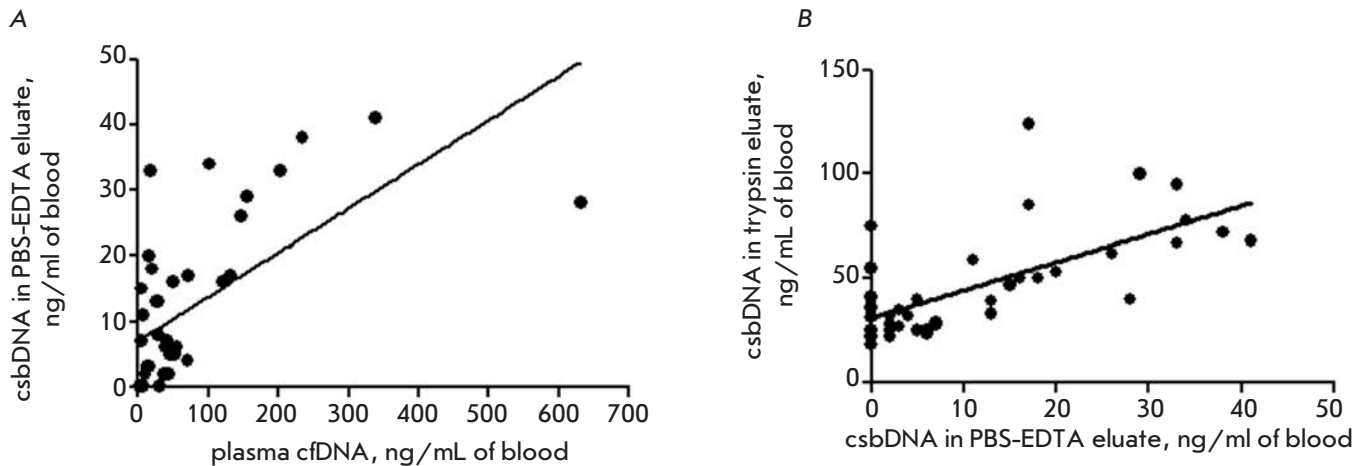


Fig. 3. Relation between the plasma cfDNA concentration and the csbDNA concentration in PBS-EDTA eluate (A); relation between the PBS-EDTA eluate csbDNA concentration and the trypsin eluate csbDNA concentration (B)

cer patients revealed an appreciable (on the Chaddock scale) inverse correlation between these parameters ( $R = -0.57$ ,  $P < 0.01$ ) (Fig. 2).

These data demonstrate that DNases, despite a statistically significant ( $P < 0.01$ ) decrease in their activity in the blood of PC patients compared to healthy donors (Fig. 2), can hydrolyze cfDNA and apparently are one of the factors negatively regulating the cfDNA concentration.

Investigation of the relationship between the blood plasma DNase activity and the csbDNA concentration demonstrated that the DNase activity is weakly correlated with the concentration of DNAs bound to the surface of blood cells via ionic interactions and is almost not correlated with the concentration of DNAs

bound to cell surface proteins ( $R = -0.36$ ,  $P < 0.01$  and  $R = -0.28$ ,  $P < 0.01$ , respectively). These data indicate that DNases do not actually hydrolyze csbDNAs strongly bound to cell surface proteins, do not contribute noticeably to the fragmentation process of csbDNA and its dissociation from the cell surface, and that the cfDNA concentration cannot increase due to the hydrolysis of csbDNA strongly bound to the cell surface.

The data from *in vitro* experiments [11] and the results of a study of blood csbDNA (Fig. 1) demonstrate that the main portion of csbDNA is removed from the cell surface upon treating cells with trypsin; i.e., it is bound to cell surface proteins. Based on the data on the correlation between the csbDNA concentration of the PBS-EDTA eluate and the DNase activity, it may be

assumed that a portion of weakly bound csbDNAs can enter into an exchange with DNAs of the extracellular environment and blood plasma. An appreciable (on the Chaddock scale) direct correlation between the change in the plasma cfDNA concentration and the weakly bound csbDNA concentration (PBS-EDTA eluate) ( $R = 0.67$ ,  $P < 0.01$ ) in PC patients (Fig. 3A) confirms this supposition.

In addition, we found a direct correlation between the csbDNA concentration in the PBS-EDTA eluate and in the trypsin eluate in PC patients ( $R = 0.65$ ,  $P < 0.001$ ) (Fig. 3B), which may indicate a redistribution of DNA between these fractions of csbDNA.

Therefore, these data indicate a possibility of partial exchange between blood cfDNAs and csbDNAs. Indirectly, this fact is also confirmed by the data on the size of circulating DNA fragments. csbDNAs of the trypsin eluate are mainly represented by high-molecular-weight (approximately 10–20 kb) DNA, and cfDNAs and csbDNAs of the PBS-EDTA eluate contain, apart from high-molecular-weight DNA, 200–500 bp fragments [3], which, apparently, can circulate as a part of one or another pool of circulating DNAs.

The causes of a decrease in the fraction of csbDNA in the total pool of circulating DNAs in the blood of PC patients are not known. It is likely that they are associ-

ated with a change in the structure of the cytoplasmic membranes of blood cells. Indeed, the development of oncologic diseases has been demonstrated to be accompanied by a change in the lipid ratio in blood cell membranes that leads to increased viscosity of the lipid bilayer, disruption of intermolecular protein-lipid interactions, and, as a consequence, disorganization of the protein composition, malfunction of the membrane cation transport systems, and disorganization of cell surface architectonics [12].

The pool of csbDNAs is known to be a valuable source of diagnostic material [4]. The possibility of cfDNA and csbDNA exchange suggests that, in the future, the most accurate diagnostic information could be obtained from an analysis of total blood-circulating DNA. Indeed, given that cfDNA and csbDNA can enter into an exchange (although the mechanisms of this process are not yet known), it is more accurate to use total blood-circulating (cfDNA + csbDNA) DNA to measure relative marker concentrations. ●

*This work was supported by the Russian Foundation for Basic Research (grant № 13-04-01460), BOR (№ VI.62.1.4), and grants from the President of the Russian Federation for young scientists and graduate students (SP-1528.2013.4 and SP-5711.2013.4).*

#### REFERENCES

1. Tamkovich S.N., Laktionov P.P., Vlasov V.V. // *Mol. Biol. (Mosk.)*. 2008. V. 42. № 1. P. 12–24.
2. Geary R., Watanabe T., Truong L., Freier S., Lesnik E.A., Sioufi N.B., Sasmor H., Manoharan M., Levin A.A. // *Pharm. Exp. Therap.* 2001. V. 296. № 3. P. 890–897.
3. Laktionov P.P., Tamkovich S.N., Rykova E.Y., Bryzgunova O.E., Starikov A.V., Kuznetsova N.P., Vlassov V.V. // *Ann. N.Y. Acad. Sci.* 2004. V. 1022. P. 221–227.
4. Skvortsova T.E., Rykova E.Y., Tamkovich S.N., Bryzgunova O.E., Starikov A.V., Kuznetsova N.P., Vlassov V.V., Laktionov P.P. // *Br. J. Cancer*. 2006. V. 94. № 10. P. 1492–1495.
5. Tamkovich S.N., Litviakov N.V., Bryzgunova O.E., Dobrodeev A.Y., Rykova E.Y., Tuzikov S.A., Zav'ialov A.A., Vlassov V.V., Cherdyntseva N.V., Laktionov P.P. // *Ann. N.Y. Acad. Sci.* 2008. V. 1137. P. 214–217.
6. Cherepanova A., Tamkovich S., Pyshnyi D., Kharkova M., Vlassov V., Laktionov P. // *J. Immunol. Methods*. 2007. V. 325. № 1–2. P. 96–103.
7. Tamkovich S.N., Bryzgunova O.E., Rykova E.I., Kolesnikova E.V., Shelestiuk P.I., Laktionov P.P., Vlasov V.V. // *Biomed. Khim.* 2005. V. 51. № 3. P. 321–328.
8. Beliaev N.D., Budker V.G., Gorokhova O.E., Sokolov A.V. // *Mol. Biol. (Mosk.)*. 1988. V. 22. P. 1667–1672.
9. Aggarwal S., Wagner R., McAllister P., Rosenberg B. // *Proc. Nat. Acad. Sci. USA*. 1975. V. 72. № 3. P. 928–932.
10. Dorsch C. // *Thromb. Res.* 1981. V. 24. № 1–2. P. 119–129.
11. Morozkin E.S., Sil'nikov V.N., Rykova E.Y., Vlassov V.V., Laktionov P.P. // *Bull. Exp. Biol. Med.* 2009. V. 147. № 1. P. 63–65.
12. Novitsky V.V., Ryazantseva N.V., Stepovaya Ye.A., Fyodorova T.S., Kravets Y.B., Ivanov V.V., Zhavoronok T.V., Chasovskikh N.Yu., Choudakova O.M., Butusova V.N., et al. // *Bull. Sib. Med.* 2006. V. 2. P. 62–69.

## GENERAL RULES

*Acta Naturae* publishes experimental articles and reviews, as well as articles on topical issues, short reviews, and reports on the subjects of basic and applied life sciences and biotechnology.

The journal is published by the Park Media publishing house in both Russian and English.

The journal *Acta Naturae* is on the list of the leading periodicals of the Higher Attestation Commission of the Russian Ministry of Education and Science

The editors of *Acta Naturae* ask of the authors that they follow certain guidelines listed below. Articles which fail to conform to these guidelines will be rejected without review. The editors will not consider articles whose results have already been published or are being considered by other publications.

The maximum length of a review, together with tables and references, cannot exceed 60,000 symbols (approximately 40 pages, A4 format, 1.5 spacing, Times New Roman font, size 12) and cannot contain more than 16 figures.

Experimental articles should not exceed 30,000 symbols (20 pages in A4 format, including tables and references). They should contain no more than ten figures. Lengthier articles can only be accepted with the preliminary consent of the editors.

A short report must include the study's rationale, experimental material, and conclusions. A short report should not exceed 12,000 symbols (8 pages in A4 format including no more than 12 references). It should contain no more than four figures.

The manuscript should be sent to the editors in electronic form: the text should be in Windows Microsoft Word 2003 format, and the figures should be in TIFF format with each image in a separate file. In a separate file there should be a translation in English of: the article's title, the names and initials of the authors, the full name of the scientific organization and its departmental affiliation, the abstract, the references, and figure captions.

## MANUSCRIPT FORMATTING

The manuscript should be formatted in the following manner:

- Article title. Bold font. The title should not be too long or too short and must be informative. The title should not exceed 100 characters. It should reflect the major result, the essence, and uniqueness of the work, names and initials of the authors.
- The corresponding author, who will also be working with the proofs, should be marked with a footnote \*.
- Full name of the scientific organization and its departmental affiliation. If there are two or more scientific organizations involved, they should be linked by digital superscripts with the authors' names. Abstract. The structure of the abstract should be very clear and must reflect the following: it should introduce the reader to the main issue and describe the experimental approach, the possibility of practical use, and the possibility of further research in the field. The average length of an abstract is 20 lines

(1,500 characters).

- Keywords (3 – 6). These should include the field of research, methods, experimental subject, and the specifics of the work. List of abbreviations.

- INTRODUCTION
- EXPERIMENTAL PROCEDURES
- RESULTS AND DISCUSSION
- CONCLUSION

The organizations that funded the work should be listed at the end of this section with grant numbers in parenthesis.

- REFERENCES

The in-text references should be in brackets, such as [1].

## RECOMMENDATIONS ON THE TYPING AND FORMATTING OF THE TEXT

- We recommend the use of Microsoft Word 2003 for Windows text editing software.
- The Times New Roman font should be used. Standard font size is 12.
- The space between the lines is 1.5.
- Using more than one whole space between words is not recommended.
- We do not accept articles with automatic referencing; automatic word hyphenation; or automatic prohibition of hyphenation, listing, automatic indentation, etc.
- We recommend that tables be created using Word software options (Table → Insert Table) or MS Excel. Tables that were created manually (using lots of spaces without boxes) cannot be accepted.
- Initials and last names should always be separated by a whole space; for example, A. A. Ivanov.
- Throughout the text, all dates should appear in the “day.month.year” format, for example 02.05.1991, 26.12.1874, etc.
- There should be no periods after the title of the article, the authors' names, headings and subheadings, figure captions, units (s – second, g – gram, min – minute, h – hour, d – day, deg – degree).
- Periods should be used after footnotes (including those in tables), table comments, abstracts, and abbreviations (mon. – months, y. – years, m. temp. – melting temperature); however, they should not be used in subscripted indexes ( $T_m$  – melting temperature;  $T_{p.t}$  – temperature of phase transition). One exception is mln – million, which should be used without a period.
- Decimal numbers should always contain a period and not a comma (0.25 and not 0,25).
- The hyphen (“-”) is surrounded by two whole spaces, while the “minus,” “interval,” or “chemical bond” symbols do not require a space.
- The only symbol used for multiplication is “×”; the “×” symbol can only be used if it has a number to its right. The “·” symbol is used for denoting complex compounds in chemical formulas and also noncovalent complexes (such as DNA·RNA, etc.).
- Formulas must use the letter of the Latin and Greek alphabets.

# GUIDELINES FOR AUTHORS

- Latin genera and species' names should be in italics, while the taxa of higher orders should be in regular font.
- Gene names (except for yeast genes) should be italicized, while names of proteins should be in regular font.
- Names of nucleotides (A, T, G, C, U), amino acids (Arg, Ile, Val, etc.), and phosphonucleotides (ATP, AMP, etc.) should be written with Latin letters in regular font.
- Numeration of bases in nucleic acids and amino acid residues should not be hyphenated (T34, Ala89).
- When choosing units of measurement, SI units are to be used.
- Molecular mass should be in Daltons (Da, KDa, MDa).
- The number of nucleotide pairs should be abbreviated (bp, kbp).
- The number of amino acids should be abbreviated to aa.
- Biochemical terms, such as the names of enzymes, should conform to IUPAC standards.
- The number of term and name abbreviations in the text should be kept to a minimum.
- Repeating the same data in the text, tables, and graphs is not allowed.

## GUIDENESS FOR ILLUSTRATIONS

- Figures should be supplied in separate files. Only TIFF is accepted.
- Figures should have a resolution of no less than 300 dpi for color and half-tone images and no less than 500 dpi.
- Files should not have any additional layers.

## REVIEW AND PREPARATION OF THE MANUSCRIPT FOR PRINT AND PUBLICATION

Articles are published on a first-come, first-served basis. The publication order is established by the date of acceptance of the article. The members of the editorial board have the right to recommend the expedited publishing of articles which are deemed to be a priority and have received good reviews.

Articles which have been received by the editorial board are assessed by the board members and then sent for external review, if needed. The choice of reviewers is up to the editorial board. The manuscript is sent on to reviewers who are experts in this field of research, and the editorial board makes its decisions based on the reviews of these experts. The article may be accepted as is, sent back for improvements, or rejected.

The editorial board can decide to reject an article if it does not conform to the guidelines set above.

A manuscript which has been sent back to the authors for improvements requested by the editors and/or reviewers is reviewed again, after which the editorial board makes another decision on whether the article can be accepted for publication. The published article has the submission and publication acceptance dates set at the beginning.

The return of an article to the authors for improve-

ment does not mean that the article has been accepted for publication. After the revised text has been received, a decision is made by the editorial board. The author must return the improved text, together with the original text and responses to all comments. The date of acceptance is the day on which the final version of the article was received by the publisher.

A revised manuscript must be sent back to the publisher a week after the authors have received the comments; if not, the article is considered a resubmission.

E-mail is used at all the stages of communication between the author, editors, publishers, and reviewers, so it is of vital importance that the authors monitor the address that they list in the article and inform the publisher of any changes in due time.

After the layout for the relevant issue of the journal is ready, the publisher sends out PDF files to the authors for a final review.

Changes other than simple corrections in the text, figures, or tables are not allowed at the final review stage. If this is necessary, the issue is resolved by the editorial board.

## FORMAT OF REFERENCES

The journal uses a numeric reference system, which means that references are denoted as numbers in the text (in brackets) which refer to the number in the reference list.

*For books:* the last name and initials of the author, full title of the book, location of publisher, publisher, year in which the work was published, and the volume or issue and the number of pages in the book.

*For periodicals:* the last name and initials of the author, title of the journal, year in which the work was published, volume, issue, first and last page of the article. Must specify the name of the first 10 authors. Ross M.T., Grafham D.V., Coffey A.J., Scherer S., McLay K., Muzny D., Platzer M., Howell G.R., Burrows C., Bird C.P., et al. // Nature. 2005. V. 434. № 7031. P. 325–337.

References to books which have Russian translations should be accompanied with references to the original material listing the required data.

References to doctoral thesis abstracts must include the last name and initials of the author, the title of the thesis, the location in which the work was performed, and the year of completion.

References to patents must include the last names and initials of the authors, the type of the patent document (the author's rights or patent), the patent number, the name of the country that issued the document, the international invention classification index, and the year of patent issue.

The list of references should be on a separate page. The tables should be on a separate page, and figure captions should also be on a separate page.

**The following e-mail addresses can be used to contact the editorial staff: vera.knorre@gmail.com, actanaturae@gmail.com, tel.: (495) 727-38-60, (495) 930-87-07**